frontiers | Research Topics

Radiation therapy using MRI-LINAC - the right way to start: A guide for physicians and physicists

Edited by
Merav Ben-David, Frank Lagerwaard and Enis Ozyar

Published in
Frontiers in Oncology

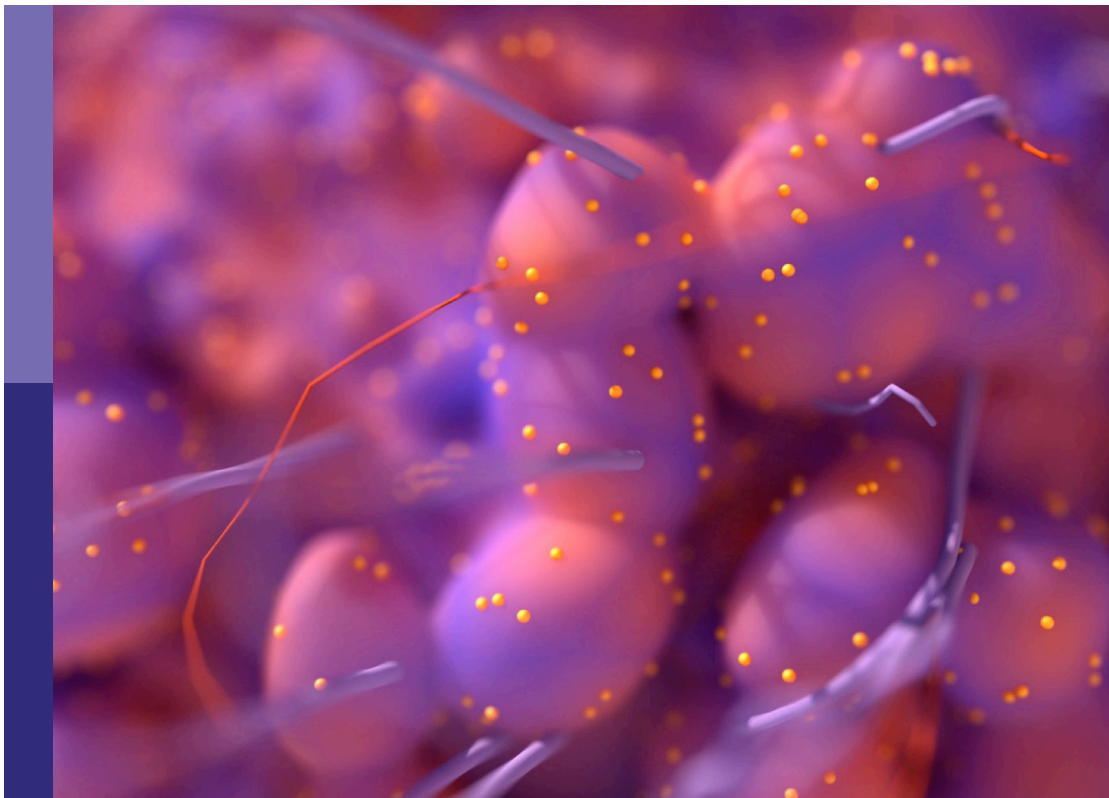

ISSN 1664-8714
ISBN 978-2-8325-3695-7
DOI 10.3389/978-2-8325-3695-7

About Frontiers

Frontiers is more than just an open access publisher of scholarly articles: it is a pioneering approach to the world of academia, radically improving the way scholarly research is managed. The grand vision of Frontiers is a world where all people have an equal opportunity to seek, share and generate knowledge. Frontiers provides immediate and permanent online open access to all its publications, but this alone is not enough to realize our grand goals.

Frontiers journal series

The Frontiers journal series is a multi-tier and interdisciplinary set of open-access, online journals, promising a paradigm shift from the current review, selection and dissemination processes in academic publishing. All Frontiers journals are driven by researchers for researchers; therefore, they constitute a service to the scholarly community. At the same time, the *Frontiers journal series* operates on a revolutionary invention, the tiered publishing system, initially addressing specific communities of scholars, and gradually climbing up to broader public understanding, thus serving the interests of the lay society, too.

Dedication to quality

Each Frontiers article is a landmark of the highest quality, thanks to genuinely collaborative interactions between authors and review editors, who include some of the world's best academicians. Research must be certified by peers before entering a stream of knowledge that may eventually reach the public - and shape society; therefore, Frontiers only applies the most rigorous and unbiased reviews. Frontiers revolutionizes research publishing by freely delivering the most outstanding research, evaluated with no bias from both the academic and social point of view. By applying the most advanced information technologies, Frontiers is catapulting scholarly publishing into a new generation.

What are Frontiers Research Topics?

Frontiers Research Topics are very popular trademarks of the *Frontiers journals series*: they are collections of at least ten articles, all centered on a particular subject. With their unique mix of varied contributions from Original Research to Review Articles, Frontiers Research Topics unify the most influential researchers, the latest key findings and historical advances in a hot research area.

Find out more on how to host your own Frontiers Research Topic or contribute to one as an author by contacting the Frontiers editorial office: frontiersin.org/about/contact

Radiation therapy using MRI-LINAC - the right way to start: A guide for physicians and physicists

Topic editors

Merav Ben-David — Assuta Medical Center, Ramat-Hahayal, Israel

Frank Lagerwaard — Amsterdam University Medical Center, Netherlands

Enis Ozyar — Acıbadem University, Türkiye

Citation

Ben-David, M., Lagerwaard, F., Ozyar, E., eds. (2023). *Radiation therapy using MRI-LINAC - the right way to start: A guide for physicians and physicists*. Lausanne: Frontiers Media SA. doi: 10.3389/978-2-8325-3695-7

Table of contents

frontiers | Frontiers in Oncology

TYPE Editorial
PUBLISHED 09 August 2023
DOI 10.3389/fonc.2023.1258257

OPEN ACCESS

EDITED AND REVIEWED BY
Timothy James Kinsella,
Brown University, United States

*CORRESPONDENCE
Enis Özyar
enis.ozyar@acibadem.com.tr

RECEIVED 13 July 2023
ACCEPTED 17 July 2023
PUBLISHED 09 August 2023

CITATION
Özyar E, Ben-David MA and Lagerwaard F (2023) Editorial: Radiation therapy using MRI-Linac - the right way to start: a guide for physicians and physicists.
Front. Oncol. 13:1258257.
doi: 10.3389/fonc.2023.1258257

Editorial: Radiation therapy using MRI-Linac - the right way to start: a guide for physicians and physicists

Enis Özyar[1]*, Merav A. Ben-David[2,3] and Frank Lagerwaard[4]

[1]Radiation Oncology Department, Acıbadem University, Istanbul, Türkiye, [2]Oncology Department, Assuta Medical Center, Tel Aviv, Israel, [3]Ben-Gurion University of the Negev, Beer-Sheva, Israel, [4]Radiation Oncology Department, VU Amsterdam, Amsterdam, Netherlands

KEYWORDS

MR guided radiotherapy, sterotactic radiotherapy, online adaptive, reoptimization, MR imaging

Editorial on the Research Topic
Radiation therapy using MRI-Linac - the right way to start: a guide for physicians and physicists

Radiotherapy iss an important method of local-regional treatment of malignancies and has witnessed impressive advancements in recent years. The main aim of radiotherapy is to increase the outcome of patients while minimizing side effects. The emergence of a new cutting-edge hybrid technology - Magnetic Resonance Image-guided Linear Accelerators (MR-Linac) - is a revolutionary breakthrough technology in the field. This new technology combines real-time MR imaging of "the anatomy of the day", prediction of the dose distribution, online adaptive optimization of the plan if needed, and continuous automatic cine-MR tracking of the target. As this technology has a significantly different workflow compared to conventional radiotherapy, it is crucial to understand the fundamentals of utilizing MR-Linac to reach the goal to obtain optimal patient outcomes. The following topics we would like to emphasize are the major important components of MR-Linac technology;

1 Exploiting the power of MR imaging during online adaptive radiotherapy

One of the key influences of MR-Linac is the ability to integrate high-quality real-time MR imaging into the MR-guided radiotherapy workflow. Physicians must notice the implication of this feature to visualize the exact location of tumors and critical structures immediately before the treatment, recontouring or editing tumors and neighboring normal organs and structures if needed, and tracking the tumors continuously during beam-on and stop the treatment automatically if the target is out of the boundaries.

2 Collaborative approach of the treatment team

The successful implementation of a new MR-Linac workflow requires close teamwork between physicians, Radiotherapy Technologists (RTTs), and Medical Physicists. Each team member has a valuable role in the different steps of the workflow. This collaborative approach aims to synergistically exploit the capabilities of MR-Linac (1).

3 Online adaptive radiotherapy: optimizing precision and personalization

Members of the team should collaborate to develop optimal personalized treatment plans based on the "anatomy of the day" imaging where needed. A recent analysis of 50 patients with localized prostate cancer who were treated with ultra-hypofractionation using MRgRT in a total of 250 fractions has shown that in 76% (190/250 fractions) of fractions, reoptimizisation is needed due to various reasons (2).

4 Continuous monitoring of the target during beam on

This new technology enables the real-time tracking of the tumors, ensuring the preplanned optimal target dose.

The goal of this Research Topic is to collect and summarise the growing knowledge from institutions using online MR-guided radiotherapy. To share the obstacles, solutions, learning curves, and innovations of this new treatment modality. Eleven top-notch manuscripts are published in this new Research Topicof Frontiers in Oncology – Radiation Oncology Journal.

The first manuscript of this Research Topic aimed to evaluate the geometrical differences and metabolic parameters (FDG-PET, DWI-MRI) as a tool for an individualized definition of the volume in need of dose escalation for squamous cell esophageal cancer (Li et al.). Second manuscript reports the dosimetric benefits of daily adaptation of SMART and the first clinical results in pancreatic tumors in 30 patients (Michalet et al.). Third manuscript assesses the quality of a new diffusion-weighted imaging (DWI) sequence implemented on an MR-Linac MRIdian system, evaluating and optimizing the acquisition parameters to explore the possibility of clinically implementing a DWI acquisition protocol in a 0.35-T MR-Linac (Nardini et al.). The fourth manuscript reported the use of MRgRT for pediatric patients over four years and describes important considerations in the selection and application of this technology in children (Hall et al.). The fifth manuscript quantitatively characterizes the dosimetric effects of long on-couch time in prostate cancer patients treatment (Gao et al.). Sixth manuscript reports the workflow and initial clinical experience of high-grade glioma radiotherapy on the 1.5 T MR-Linac (MRL), with a focus on the temporal variations of the tumor and feasibility of multi-parametric image (mpMRI) acquisition during routine treatment workflow. (Tseng et al.) The seventh manuscript documented the critical steps needed for the appropriate delivery of MRgART for lung tumors safely and effectively. (Bryant et al.). The eight manuscripts reported one of the largest cohorts of patients treated with online MRgRT of liver metastases focusing on oncological outcome, toxicity, patient-reported outcome measures (PROMs), and quality of life (Uder et al.). The ninth manuscript analyzed the role of MRgRT as a potential to become a widely utilized treatment platform and transform the radiation oncology treatment process just as earlier disruptive radiation therapy technologies have done (Ng et al.). Tenth manuscript, aimed to optimize patient selection for stereotactic ablative radiotherapy in patients with locally advanced pancreatic cancer after initial chemotherapy (Doppenberg et al.). The eleventh manuscript reported the outcome and toxicity of the first 200 patients with prostate cancer treated with MRI-Linac (Pridan et al.).

This editorial highlights the implications of recent research findings in this breakthrough technology. This Research Topic of the journal guide Physicians and Medical Physicists who are starting their voyage with this new technology and speed up their learning curve time in their new journey.

Author contributions

All authors listed have made a substantial, direct, and intellectual contribution to the work and approved it for publication.

Conflict of interest

Authors received honorarium, travel grants from Viewray Inc.

Publisher's note

References

1. Botman R, Tetar SU, Palacios MA, Slotman BJ, Lagerwaard FJ, Bruynzeel AME. The clinical introduction of MR-guided radiation therapy from an RTT perspective. *Clin Transl Radiat Oncol* (2019) 18:140–5. doi: 10.1016/j.ctro.2019.04.019

2. Ugurluer G, Atalar B, Zoto Mustafayev T, Gungor G, Aydin G, Sengoz M, et al. Magnetic resonance image-guided adaptive stereotactic body radiotherapy for prostate cancer: preliminary results. *Br J Radiol* (2020) 93:20200696. doi: 10.1259/bjr.20200696

frontiers in Oncology

ORIGINAL RESEARCH
published: 22 December 2021
doi: 10.3389/fonc.2021.772428

Geometrical Comparison and Quantitative Evaluation of ^{18}F-FDG PET/CT- and DW-MRI-Based Target Delineation Before and During Radiotherapy for Esophageal Squamous Carcinoma

Huimin Li[1,2], Jianbin Li[3], Fengxiang Li[3]*, Yingjie Zhang[3], Yankang Li[3], Yanluan Guo[4] and Liang Xu[5]*

[1] Weifang Medical University, Weifang, China, [2] Department of Respiratory and Neurology, The Affiliated Tumor Hospital of Xinjiang Medical University, Urumqi, China, [3] Department of Radiation Oncology, Shandong Cancer Hospital and Institute, Shandong First Medical University and Shandong Academy of Medical Sciences, Jinan, China, [4] Department of Positron Emission Tomography-Computed Tomograph (PET-CT), Shandong Cancer Hospital and Institute, Shandong First Medical University and Shandong Academy of Medical Sciences, Jinan, China, [5] Department of Medical Imaging, Shandong Cancer Hospital and Institute, Shandong First Medical University and Shandong Academy of Medical Sciences, Jinan, China

OPEN ACCESS

Edited by:
Enis Ozyar, Acıbadem University, Turkey

Reviewed by:
Christiane Matuschek, University Hospital of Düsseldorf, Germany
Joseph Weygand, Moffitt Cancer Center, United States

***Correspondence:**
Jianbin Li
lijianbin@msn.com
Fengxiang Li
lifengxiangli@aliyun.com

Specialty section:
This article was submitted to Radiation Oncology, a section of the journal Frontiers in Oncology

Received: *08 September 2021*
Accepted: *30 November 2021*
Published: *22 December 2021*

Citation:
Li H, Li J, Li F, Zhang Y, Li Y, Guo Y and Xu L (2021) Geometrical Comparison and Quantitative Evaluation of ^{18}F-FDG PET/CT- and DW-MRI-Based Target Delineation Before and During Radiotherapy for Esophageal Squamous Carcinoma. Front. Oncol. 11:772428. doi: 10.3389/fonc.2021.772428

Background and Purpose: This study aimed to evaluate the geometrical differences in and metabolic parameters of ^{18}F-fluorodeoxyglucose positron emission tomography–computed tomography (^{18}F-FDG PET-CT) and diffusion-weighted magnetic resonance imaging (DW-MRI) performed before and during radiotherapy (RT) for patients with esophageal cancer based on the three-dimensional CT (3DCT) medium and explore whether the high signal area derived from DW-MRI can be used as a tool for an individualized definition of the volume in need of dose escalation for esophageal squamous cancer.

Materials and Methods: Thirty-two patients with esophageal squamous cancer sequentially underwent repeated 3DCT, ^{18}F-FDG PET-CT, and enhanced MRI before the initiation of RT and after the 15th fraction. All images were fused with 3DCT images through deformable registration. The gross tumor volume (GTV) was delineated based on PET Edge on the first and second PET-CT images and defined as GTV_{PETpre} and GTV_{PETdur}, respectively. GTV_{DWIpre} and GTV_{DWIdur} were delineated on the first and second DWI and corresponding T_2-weighted MRI (T_2W-MRI)-fused images. The maximum, mean, and peak standardized uptake values (SUVs; SUV_{max}, SUV_{mean}, and SUV_{peak}, respectively); metabolic tumor volume (MTV); and total lesion glycolysis(TLG) and its relative changes were calculated automatically on PET. Similarly, the minimum and mean apparent diffusion coefficient (ADC; ADC_{min} and ADC_{mean}) and its relative changes were measured manually using ADC maps.

Results: The volume of GTV_{CT} exhibited a significant positive correlation with that of GTV_{PET} and GTV_{DWI} (both $p < 0.001$). Significant differences were observed in both ADCs and ^{18}F-FDG PET metabolic parameters before and during RT (both $p < 0.001$). No significant correlation was observed between SUVs and ADCs before and during RT ($p = 0.072$–0.944) and between ΔADCs and ΔSUVs ($p = 0.238$–0.854). The conformity index and degree of inclusion of GTV_{PETpre} to GTV_{DWIpre} were significantly higher than those of GTV_{PETdur} to GTV_{DWIdur} (both $p < 0.001$). The maximum diameter shrinkage rate (ΔLD_{DWI}) (24%) and the tumor volume shrinkage rate (VRR_{DWI}) (60%) based on DW-MRI during RT were significantly greater than the corresponding PET-based ΔLD_{PET} (14%) and VRR_{PET} (41%) rates ($p = 0.017$ and 0.000, respectively).

Conclusion: Based on the medium of CT images, there are significant differences in spatial position, biometabolic characteristics, and the tumor shrinkage rate for GTVs derived from ^{18}F-FDG PET-CT and DW-MRI before and during RT for esophageal squamous cancer. Further studies are needed to determine if DW-MRI will be used as tool for an individualized definition of the volume in need of dose escalation.

Keywords: esophageal squamous carcinoma, diffusion magnetic resonance imaging, positron emission tomography, gross target volume, standard uptake value (SUV), apparent diffusion coefficient (ADC)

INTRODUCTION

Radiotherapy—one of the main effective and relatively safe treatment modalities—is now fully integrated in the multidisciplinary treatment of esophageal cancer (EC). Currently, with substantial evidence, radiotherapy can be applied as a sole treatment or as part of a comprehensive treatment in combination with systemic treatments such as surgery, chemotherapy, targeted therapy, and, more recently, immunotherapy (1). Regional recurrence accounts for most radiation treatment failures in EC cases, with a local relapse rate of 40% (2). In particular, 90% of locoregional failures after definitive chemoradiotherapy (dCRT) occurred within the gross tumor volume (GTV) (3). Hence, there is an urgent need to escalate the radiation dose to the area at highest risk of recurrence to improve locoregional control. Currently, there is a growing interest in the delivery of intensity-modulated radiotherapy (IMRT)-based late course boost or simultaneously integrated boost techniques (4, 5), which could selectively deliver high radiation doses to radioresistant regions and a relatively low dose to subclinical tissues.

Currently, metabolic and functional imaging modalities such as ^{18}F-fluorodeoxyglucose positron emission tomography–computed tomography (^{18}F-FDG PET-CT) and diffusion-weighted magnetic resonance imaging (DW-MRI) are gaining increasing clinical significance in the management of patients undergoing radiotherapy since these allow visualization and quantification of treatment-induced changes on a molecular level before volumetric changes become apparent (6–8). It is well known that PET-based parameters such as standardized uptake value (SUV), metabolic tumor volume (MTV), and total lesion glycolysis (TLG) have been established and validated as prognostic biomarkers in EC (8, 9). Escalating the radiation dose to 64.8 Gy, which had been previously established, failed to improve survival or locoregional control (10). It is warranted to explore potential tools for an individualized definition of the volume in need of dose escalation. The current analysis demonstrates that high FDG uptake on initial PET-CT can identify tumor areas at high risk of relapse in EC (9, 11). Another study by Yu et al. (5) showed that the FDG hotspot within the residual area was completely within the GTV and remained stable during RT. They also reported that adaptive RT based on target volume reduction assessed on PET-CT could facilitate dose escalation up to 70 Gy, with a 1-year overall survival and local control of 69.2% and 77.4%, respectively. Therefore, it is feasible and safe to select boosting of high ^{18}F-FDG uptake zones within the tumor based on FDG PET-CT for the definition of the volume in need of dose escalation.

However, repeated PET imaging has not been widely adopted regardless of its clinical benefit owing to radiation exposure and uncertain segmentation algorithms obtained during PET (12, 13). In contrast, considering patient acceptability, repeated MRI is generally well tolerated for response assessment (14). High-resolution MRI for target volume delineation and response assessment in EC is currently of immense clinical interest (15, 16). The apparent diffusion coefficient (ADC) map from DW-MRI is a quantitative measure for the motion of water molecules and inversely correlates with tissue density. Relevant studies have shown that lower ADC values were associated with a higher histological grade and aggressiveness (17). Furthermore, it has been recently recognized that relative ADC changes from baseline to interim DW-MRI scans can help identify pathologic response in EC patients (7). Hence, we could theoretically observe the feasibility of selective boosting of the high signal areas of EC based on DW-MRI for definition of the volume in need of dose escalation.

Currently, selective boosting of high ^{18}F-FDG uptake zones based on FDG PET-CT within the tumor has been suggested for radioresistance (5, 9, 11). To date, CT imaging of the tumor extension remains the gold standard for target volume contouring and plan evaluation. Therefore, based on the medium of CT images, we evaluated the spatial position and functional parameters of ^{18}F-FDG PET-CT and DW-MRI performed before and during radiotherapy in patients with esophageal squamous carcinoma. The aim of this study was to explore whether the high signal area derived from DW-MRI can be used as tool for an individualized definition of the volume in need of dose escalation for esophageal squamous cancer.

MATERIALS AND METHODS

Patient Selection and Characteristics

After receiving approval from the local research ethics committee, a total of 35 patients with newly diagnosed, biopsy-proven, nonmetastatic esophageal squamous cancer suitable for concurrent chemoradiotherapy were recruited for this prospective study between November 2016 and May 2020. All patients scheduled to receive neoadjuvant or definitive chemoradiation for EC underwent 3DCT, ^{18}F-FDG PET-CT, and MRI simulation scanning prior to the initiation of RT and after 15 fractions of RT. Written informed consent was obtained from every patient included in this study. Patients were excluded if either pre-RT ^{18}F-FDG PET-CT or DW-MRI data were not available (n = 1), the volume of the tumor on baseline metabolic imaging was extremely small (≤1 cm^3) (n = 1), or they did not complete RT (n = 1). Consequently, image data of 32 patients were available for analysis. Patient and treatment characteristics are presented in **Table 1**.

TABLE 1 | Patient and treatment characteristics.

	Number	Percent
Patient characteristics		
Age (year), median (range)	67	(47–76)
Sex		
Female	6	18.8
Male	26	81.3
ECOG PS		
0–1	32	100.0
2	0	0.0
Pathology		
Squamous cell carcinoma	32	100.0
Adenocarcinoma	0	0.0
Site[a]		
Upper thoracic (UI 20–25 cm)	12	37.5
Middle thoracic (UI 25–30 cm)	11	34.4
Lower thoracic (UI 30–40 cm)	9	28.1
Stage[b]		
II	3	9.3
IIIA	4	12.5
IIIB	23	71.9
IVA	3	9.3
Treatment characteristics		
Aim		
Definitive chemoradiation	28	87.5
Neoadjuvant chemoradiation	4	12.5
Chemotherapy regimen		
5-Fluorouracil+cisplatin	30	93.8
5-Fluorouracil monotherapy	2	6.2
RT modality		
IMRT	32	100.0
3D-CRT	0	0.0
Total dose (Gy), median (range)	60	(41.4-60)
Fraction dose (Gy), median (range)	2.0	(1.8-2.0)
Fractions of RT completed before midradiotherapy	15	100.00
PET/DWI (fractions)		
Dose of RT completed before midradiotherapy	30	(27.30)
PET/DWI (Gy), median (range)		

ECOG, PS Eastern Cooperative Oncology Group performance status; UI, upper incisor; RT, radiotherapy; IMRT, intensity-modulated radiotherapy; 3D-CRT, 3-dimensional conformal radiotherapy.

[a]*American Joint Committee on Cancer classification 2017.*

[b]*Clinical tumor-node-metastasis (cTNM) stage according to 8th edition TNM classification.*

Image Simulation and Acquisition

Each patient underwent contrast-enhanced CT using a 16-slice CT scanner (Philips Brilliance Bores CT, Cleveland, OH, USA), with a 3-mm slice thickness during free breathing. All patients were scanned in the supine position, followed by laser alignment. The ^{18}F-FDG PET–CT examinations were performed within 2 weeks before the initiation of RT (PET_{pre}) and after 15 fractions (median 27 Gy, 1.8 Gy per fraction) of RT (PET_{dur}). Following CT, PET_{pre} was performed from the proximal thigh to the base of the skull in 3D acquisition mode with 2–5 min per bed position, while PET_{dur} was acquired from the skull base to the diaphragm. PET images were reconstructed using iterative 3D reconstruction.

Patients underwent MRI scanning with anatomical (T_2-weighted) and functional (diffusion-weighted) MRI sequences at the same two time points as that for ^{18}F-FDG PET-CT. MRI examinations were performed on a 3.0-T scanner equipped with a 32-tunnel body phased-array coil (Discovery MR 750, GE Medical Systems, Milwaukee, WI, USA). Patients were scanned in the supine position, with arms parallel to the body for both pre- and mid-RT scanning. Transverse DW images were obtained under free breathing conditions with the following scan parameters: repetition time (TR) 13,333 ms, echo time (TE) 64 ms, acquisition matrix 128 × 128 mm, field of view (FOV) 500 × 500 mm, slice thickness = 3.6 mm, and NE_X 5. A diffusion-sensitive gradient b-value of 600 s/mm^2 was applied for DWI. T_2W-MRI adopts fast spin echo to scan cross and axial sections, with the following specific parameters: TR 12,000 ms, TE 84 ms, thickness and spacing 3 mm, FOV 500 × 500 mm, acquisition matrix 384 × 384, and NE_X 1.8. Additionally, conventional T_2W-MR images were obtained using pulse and respiratory gating techniques to trigger scanning exclusively during the end of expiration (18).

Image Registration and Target Delineation

The ^{18}F-FDG PET-CT and MR images were registered to the planning CT using deformable image registration (DIR) in the software MIM Vista® (MIM Software Inc., version 6.8.3,

Cleveland, OH, USA). The main role of DIR is to define spatial correspondence between two considered image sets. To ensure the accuracy and repeatability of the delineation of target volumes, all structures were delineated by the same experienced radiation oncologist according to the consensus guidelines. GTVs were manually contoured on the first and second planning CT images, referred to as GTV_{CTpre} and GTV_{CTdur}, with a mediastinal window (window width = 400 HU, window level = 40 HU) setting and by the following standards: the GTVs were defined as any enlargement of the esophagus over its standard dimensions, 5 mm for wall thickness and 10 mm for wall diameter. On the basis of the reconstructed ^{18}F-FDG PET-CT image, given that no single absolute and relative methods of PET-based target volume delineation were validated, a gradient-based segmentation algorithm (PET_{Edge}) was applied, which identified tumors on the basis of changes in intensity/activity concentration at the tumor borders (19). The GTVs based on the first and second PET-CT images were determined using thresholds of PET_{Edge} and defined as GTV_{PETpre} and GTV_{PETdur}, respectively. All noncancerous regions within the GTV_{PET}, including areas overlaid by the heart, bone, and great vessels, were corrected to be excluded manually with the help of the CT component of PET-CT. Similarly, GTV_{DWIpre} and GTV_{DWIdur} were delineated on the first and second DWI and corresponding T_2-weighted MRI-fused images.

Functional Parameter Extraction

Images were analyzed and measured by two observers (a senior radiologist and an imaging physician in diagnostic PET/MRI) who were blinded to the histopathological results. Regions of interest (ROIs) were automatically drawn on the first and second PET based on PET_{Edge} and were modified to exclude any overlap with the heart, bone, and great vessels on CT images of PET-CT. The maximum, mean, and peak standardized uptake values (SUV_{max}, SUV_{mean}, and SUV_{peak}, respectively), MTV, and TLG were calculated automatically using the MIM software. TLG is defined as MTV from PET multiplied by SUV_{mean} within that volume (20).

For ADC measurements, an ADC map in grayscale was automatically generated in DW-MRI using ADW 4.7 Workstation (GE Healthcare, Waukesha, WI, USA). The manifested largest and clearest sections of esophageal lesions were selected as the ROIs. Subsequently, ROIs on the DWI and corresponding T_2-weighted MRI fused images were edited manually by two physicians in consensus to ensure that areas of hemorrhage, necrosis, edema, cystic change, and normal vessels were excluded. Finally, through the MIM software, the positions of ROIs on the ADC map were set to the same layers and locations prior to RT and after the 15th treatment cycle. The mean and minimum ADCs (ADC_{mean} and ADC_{min}, respectively) of the lesion were automatically calculated. The relative changes in percent (Δ%) of these ^{18}F-FDG PET-CT and DW-MRI parameters (i.e., ΔADCs, ΔSUVs, ΔMTV, and ΔTLG) between baseline scans and scans during RT were calculated.

Overlap Analysis

To quantify the overlap between PET-CT- and DW-MRI-based delineations before and during RT, the conformity index (CI) and degree of inclusion (DI) were calculated for GTV_{PETpre} and GTV_{DWIpre} and GTV_{PETdur} and GTV_{DWIdur}, respectively. The CI of volume A and B (CI[A, B]) was computed according to that described in a study by Struikmans et al. (21). A CI of 1 indicates 100% agreement between GTVs, and a CI of 0 indicates no overlap in delineation. The formula was as follows:

$$\mathrm{CI}(A,\ B) = \frac{A \cap B}{A \cup B}$$

The definition of DI of volume A included in volume B (DI[A in B]) was the intersection between volume A and volume B divided by volume A (22). The DI was defined as follows:

$$\mathrm{DI}(A \text{ in } B) = \frac{A \cap B}{A}$$

Tumor Shrinkage Analysis

Based on the Response Evaluation Criteria in Solid Tumors version 1.1, measurements of tumor volume and tumor maximal diameters were performed on PET-CT or MR images prior to and during RT. Four diameters measured on the first and second PET and DWI images were defined as LD_{PETpre} and LD_{PETdur} and LD_{DWIpre} and LD_{DWIdur}, respectively. The percentage maximum diameter shrinkage rate (ΔLD) was calculated using the following equation:

$$\Delta\mathrm{LD} = \frac{[(\mathrm{LD_{pre}} - \mathrm{LD_{dur}})]}{\mathrm{LD_{pre}}} \times 100\,\%$$

By the same method, the volume reduction rate (VRR) was calculated as follows:

$$\mathrm{VRR} = \frac{([\mathrm{GTVpre}] - [\mathrm{GTVdur}])}{\mathrm{GTVpre}} \times 100\,\%$$

Statistical Analysis

Statistical analysis was performed using SPSS 21.0 software (IBM Corp, Armonk, NY, USA). Data with skewed distribution are presented as medians with ranges. The Wilcoxon signed-rank test was used to compare the target volumes and relevant parameters. Spearman's rank correlation analysis was performed to analyze the relativity between SUVs and ADCs. A p-value <0.05 indicated statistical significance.

RESULTS

Correlation Analysis of GTVs and GTV_{CT}

The volume of GTV_{CTpre} was 26.34 (4.50–118.71) cm^3, leading to a significantly positive correlation with both GTV_{PETpre} (**Figure 1A**) and GTV_{DWIpre} (**Figure 1D**) (r = 0.763 and r = 0.809, both $p < 0.001$). The volume of GTV_{CTdur} was 16.74 (2.92–

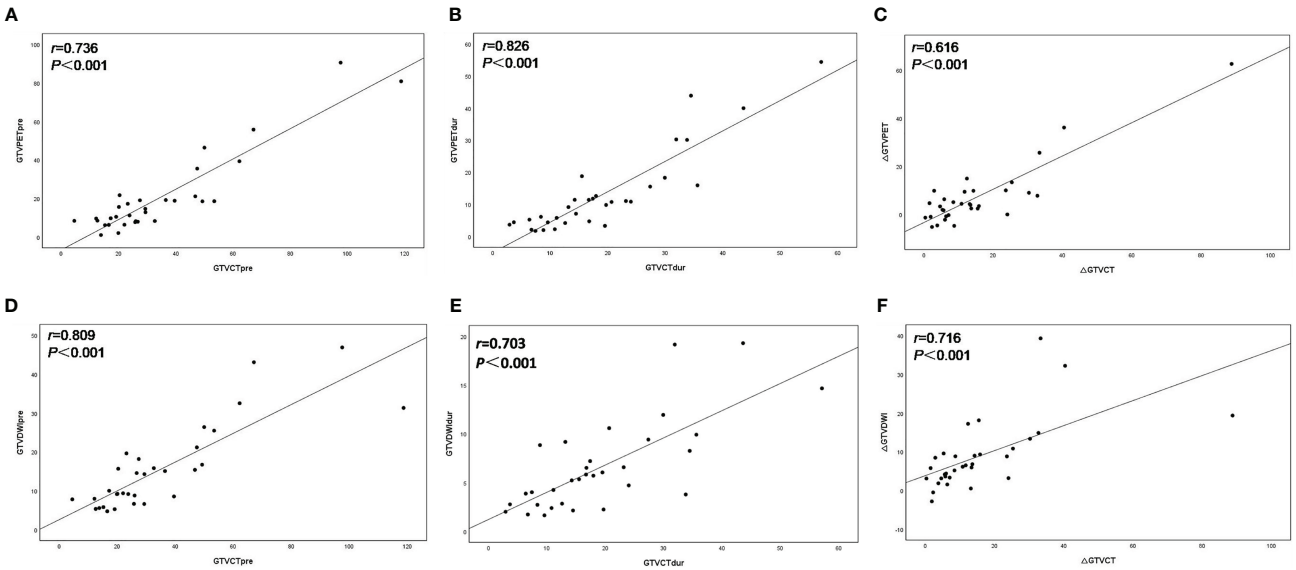

FIGURE 1 | Scatter plots of correlation between the target volume delineated on ^{18}F-FDG PET–CT (GTV_{PET}) and DW-MRI (GTV_{DWI}) and on the corresponding CT (GTV_{CT}) before and during radiotherapy. The best-fit line is shown as the solid line for each scatterplot. **(A)** GTV_{PETpre} versus GTV_{CTpre}; **(B)** GTV_{PETdur} versus GTV_{CTdur}; **(C)** ΔGTV_{PET} versus ΔGTV_{CT}; **(D)** GTV_{DWIpre} versus GTV_{CTpre}; **(E)** GTV_{DWIdur} versus GTV_{CTdur}; **(F)** ΔGTV_{DWI} versus ΔGTV_{CT}.

57.13) cm^3 and exhibited a significant positive correlation with both GTV_{PETdur} (**Figure 1B**) and GTV_{DWIdur} (**Figure 1E**) (r = 0.826 and r = 0.703, both p< 0.001). Similarly, the relative changes in the volume of PET-CT and DW-MRI (ΔGTV_{PET}, ΔGTV_{DWI}) before and during RT demonstrated a significantly positive correlation with that of CT (ΔGTV_{CT}) before and during RT (r = 0.616 and r = 0.716, both p < 0.001) (**Figure 1**).

SUV and ADC Values

Table 2 summarizes the results of SUVs (SUV_{max}, SUV_{mean}, and SUV_{peak}) and ADCs (ADC_{mean} and ADC_{min}) performed before and during RT. The differences in SUVs (SUV_{max}, SUV_{mean}, and SUV_{peak}), MTV, TLG, and ADCs (ADC_{mean} and ADC_{min}) values as determined on ^{18}F-FDG PET-CT and DW-MRI before and during RT were significant (both p < 0.001). A trend toward lower SUV and higher ADC was observed during the treatment process.

Correlation of ADC and SUV Values

The tumor ADC and SUV values before and during RT showed negligible correlations (pre-RT: SUV_{max} vs. ADC_{min} r = −0.322, p = 0.072; SUV_{max} vs. ADC_{mean} r = −0.217, p = 0.232; SUV_{mean} vs. ADC_{min} r = −0.258, p = 0.153; SUV_{mean} vs. ADC_{mean} r = −0.256, p = 0.158; dur-RT: SUV_{max} vs. ADC_{min} r = −0.133, p = 0.496; SUV_{max} vs. ADC_{mean} r = −0.133, p = 0.496; SUV_{mean} vs. ADC_{min} r = −0.013, p = 0.944; SUV_{mean} vs. ADC_{mean} r = −0.121, p = 0.510). There was no correlation between ΔSUV values (ΔSUV_{max}, ΔSUV_{mean}, and ΔSUV_{peak}) and ΔADC values (ΔADC_{min} and ΔADC_{mean}) (p = 0.238–0.854) (**Table 3**).

Associations of SUVs and ADCs With Clinical Prognostic Factors

Table 4 shows associations of SUVs and ADCs with clinical T-stage and longitudinal length of GTVs. The SUVs (SUV_{max},

TABLE 2 | Comparison of tumor ADC and SUV values before and during radiotherapy.

Parameters	$PET(DWI)_{pre}$	$PET(DWI)_{dur}$	$\Delta[PET(DWI)_{dur}\text{-}PET(DWI)_{pre}]$	*Z*-value	*p*-value
SUV_{max}	14.10 [3.02–22.94]	8.21 [1.74–13.75]	5.25 [–5.21–15.45]	–4.394	<0.001
SUV_{mean}	6.87 [1.32–12.75]	4.93 [2.14–8.04]	2.29 [–2.63–9.70]	–4.133	<0.001
SUV_{peak}	9.98 [3.57–19.34]	5.97 [2.03–11.10]	4.42 [0.03–10.53]	–4.937	<0.001
MTV	13.77 [1.07–90.50]	10.3 [1.74–54.38]	4.23 [–5.10–62.51]	–3.571	<0.001
TLG	94.7 [4.49–833.10]	35.13 [9.72–285.20]	47.62 [–12.44–721.10]	–4.600	<0.001
ADC^{a}_{min}	0.51 [0.30–1.04]	0.79 [0.22–2.09]	0.33 [–0.40–1.19]	–3.909	<0.001
ADC^{b}_{mean}	1.30 [0.92–1.83]	2.28 [1.13–4.24]	0.9 [0.21–2.51]	–4.937	<0.001

[a] *ADC_{min} and ADC_{mean} are expressed in $10^{-3}mm^2/s$.*

PET, positron emission tomography; DWI, diffusion-weighted imaging; SUV_{max}, maximum standardized uptake value; SUV_{mean}, mean standardized uptake value; SUV_{peak}, peak standardized uptake value; MTV, metabolic tumor volume; TLG, total lesion glycolysis; ADC_{min}, the minimum apparent diffusion coefficient; ADC_{mean}, the mean apparent diffusion coefficient.

SUV_{mean}, and SUV_{peak}), MTV, and TLG pre-RT and its relative changes between pre-RT and after 15 fractions of RT were significantly higher in stages T3–4 than in stage T2 and in the group with a longitudinal length of GTVs ≥4 cm than <4 cm (p = 0.000–0.041). The ADC_{min} dur-RT and its relative changes between pre-RT and after 15 fractions of RT were significantly lower in the group with a longitudinal length of GTVs ≥4 cm than <4 cm, but these were not significantly associated with clinical T-stage (**Table 4**).

Differences in Volumes, CI, and DI

The target volumes defined using PET-CT and DW-MRI before and during RT are listed in **Table 5**. The median volume variabilities between GTV_{PETpre} and GTV_{DWIpre} and between GTV_{PETdur} and GTV_{DWIdur} were significant (p =0.026 and 0.000, respectively). Significant differences were observed between the CI of GTV_{PETpre} to GTV_{DWIpre} (0.47 [0.20–0.77]) and GTV_{PETdur} to GTV_{DWIdur} (0.29 [0.11–0.48]) (Z = −4.750, p < 0.001). Meanwhile, the DI of GTV_{PETpre} in GTV_{DWIpre} (0.63

TABLE 3 | Correlation analysis of relative changes in SUV and ADC values before and during radiotherapy.

	Parameters	ΔSUV_{max}	ΔADC_{mean}	ΔSUV_{peak}	ΔMTV	ΔTLG	ΔADC_{min}	ΔADC_{mean}
ΔSUV_{max}	*r*-value	1	0.894	0.833	0.154	0.622	−0.196	−0.087
	p-value		<0.001	<0.001	0.399	<0.001	0.238	0.635
ΔSUV_{mean}	*r*-value		1	0.870	0.236	0.715	−0.179	−0.035
	p-value			<0.001	0.193	<0.001	0.327	0.848
ΔSUV_{peak}	*r*-value			1	0.316	0.784	−0.139	−0.034
	p-value				0.078	<0.001	0.448	0.854
ΔMTV	*r*-value				1	0.739	−0.253	−0.238
	p-value					<0.001	0.163	0.190
ΔTLG	*r*-value					1	−0.286	−0.163
	p-value						0.112	0.372
ΔADC_{min}	*r*-value						1	0.179
	p-value							0.327
ΔADCmean	*r*-value							1
	p-value							

SUV_{max}, maximum standardized uptake value; SUV_{mean}, mean standardized uptake value; SUV_{peak}, peak standardized uptake value; MTV, metabolic tumor volume; TLG, total lesion glycolysis; ADC_{min}, the minimum apparent diffusion coefficient; ADC_{mean}, the mean apparent diffusion coefficient.

TABLE 4 | Associations of SUVs and ADCs with clinical T-stage and longitudinal length of GTVs.

Parameters	Clinical T-stage			Longitudinal length of GTVs		
	cT2 (n = 11)	≥cT3 (n = 21)	p-value	<4 cm (n = 15)	≥4 cm (n = 17)	p-value
Preradiotherapy PET(DWI)						
SUV_{max}	7.67 [3.02–15.67]	16.89 [10.75–22.94]	0.001	10.75 [3.02–19.91]	17.23 [11.7–22.94]	0.000
SUV_{mean}	4.02 [1.32–8.83]	9.21 [5.33–12.75]	0.000	5.8 [1.32–12.75]	9.45 [5.33–12.63]	0.002
SUV_{peak}	5.86 [3.57–11.31]	12.65 [8.69–19.34]	0.000	7.16 [3.57–11.31]	13.73 [9.54–19.34]	0.000
MTV	7.99 [1.07–14.67]	18.86 [2.11–90.50]	0.000	8.26 [1.07–14.67]	19.21 [8.52–90.50]	0.000
TLG	24.89 [4.49–72.94]	144.86 [26.9–833.1]	0.000	26.90 [4.49–88.8]	196.71 [82.3–833.1]	0.000
ADC_{min}	0.55 [0.30–1.04]	0.39 [0.31–0.63]	0.074	0.57 [0.30–1.04]	0.46 [0.31–0.63]	0.079
ADC_{mean}	1.31 [0.92–1.52]	1.27 [1.07–1.83]	0.706	1.3 [1.07–1.83]	1.3 [0.92–1.64]	0.584
Dur-radiotherapy PET(DWI)						
SUV_{max}	4.91 [1.74–13.69]	10.46 [3.76–13.75]	0.025	6.68 [1.74–13.69]	10.46 [3.76–13.75]	0.011
SUV_{mean}	3.31 [2.14–8.04]	5.10 [2.43–7.33]	0.088	3.43 [2.14–8.04]	5.14 [2.43–7.33]	0.076
SUV_{peak}	3.07 [2.03–6.53]	7.56 [3.20–11.10]	0.000	3.33 [2.03–6.53]	7.79 [3.2–11.10]	0.000
MTV	4.45 [1.74–15.55]	10.85 [2.13–54.38]	0.077	4.74 [1.74–15.55]	11.81 [2.13–54.38]	0.012
TLG	24.44 [9.72–45.56]	53.84 [10.18–285.20]	0.006	24.44 [9.72–45.56]	62.41 [14.1–285.20]	0.001
ADC_{min}	0.92 [0.27–2.09]	0.67 [0.22–1.19]	0.131	1.03 [0.27–2.09]	0.67 [0.22–1.19]	0.010
ADC_{mean}	2.42 [1.66–4.24]	2.23 [1.13–2.73]	0.126	2.37 [1.66–4.24]	2.23 [1.13–2.73]	0.355
Relative change from preradiotherapy PET(DWI)to dur-radiotherapy PET(DWI)						
$\triangle SUV_{max}$	1.59 [−5.21–11.56]	6.74 [0.21–15.45]	0.010	1.97 [−5.21–15.45]	6.77 [0.87–14.13]	0.013
$\triangle SUV_{mean}$	0.44 [−2.63–4.07]	2.90 [−0.33–9.7]	0.002	0.71 [−2.63–9.7]	3.08 [−0.33–7.02]	0.005
$\triangle SUV_{peak}$	3.11 [0.75–4.78]	5.36 [0.03–10.53]	0.004	3.47 [0.75–5.36]	5.72 [0.03–10.53]	0.003
$\triangle MTV$	−0.20 [−5.10–5.18]	7.84 [−4.45–62.51]	0.005	1.81 [−5.1–5.18]	9.48 [−4.45–62.51]	0.001
$\triangle TLG$	9.56 [−12.44–48.7]	88.96 [4.06–721.10]	0.000	16.72 [−12.44–48.70]	123.98 [4.06–721.10]	0.000
$\triangle ADC_{min}$	0.34 [−0.40–1.19]	0.30 [−0.37–0.56]	0.525	0.38 [−0.40–1.19]	0.20 [−0.37–0.56]	0.041
$\triangle ADC_{mean}$	0.99 [0.23–2.51]	0.75 [0.21–1.42]	0.132	0.99 [0.23–2.51]	0.87 [0.21–1.46]	0.45

SUV_{max}, maximum standardized uptake value; SUV_{mean}, mean standardized uptake value; SUVpeak, peak standardized uptake value; MTV, metabolic tumor volume; TLG, total lesion glycolysis; ADC_{min}, the minimum apparent diffusion coefficient; ADC_{mean}, the mean apparent diffusion coefficient.

[0.24–2.60]) was significantly larger than that of GTV_{PETdur} in GTV_{DWIdur} (0.38 [0.11–0.92]) ($Z = -4.675$, $p < 0.001$).

Tumor Maximum Diameter/Volume Shrinkage Rate

There was no significant difference between LD_{PETpre} and LD_{DWIpre} and between LD_{PETdur} and LD_{DWIdur} (median 2.85 cm [1.48–6.31] vs. 2.92 cm [1.89–5.33], median 2.36 cm [1.47–4.79] vs. 2.22 cm [1.35–3.47], $Z = -1.169$ and -1.187, $p = 0.243$ and 0.235, respectively). There was a significant positive correlation between LD_{PETpre} and LD_{DWIpre} and between VRR_{PET} and VRR_{DWI} ($r = 0.631$ and 0.547, $p = 0.000$ and 0.001, respectively). $\triangle LD_{DWI}$ (24%) and VRR_{DWI} (60%) based on DWI during RT were significantly greater than the corresponding PET-based $\triangle LD_{PET}$ (14%) and VRR_{PET} (41%) ($Z = -2.393$ and -3.758, $p = 0.017$ and 0.000, respectively) (**Figure 2**).

DISCUSSION

In this single-center prospective study, comparisons of the spatial overlap and functional markers derived from ^{18}F-FDG PET-CT and DW-MRI before and during RT based on the medium of CT imaging were evaluated. The results of the current study show that it is feasible to select boosting of high ^{18}F-FDG uptake zones within the GTV based on FDG PET-CT for definition of the volume in need of dose escalation (4, 5, 23). However, owing to exorbitant costs and physical burden to patients undergoing repeated PET procedures, MRI-guided Linear Accelerator (MRI-LINAC) with online MR-guided adaptive radiotherapy (MRgRT) in EC has been widely applied (24). Furthermore, ADC measurements on DW-MRI have potential for prediction of response to treatment in esophageal cancer patients, especially the relative ADC increase during and after treatment showed a trend towards a larger increase of ADC in good responders compared with poor responders (16). Hence, we aimed to explore whether the high signal area derived from DW-MRI can be used as tool for an individualized definition of the volume in need of dose escalation for EC. To our knowledge, this is the first prospective trial assessing the geometrical differences and metabolic parameters between two imaging modalities in the reirradiation treatment planning for esophageal squamous cancer.

Currently, the method of gradient-based algorithm (PET_{Edge}) has been found to correspond better to pathological specimens

TABLE 5 | Summary of the volume of GTVs contoured using PET-CT and DW-MRI before and during radiotherapy.

Modality	Target volumes			*Z*-value	*p*-value
	Median	Range			
		Min	Max		
GTV_{PETpre}	13.77	1.07	90.50	−2.225	0.026
GTV_{DWIpre}	12.16	4.74	46.86		
GTV_{PETdur}	10.30	1.74	54.38	−3.815	0.000
GTV_{DWIdur}	5.54	1.65	19.30		

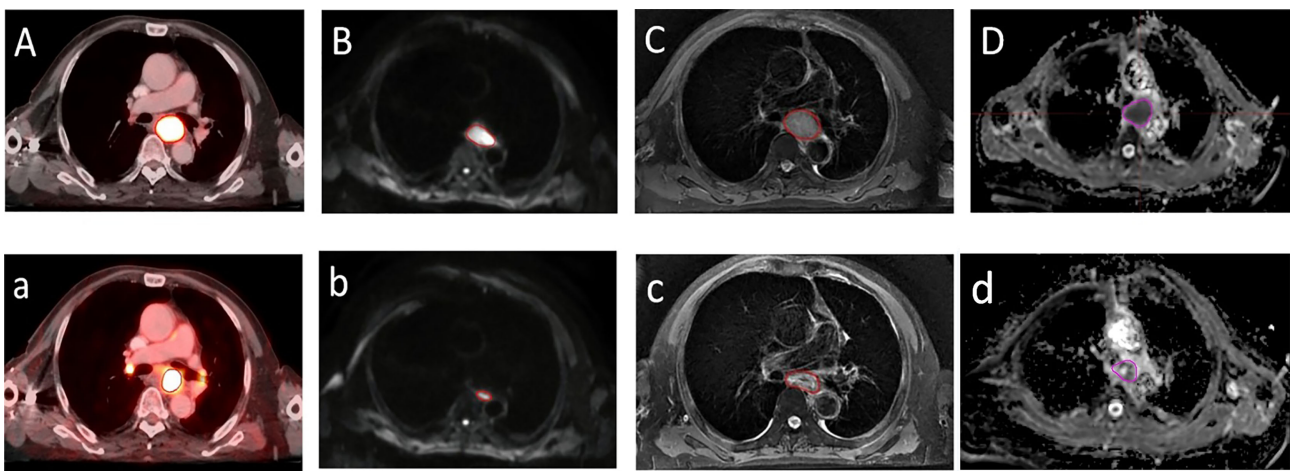

FIGURE 2 | A transversal diagram of gross target volumes on esophageal cancer with high uptake on ^{18}F fluorodeoxyglucose positron emission tomography/computed tomography fused images. **(A,a)** Corresponding tumor on T_2-weighted imaging **(C,c)** with a high signal on diffusion weighted magnetic resonance imaging (b=600 s/mm^2) **(B,b)** and corresponding apparent diffusion coefficient map **(D,d)** with restricted diffusion at the location of the tumor before radiotherapy **(A–D)** and during radiotherapy **(a–d)**.

than manual or relative threshold-based methods (19). However, no single PET-based segmentation algorithm has yet performed better than manual CT delineation alone (16), implying that PET-guided adaptive radiotherapy was insufficient for clinical decision-making. Till date, CT imaging remains the gold standard for GTV delineation and treatment planning evaluation. On this basis, our data suggest that the volume of GTV_{CT} exhibited a significant positive correlation with that of GTV_{PET} and GTV_{DWI}.

Based on our analysis, the results showed that the differences in SUV and ADC values before and during RT were significant, consistent with the findings of more recent studies (25, 26). There is also clear evidence that higher SUV and lower ADC values are associated with a higher histological grade and aggressiveness (17, 27). With high cellular density and enhanced glucose metabolism, malignant tumors generally exhibit low ADCs and high SUVs. Several studies indicate that the change in tumor ^{18}F-FDG uptake for EC seemed highly predictive for assessing response during and after treatment (7, 28). Another recent study by Aerts et al. (29) has demonstrated that the recurrent areas within the tumor after therapy largely corresponded with the high FDG uptake area of the pretreatment PET scan. As a result, selective boosting of high ^{18}F-FDG uptake zones within the tumor for radioresistance has been suggested. However, part of the limitations of PET can be attributed to the fact that no consensus for the accurate segmentation algorithm is recommended. Meanwhile, DW-MRI is emerging as an advanced imaging technique with noninvasive, well-tolerated, and excellent soft-tissue contrast features for diagnosing EC. ADC value is the most common DWI-derived imaging biomarker with broad clinical applications. More importantly, recent exploratory studies have shown that changes in ADC appears to provide valuable information on the prediction and assessment of treatment response early after RT (7, 16, 17). Consequently, regions of restricted diffusion may serve as a surrogate for active tumor tissue. DW-MRI may be a technically and clinically available alternative to PET-CT for an individualized definition of the volume in need of dose escalation for EC.

Concerning the possible correlation between ADCs and SUVs for the prediction of survival or evaluation of response to treatment in EC, our current data suggest that the tumor ADCs and SUVs before and during RT showed negligible correlations. Similar to our findings, previous studies also found no significant correlations between pretreatment SUVs and ADCs (30–32). Our results also revealed that pretreatment SUVs, MTV, and TLG were significantly higher in tumor stage $\geq T_3$ than in tumor stage $< T_2$, while ADC_{min} values has not yet been found to correlate with the clinical T-stage, indicating the effect of tumor load on ^{18}F-FDG metabolism, consistent with the literature (8, 33). These results suggest that enhanced glucose metabolism as measured on FDG PET and restricted water diffusion as measured using ADC represent independent biological properties and refer to different aspects of tumor pathophysiology. This is likely owing to the variety of pathogenic mechanisms because of which elevated ^{18}F-FDG uptake was detected in the sites of glucose metabolism and active inflammation, while no significant changes in cell density were detected in the activity of inflammatory cells (28, 33, 34). Additionally, necrosis and liquefaciens induced by radiation can impede movement of water molecules, leading to increased ADC values. Finally, it is likely that the timing and distribution of decreased glucose metabolism and cellular density are asynchronous and inconsistent.

In addition, we evaluated the difference in matching and inclusion relation between the GTVs derived from PET-CT and DW-MRI simulation before and during RT. Our results indicate that the CI of GTV_{PETpre} to GTV_{DWIpre} was significantly larger than that of GTV_{PETdur} to GTV_{DWIdur}. Meanwhile, a significant difference was observed between the DI of GTV_{PETpre} in GTV_{DWIpre} and GTV_{PETdur} in GTV_{DWIdur}. Our study results are also consistent with the findings of Popp et al. (34) and Houweling et al. (35), who showed that the GTV of restricted diffusion on ADC overlapped only partially with that of increased glucose uptake for reirradiation treatment planning, suggesting that there were great mismatches between the regions of residual high FDG uptake based on PET-CT and the areas of residual high signal based on DW-MRI. Moreover, given the data from our study, the rate of tumor maximum diameter/volume regression based on DW-MRI during RT is significantly faster than that based on PET-CT. This suggests that the regions of high cellularity may not cover the entire biologically active tumor, agreeing with earlier studies comparing DWI and PET in reirradiation of recurrent primary brain tumors (34, 35).

Some limitations of the current study must be considered. A potential disadvantage of EPI-DWI is that the technique is prone to artifact contamination caused by variations in magnetic susceptibility (36). To minimize this, the study excluded some cases with a small volume and severe image distortions. Additionally, The magnitude of the geometric distortion scales with magnetic field strength (37). Considering that the use of 3.0 T MRI was applied, the limitation of the geometric distortion caused by high field strength must be considered. Owing to the partial-volume and pseudo-diffusion effect caused by tumor vascular permeability and microcirculation perfusion, tumor shrinkage upon initiation of treatment may lead to underestimation of the FDG uptake observed on midtreatment imaging modalities and a consequent overestimation of the change in parameters such as the SUV. Further dosimetric investigations are necessary to evaluate whether it is safe to select boosting of the high signal areas within the tumor based on DW-MRI for definition of the volume in need of dose escalation.

CONCLUSIONS

The location of high residual FDG uptake based on ^{18}F-FDG PET-CT yielded poorer spatial matching than that of high residual signal based on DW-MRI during RT. Furthermore, tumor ADC and SUV values may play complementary roles as imaging markers for the prediction of patterns of failure and for definition of the volume in need of dose escalation. In addition, the rate of tumor maximum diameter/volume regression based

on DW-MRI during RT is significantly faster than that based on PET-CT. Based on the medium of CT images, the volume of GTV_{CT} exhibited a significant positive correlation with that of GTV_{PET} and GTV_{DWI}. Under this premise, there are significant differences in spatial position, biometabolic characteristics, and the tumor shrinkage rate for GTVs derived from ^{18}F-FDG PET-CT and DW-MRI before and during RT for esophageal squamous cancer. Further studies are needed to determine if DW-MRI will be used as tool for an individualized definition of the volume in need of dose escalation.

DATA AVAILABILITY STATEMENT

The original contributions presented in the study are included in the article/supplementary material. Further inquiries can be directed to the corresponding authors.

ETHICS STATEMENT

The studies involving human participants were reviewed and approved by the Shandong Tumor Hospital Ethics Committee. The patients/participants provided their written informed consent to participate in this study. Written informed consent was obtained from the individual(s) for the publication of any potentially identifiable images or data included in this article.

AUTHOR CONTRIBUTIONS

HL contributed to the study design, the patient enrollment, the data statistics, and analysis and writing of the manuscript. JL and FL participated in the study design and revised the content. YZ and YL contributed to reviewing the delineation. YG and LX made important contributions in collecting the data and revising the content. All authors read and approved the final version of the manuscript.

FUNDING

This work was supported by the National Natural Science Foundation of China (grant number 81773287) and Taishan Scholars Program of Shandong Province (grant number ts20190982).

ACKNOWLEDGMENTS

This manuscript underwent American-language editing by Elsevier Limited.

REFERENCES

1. Kakeji Y, Oshikiri T, Takiguchi G, Kanaji S, Matsuda T, Nakamura T, et al. Multimodality Approaches to Control Esophageal Cancer: Development of Chemoradiotherapy, Chemotherapy, and Immunotherapy. *Esophagus* (2021) 18(1):25–32. doi: 10.1007/s10388-020-00782-1
2. Button MR, Morgan CA, Croydon ES, Roberts SA, Crosby TD. Study to Determine Adequate Margins in Radiotherapy Planning for Esophageal Carcinoma by Detailing Patterns of Recurrence After Definitive Chemoradiotherapy. *Int J Radiat Oncol Biol Phys* (2009) 73(3):818–23. doi: 10.1016/j.ijrobp.2008.04.062
3. Welsh J, Settle SH, Amini A, Xiao L, Suzuki A, Hayashi Y, et al. Failure Patterns in Patients With Esophageal Cancer Treated With Definitive Chemoradiation. *Cancer* (2012) 118(10):2632–40. doi: 10.1002/cncr.26586
4. Grover A, Soni TP, Patni N, Singh DK, Jakhotia N, Gupta AK, et al. A Randomized Prospective Study Comparing Acute Toxicity, Compliance and Objective Response Rate Between Simultaneous Integrated Boost and Sequential Intensity-Modulated Radiotherapy for Locally Advanced Head and Neck Cancer. *Radiat Oncol J* (2021) 39(1):15–23. doi: 10.3857/roj.2020.01018
5. Yu W, Cai XW, Liu Q, Zhu ZF, Feng W, Zhang Q, et al. Safety of Dose Escalation by Simultaneous Integrated Boosting Radiation Dose Within the Primary Tumor Guided by (18)FDG-PET/CT for Esophageal Cancer. *Radiother Oncol* (2015) 114(2):195–200. doi: 10.1016/j.radonc.2014.12.007
6. Kim N, Cho H, Yun M, Park KR, Lee CG. Prognostic Values of Mid-Radiotherapy ^{18}F-FDG PET/CT in Patients With Esophageal Cancer. *Rad Oncol* (2019) 14(1):27. doi: 10.1186/s13014-019-1232-1
7. Borggreve AS, Goense L, van Rossum PSN, Heethuis SE, van Hillegersberg R, Lagendijk JJW, et al. Preoperative Prediction of Pathologic Response to Neoadjuvant Chemoradiotherapy in Patients With Esophageal Cancer Using ^{18}F-FDG PET/CT and DW-MRI: A Prospective Multicenter Study. *Int J Radiat Oncol Biol Phys* (2020) 106(5):998–1009. doi: 10.1016/j.ijrobp.2019.12.038
8. Yu CW, Chen XJ, Lin YH, Tseng YH, Lu CC, Chen BB, et al. Prognostic Value of ^{18}F-FDG PET/MR Imaging Biomarkers in Oesophageal Squamous Cell Carcinoma. *Eur J Radiol* (2019) 120:108671. doi: 10.1016/j.ejrad.2019.108671
9. Chang S, Kim SJ. Prediction of Recurrence and Mortality of Locally Advanced Esophageal Cancer Patients Using Pretreatment F-18 FDG PET/CT Parameters: Intratumoral Heterogeneity, SUV, and Volumetric Parameters. *Cancer Biother Radiopharm* (2016) 31(1):1–6. doi: 10.1089/cbr.2015.1932
10. Minsky BD, Pajak TF, Ginsberg RJ, Pisansky TM, Martenson J, Komaki R, et al. Int 0123 (Radiation Therapy Oncology Group 94-05) Phase III Trial of Combined-Modality Therapy for Esophageal Cancer: High-Dose Versus Standard-Dose Radiation Therapy. *J Clin Oncol Radiat Ther Oncol Group* (2002) 20(5):1167–74. doi: 10.1200/JCO.2002.20.5.1167
11. Calais J, Dubray B, Nkhali L, Thureau S, Lemarignier C, Modzelewski R, et al. High FDG Uptake Areas on Pre-Radiotherapy PET/CT Identify Preferential Sites of Local Relapse After Chemoradiotherapy for Locally Advanced Oesophageal Cancer. *Eur J Nucl Med Mol Imaging* (2015) 42(6):858–67. doi: 10.1007/s00259-015-3004-y
12. Huang B, Law MW, Khong PL. Whole-Body PET/CT Scanning: Estimation of Radiation Dose and Cancer Risk. *Radiology* (2009) 251(1):166–74. doi: 10.1148/radiol.2511081300
13. Cremonesi M, Garibaldi C, Timmerman R, Ferrari M, Ronchi S, Grana CM, et al. Interim ^{18}f-FDG-PET/CT During Chemo-Radiotherapy in the Management of Oesophageal Cancer Patients. *A Syst Rev Radiother Oncol* (2017) 125(2):200–12. doi: 10.1016/j.radonc.2017.09.022
14. Goense L, Borggreve AS, Heethuis SE, van Lier AL, van Hillegersberg R, Mook S, et al. Patient Perspectives on Repeated MRI and PET/CT Examinations During Neoadjuvant Treatment of Esophageal Cancer. *Br J Radiol* (2018) 91(1086):20170710. doi: 10.1259/bjr.20170710
15. Li H, Li F, Li J, Zhu Y, Zhang Y, Guo Y, et al. Comparison of Gross Target Volumes Based on Four-Dimensional CT, Positron Emission Tomography-Computed Tomography, and Magnetic Resonance Imaging in Thoracic Esophageal Cancer. *Cancer Med* (2020) 9(15):5353–61. doi: 10.1002/cam4.3072

16. Vollenbrock SE, Voncken FEM, Bartels LW, Beets-Tan RGH, Bartels-Rutten A. Diffusion-Weighted MRI With ADC Mapping for Response Prediction and Assessment of Oesophageal Cancer: A Systematic Review. *Radiother Oncol* (2020) 142:17–26. doi: 10.1016/j.radonc.2019.07.006
17. Giganti F, Salerno A, Ambrosi A, Chiari D, Orsenigo E, Esposito A, et al. Prognostic Utility of Diffusion-Weighted MRI in Oesophageal Cancer: Is Apparent Diffusion Coefficient a Potential Marker of Tumour Aggressiveness? *Radiol Med* (2016) 121(3):173–80. doi: 10.1007/s11547-015-0585-2
18. Lever FM, Lips IM, Crijns SP, Reerink O, van Lier AL, Moerland MA, et al. Quantification of Esophageal Tumor Motion on Cine-Magnetic Resonance Imaging. *Int J Radiat Oncol Biol Phys* (2014) 88(2):419–24. doi: 10.1016/j.ijrobp.2013.10.036
19. Werner-Wasik M, Nelson AD, Choi W, Arai Y, Faulhaber PF, Kang P, et al. What is the Best Way to Contour Lung Tumors on PET Scans? Multiobserver Validation of a Gradient-Based Method Using a NSCLC Digital PET Phantom. *Int J Radiat Oncol Biol Phys* (2012) 82(3):1164–71. doi: 10.1016/j.ijrobp.2010.12.055
20. Larson SM, Erdi Y, Akhurst T, Mazumdar M, Macapinlac HA, Finn RD, et al. Tumor Treatment Response Based on Visual and Quantitative Changes in Global Tumor Glycolysis Using PET-FDG Imaging. The Visual Response Score and the Change in Total Lesion Glycolysis. *Clin Positron Imaging* (1999) 2(3):159–71. doi: 10.1016/s1095-0397(99)00016-3
21. Struikmans H, Wárlám-Rodenhuis C, Stam T, Stapper G, Tersteeg RJ, Bol GH, et al. Interobserver Variability of Clinical Target Volume Delineation of Glandular Breast Tissue and of Boost Volume in Tangential Breast Irradiation. *Radiother Oncol* (2005) 76(3):293–9. doi: 10.1016/j.radonc.2005.03.029
22. Hof H, Rhein B, Haering P, Kopp-Schneider A, Debus J, Herfarth K. 4d-CT-Based Target Volume Definition in Stereotactic Radiotherapy of Lung Tumours: Comparison With a Conventional Technique Using Individual Margins. *Radiother Oncol* (2009) 93(3):419–23. doi: 10.1016/j.radonc.2009.08.040
23. Nkhali L, Thureau S, Edet-Sanson A, Doyeux K, Benyoucef A, Gardin I, et al. FDG-PET/CT During Concomitant Chemo Radiotherapy for Esophageal Cancer: Reducing Target Volumes to Deliver Higher Radiotherapy Doses. *Acta Oncol* (2015) 54(6):909–15. doi: 10.3109/0284186X.2014.973062
24. Boekhoff MR, Defize IL, Borggreve AS, Takahashi N, van Lier ALHMW, Ruurda JP, et al. 3-Dimensional Target Coverage Assessment for MRI Guided Esophageal Cancer Radiotherapy. *Radiother Oncol* (2020) 147:1–7. doi: 10.1016/j.radonc.2020.03.007
25. Heijmen L, ter Voert EE, Oyen WJ, Punt CJ, van Spronsen DJ, Heerschap A, et al. Multimodality Imaging to Predict Response to Systemic Treatment in Patients With Advanced Colorectal Cancer. *PloS One* (2015) 10(4):e0120823. doi: 10.1371/journal.pone.0120823
26. Weber MA, Bender K, von Gall CC, Stange A, Grünberg K, Ott K, et al. Assessment of Diffusion-Weighted MRI and 18F-Fluoro-Deoxyglucose PET/CT in Monitoring Early Response to Neoadjuvant Chemotherapy in Adenocarcinoma of the Esophagogastric Junction. *J Gastrointestin Liver Dis* (2013) 22(1):45–52.
27. Shimizu D, Yuasa N, Miyake H, Takeuchi E, Miyata K, Itoh S. Clinical Significance of SUVmax on Preoperative 18F-fluorodeoxyglucose Positron Emission Tomography in Patients Who Underwent R0-Esophagectomy for Esophageal Cancer. *Nagoya J Med Sci* (2018) 80(3):401–9. doi: 10.18999/nagjms.80.3.401
28. Unterrainer M, Eze C, Ilhan H, Marschner S, Roengvoraphoj O, Schmidt-Hegemann NS, et al. Recent Advances of PET Imaging in Clinical Radiation Oncology. *Rad Oncol* (2020) 15(1):88. doi: 10.1186/s13014-020-01519-1
29. Aerts HJ, van Baardwijk AA, Petit SF, Offermann C, Loon Jv, Houben R, et al. Identification of Residual Metabolic-Active Areas Within Individual NSCLC Tumours Using a Pre-Radiotherapy (18)Fluorodeoxyglucose-PET-CT Scan. *Radiother Oncol* (2009) 91(3):386–92. doi: 10.1016/j.radonc.2009.03.006
30. Varoquaux A, Rager O, Lovblad KO, Masterson K, Dulguerov P, Ratib O, et al. Functional Imaging of Head and Neck Squamous Cell Carcinoma With Diffusion-Weighted MRI and FDG PET/CT: Quantitative Analysis of ADC and SUV. *Eur J Nucl Med Mol Imaging* (2013) 40(6):842–52. doi: 10.1007/s00259-013-2351-9
31. Goense L, Heethuis SE, van Rossum PSN, Voncken FEM, Lagendijk JJW, Lam MGEH, et al. Correlation Between Functional Imaging Markers Derived From Diffusion-Weighted MRI and 18F-FDG PET/CT in Esophageal Cancer. *Nucl Med Commun* (2018) 39(1):60–7. doi: 10.1097/MNM.0000000000000771
32. de Jong A, Kwee TC, de Klerk JM, Adam JA, de Keizer B, Fijnheer R, et al. Relationship Between Pretreatment FDG-PET and Diffusion-Weighted MRI Biomarkers in Diffuse Large B-Cell Lymphoma. *Am J Nucl Med Mol Imaging* (2014) 4(3):231–8.
33. Qu YH, Long N, Ran C, Sun J. The Correlation of ^{18}F-FDG PET/CT Metabolic Parameters, Clinicopathological Factors, and Prognosis in Breast Cancer. *Clin Transl Oncol* (2021) 23(3):620–7. doi: 10.1007/s12094-020-02457-w
34. Popp I, Bott S, Mix M, Oehlke O, Schimek-Jasch T, Nieder C, et al. Diffusion-Weighted MRI and ADC Versus FET-PET and GdT1w-MRI for Gross Tumor Volume (GTV) Delineation in Re-Irradiation of Recurrent Glioblastoma. *Radiother Oncol* (2019) 130:121–31. doi: 10.1016/j.radonc.2018.08.019
35. Houweling AC, Wolf AL, Vogel WV, Hamming-Vrieze O, van Vliet-Vroegindeweij C, van de Kamer JB, et al. FDG-PET and Diffusion-Weighted MRI in Head-and-Neck Cancer Patients: Implications for Dose Painting. *Radiother Oncol* (2013) 106(2):250–4. doi: 10.1016/j.radonc.2013.01.003
36. Min LA, Vacher YJL, Dewit L, Donker M, Sofia C, van Triest B, et al. Gross Tumour Volume Delineation in Anal Cancer on T2-Weighted and Diffusion-Weighted MRI - Reproducibility Between Radiologists and Radiation Oncologists and Impact of Reader Experience Level and DWI Image Quality. *Radiother Oncol* (2020) 150:81–8. doi: 10.1016/j.radonc.2020.06.01
37. Weygand J, Fuller CD, Ibbott GS, Mohamed AS, Ding Y, Yang J, et al. Spatial Precision in Magnetic Resonance Imaging-Guided Radiation Therapy: The Role of Geometric Distortion. *Int J Radiat Oncol Biol Phys* (2016) 95(4):1304–16. doi: 10.1016/j.ijrobp.2016.02.059

Conflict of Interest: The authors declare that the research was conducted in the absence of any commercial or financial relationships that could be construed as a potential conflict of interest.

Publisher's Note: All claims expressed in this article are solely those of the authors and do not necessarily represent those of their affiliated organizations, or those of the publisher, the editors and the reviewers. Any product that may be evaluated in this article, or claim that may be made by its manufacturer, is not guaranteed or endorsed by the publisher.

frontiers in Oncology

ORIGINAL RESEARCH
published: 09 March 2022
doi: 10.3389/fonc.2022.842402

Stereotactic MR-Guided Radiotherapy for Pancreatic Tumors: Dosimetric Benefit of Adaptation and First Clinical Results in a Prospective Registry Study

*Morgan Michalet[1], Karl Bordeau[1], Marie Cantaloube[1], Simon Valdenaire[1], Pierre Debuire[1], Sebastien Simeon[1], Fabienne Portales[2], Roxana Draghici[1], Marc Ychou[2], Eric Assenat[3], Marie Dupuy[3], Sophie Gourgou[4], Pierre-Emmanuel Colombo[5], Sebastien Carrere[5], François-Regis Souche[6], Norbert Aillères[1], Pascal Fenoglietto[1], David Azria[1] and Olivier Riou[1]**

[1] University Federation of Radiation Oncology of Mediterranean Occitanie, Montpellier Cancer Institute (ICM), Univ Montpellier, INSERM U1194 Institut de Recherche en Cancérologie de Montpellier (IRCM), Montpellier, France, [2] Medical Oncology Department, Institut du Cancer de Montpellier (ICM), Montpellier Cancer Institute, Univ Montpellier, Montpellier, France, [3] Medical Oncology Department, Centre Hospitalier Universitaire (CHU) St Eloi, Montpellier, France, [4] Biometrics Unit Institut du Cancer de Montpellier (ICM), Montpellier Cancer Institute, Univ Montpellier, Montpellier, France, [5] Digestive Surgery Department, Institut du Cancer de Montpellier (ICM), Montpellier Cancer Institute, Univ Montpellier, Montpellier, France, [6] Surgical Department, Centre Hospitalier Universitaire (CHU) St Eloi, Montpellier, France

OPEN ACCESS

Edited by:
Enis Ozyar,
Acıbadem University, Turkey

Reviewed by:
Raphael Pfeffer,
Assuta Medical Center, Israel
Brígida Ferreira,
University of Lisbon, Portugal
Anna Bruynzeel,
VU Medical Center, Netherlands

***Correspondence:**
Olivier Riou
olivier.riou@icm.unicancer.fr

Specialty section:
This article was submitted to Radiation Oncology, a section of the journal Frontiers in Oncology

Received: 23 December 2021
Accepted: 31 January 2022
Published: 09 March 2022

Citation:
Michalet M, Bordeau K, Cantaloube M, Valdenaire S, Debuire P, Simeon S, Portales F, Draghici R, Ychou M, Assenat E, Dupuy M, Gourgou S, Colombo P-E, Carrere S, Souche F-R, Aillères N, Fenoglietto P, Azria D and Riou O (2022) Stereotactic MR-Guided Radiotherapy for Pancreatic Tumors: Dosimetric Benefit of Adaptation and First Clinical Results in a Prospective Registry Study. Front. Oncol. 12:842402. doi: 10.3389/fonc.2022.842402

Introduction: Stereotactic MR-guided adaptive radiotherapy (SMART) is an attractive modality of radiotherapy for pancreatic tumors. The objectives of this prospective registry study were to report the dosimetric benefits of daily adaptation of SMART and the first clinical results in pancreatic tumors.

Materials and Methods: All patients treated in our center with SMART for a pancreatic tumor were included. Patients were planned for five daily-adapted fractions on consecutive days. Endpoints were acute toxicities, late toxicities, impact of adaptive treatment on target volume coverage and organs at risk (OAR) sparing, local control (LC) rate, distant metastasis-free survival (DMFS), and overall survival (OS).

Results: Thirty consecutive patients were included between October 2019 and April 2021. The median dose prescription was 50 Gy. No patient presented grade > 2 acute toxicities. The most frequent grade 1–2 toxicities were asthenia (40%), abdominal pain (40%), and nausea (43%). Daily adaptation significantly improved planning target volume (PTV) and gross tumor volume (GTV) coverage and OAR sparing. With a median follow-up of 9.7 months, the median OS, 6-month OS, and 1-year OS were 14.1 months, 89% (95% CI: 70%–96%), and 75% (95% CI: 51%–88%), respectively, from SMART completion. LC at 6 months and 1 year was respectively 97% (95% CI: 79–99.5%) and 86% (95% CI: 61%–95%). There were no grade > 2 late toxicities. With a median follow-up of 10.64 months, locally advanced pancreatic cancer (LAPC) and borderline resectable pancreatic cancer (BRPC) patients (22 patients) had a median OS, 6-month OS, and 1-year OS from

SMART completion of 14.1 months, 76% (95% CI: 51%–89%), and 70% (95% CI: 45%–85%), respectively. Nine patients underwent surgical resection (42.1% of patients with initial LAPC and 33.3% of patients with BRPC), with negative margins (R0). Resected patients had a significantly better OS as compared to unresected patients (p = 0.0219, hazard ratio (HR) = 5.78 (95% CI: 1.29–25.9)).

Conclusion: SMART for pancreatic tumors is feasible without limiting toxicities. Daily adaptation demonstrated a benefit for tumor coverage and OAR sparing. The severity of observed acute and late toxicities was low. OS and LC rates were promising. SMART achieved a high secondary resection rate in LAPC patients. Surgery after SMART seemed to be feasible and might increase OS in these patients.

Keywords: stereotactic MR-guided adaptive radiotherapy, stereotactic body radiation therapy, pancreatic cancer, pancreatic tumors, locally advanced pancreatic cancer, borderline resectable pancreatic cancers, adaptive radiotherapy, image guided radiotherapy (IGRT)

INTRODUCTION

Pancreatic adenocarcinoma (PA) is the 10th cause of cancer in Europe and the United States and the 4th cause of cancer mortality. The 5-year overall survival (OS) is 9% for all stages, mainly due to a frequent metastatic spread (1). Surgical resection is the only curative modality, but only 10% of these cancers are resectable at diagnosis. On the other hand, 30% are considered unresectable or locally advanced (2). In locally advanced pancreatic cancer (LAPC), chemoradiotherapy is a frequent option after induction chemotherapy, since the phase III trial GERCOR LAP 07 demonstrated a benefit in terms of local control (LC) and delayed chemotherapy reintroduction as compared to chemotherapy (gemcitabine) alone, despite no advantage in terms of OS (3). These results were later confirmed by other studies on chemoradiotherapy, as suggested by a meta-analysis (4).

Stereotactic body radiotherapy (SBRT) is an attractive modality of radiotherapy in this indication for three main reasons: 1) possibility to deliver higher biologically equivalent doses (BED) in these radioresistant tumors, 2) modality allowing better organ at risk (OAR) sparing, and 3) decreased number of fractions in these patients with limited life expectancy with consequential improved quality of life. Recent data suggest an excellent LC with this treatment modality (5, 6), but the proximity of OARs limits the use of this technique.

Stereotactic MR-guided adaptive radiotherapy (SMART) is a technique combining X-ray beam delivery, daily adaptive treatment planning, and gating/tracking possibility through continuous cine-MR images (7, 8). MRIdian Linac® is a radiotherapy device developed by ViewRay, coupling a 0.35-tesla MR-imaging system with a multileaf collimator-equipped linear accelerator (9). It is particularly adapted to pancreatic SBRT, improving the delineation accuracy thanks to better soft tissue MR contrast as compared to CT scan, sparing OARs by adaptation of treatment to the daily anatomy, and tracking the target with cine-MRI during irradiation. A retrospective study suggested an increase of OS with dose-escalated SMART in unresectable pancreatic cancers (10).

The objective of this study was to report the dosimetric benefits of daily adaptation of SMART and the first clinical results in pancreatic tumors.

METHODS AND MATERIALS

Patient Selection

All patients treated with SMART for a pancreatic tumor at the Montpellier Cancer Institute from October 2019 to April 2021 were included.

Patients with non-metastatic unresectable pancreatic adenocarcinoma were first treated with induction chemotherapy and had stable or responsive disease. Metastatic pancreatic adenocarcinoma patients could be included in the study in case of metastatic complete or near-complete response to chemotherapy with a residual primary tumor. Primary tumors other than adenocarcinoma and metastatic lesions to the pancreas from other primaries could be included in the study. The indication of SMART had to be validated in a multidisciplinary tumor board. Histological confirmation was required. Other inclusion criteria were Eastern Cooperative Oncology Group (ECOG) performance status = 0 or 1, no previous abdominal radiotherapy, no MRI contraindication (presence of non-MRI compatible implanted cardiac devices, claustrophobia, psychiatric disorders, and metal objects), and no duodenal invasion on endoscopy.

This study was registered in the Health Data Hub (registration number: #1802) and was approved by our local research committee (2020/01). All patients signed an informed consent form before treatment.

Simulation

All patients underwent CT simulation directly followed by 0.35-T MRI simulation using the MRIdian® apparatus to ensure reproducibility of the anatomic configuration. MR and CT images were rigidly registered for target volume delineation, while only the MR images were used for OAR delineation. A 1.5-T MRI simulation in our radiology department was also required to allow better tumor visualization and improve gross

tumor volume (GTV) delineation after registration with MRIdian® images. Patients in all simulation exams were injected with contrast agents unless contraindication. Patients were asked to fast for at least 3 to 4 h prior to all simulation exams (and every fraction). Patients were in a supine position with arms down at their sides, and immobilization was obtained with a Totim® device. Furthermore, for dose calculation, CT to MR image registration was performed using an elastic registration algorithm. During the CT simulation, MRI dummy surface coils with similar electron attenuation properties to real MRI coils were placed on the custom immobilization device. MR images were acquired with true fast imaging with steady-state free precession (TRUFISP) sequences (T1/T2 weighted, breath-hold technique (physiologic end-expiration), 17 to 25 s, 1.6 × 1.6 × 3 mm or 1.5 × 1.5 × 3 mm resolution, 45 × 45 × 24 to 54 × 47 × 43 maximum field of view).

Breath-Hold Procedure

All patients were simulated and treated with a breath-hold technique. All the patients benefited after the first medical consultation from a respiratory coaching session by a radiotherapy nurse. They received a document explaining the respiratory breath-hold procedure and the terms that were going to be used during simulation and treatment. Patients were asked to perform respiratory breath-hold exercises at home. Another respiratory coaching session was performed directly before the first simulation. Breath-hold was achieved by voice guidance by the radiotherapy technicians at simulation and treatment. No abdominal compression was used. No specific visual coaching system was used. The quality and reproducibility of breath-hold were checked by continuous cine-MR guidance during simulation and treatment. Breath-hold was performed in physiologic end-expiration.

Treatment Planning

The tumoral GTV (GTV T) was delineated using the data from CT and MRI. Suspect regional lymph nodes were also delineated if required (nodal GTV (GTV N)). An isotropic margin of 3 mm was used for the planning target volume (PTV) extension. OAR was delineated on MRIdian® simulation images. OAR dose constraints are listed in **Table 1**. Priority was given to OAR dose constraints. An optimization structure (PTV optimized or PTVopt) was created as follows: PTVopt = PTV − (digestive OAR + 5 mm). The median prescribed dose was 50 Gy (range 30–50) in 5 consecutive fractions. Actually, only one patient had a prescription of 30 Gy, two patients had a prescription of 35 Gy, 3 patients had a prescription of 40 Gy, and 24 patients had a prescription of 50 Gy. The reason for a different level of dose prescription is related to the characteristics of the patients and the tumors treated. Indeed, our reference dose level was 50 Gy in 5 fractions. However, we delivered lower dose levels for 3 patients who did not have pancreatic adenocarcinoma. One patient with a primary pancreatic neuroendocrine tumor with a single liver metastasis was treated with 30 Gy in 5 fractions because of the tumor size and metastatic status. Two patients with oligometastatic renal clear cell carcinoma were treated with 35 Gy and 40 Gy in 5 fractions due to the oligometastatic status outside the pancreas. One patient with metastatic pancreatic adenocarcinoma was treated with 35 Gy in 5 fractions. Finally, two patients with borderline resectable pancreatic cancer (BRPC) in whom pancreatic surgery was considered after SMART received 40 Gy in 5 fractions. In the end, only one of these two patients underwent surgery. Treatment planning was done using the ViewRay® Treatment Planning System (TPS), using a Monte Carlo algorithm, with normalization on D50 (100% of the prescribed dose covers 50% of the target volume), trying to ensure 95% PTVopt coverage within the 95% isodose and 99% GTV coverage with the 95% isodose. Treatment was delivered using step-and-shoot intensity-modulated radiation therapy (IMRT) with 6-MV photons and approximately 15–20 beams and 70–90 segments. No concomitant chemotherapy was administered during radiotherapy.

TABLE 1 | Organ at risk dose constraints.

Organ	Dose constraints (5 fractions)
Esophagus	Dmax < 35 Gy $V_{19.5Gy}$ < 5 cm^3
Stomach	Dmax < 32 Gy V_{18Gy} < 10 cm^3
Duodenum	Dmax < 32 Gy V_{18Gy} < 5 cm^3
Small intestine	Dmax < 32 Gy $V_{19.5Gy}$ < 5 cm^3
Large intestine	Dmax < 32 Gy V_{25Gy} < 5 cm^3
Liver	$V_{< 15Gy}$ > 700 cm^3
Kidneys	$V_{< 17.5Gy}$ > 200 cm^3 V_{18Gy} < 33% $V_{< 14.5Gy}$ > 130 cm^3 (if single kidney)
Spinal cord	Dmax < 25 Gy
Heart	Dmax < 30 Gy V_{24Gy} < 15 cm^3

Daily Adaptive Treatment Workflow

After daily TRUFISP image acquisition, patients were positioned to the pancreatic area. After rigid registration of the GTV, OAR contours were propagated on the daily MR image using deformable image registration. OAR contours not considered optimal were modified by the physician (especially digestive OAR contours). The initial plan was then evaluated by the physician and the physicist. If all dose constraints were met, no adaptation was required (non-adapted fractions). If a decrease in tumor coverage and/or unacceptable OAR dose constraints were observed, the initial plan was optimized on the integrated TPS (adapted fractions). The electron density map (transferred from the CT to MR images) and the skin contour were checked to ensure correct dose recalculation (11). Quality assurance of the newly optimized plan was performed by recalculating the plan with a secondary Monte Carlo algorithm before irradiation. Tracking was ensured by following a structure with good spontaneous contrast on MRIdian acquisition (usually the GTV itself) on sagittal images obtained by cine-MR. The beam was turned off when more than 5% of the tracked structure was outside the threshold of 3 mm from its initial position.

Clinical Assessment, Dosimetric Evaluation, and Endpoints

The primary endpoint was acute toxicities. Secondary endpoints were late toxicities; the impact of the adaptive treatment on the

target volume coverage and OAR sparing; the LC rate defined by the Response Evaluation Criteria in Solid Tumors (RECIST) criteria including local complete response (CR), local partial response (PR), and local stable disease (SD); the distant metastasis-free survival (DMFS) based on clinical, radiological, and biological assessment; and OS.

Follow-up started on the first day of SMART treatment until the death or latest news for each patient. Acute toxicities were defined as toxicities occurring during treatment until 3 months posttreatment. Late toxicities were defined as toxicities occurring after 3 months posttreatment.

All patients were assessed after treatment at 1 month and then every 3 months. The assessment consisted of clinical, radiological (CT scan, MRI, or PET scan), and biological (including tumoral markers carcinoembryonic antigen (CEA) and CA 19.9) evaluations at each visit. All toxicity events were reported according to the Common Terminology Criteria for Adverse Events (CTCAE) v5.0 at each clinical examination.

For each adapted fraction delivery, the predicted plan (initial plan on the daily image) and the delivered plan (new plan on the daily image) were compared *a posteriori* with the initial plan. PTV and GTV coverage (D2%, D95%, D98%, V100%, V95%, and V90%) values as well as OAR maximum dose and volumetric doses were recorded.

Statistical Analysis

For survival analysis, median follow-up was estimated using the Kaplan–Meier method. OS was defined as the time between the end of chemotherapy or SMART and death by any cause. Alive patients were censured at the date of the last follow-up. Progression-free survival (PFS) was defined as the time between the end of chemotherapy or SMART and local relapse, metastatic relapse, or death by any cause. DMFS was defined as the time between the end of chemotherapy or SMART and distant relapse or death by any cause. LC was defined as the absence of progression of the primary pancreatic tumor. A subgroup analysis of each of these parameters was realized for LAPC and BRPC and, among those, between resected and non-resected patients. Comparison of the survival curves between the resected patients and the non-resected patients was performed by the log-rank (Mantel–Cox) test with hazard ratio (HR) (Mantel–Haenszel) calculation.

For each adapted fraction delivery, the predicted plan (initial plan on the daily image) and the delivered plan (new plan on the daily image) were compared *a posteriori* by a paired Wilcoxon test. PTV and GTV coverage values as well as OAR maximum doses and volumetric doses were recorded. Statistical analyses were performed using Stata v16.0, RStudio, and GraphPad PRISM v9.

RESULTS

Patient and Treatment Characteristics

Between October 2019 and April 2021, thirty consecutive patients treated with SMART for an unresectable pancreatic tumor were included in our prospective registry study. Median follow-up was 9.7 months (95% CI: 5.85–11.86) for the whole cohort and 10.64 months (95% CI: 5.85–11.86) for pancreatic adenocarcinoma patients. Patient and treatment characteristics are described in **Table 2**. The median age was 64.5 years (range 44–85). The proportion of men and women was well balanced. Borderline or locally advanced pancreatic adenocarcinomas represented 22 patients (77%). There were also 1 patient (3%) with resectable pancreatic adenocarcinoma but unfit for surgery, 3 patients (10%) with oligometastatic disease from pancreatic adenocarcinoma, 1 patient (3%) with pancreatic neuroendocrine tumor, and 2 patients (6%) with pancreatic metastasis from kidney tumors. Twenty-eight patients (94%) received chemotherapy before radiotherapy, mainly induction FOLFIRINOX regimen (73%) with a median of eight cycles (range 4–14). Four of these patients had to switch for FOLFOX, FOLFIRI, GEMCITABINE alone, or GEMCITABINE-ABRAXANE protocol because of tolerance issues. Serum CA

TABLE 2 | Baseline characteristics.

Sex	
Women	15 (50%)
Men	15 (50%)
Median age (range)	64.5 years (44–85)
Pathology	
Pancreatic adenocarcinoma (PA)	27 (90%)
Pancreatic neuroendocrine tumor	1 (3.33%)
Metastasis from kidney tumor	2 (6.67%)
Stage among PA	
Resectable	1 (3.33%)
Borderline	3 (10%)
Locally advanced	19 (63.33%)
Local relapse	1 (3.33%)
Metastatic	3 (10%)
Previous treatment	
Chemotherapy	28 (93.33%)
Pancreatic surgery	3 (10%)
CAR-T cells	1 (3.33%)
None	1 (3.33%)
ECOG score	
0	11 (36.67%)
1	17 (56.67%)
2	2 (6.67%)
3	0 (0%)
Chemotherapy regimen for PA	
FOLFIRINOX	22 (73.33%)
GEMCITABINE-ABRAXANE	2 (6.67%)
FOLFOX	4 (13.33%)
GEMCITABINE	2 (6.67%)
FOLFIRI	1 (3.33%)
Several protocols*	4 (13.33%)
Localization	
Head	16 (57.17%)
Body/tail	12 (42.86%)
Unknown	2
Lymph node involvement°	
Yes	7 (23.33%)
No	23 (76.67%)
Median CA 19.9 at diagnosis (range)	321 UI/ml (6–1,884)
Median CA 19.9 before SMART (range)	108 UI/ml (6–802)
Average size of pancreatic tumor (range)	31.5 mm (16–53)

ECOG, Eastern Cooperative Oncology Group; SMART, stereotactic MR-guided adaptive radiotherapy.
**Because of tolerance issues with FOLFIRINOX.*
°On CT/MRI/PET.

19.9 was initially available for 25 (83%) patients. The median value of serum CA 19.9 decreased from 321 (range, 6–1884) to 108 UI/ml (range, 6–802) between diagnosis and the start of SMART. Based on MRI or CT findings at diagnosis, 77% of patients were without nodal invasion. The average size of a pancreatic tumor before SMART was 31.5 mm (range 16–53). The tumor was mainly localized in the pancreas head (57%).

Initial Treatment Plans

All patients underwent five daily consecutive fractions. The prescribed dose was 50 Gy for 24 patients, 40 Gy for 3 patients, 35 Gy for 2 patient, and 30 Gy for one patient. The median fraction duration was 86 min (range 64–133). The median PTV was 67.4 cm^3 (range 6.9–138.7). **Table 3** presents the dosimetric data of initial plans.

Dosimetric Benefits of Adaptive Method

All fractions (150) were adapted because of a dosimetric benefit obtained either on PTV coverage or on OAR protection. Adaptation was performed because of stomach, duodenum, or jejunum Dmax violation on predicted plans, as follows:

- 2 out of 5 fractions (40%) for a prescription dose of 30 Gy
- 7 out of 10 fractions (70%) for a prescription dose of 35 Gy
- 15 out of 15 fractions (100%) for a prescription dose of 40 Gy
- 110 out of 120 fractions (91.67%) for a prescription dose of 50 Gy

The remaining fractions were adapted to improve target volume coverage.

The mean treatment duration of adapted fractions was 90 min, including patient preparation, positioning, image acquisition, image registration, OAR recontouring, plan adaptation, and treatment delivery. Average dosimetric data and comparison between predicted and adapted plans are available in **Table 4**. PTV coverage was significantly improved for adapted plans compared to predicted plans (mean PTV V95% increase of 2.2%, $p < 0.01$), as was the PTV optimized coverage (mean PTV V95% increase of 4.3%, $p < 0.01$). The adaptation of the plan also significantly improved dosimetric measures for OAR, except for the kidneys. **Figure 1** shows an example of the benefit of adaptation on PTV coverage for a given fraction. **Figure 2** shows a dosimetric comparison between predicted and adapted plans for target volumes coverage (GTV V100%, PTVopt V100%, and PTVopt V95%) (**Figure 2A**) and for OAR sparing (Dmax to the stomach, duodenum, and jejunum) (**Figure 2B**). The benefit of adaptive plans vs. predicted plans on target volumes is less obvious than on OARs because PTV coverage values on predicted plans are often in parallel with unacceptable OAR values (unacceptable plans that cannot be delivered to patients).

Toxicities

No patients presented grade > 2 acute toxicities, and 13 patients presented grade 1–2 acute toxicities (asthenia (grade 1: 40%), abdominal pain (grade 1: 40%), nausea/vomiting (grade 1: 23.3%, grade 2: 20%), and diarrhea (grade 1: 23.3%, grade 2: 3.3%).

TABLE 3 | Median (min–max) dosimetric data for initial plans.

Total dose (Gy)	50 (24 patients) 40 (3 patients) 35 (2 patient) 30 (1 patient)
Total treatment duration (days)	6 (5 – 14)
Fraction dose (Gy)	10 (6 – 10)
Median PTV (cm^3)	68.6 (6.9 – 138.7)
Fraction duration (min)	89.8 (64 – 133)
PTVopt	
V100% (%)	58.1 (40.5 – 83.1)
V95% (%)	90.6 (68.9 – 99.9)
V80% (%)	99.6 (92.9 – 100)
D98% (Gy)	41.9 (28.5 – 47.8)
D95% (Gy)	44.6 (29.1 – 48.6)
D2% (Gy)	53 (32.2 – 55.2)
PTV	
V100% (%)	50 (33.8 – 78.5)
V95% (%)	78.9 (57.5 – 98.5)
V80% (%)	90.9 (72.7 – 99.9)
D98% (Gy)	23.5 (12.6 – 84.4)
D95% (Gy)	29.3 (15.2 – 48.6)
D2% (Gy)	53 (32.1 – 55.1)
GTV	
V100% (%)	61.7 (40.5 – 93.3)
V95% (%)	89.8 (65.1 – 100)
V80% (%)	96.1 (77.9 – 100)
D98% (Gy)	32.9 (17.8 – 49.2)
D95% (Gy)	38.6 (22.3 – 49.6)
D2% (Gy)	53 (32.3 – 55.9)
Kidney	
V_{18Gy} (cm^3)	2.5 (0 – 16.6)
Spinal cord	
Dmax (Gy)	18 (7.61 – 22.9)
Stomach	
Dmax (Gy)	29.5 (0.9 – 32.8)
V_{18Gy} (cm^3)	9.8 (0 – 30.5)
Duodenum	
Dmax (Gy)	29.4 (20.4 – 33.4)
V_{18Gy} (cm^3)	4.2 (0.9 – 11.4)
Small intestine	
Dmax (Gy)	27.6 (2.8 – 34)
$V_{19.5Gy}$ (cm^3)	3.1 (0 – 9.1)
Large intestine	
Dmax (Gy)	27.8 (5.9 – 32.9)
V_{25Gy} (cm^3)	1.8 (0 – 2.5)

PTV, planning target volume; GTV, gross tumor volume; PTVopt, PTV optimized.

After surgery, one patient presented a digestive fistula, and another one presented an abdominal aneurism, highly suggestive of immediate postoperative complications from head pancreatic surgery consecutive to the anastomosis and vascular reconstruction problems. Both underwent additional surgical procedures with complete resolution afterwards.

With a median follow-up of 9.7 months for the whole cohort (95% CI: 5.85–11.86), no grade > 2 late toxicities were observed. Toxicities between resected and non-resected patients were not significantly different. More details are available in **Table 5**.

Survival Analysis

Whole Cohort

The median OS was 14.1 months. The 6-month OS from SMART completion was 89% (95% CI: 70%–96%). The 1-year

TABLE 4 | Average target volume and OAR dosimetric results for predicted and adapted plans.

Target volume / OAR	Predicted plan [standard deviation]	Adapted plan [standard deviation]	p-Value
PTVopt			
V100%	53.7% [14.5%]	60.2% [14.4%]	**<0.01**
V95%	84% [9.1%]	88.3% [9.4%]	**<0.01**
V80%	95.4% [4.8%]	98.4% [2.2%]	**<0.01**
D98%	34.7 Gy [7.3 Gy]	40.1 Gy [5 Gy]	**<0.01**
D95%	38.9 Gy [6.4 Gy]	42.3 Gy [4.9 Gy]	**<0.01**
D2%	50.7 Gy [6.3 Gy]	50.6 Gy [6 Gy]	0.31
PTV			
V100%	47% [12.6%]	51.7% [13%]	**<0.01**
V95%	74.4% [10.6%]	76.6% [12%]	**<0.01**
V80%	87.9% [8.1%]	88.6% [8.2%]	0.22
D98%	25.4 Gy [8.5 Gy]	26.2 Gy [9.8 Gy]	0.5
D95%	30.4 Gy [8.8 Gy]	31.4 Gy [10.1 Gy]	0.35
D2%	50.7 Gy [6.3 Gy]	50.3 Gy [6.5 Gy]	0.2
GTV			
V100%	60% [15.9%]	65.1% [14.3%]	**<0.01**
V95%	85.9% [9.9%]	86.8% [10.4%]	0.15
V80%	93.7% [6.4%]	93.8% [6.8%]	0.72
D98%	32.7 Gy [8.9 Gy]	33 Gy [10.9 Gy]	0.93
D95%	37.2 Gy [8.4 Gy]	37.4 Gy [9.9 Gy]	0.65
D2%	50.9 Gy [6.3 Gy]	50.8 Gy [6 Gy]	0.60
Kidney			
V_{18Gy}	4.2 cm^3 [4.6%]	4.7 cm^3 [5.1%]	**<0.01**
Spinal cord			
Dmax	17.2 Gy [3.7 Gy]	17.5 Gy [3.2 Gy]	0.25
Stomach			
V_{18Gy}	15.2 cm^3 [11.2 cm^3]	12.1 cm^3 [8.8 cm^3]	**<0.01**
Dmax	35.2 Gy [11.8 Gy]	27.2 Gy [6.6 Gy]	**<0.01**
Duodenum			
V_{18Gy}	6.6 cm^3 [5.7 cm^3]	4.5 cm^3 [3 cm^3]	**<0.01**
Dmax	35.4 Gy [10.1 Gy]	28.1 Gy [3.52 Gy]	**<0.01**
Small intestine			
$V_{19.5Gy}$	3.8 cm^3 [5.1 cm^3]	2.4 cm^3 [2.7 cm^3]	**<0.01**
Dmax	29.5 Gy [10.9 Gy]	25 Gy [6.2 Gy]	**<0.01**
Large intestine			
V_{25Gy}	1 cm^3 [1.9 cm^3]	0.4 cm^3 [0.8 cm^3]	**<0.01**
Dmax	24.7 Gy [10.3 Gy]	23.1 Gy [7.3 Gy]	**<0.01**

OAR, organ at risk; PTV, planning target volume; GTV, gross tumor volume; PTVopt, PTV optimized.
Bold values are statistically significant differences (p< 0.05).

OS from SMART completion was 75% (95% CI: 51%–88%) (**Figure 3A**).

LC at 6 months and 1 year was respectively 97% (95% CI: 79–99.5%) and 86% (95% CI: 61%–95%) (**Figure 3B**). Among 3 local relapses (10%), 2 were located on the field edge and 1 inside the field.

Locally Advanced Pancreatic Cancer and Borderline Resectable Pancreatic Cancer Patients

LAPC and BRPC patients had a median follow-up of 10.64 months (95% CI: 5.85–11.86) from SMART.

The median OS was 14.1 months. The 6-month OS from SMART completion was 76% (95% CI: 51%–89%). The 1-year OS from SMART completion was 70% (95% CI: 45%–85%) (**Figure 4A**). The median DMFS from SMART completion was 10.5 months. The 6-month DMFS from SMART completion was 73% (95% CI: 49%–87%). The 1-year DMFS from SMART completion was 34% (95% CI: 11%–58%) (**Figure 4B**).

The median OS and 1-year OS from initiation of induction chemotherapy were 19.1 months and 91% (95% CI: (68%–98%), respectively (**Figure 4C**).

The median DMFS and 1-year DMFS from initiation of induction chemotherapy were 16.3 months and 72% (95% CI: 49%–87%), respectively (**Figure 4D**).

The median serum CA 19.9 initially decreased with a nadir at 6 months (70 UI/ml range, 1.1–692) and increased at 1 year (147 UI/ml range, 9–792).

Primary adenocarcinoma patients considered with a responsive disease (CA 19.9 decrease and radiological assessment classified as stable, or in response according to RECIST 1.1 classification) and clinically fit were proposed for pancreatic surgery. For the selected patient, after agreement of the multidisciplinary staff, including trained surgeons, duodeno-pancreatectomy or spleno-pancreatectomy was realized, depending on initial tumor location. Consequently, nine patients (8 out of 19 patients (42.1%) with initial LAPC and one out of 3 patients (33.3%) with BRPC) were resected. Histologically, the average pathologic therapeutic effect was evaluated at 64% (range 10%–95%), mainly classified ypT2N0 (56%). There was no CR. All patients underwent complete surgery with negative margins (R0). Among them, 3 patients had a metastatic relapse, and one of them had also a local relapse on the field boundary. To date, all resected patients are still alive. Resected patients had a significantly better OS as compared to unresected patients (p = 0.0219, HR = 5.78 (95% CI: 1.29–25.9) (**Figure 5A**). DMFS was not significantly different between resected and unresected patients (**Figure 5B**).

DISCUSSION

Management of pancreatic tumors remains a major challenge for surgeons, radiation oncologists, and medical oncologists due to the anatomical location of the pancreas in contact with vascular and digestive structures and because of the poor prognosis of pancreatic adenocarcinoma. Until now, surgical resection is the only curative modality of pancreatic adenocarcinoma, and the publication of adjuvant FOLFIRINOX results for resected patients has dramatically improved OS in this population with a median OS of 54.4 months (12). Unfortunately, only 10% of patients are resectable at diagnosis; 10% are considered borderline resectable and 30% unresectable or locally advanced (2). Unresected patients have a poor prognosis, with median OS of approximately 11 months (13). In a recent study on LAPC, the 3-year OS was 43% in the resected group vs. 6.5% in the unresected group (14). However, the better prognosis of resected patients may also reflect a better response to neoadjuvant treatment, since only good responders will ultimately undergo surgery. Thus, it seems important to try to improve induction treatments in order to increase the therapeutic response and make more patients resectable.

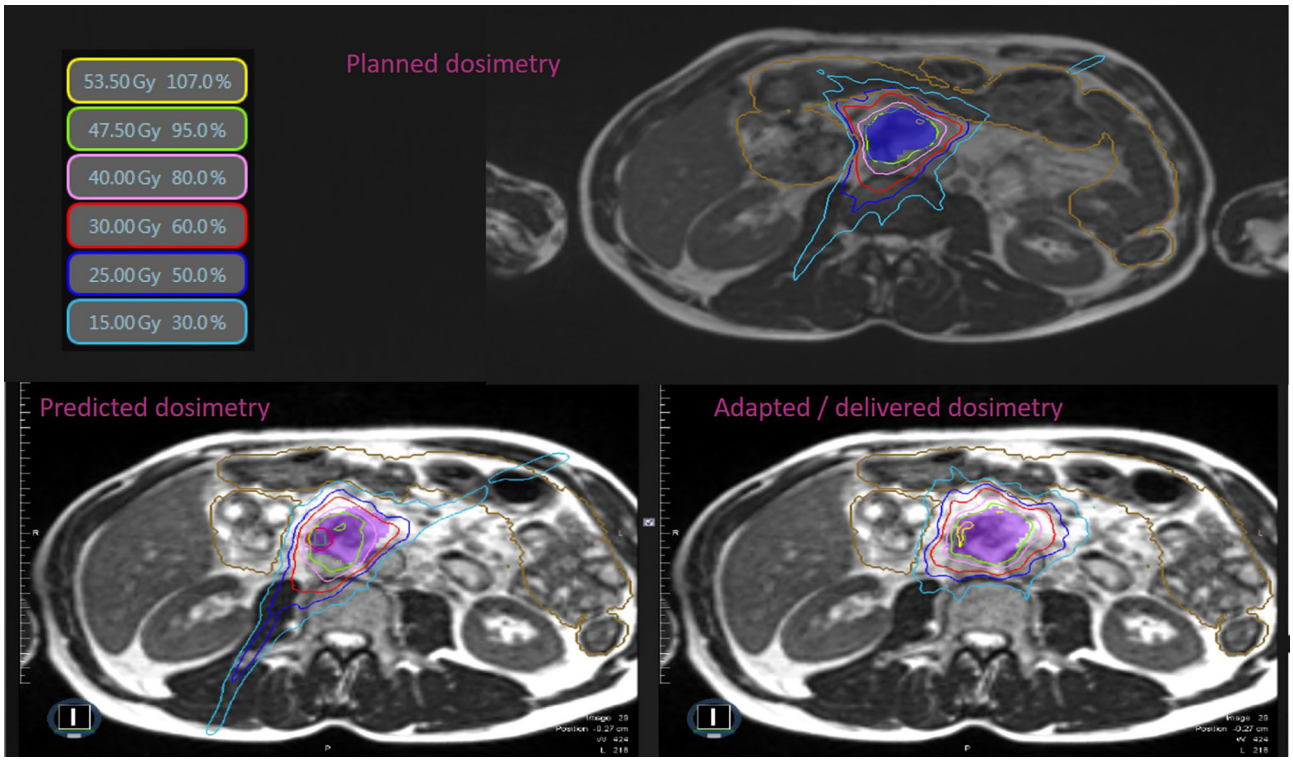

FIGURE 1 | Typical SMART dosimetry showing planned, predicted, and adapted/delivered dosimetry. Comparison of dose distribution between planned, predicted, and adapted/delivered dosimetry on MR 0.35-T TRUFISP images for a prescription of 50 Gy in 5 fractions in LAPC. Isodose line 53.5 Gy in yellow, 47.5 Gy in green, 40 Gy in rose, 30 Gy in red, 25 Gy in blue, and 15 Gy in cyan. Small intestine in brown. LAPC, locally advanced pancreatic cancer; SMART, stereotactic MR-guided adaptive radiotherapy.

Radiotherapy remains a controversial treatment in LAPC since the LAP07 trial failed to prove a survival benefit in patients receiving fractionated radiochemotherapy after induction chemotherapy. Nevertheless, the reference protocols for induction chemotherapy, but especially the available radiotherapy techniques, have evolved considerably as compared to the treatments used in this clinical trial. SBRT uses an advanced technological approach to improve nearby OAR sparing while ensuring a correct coverage of the target volumes. Moreover, this treatment is delivered in a limited number of fractions, which improves the comfort and quality of life of patients. Finally, SBRT appears to be an attractive modality for the treatment of this radioresistant tumor type (15). A recent meta-analysis comparing SBRT and radiochemotherapy with conventional fractionation suggested a benefit in favor of SBRT, with 2-year OS of 26.9% vs. 13.7%. In addition, this study demonstrated also a benefit in terms of tolerance, with 5.6% acute grade 3/4 toxicities versus 37.7%, without differences of late grade 3/4 toxicities (16). Looking individually at the prospective studies evaluating SBRT in LAPC, the prescription dose varied from 15 Gy in 1 fraction to 45 Gy in 6 fractions (17–21). The proximity of digestive organs was the main issue of these studies with the rate of severe (grade > 2) gastrointestinal (GI) toxicities ranging from 5% up to 22%, especially for treatment in one fraction (19, 22–25). All of these trials used Linac or CyberKnife, with no possibility of daily adaptation, probably partially explaining the rate of GI toxicities (5, 6).

For this reason, adaptive radiotherapy seems to be a good solution to improve digestive organs sparing while keeping a high prescription dose, by daily adaptation of dosimetric plan to daily anatomy. With the development of MR-guided radiotherapy, new possibilities are offered for the treatment of LAPC. SMART is a technique allowing high prescription doses by 1) using good soft-tissue contrast of MRI for a precise delineation of target volumes and OAR, 2) using integrated TPS for daily adaptation of dosimetry, and 3) tracking of target volume using continuous cine-MR acquisitions (7, 8, 26).

Two series of SMART for the treatment of LAPC recently reported very encouraging results. The prescribed dose was 40 Gy (one patient), 45 Gy (4 patients), and 50 Gy (30 patients) in 5 fractions in the first study with a median follow-up of 10.3 months from SMART completion (27). In the second study, the prescribed dose was 50 Gy in 5 fractions for all patients with a median follow-up of 16 months from diagnosis and not SMART

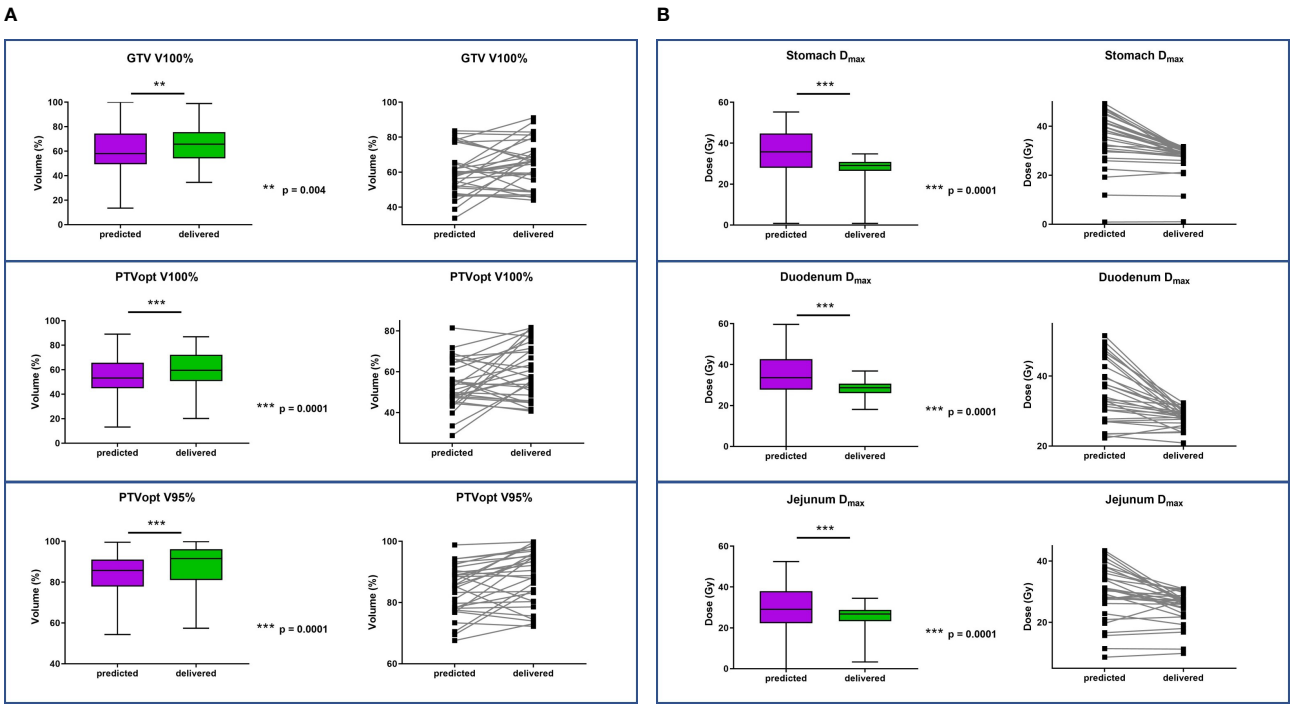

FIGURE 2 | Dosimetric comparison between predicted and adapted plans. **(A)** Target volumes coverage (GTV V100%, PTVopt, V100% and PTVopt V95%). **(B)** OAR sparing (Dmax to stomach, duodenum, and jejunum). The three images on the left part of the figures represent the 150 predicted fractions vs. 150 adapted fractions (5 fractions for 30 patients). Whiskers show minimal to maximal values, and boxes show the mean values with standard deviations. The three images on the right part of the figures represent the variation for each patient (one line represents one patient) from the predicted values (left) to the adapted values (right). In order to limit the number of lines (30 lines) and to make the figure readable, we have calculated and plotted the average values of the 5 predicted plans (left) and the average values of the 5 adapted plans (right). GTV, gross tumor volume; PTVopt, planning target volume optimized; OAR, organ at risk.

completion. The tolerance was excellent with only one (3%) acute grade 3 toxicity and one (3%) late grade 3 toxicity in the first study (27) and no late grade 3 toxicity and only 2 (4.6%) acute grade 3 toxicities in the second one (28). There were no grade > 3 toxicities in both studies. Our results are in accordance with their results, as we did not report any grade > 2 toxicities. The most frequent acute toxicities were asthenia (40%), abdominal pain (40%), and nausea/vomiting (43%), with no need for treatment interruption. Late tolerance was excellent too, with only grade 1 toxicities. Two patients had postoperative complications that resolved and can be considered unrelated to radiotherapy.

The benefits of adaptive treatment have already been demonstrated in other studies using SMART for different clinical indications. In lung tumors, the average gain per fraction for the PTV coverage (V100%) was 4.4% (29). For prostate reirradiation, we showed a benefit of adaptation on PTV coverage, without exceeding doses to OAR (30). In another study of different tumor localizations treated with SMART, 35/61 fractions were adapted because of OAR violation and led to better PTV coverage (7). In our study, we chose to prioritize OAR dose constraints. All patients had a daily adaptive treatment, usually for OAR dose constraints violation. Similarly, our adapted plans showed a significantly better PTV and PTV optimized coverage (an increase of mean PTV V95% of 2.2% and 4.3% respectively, $p < 0.01$). There was also a significant benefit of adaptation on stomach, duodenum, and small and large intestine dose constraints. In our experience, adaptive radiotherapy seems to be compulsory for the treatment of abdominal targets at this dose level (>40 Gy in 5 fractions).

In our study, the median OS calculated from SMART was 14.1 months in both the whole cohort and the BRPC and LAPC cohorts. In the other SMART series for LAPC and BRPC with the same dose prescription (50 Gy in 5 fractions), the median OS was 9.8 and 15.7 months (27, 28). The 1-year LC in our cohort was 86%, similar to respectively 87% and 84.3% in the studies of Chuong *et al.* and Hassanzadeh *et al.*, confirming that SMART achieves a high LC rate in LAPC. LC is of particular importance for LAPC patients, as local progression is a frequent cause of morbidity and mortality (31). Indeed, Rudra *et al.* showed that increasing the BED_{10} over 70 Gy translated into OS benefit (2-year OS of 49% when $BED_{10} > 70$ Gy vs. 30% when $BED_{10} < 70$ Gy) (10). This suggests that LC plays a role in OS too. A recent review demonstrated the dose–response effect using SBRT for

TABLE 5 | SMART-related acute and late toxicities.

CTCAE v5.0	Acute toxicity (0–90 days)	Late toxicity (90 days–1 year)
Abdominal pain		
g0	18 (60%)	13 (43.3%)
g1	12 (40%)	8 (26.7%)
g2	0	1 (3.3%)
g3	0	0
Ongoing	0	7 (23.3%)
Nausea/Vomiting		
g0	17 (56.7%)	19 (63.3%)
g1	7 (23.3%)	2 (6.7%)
g2	6 (20%)	2 (6.7%)
g3	0	0
Ongoing	0	7 (23.3%)
Gastritis/enteritis		
g0	29 (96.7%)	23 (66.7%)
g1	1 (3.3%)	0
g2	0	0
g3	0	0
Ongoing	0	7 (23.3%)
Gastroduodenal ulcer		
g0	30 (100%)	23 (66.7%)
g1	0	0
g2	0	0
g3	0	0
Ongoing	0	7 (23.3%)
Digestive fistula		
g0	30 (100%)	23 (66.7%)
g1	0	0
g2	0	0
g3	0	0
Ongoing	0	7 (23.3%)
Diarrhea		
g0	22 (63.3%)	16 (53.3%)
g1	7 (23.3%)	4 (13.3%)
g2	1 (3.3%)	3 (10%)
g3	0	0
Ongoing	0	7 (23.3%)

SMART, stereotactic MR-guided adaptive radiotherapy; CTCAE, Common Terminology Criteria for Adverse Events.

pancreatic cancers, from 70% 1-year LC for equivalent 24 Gy in 3 fractions to 86% for equivalent 30 to 36 Gy in 3 fractions, confirming the necessity to prescribe high doses in this population (32). This is also suggested by the results of other retrospective studies using non-MR Linac and non-adaptive techniques, where 1-year LC ranged from 48.5% to 78% for prescription of 1 fraction of 24 Gy to 5 fractions of 6.6 Gy (33–36).

However, the median DMFS and 1-year DMFS from initiation of induction chemotherapy in our study were 16.3 months and 72%, but only 10.5 months and 34% from SMART, showing the frequent and quick metastatic dissemination of these cancers.

Our study is the first to report a high rate of secondary resection after SMART. Indeed, nine patients (8 out of 19 patients (42.1%) with initial LAPC and one out of 3 patients (33.3%) with BRPC) were resected. In the studies published by the Washington University and Miami teams on SMART for pancreatic cancers, the resection rate was respectively 9% (28) and 14% (27). All our patients had an R0 resection, and the average pathologic therapeutic effect was 64%. Resected patients in our study had a significant increase in OS (HR = 5.78 (95% CI: 1.29–25.9); p = 0.0219). We report the feasibility of pancreatic surgery after SMART, provided that these high-risk surgeries are carried out by trained surgical teams with significant experience in these procedures. These results lead us to pursue our aggressive strategy in this situation, especially as some lesions that appeared inoperable on the post-SMART scan were finally able to benefit from an R0 resection and a probable therapeutic benefit. Indeed, we confirmed the imaging struggles to assess resectability after neoadjuvant treatment.

Our study presents some limits. First, the number of patients is limited and the study is monocentric, but we must consider that SMART is a new technique available in a few centers. Second, our study population is heterogeneous, with three patients presenting a neuroendocrine tumor or pancreatic metastases of another primary. We decided to keep these patients for dosimetric and toxicity analysis, as the treatment site and anatomical and dosimetric characteristics were similar, but a subgroup analysis on BRPCs and LAPCs regarding survival data had to be performed. Then, our follow-up is limited, and our results need to be confirmed with a longer follow-up.

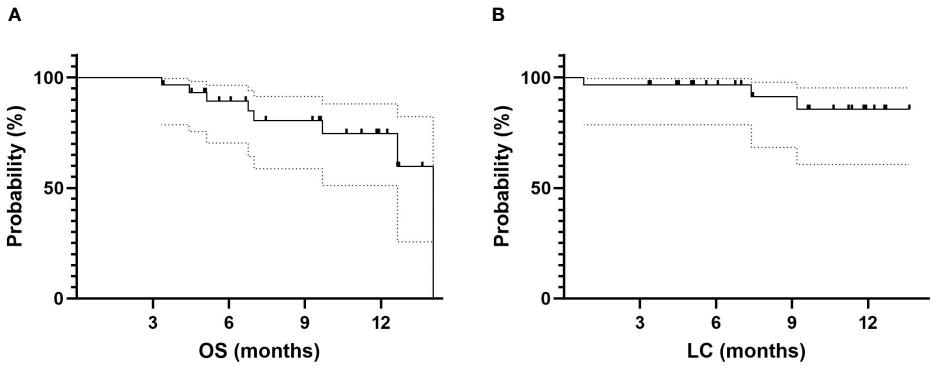

FIGURE 3 | Survival date for the whole cohort. **(A)** OS for the whole cohort. **(B)** LC for the whole cohort. OS, overall survival; LC, local control.

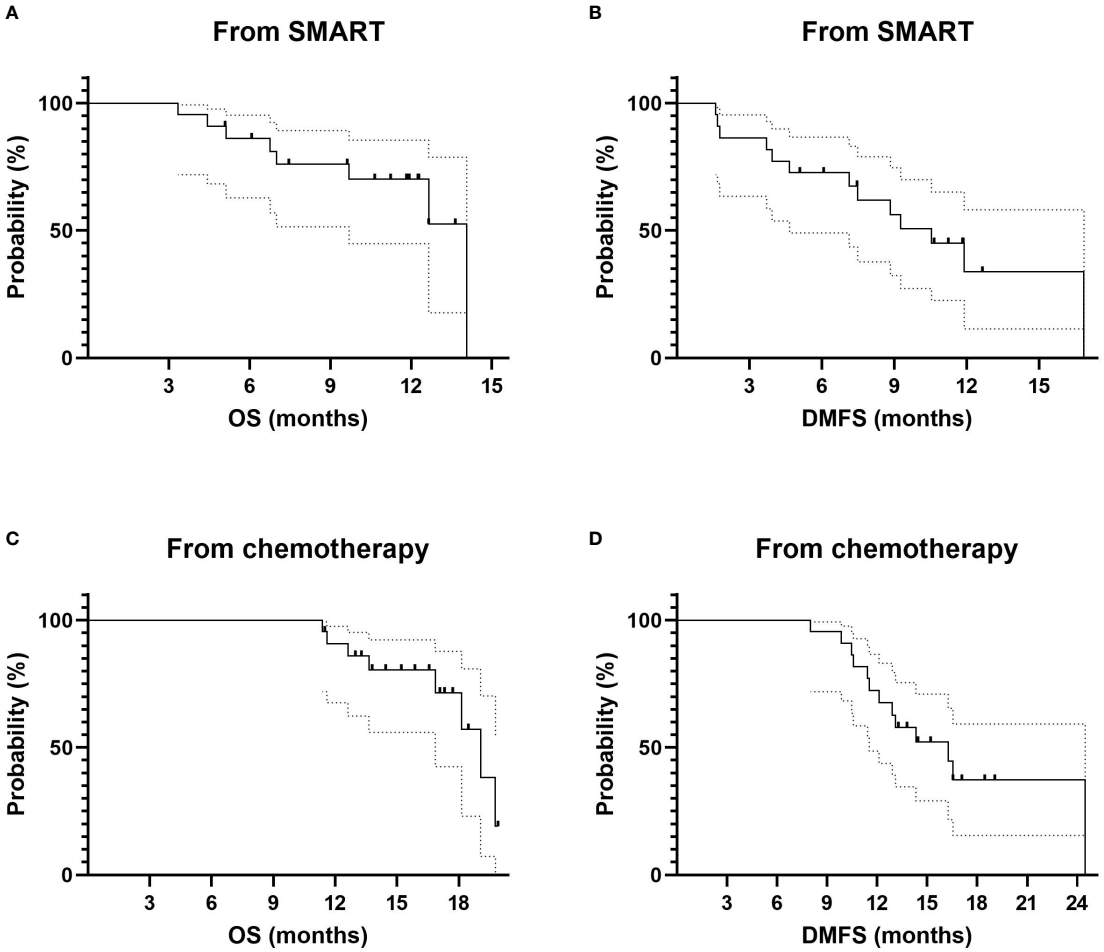

FIGURE 4 | Survival data for LAPC and BRPC patients: comparison between resected and unresected patients. **(A)** OS from SMART completion. **(B)** DMFS from SMART completion. **(C)** OS from chemotherapy start. **(D)** DMFS from chemotherapy start. LAPC, locally advanced pancreatic cancer; BRPC, borderline resectable pancreatic cancer; OS, overall survival; SMART, stereotactic MR-guided adaptive radiotherapy; DMFS, distant metastasis-free survival.

In our study, OS from SMART completion was 14.1 months, highlighting the poor prognosis of this patient population, despite a good LC rate (86% at 1 year). This result highlights the need for intensification of therapy and personalization of treatment according to the characteristics of the disease. We believe that the use of radiomics could play a part in this therapeutic personalization. Cusumano et al. used a delta radiomics approach for patients treated with SMART for pancreatic cancer. They identified a feature capable to predict 1-year LC with an AUC of 0.78 (37). Patients with a poor prognosis may be offered intensified systemic therapy or dose-escalated radiation therapy.

The first published results of SMART in the treatment of pancreatic tumors seem encouraging, and our clinical results in a prospective registry confirm the safety data and seem to show therapeutic benefit for patients. However, we need more prospective, multicenter data to confirm these trends. The first encouraging results of the multicenter SMART pancreas study sponsored by ViewRay were presented at ASTRO 2021 and seem to confirm the interest in the technique. In France, the GABRINOX ART trial is ongoing (38). This trial is evaluating an intensified and sequential chemotherapy regimen (Gabrinox) comprising Gembrax (Gemcitabine-Abraxane) and Folfirinox (5FU, oxaliplatin, and irinotecan) in patients with LAPC, followed by SMART in non-progressive patients after induction chemotherapy. In the United States, a trial is evaluating a combination of SMART and concomitant chemotherapy by gemcitabine or capecitabine (39). We hope that the results of these trials will give us robust results confirming the benefit of this technique for patients with pancreatic tumors.

CONCLUSION

SMART for pancreatic tumors is feasible without limiting toxicities. Daily adaptation demonstrated a benefit for tumor coverage and

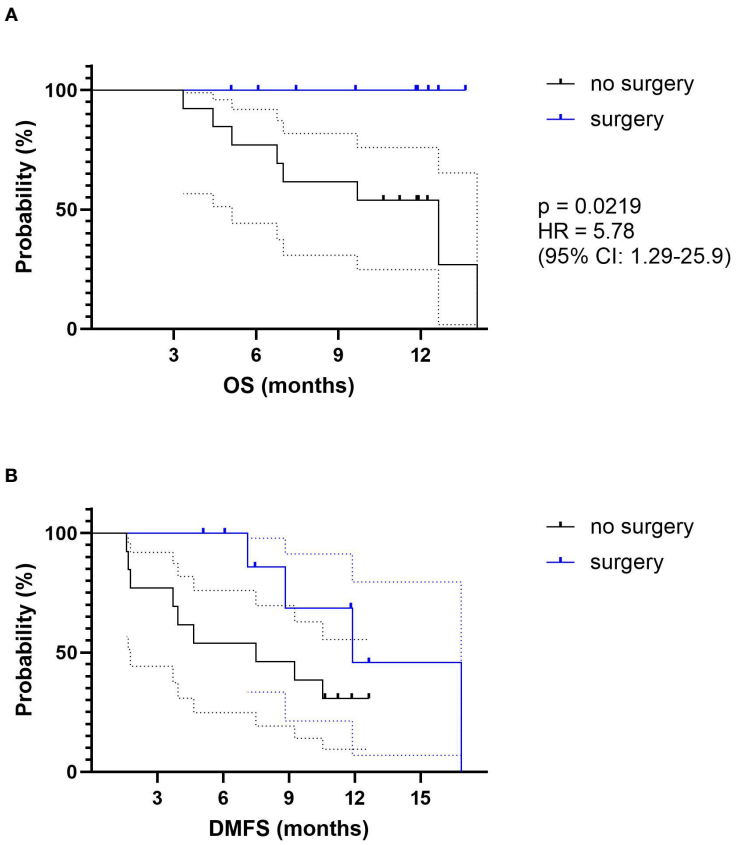

FIGURE 5 | Survival data for LAPC and BRPC patients: comparison between resected (in blue) and unresected patients (in black). **(A)** OS from SMART completion. **(B)** DMFS from SMART completion. OS, overall survival, DMFS, distant metastasis-free survival.

OAR sparing. Acute and late toxicities were low. OS and LC rates were promising. SMART achieved a high secondary resection rate in LAPC patients. Surgery after SMART seemed to be feasible and might increase OS in these patients.

DATA AVAILABILITY STATEMENT

The raw data supporting the conclusions of this article will be made available by the authors, without undue reservation.

ETHICS STATEMENT

The studies involving human participants were reviewed and approved by COMERE ICM. The patients/participants provided their written informed consent to participate in this study.

AUTHORS CONTRIBUTIONS

Conceptualization: OR, KB, and MM. Methodology: SG and OR. Investigation: KB, MM, and OR. Supervision: OR. Writing—original draft preparation: OR, MM, and KB. Writing—review and editing: OR, MM, KB, MC, SG, EA, FP, MD, SV, PD, SS, MY, NA, PF, DA, RD, PEC, FRS, and SC. All authors have read and agreed to the published version of the manuscript.

REFERENCES

1. Siegel RL, Miller KD, Jemal A. Cancer Statistics, 2019. *CA Cancer J Clin* (2019) 69(1):7–34. doi: 10.3322/caac.21551
2. Vincent A, Herman J, Schulick R, Hruban RH, Goggins M. Pancreatic Cancer. *Lancet* (2011) 378(9791):607–20. doi: 10.1016/S0140-6736(10)62307-0
3. Hammel P, Huguet F, Laethem J-Lv, Goldstein D, Glimelius B, Artru P, et al. Effect of Chemoradiotherapy vs Chemotherapy on Survival in Patients With Locally Advanced Pancreatic Cancer Controlled After 4 Months of Gemcitabine With or Without Erlotinib: The LAP07 Randomized Clinical Trial. *JAMA* (2016) 315(17):1844–53. doi: 10.1001/jama.2016.4324

4. Wan X, Yang Y-F, Cao X-H, Bao C-E. Concurrent Radiotherapy With Oral Fluoropyrimidine Versus Gemcitabine in Locally Advanced Pancreatic Cancer: A Systematic Review and Meta-Analysis. *OncoTargets Ther nov* (2015) 8:3315–22. doi: 10.2147/OTT.S91292
5. Panje C, Andratschke N, Brunner TB, Niyazi M, Guckenberger M. Stereotactic Body Radiotherapy for Renal Cell Cancer and Pancreatic Cancer: Literature Review and Practice Recommendations of the DEGRO Working Group on Stereotactic Radiotherapy. *Strahlenther Onkol* (2016) 192 (12):875–85. doi: 10.1007/s00066-016-1053-1
6. Tonneau M, Lacornerie T, Mirabel X, Pasquier D. Radiothérapie Stéréotaxique Dans Le Cancer Du Pancréas Localement Avancé : Revue De La Littérature. *Cancer/Radiothérapie* (2021) 25(3):283-95. doi: 10.1016/j.canrad.2020.08.047
7. Henke L, Kashani R, Robinson C, Curcuru A, DeWees T, Bradley J, et al. Phase I Trial of Stereotactic MR-Guided Online Adaptive Radiation Therapy (SMART) for the Treatment of Oligometastatic or Unresectable Primary Malignancies of the Abdomen. *Radiother Oncol* (2018) 126(3):519–26. doi: 10.1016/j.radonc.2017.11.032
8. Bohoudi O, Bruynzeel AME, Senan S, Cuijpers JP, Slotman BJ, Lagerwaard FJ, et al. Fast and Robust Online Adaptive Planning in Stereotactic MR-Guided Adaptive Radiation Therapy (SMART) for Pancreatic Cancer. *Radiother Oncol* (2017) 125(3):439–44. doi: 10.1016/j.radonc.2017.07.028
9. Mutic S, Dempsey JF. The ViewRay System: Magnetic Resonance–Guided and Controlled Radiotherapy. *Semin Radiat Oncol* (2014) 24(3):196–9. doi: 10.1016/j.semradonc.2014.02.008
10. Rudra S, Jiang N, Rosenberg SA, Olsen JR, Roach MC, Wan L, et al. Using Adaptive Magnetic Resonance Image-Guided Radiation Therapy for Treatment of Inoperable Pancreatic Cancer. *Cancer Med* (2019) 8(5):2123–32. doi: 10.1002/cam4.2100
11. Mittauer KE, Hill PM, Bassetti MF, Bayouth JE. Validation of an MR-Guided Online Adaptive Radiotherapy (MRgoART) Program: Deformation Accuracy in a Heterogeneous, Deformable, Anthropomorphic Phantom. *Radiother Oncol* (2020) 146:97–109. doi: 10.1016/j.radonc.2020.02.012
12. Conroy T, Hammel P, Hebbar M, Ben Abdelghani M, Wei AC, Raoul J-L, et al. FOLFIRINOX or Gemcitabine as Adjuvant Therapy for Pancreatic Cancer. *N Engl J Med* (2018) 379(25):2395–406. doi: 10.1056/NEJMoa1809775
13. Huguet F, Mukherjee S, Javle M. Locally Advanced Pancreatic Cancer: The Role of Definitive Chemoradiotherapy. *Clin Oncol* (2014) 26(9):560–8. doi: 10.1016/j.clon.2014.06.002
14. Teriaca MA, Loi M, Suker M, Eskens FALM, van Eijck CHJ, Nuyttens JJ. A Phase II Study of Stereotactic Radiotherapy After FOLFIRINOX for Locally Advanced Pancreatic Cancer (LAPC-1 Trial): Long-Term Outcome. *Radiother Oncol* (2021) 155:232–6. doi: 10.1016/j.radonc.2020.11.006
15. Deorukhkar A, Shentu S, Park Hc, Diagaradjane P, Puduvalli V, Aggarwal B, et al. Inhibition of Radiation-Induced DNA Repair and Prosurvival Pathways Contributes to Vorinostat-Mediated Radiosensitization of Pancreatic Cancer Cells. *Pancreas* 39(8):1277–83. doi: 10.1097/MPA.0b013e3181dd63e1
16. Tchelebi LT, Lehrer EJ, Trifiletti DM, Sharma NK, Gusani NJ, Crane CH, et al. Conventionally Fractionated Radiation Therapy Versus Stereotactic Body Radiation Therapy for Locally Advanced Pancreatic Cancer (CRiSP): An International Systematic Review and Meta-Analysis. *Cancer* (2020) 126 (10):2120–31. doi: 10.1002/cncr.32756
17. Koong AC, Le QT, Ho A, Fong B, Fisher G, Cho C, et al. Phase I Study of Stereotactic Radiosurgery in Patients With Locally Advanced Pancreatic Cancer. *Int J Radiat Oncol Biol Phys* (2004) 58(4):1017–21. doi: 10.1016/j.ijrobp.2003.11.004
18. Schellenberg D, Kim J, Christman-Skieller C, Chun CL, Columbo LA, Ford JM, et al. Single-Fraction Stereotactic Body Radiation Therapy and Sequential Gemcitabine for the Treatment of Locally Advanced Pancreatic Cancer. *Int J Radiat Oncol Biol Phys* (2011) 81(1):181–8. doi: 10.1016/j.ijrobp.2010.05.006
19. Hoyer M, Roed H, Sengelov L, Traberg A, Ohlhuis L, Pedersen J, et al. Phase-II Study on Stereotactic Radiotherapy of Locally Advanced Pancreatic Carcinoma. *Radiother Oncol J Eur Soc Ther Radiol Oncol* (2005) 76(1):48 –53. doi: 10.1016/j.radonc.2004.12.022
20. Comito T, Cozzi L, Clerici E, Franzese C, Tozzi A, Iftode C, et al. Can Stereotactic Body Radiation Therapy Be a Viable and Efficient Therapeutic Option for Unresectable Locally Advanced Pancreatic Adenocarcinoma? *Results Phase 2 Study Technol Cancer Res Treat* (2017) 16(3):295–301. doi: 10.1177/1533034616650778
21. Schellenberg D, Goodman KA, Lee F, Chang S, Kuo T, Ford JM, et al. Gemcitabine Chemotherapy and Single-Fraction Stereotactic Body Radiotherapy for Locally Advanced Pancreatic Cancer. *Int J Radiat Oncol Biol Phys* (2008) 72(3):678–86. doi: 10.1016/j.ijrobp.2008.01.051
22. Goyal K, Einstein D, Ibarra RA, Yao M, Kunos C, Ellis R, et al. Stereotactic Body Radiation Therapy for Nonresectable Tumors of the Pancreas. *J Surg Res* (2012) 174(2):319–25. doi: 10.1016/j.jss.2011.07.044
23. Koong AC, Christofferson E, Le Q-T, Goodman KA, Ho A, Kuo T, et al. Phase II Study to Assess the Efficacy of Conventionally Fractionated Radiotherapy Followed by a Stereotactic Radiosurgery Boost in Patients With Locally Advanced Pancreatic Cancer. *Int J Radiat Oncol Biol Phys* (2005) 63(2):320 –3. doi: 10.1016/j.ijrobp.2005.07.002
24. Suker M, Nuyttens JJ, Eskens FALM, Haberkorn BCM, Coene P-PLO, van der Harst E, et al. Efficacy and Feasibility of Stereotactic Radiotherapy After Folfirinox in Patients With Locally Advanced Pancreatic Cancer (LAPC-1 Trial). *EClinicalMedicine* (2019) 17:100200. doi: 10.1016/j.eclinm.2019.10.013
25. Herman JM, Chang DT, Goodman KA, Dholakia AS, Raman SP, Hacker-Prietz A, et al. Phase 2 Multi-Institutional Trial Evaluating Gemcitabine and Stereotactic Body Radiotherapy for Patients With Locally Advanced Unresectable Pancreatic Adenocarcinoma. *Cancer* (2015) 121(7):1128–37. doi: 10.1002/cncr.29161
26. Kersemans V, Beech JS, Gilchrist S, Kinchesh P, Allen PD, Thompson J, et al. An Efficient and Robust MRI-Guided Radiotherapy Planning Approach for Targeting Abdominal Organs and Tumours in the Mouse. Zhang Q, Éditeur. *PloS One 28 avr* (2017) 12(4):e0176693. doi: 10.1371/journal.pone.0176693
27. Chuong MD. Ablative 5-Fraction Stereotactic Magnetic Resonance-Guided Radiation Therapy With On-Table Adaptive Replanning and Elective Nodal Irradiation for Inoperable Pancreas Cancer. *Pract Radiat Oncol* (2020) 14:134-47. doi: 10.1016/j.prro.2020.09.005
28. Hassanzadeh C, Rudra S, Bommireddy A, Hawkins WG, Wang-Gillam A, Fields RC, et al. Ablative Five-Fraction Stereotactic Body Radiation Therapy for Inoperable Pancreatic Cancer Using Online MR-Guided Adaptation. *Adv Radiat Oncol janv* (2021) 6(1):100506. doi: 10.1016/j.adro.2020.06.010
29. Finazzi T, Haasbeek CJA, Spoelstra FOB, Palacios MA, Admiraal MA, Bruynzeel AME, et al. Clinical Outcomes of Stereotactic MR-Guided Adaptive Radiation Therapy for High-Risk Lung Tumors. *Int J Radiat Oncol* (2020) 107(2):270–8. doi: 10.1016/j.ijrobp.2020.02.025
30. Michalet M, Riou O, Valdenaire S, Debuire P, Ailleres N, Draghici R, et al. Magnetic Resonance–Guided Reirradiation for Local Recurrence Within the Prostate or in the Prostate Bed: Preliminary Results of a Prospective Registry Study. *Adv Radiat Oncol* (2021) 6(5):100748. doi: 10.1016/j.adro.2021.100748
31. Ke P, Cl W. Palliative Management of Unresectable Pancreas Cancer. *Surg Oncol Clin N Am* (2016) 25(2):327–37. doi: 10.1016/j.soc.2015.11.005
32. Mahadevan A, Moningi S, Grimm J, XA Li, Forster KM, Palta M, et al. Maximizing Tumor Control and Limiting Complications With Stereotactic Body Radiation Therapy for Pancreatic Cancer. *Int J Radiat Oncol* (2021) 110 (1):206–16. doi: 10.1016/j.ijrobp.2020.11.017
33. Mahadevan A, Jain S, Goldstein M, Miksad R, Pleskow D, Sawhney M, et al. Stereotactic Body Radiotherapy and Gemcitabine for Locally Advanced Pancreatic Cancer. *Int J Radiat Oncol* (2010) 78(3):735–42. doi: 10.1016/j.ijrobp.2009.08.046
34. Gurka MK, Kim C, AR He, Charabaty A, Haddad N, Turocy J, et al. Stereotactic Body Radiation Therapy (SBRT) Combined With Chemotherapy for Unresected Pancreatic Adenocarcinoma. *Am J Clin Oncol* (2017) 40(2):152. doi: 10.1097/COC.0000000000000118
35. Song Y, Yuan Z, Li F, Dong Y, Zhuang H, Wang J, et al. Analysis of Clinical Efficacy of CyberKnife(®) Treatment for Locally Advanced Pancreatic Cancer. *OncoTargets Ther* (2015) 8:1427–31. doi: 10.2147/OTT.S81939
36. Rwigema JC, Parikh SD, Heron DE, Howell M, Zeh H, Moser AJ, et al. Stereotactic Body Radiotherapy in the Treatment of Advanced Adenocarcinoma of the Pancreas. *Am J Clin Oncol* (2011) 34(1):63–9. doi: 10.1097/COC.0b013e3181d270b4
37. Cusumano D, Boldrini L, Yadav P, Casà C, Lee SL, Romano A, et al. Delta Radiomics Analysis for Local Control Prediction in Pancreatic Cancer

Patients Treated Using Magnetic Resonance Guided Radiotherapy. *Diagnostics* (2021) 11(1):72. doi: 10.3390/diagnostics11010072

38. Institut du Cancer de Montpellier. *Val D'aurelle. Phase II Study to Assess the Interest of a Sequential Treatment With Gemcitabine/Nab-Paclitaxel (GEMBRAX) and Then FOLFIRINOX Followed by Stereotactic Magnetic Resonance-Guided Adaptive Radiotherapy in Patients With Locally Advanced Pancreatic Cancer* (2020). Available at: https://clinicaltrials.gov/ct2/show/NCT04570943.
39. Erickson B. *MR Guided Phase II Radiotherapy Dose Escalation in Unresectable Non-Metastatic Pancreatic Cancer* (2021). Available at: https://clinicaltrials.gov/ct2/show/NCT01972919.

Conflict of Interest: The authors declare that the research was conducted in the absence of any commercial or financial relationships that could be construed as a potential conflict of interest.

Publisher's Note: All claims expressed in this article are solely those of the authors and do not necessarily represent those of their affiliated organizations, or those of the publisher, the editors and the reviewers. Any product that may be evaluated in this article, or claim that may be made by its manufacturer, is not guaranteed or endorsed by the publisher.

frontiers | Frontiers in Oncology

TYPE Original Research
PUBLISHED 28 November 2022
DOI 10.3389/fonc.2022.1060098

OPEN ACCESS

EDITED BY
Enis Ozyar,
Acıbadem University, Turkey

REVIEWED BY
Archya Dasgupta,
Tata Memorial Hospital, India
Colette Shen,
University of North Carolina Hospitals, United States

*CORRESPONDENCE
Chia-Lin Tseng
chia-lin.tseng@sunnybrook.ca

SPECIALTY SECTION
This article was submitted to Radiation Oncology, a section of the journal Frontiers in Oncology

RECEIVED 02 October 2022
ACCEPTED 10 November 2022
PUBLISHED 28 November 2022

CITATION
Tseng C-L, Chen H, Stewart J, Lau AZ, Chan RW, Lawrence LSP, Myrehaug S, Soliman H, Detsky J, Lim-Fat MJ, Lipsman N, Das S, Heyn C, Maralani PJ, Binda S, Perry J, Keller B, Stanisz GJ, Ruschin M and Sahgal A (2022) High grade glioma radiation therapy on a high field 1.5 Tesla MR-Linac - workflow and initial experience with daily adapt-to-position (ATP) MR guidance: A first report. *Front. Oncol.* 12:1060098. doi: 10.3389/fonc.2022.1060098

High grade glioma radiation therapy on a high field 1.5 Tesla MR-Linac - workflow and initial experience with daily adapt-to-position (ATP) MR guidance: A first report

Chia-Lin Tseng[1]*, Hanbo Chen[1], James Stewart[1], Angus Z. Lau[2,3], Rachel W. Chan[2], Liam S. P. Lawrence[3], Sten Myrehaug[1], Hany Soliman[1], Jay Detsky[1], Mary Jane Lim-Fat[4], Nir Lipsman[5], Sunit Das[6], Chinthaka Heyn[7], Pejman J. Maralani[7], Shawn Binda[1], James Perry[4], Brian Keller[1], Greg J. Stanisz[2,3,8], Mark Ruschin[1] and Arjun Sahgal[1]

[1]Department of Radiation Oncology, Sunnybrook Health Sciences Centre, University of Toronto, Toronto, ON, Canada, [2]Physical Sciences Platform, Sunnybrook Research Institute, Toronto, ON, Canada, [3]Medical Biophysics, University of Toronto, Toronto, ON, Canada, [4]Department of Medicine, Division of Neurology, Sunnybrook Health Sciences Centre, University of Toronto, Toronto, ON, Canada, [5]Division of Neurosurgery, Sunnybrook Health Sciences Centre, University of Toronto, Toronto, ON, Canada, [6]Division of Neurosurgery, St. Michael's Hospital, University of Toronto, Toronto, ON, Canada, [7]Department of Medical Imaging, Sunnybrook Health Sciences Centre, University of Toronto, Toronto, ON, Canada, [8]Department of Neurosurgery and Paediatric Neurosurgery, Medical University, Lublin, Poland

Purpose: This study reports the workflow and initial clinical experience of high grade glioma (HGG) radiotherapy on the 1.5 T MR-Linac (MRL), with a focus on the temporal variations of the tumor and feasibility of multi-parametric image (mpMRI) acquisition during routine treatment workflow.

Materials and methods: Ten HGG patients treated with radiation within the first year of the MRL's clinical operation, between October 2019 and August 2020, were identified from a prospective database. Workflow timings were recorded and online adaptive plans were generated using the Adapt-To-Position (ATP) workflow. Temporal variation within the FLAIR hyperintense region (FHR) was assessed by the relative FHR volumes (n = 281 contours) and migration distances (maximum linear displacement of the volume). Research mpMRIs were acquired on the MRL during radiation and changes in selected functional parameters were investigated within the FHR.

Results: All patients completed radiotherapy to a median dose of 60 Gy (range, 54-60 Gy) in 30 fractions (range, 30-33), receiving a total of 287 fractions on the MRL. The mean in-room time per fraction with or without post-beam

research imaging was 42.9 minutes (range, 25.0–69.0 minutes) and 37.3 minutes (range, 24.0–51.0 minutes), respectively. Three patients (30%) required re-planning between fractions 9 to 12 due to progression of tumor and/or edema identified on daily MRL imaging. At the 10, 20, and 30-day post-first fraction time points 3, 3, and 4 patients, respectively, had a FHR volume that changed by at least 20% relative to the first fraction. Research mpMRIs were successfully acquired on the MRL. The median apparent diffusion coefficient (ADC) within the FHR and the volumes of FLAIR were significantly correlated when data from all patients and time points were pooled (R=0.68, p<.001).

Conclusion: We report the first clinical series of HGG patients treated with radiotherapy on the MRL. The ATP workflow and treatment times were clinically acceptable, and daily online MRL imaging triggered adaptive re-planning for selected patients. Acquisition of mpMRIs was feasible on the MRL during routine treatment workflow. Prospective clinical outcomes data is anticipated from the ongoing UNITED phase 2 trial to further refine the role of MR-guided adaptive radiotherapy.

KEYWORDS

MR-Linac, glioma radiation, tumor dynamics, functional imaging, adapt-to-position

Introduction

The development of magnetic resonance imaging (MRI)-guided radiotherapy with an integrated high-field strength (1.5 Tesla) MRI-linear accelerator (MR-Linac) enables the daily acquisition of an MRI which allows for on-line soft tissue visualization. Therefore, alignment on the tumor itself is now possible as opposed to relying on a bony surrogate or implanted fiducial and, most importantly, the ability to adapt treatment in real time (1–3). Moreover, a high-field strength MR-Linac permits the acquisition of functional imaging such as diffusion, chemical exchange saturation transfer (CEST), perfusion, and other quantitative MRI (qMRI) biomarkers which introduces the possibility to further individualize treatment (4–10).

At the Sunnybrook Odette Cancer Centre (Toronto, Canada), as a founding member of the Elekta MR-Linac Consortium, our role was to develop the technology primarily for central nervous system tumors (11). Our focus was on the management of intracranial high grade gliomas (HGG) given that following maximal safe resection, radiotherapy with or without concurrent and adjuvant chemo is the standard of care (12–16). The motivation to study this population was based on the lack of any meaningful advances in radiotherapy margin design despite the integration of MRI into radiation planning for almost three decades. In order to determine if personalized margins would be beneficial, predicate work to determine tumor dynamics was undertaken by prospectively imaging patients during a 6-week course of therapy. Stewart et al. reported that inter-fraction volume changes and migration distances are indeed a factor to consider, and challenged the dogma that HGGs are static during a course of chemo-radiotherapy (17). Therefore, when clinical operations of the Unity MR-Linac (Elekta AB, Stockholm, Sweden) began at our institution, we started by treating patients with HGG based on standard margins and contouring practices (18), and evaluated the entire process including our in-house developed workflow, treatment toxicities, and imaging outcomes to inform future directions. In the present study, we report the clinical experience of an initial cohort of 10 HGG patients with an additional focus on the temporal variations of the tumor and the feasibility of acquiring research based multi-parametric images during routine treatment workflow.

Methods and materials

Ten HGG patients treated on our MR-Linac (MRL) between October 2019 and August 2020 within the first year of the MRL's clinical operation were identified from a prospective database and retrospectively analyzed. All patients had histologically confirmed WHO Grade 3 or 4 glioma. The study was approved by the institutional ethics review board and all

patients provided written consent to be enrolled on the MOMENTUM trial, an international prospective registry designed to facilitate evidence-based implementation of the first MRL and collect outcomes data (19).

MRL glioma adapt-to-position workflow

The patient workflow was categorized into offline and online components, and this is depicted in Figure 1. The offline (pre-treatment) component began with CT and MRI simulation scans. A CT overlay was placed on the CT simulation couch which mimicked the couch top of the MRL. An MR-safe Orfit (Orfit Industries NV, Belgium) base plate was affixed to the couch overlay and a 3-point mask was used for immobilization. A dummy coil, mimicking the true MRL anterior coil, was used to ensure that there were no collisions between the patient and the coil. The slice thickness for CT scanning was 1 mm. MRI simulation sequences included a post-gadolinium T_1-weighted 3D sequence, a T_1-weighted DIXON (fat sat), a T_2-weighted fluid-attenuated inversion recovery (FLAIR), and a DWI sequence.

The CT and MRI data sets were imported into the Monaco treatment planning system (TPS) to generate a reference plan. The Monaco TPS uses a Monte Carlo dose calculation algorithm that models the effects of the magnetic field (20). The MRI data set was co-registered to the CT data set, and contouring was completed by the treating radiation oncologist. The gross tumor volume (GTV) was defined as the T_1-weighted gadolinium-enhancing disease for Grade 4 tumors, or FLAIR hyperintense disease for Grade 3 tumors. The clinical target volume (CTV) consisted of a standard 1.5 cm or 1.0 cm expansion beyond the GTV for grade 4 and grade 3 disease, respectively, adjusted for anatomical barriers and routes of spread (18). The PTV expansion was 0.3 cm beyond the CTV. Planning was based on a pre-defined template in the Monaco TPS, which pre-loads the prescription dose, IMRT optimization parameters, beam arrangement (typically 9 beams), dosimetric criteria and reference dose. Treatment plans were calculated using the following parameters: 1% statistical uncertainty, a 3 mm dose grid in all directions, dose calculated to medium using the GPUMCD Monte Carlo algorithm, a minimum segment monitor unit of 2 MU and a minimum segment size setting of 4 cm^2. A dose reference point was placed in the centre of the

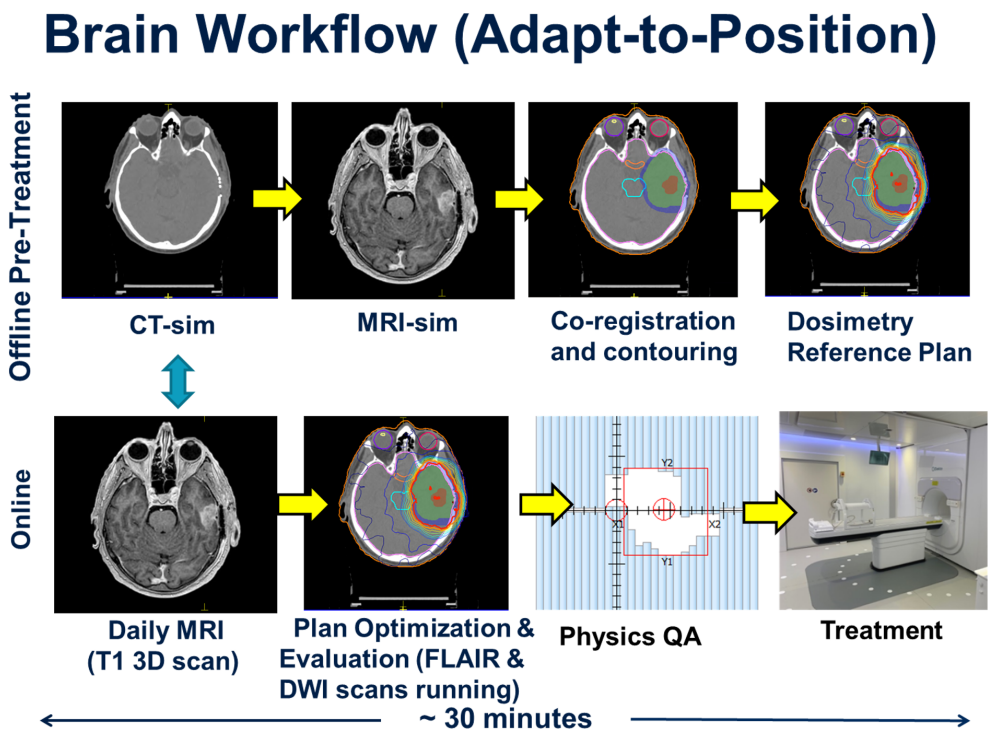

FIGURE 1
Workflow for both the offline (upper figures) and online (lower figures) series of events in the treatment of the 10 glioma patients. The offline pre-treatment workflow involves initial simulations and treatment planning that leads to a reference plan. The online portion involves a daily MRI scan used to account for patient setup variations and the generation of a new daily online treatment plan as per the adapt-to-position workflow followed by physics quality assurance checks prior to and post treatment. The turquoise arrow indicates the online co-registration between the acquired daily MRI and the reference CT primary data set.

PTV, in order to perform an independent dose check during the online planning stage of the patient's treatment. The reference treatment plan was sent for patient specific quality assurance (QA) measurement using the Arccheck-MR device (Sun Nuclear, Melbourne, Fl) prior to the start of treatment. Backup treatment plans for conventional Linacs were generated in case the MRL was not operational due to unexpected downtime or preventative maintenance.

The online workflow began with acquisition of daily pre-beam non-contrast enhanced MRI sequence (T_1-weighted 3D volumetric scan), which was co-registered to the pre-treatment reference CT scan. The shift information was used to adjust the patient isocenter location prior to re-optimizing the daily treatment plan. This type of workflow, where the new daily online plan accounts only for rigid translational shifts of the patient, is referred to as the ATP workflow within the Monaco TPS. The Adapt-to-Shape (ATS) workflow, which was not applied to this initial cohort, describes a process by which the organs-at-risk (OAR) and target contours are deformed or re-contoured to reflect the anatomy of the day based on the online MRI, with which the plan is then re-optimized.

All workflow timings were recorded for each patient. During co-registration and planning, FLAIR and DWI MRI sequences were acquired. The new online plan was then reviewed and accepted by the radiation oncologist, or reviewed by the MRL radiation therapist after the first 5 fractions based on a set of pre-defined target coverage objectives and OAR tolerance thresholds, where the treating physician would be paged if tolerances were exceeded. Upon approval of the online plan, an independent dose check was performed using the RadCalc software (Lifeline Software, Tyler, TX), and the dose to a point in the center of the PTV validated. The dose difference between the Monaco TPS and the RadCalc software must be within 4% otherwise an investigation was warranted. For all 10 HGG patients, post treatment patient specific QA measurements were performed using the same criteria as the pre-treatment reference plan measurements.

FLAIR hyperintense region dynamics assessment

All T2-FLAIR images acquired on the MRL were imported into a research version of the Monaco TPS (Monaco Research v. 5.19.03d; Elekta AB, Stockholm, Sweden). The FLAIR hyperintense region (FHR) was then manually contoured by an attending radiation oncologist (H.C.), and verified by a second radiation oncologist (C.L.T.) at each time point. For each patient, the daily T2-FLAIR image sets from fraction 2 onwards were registered with six degree-of-freedom translational and rotational fusion using a mutual information registration algorithm to the respective 1st fraction T2-FLAIR image set. Following registration, all contours (total n = 281) for each patient were copied to the 1st fraction T2-FLAIR image set, and the RT structure set exported for further analysis. The volumes and migration distances of the contoured FHRs were then computed using the exported structure sets by a custom MATLAB script (MATLAB 2020a; The Mathworks Inc., Natick, Massachusetts). The migration distance was defined as the maximum linear distance in any direction that the contoured FHR volume departs from its respective first fraction volume (17).

Multi-parametric imaging acquisition and analysis

Research multi-parametric images were acquired on the MRL during radiation treatment, typically post beam-on. The microstructural and functional sequences included DWI, CEST, magnetization transfer (MT), and blood oxygenation level dependent (BOLD) resting-state fMRI. Additionally, variable flip angle and multi-echo sequences were acquired for T_1 and T_2 mapping, respectively. All sequences were obtained with whole-brain volumetric coverage, except for the single-slice CEST and three-slice MT scans. Each sequence was obtained at separate treatment fractions, with up to 1 week between repeated measurements for certain sequences. These sequences were not directly used for planning, but were prospectively acquired for research and development. The acquisition protocols are detailed in Supplementary Material.

ADC maps were fitted using the mono-exponential model $\log S(b)=\log S_0-b\cdot ADC$ with b-values of [100,200,400,800] s/mm^2 with a two-step weighted linear-least squares procedure (21, 22). CEST parameter maps were calculated as described previously (23). The T_1 map was estimated from the variable flip angle data using the method described in Liberman et al. (24), incorporating uniform weighting of all flip angles and B_1 inhomogeneity correction applied to the T_1 map, except that the nominal flip angles were used for fitting. The T_2 map was estimated from the multi-echo data using a mono-exponential model with linear least-squares fitting of the log-signal versus echo time.

The temporal behaviors of selected functional parameter values within the FHR were investigated. These parameters included ADC, T_1, T_2 and CEST asymmetry. For each patient, the medians of the functional parameter values within the FHR contour of the day were computed.

In order to determine the association between ADC values and FHR, the Pearson correlation coefficient between the median ADC and FHR using all treatment fractions was computed per patient. The hypothesis of a non-zero correlation coefficient was tested using a threshold adjusted for multiple comparisons (α=0.05/10=0.005). The correlation coefficient was also computed using the median ADC values and FHR for all patients and time points pooled together.

The FLAIR and diffusion-weighted images were co-registered to a reference MRL T_1-weighted image and the FLAIR-to-reference transformation was then applied to the FLAIR contours. For greater concordance with the b-value range used in previous literature, the ADC maps were re-fitted from the co-registered DWI using b-values of [0,200,400,800] s/mm^2. A region of low ADC was defined from the maps by taking the largest connected component of the set of voxels within the region of FLAIR hyperintensity having an ADC less than 1.25 μm^2/ms (25). For those patients who exhibited progressive disease per RANO-HGG (26), the region of recurrent tumor was contoured on the first MRI scan at which progression occurred. The recurrent tumor was defined as the enhancing tumor for Grade 4 patients, and as the FHR for Grade 3 patients. For each patient, the T_1-weighted image at recurrence was registered to the reference MRL T_1-weighted image and the same transformation was applied to the contour of recurrent tumor. The overlap between low-ADC regions measured during radiotherapy and the region of recurrence was evaluated.

Overlap was quantified using the Dice score, as well as the sensitivity and positive predictive value (PPV) for the voxel-wise prediction of the region of recurrence by the low-ADC region. These metrics are given by the following equations:

$$\text{Dice} = \frac{2|A \cap R|}{|A| + |R|}$$

$$\text{Sensitivity} = \frac{|A \cap R|}{|R|}$$

$$\text{PPV} = \frac{|A \cap R|}{|A|}$$

Where A is the set of low-ADC voxels, R is the set of recurrence region voxels, $|\,|$ denotes the number of voxels in a set, and $A \cap R$ is the intersection of A and R. The sensitivity corresponds to the fraction of the recurrence region contained in the low-ADC region and the PPV with the fraction of the low-ADC region contained in the recurrence region.

Statistical analysis

Descriptive statistics were used to assess patient demographics, disease characteristics and treatment details. Categorical variables were expressed as counts and proportions, whereas continuous variables such as age and follow-up were expressed as median and range.

Time-to-death was calculated in months from the start date of radiation to date-of-death. Overall survival rates (OS) and progression-free-survival rates (PFS) were obtained using the Kaplan-Meier product-limit method. For OS, patients who were alive at time of analysis or who have become lost to follow-up were censored at their last follow-up date. PFS was defined as the time interval between the start date of radiation until date of disease progression (per RANO-HGG) (26) or death, whichever came first. If neither event had been observed, then the patient was censored at the date of last disease assessment. Statistical analysis was performed using open source statistical software R version 4.0.2 of R for Windows (The R Foundation for Statistical Computing, Vienna, Austria, 2022), and packages prodlim (v2019.11.13) and tableone (v0.12.0).

Results

All 10 HGG patients completed radiotherapy to a median dose of 60 Gy (range, 54 – 60 Gy) in 30 fractions (range, 30 – 33), receiving a total of 287 fractions on the MRL. Sixteen fractions were delivered with a conventional Linac as a result of either machine downtime or maintenance requirements. The mean in-room time per fraction was 37.3 minutes (range, 24.0 – 51.0 minutes) excluding post-beam research imaging, and 42.9 minutes (range, 25.0 – 69.0 minutes) when post-beam research imaging was performed. All patients met the independent dose check tolerance criterion. Nearly all (90%) received concurrent chemotherapy, and all patients received adjuvant chemotherapy. Patient, tumor, and treatment characteristics are summarized in Table 1, and treatment characteristics and clinical outcomes in Table 2. The median follow-up time was 25.1 months (range, 3.4 – 31.6 months). The 1-year and 2-year OS rates were 80.0% and 70.0%, respectively. The 1-year and 2-year PFS rates were 60.0% and 50.0%, respectively. No acute grade 3 or higher toxicities were observed.

For all patients, contours from each daily MRI were analyzed for tumor dynamics (n = 281 contours). The FHR dynamics are summarized in Figure 2. At the 10, 20, and 30-day post-1st fraction time points 3, 3, and 4 patients, respectively, had a FHR volume that changed by at least 20% relative to the 1st MRL fraction. A relative increase in volume of more than 250% in the FHR was observed in one patient during chemoradiation who required re-planning. In this patient, the change was also associated with a FHR migration distance of more than 25 mm.

Three patients (30%) on temozolomide (TMZ) concurrent with 6 weeks of radiation required re-planning between fractions 9 to 12 due to progression of tumor and/or edema identified on daily MRL imaging. More specifically, Patient 1 was a young woman with a large right frontal GBM, IDH-wild type, who underwent subtotal resection. Progression of edema and associated mass effect was noted on daily MRL FLAIR imaging, and adaptive re-planning performed at fraction 12. The gadolinium-enhanced MRI at the time of re-planning confirmed increased rim enhancement with diffusion restriction concerning for high cellularity. Dexamethasone dosing was increased with improvement in headaches and

TABLE 1 Summary of patient, tumor and treatment characteristics.

Characteristics	n = 10
Median age, years (range)	40.0 (29.0 – 69.0)
Gender	
Male	3 (30.0%)
Female	7 (70.0%)
WHO Tumor Classification	
GBM, IDH-wild type	4 (40.0%)
Astrocytoma, IDH-wild type, grade 3	2 (20.0%)
Astrocytoma, IDH-mutant, grade 4	2 (20.0%)
Astrocytoma, IDH-mutant, grade 3	1 (10.0%)
Oligodendroglioma, IDH-mutant, 1p/19q co-deleted	1 (10.0%)
MGMT Promoter Methylation	
Unmethylated	4 (40.0%)
Unknown	6 (60.0%)
Surgery	
Gross Total Resection	1 (10.0%)
Subtotal Resection	8 (80.0%)
Biopsy	1 (10.0%)
Median no. days from surgery to start of radiation (range)	23.5 (12.0 – 39.0)
Fractionation Scheme	
60 Gy/30 fractions	7 (70.0%)
59.4 Gy/33 fractions	1 (10.0%)
54 Gy/30 fractions	2 (20.0%)
Median % fractions completed on MRL (range)	96.8 (70.0 – 100.0)
Mean in-room time in minutes per fraction* (range)	37.3 (24.0 – 51.0)
Mean in-room time in minutes per fraction including post-beam research imaging (range)	42.9 (25.0 – 69.0)
Radiation Re-plan During Treatment	
Yes	3 (30.0%)
No	7 (70.0)
Chemotherapy	
Concurrent TMZ	9 (90.0%)
Adjuvant TMZ	10 (100.0%)

GBM, Glioblastoma; MRL, high-field MR-Linac; TMZ, Temozolomide.
*Excluding post-beam research imaging.

nausea, and the patient was transitioned to the new adapted plan on the MRL at fraction 15. There was no treatment interruption. Patient 4 was a young man with a right frontal opercular astrocytoma, IDH mutant (non-canonical), WHO grade 4 and underwent subtotal resection. At fraction 9, increased edema with midline shift was observed on the daily MRL FLAIR imaging. The patient's treatment was held for 2 days while he underwent re-planning and observation on high dose dexamethasone. He was transitioned to the new adapted plan on the MRL at fraction 10 given neurologic stability. Patient 10 was a young man with a left insula, primarily T_2-weighted hyperintense astrocytoma, IDH mutant, WHO grade 4 who underwent subtotal resection. Interval increased FLAIR hyperintensity surrounding the lesion, with increased midline shift compared to the reference planning images, was observed requiring re-planning at fraction 12. His dexamethasone dosing was adjusted, and he continued radiation with the adapted re-plan started at fraction 15 without any treatment interruption.

The trends of functional imaging parameters (n = 550 image sequences) during MRL treatment are summarized in Figure 3. The correlation between the median ADC value within the FHR and the volume of FHR was statistically significant for 6 of 10 patients ($p<.05$). The magnitude of the correlation coefficient exceeded 0.60 for these 6 patients. The median ADC and FHR volume were also significantly correlated when the data from all patients and time points were pooled ($R=0.68$, $p<.001$).

For each of the four patients who exhibited progressive disease during follow-up, the region of recurrence included most of the low-ADC region measured during treatment as illustrated in Figure 4. The positive predictive value, reflecting the fraction of the low-ADC region contained in the region of recurrence ranged from 43 – 94% over all patients/time points, and was greater than 68% by the final MRL fraction for all four patients. The sensitivity and Dice scores were lower (1 – 25% and 0.02-0.38, respectively) due to regions of recurrent tumor outside of the low-ADC region.

TABLE 2 Detailed patient treatment characteristics and clinical outcomes.

Patient	Diagnosis	Age	Surgery	RT Dose (Gy)/No. of Fx	Chemo (TMZ)	Re-plan During RT (Fx No. at transition to re-plan; Reason)	No. of Fx on delivered on MRL	Acute Toxicity	Oncologic Outcomes
1	GBM, IDH wild type	32	STR	60/30	Conc and Adj	Yes (15; tumor and edema progression)	27	Grade 2 headaches, nausea, fatigue	Died
2	GBM, IDH wild type	65	GTR	60/30	Conc and Adj	No	29	None	Died
3	GBM, IDH wild type	62	STR	60/30	Conc and Adj	No	30	None	Died
4	Astrocytoma, IDH mutant, WHO Grade 4	29	STR	60/30	Conc and Adj	Yes (10; edema with midline shift)	21	Grade 2 headaches, nausea, fatigue	Stable Disease
5	Astrocytoma, IDH mutant, WHO Grade 3	36	STR	60/30	Conc and Adj	No	30	None	Stable Disease
6	Oligodendroglioma, IDH mutant, 1p/19q co-deleted, WHO Grade 3	69	STR	59.4/33	Adj	No	32	None	Stable Disease
7	Astrocytoma, IDH wild type, WHO Grade 3	42	Biopsy	60/30	Conc and Adj	No	30	None	Progressed
8	GBM, IDH wild type	57	STR	60/30	Conc and Adj	No	30	None	Stable Disease
9	Astrocytoma, IDH wild type, WHO Grade 3	38	STR	54/30	Conc and Adj	No	29	None	Progressed
10	Astrocytoma, IDH mutant, WHO Grade 4	34	STR	54/30	Conc and Adj	Yes (15; edema)	29	Grade 1 headaches, nausea, fatigue	Stable Disease

RT, Radiation; Fx, Fractions; TMZ, Temozolomide; MRL, high-field MR-Linac; GBM, Glioblastoma; STR, Subtotal resection; GTR, Gross total resection; Conc, Concurrent; Adj, Adjuvant.

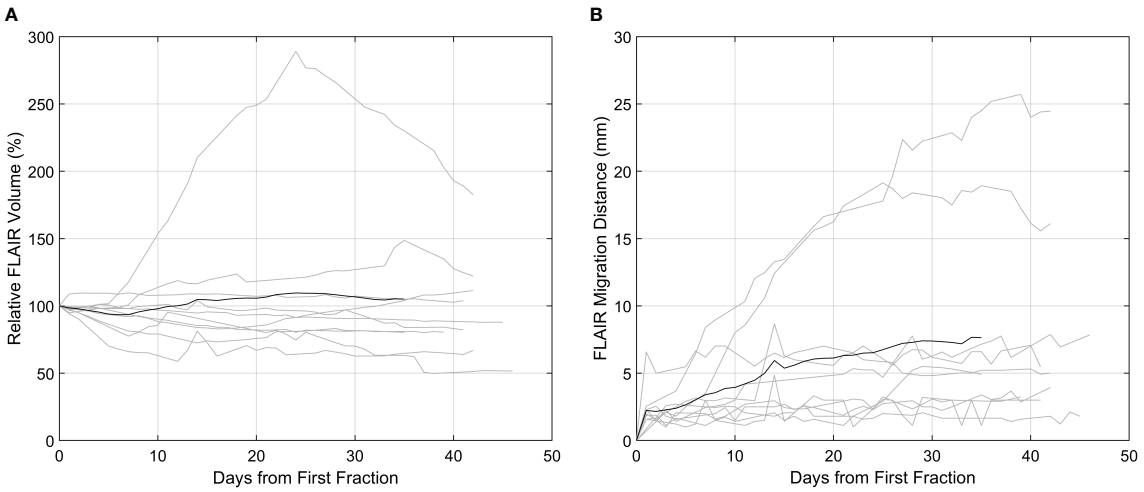

FIGURE 2
FLAIR hyperintense region (FHR) dynamics as captured on the high-field MR-Linac. In both plots, the patients (n = 10) are delineated by the grey lines, and the black line the mean across all patients. **(A)** T2-FLAIR hyperintense volume relative to the first fraction. **(B)** The migration distance relative to the first fraction.

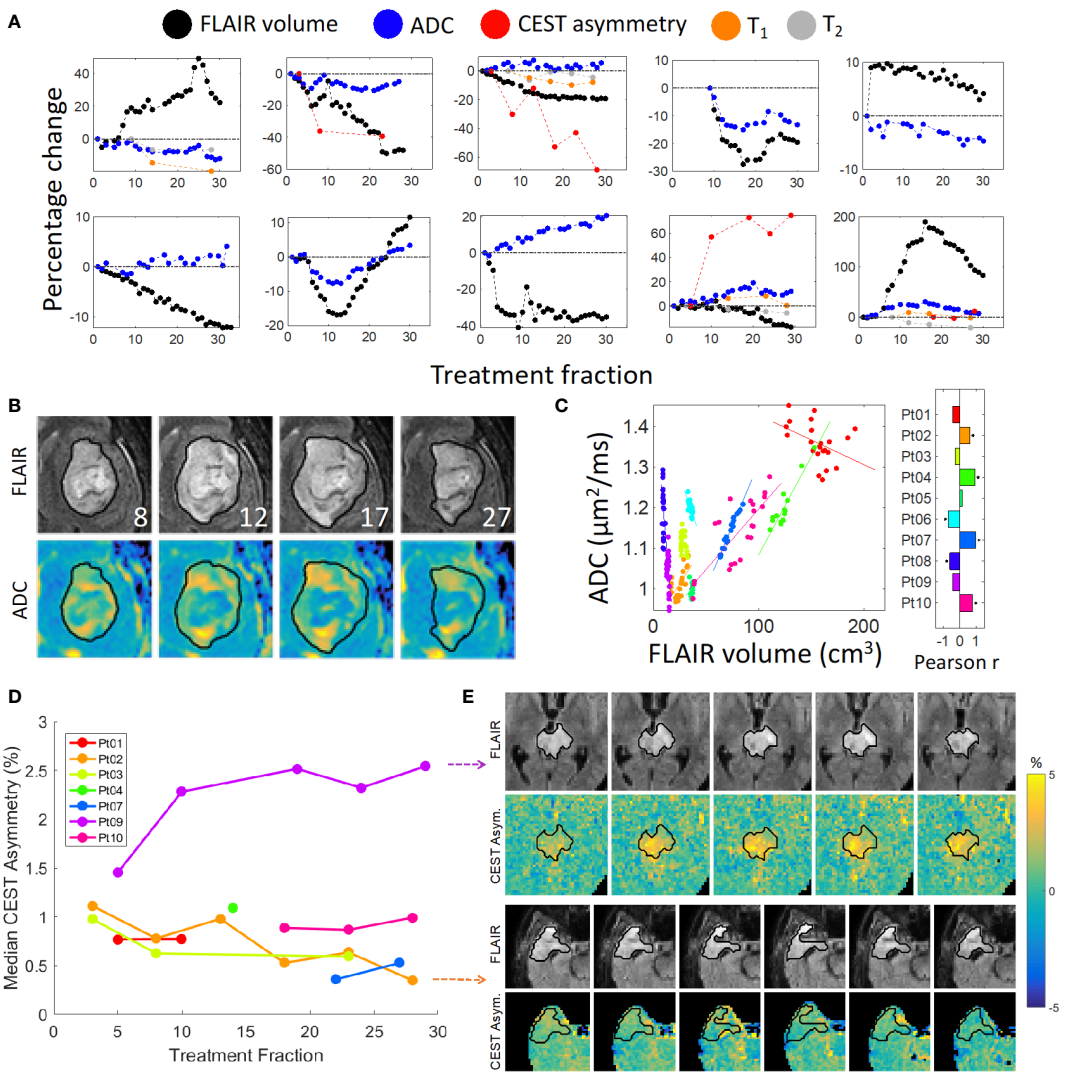

FIGURE 3
Quantitative imaging and FLAIR contours: **(A)** FLAIR volume and median functional parameter values plotted over time. Zoomed images are shown in **(B)** of the ADC maps for Patient 10 with corresponding FLAIR images with overlaid daily FLAIR contours (in black); the treatment fraction is shown in the lower-right corner of each FLAIR image. A plot of the ADC values vs FLAIR volumes is shown in **(C)**, where each color represents a different patient. The correlation coefficients are shown in the bar plot; an asterisk indicates a statistically significant correlation. **(D)** Median CEST asymmetry with respect to treatment fraction computed over a single slice for the time points with available CEST imaging. Zoomed images are shown for Patient 2 (bottom panel) and Patient 9 (top panel) over time in **(E)** exhibiting decreasing and increasing asymmetry, respectively.

Discussion

Daily MRI-guided radiation treatment delivery permits online visualization of tumor- and treatment-related temporal changes for HGG patients, which cannot be adequately identified on CT-guided radiation delivery systems. The present study is the first reported clinical series of HGG patients treated with radiotherapy on a high field strength MRL. The ATP workflow and treatment times were clinically acceptable and significant anatomic changes were noted in three of the ten patients which triggered adaptive re-planning. Our observations support the potential for this technology to improve outcomes.

All patients in this study completed radiotherapy as planned with over 96% of fractions delivered on the MRL. Remaining fractions were delivered on conventional Linacs due to machine maintenance or downtime. Despite early concerns of claustrophobia or discomfort as a result of prolonged treatment times on the MRL, no patient discontinued treatment. The tissue-air interface effects have been elucidated

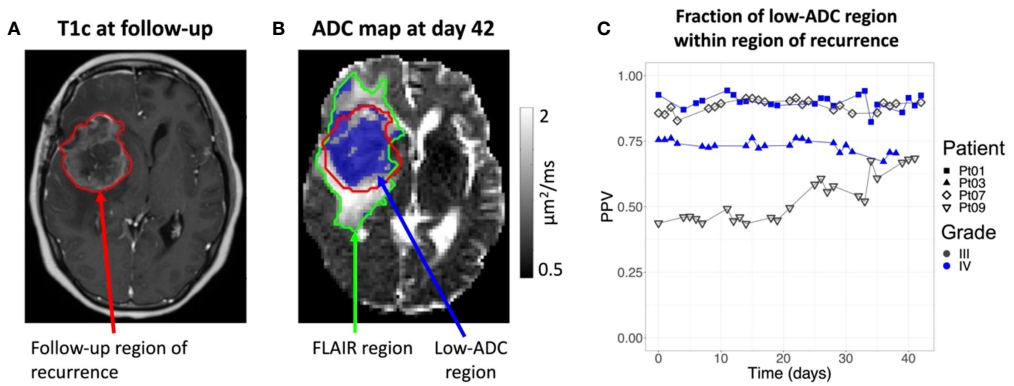

FIGURE 4
Overlap between intra-treatment low-ADC regions and recurrent tumor: **(A)**: The post-contrast T_1-weighted image (T1c) of Patient 1 from a diagnostic scanner with the region of recurrence indicated by the red contour. Note that the recurrence region was taken as the enhancing tumor for the Grade 4 patients and the FLAIR hyperintensity for the Grade 3 patients. **(B)**: The ADC map from the MR-Linac for Day 42 from first fraction of radiotherapy, corresponding to the last day of radiation for Patient 1, with the future recurrence region (red contour), FLAIR region (green contour), and low-ADC region (blue colorwash). The low-ADC region is mostly contained in the recurrence region. **(C)**: The positive predictive value (PPV) over time for the voxel-wise prediction of the recurrence region by the low-ADC region. By the end of treatment, most of the low-ADC region is contained within the recurrence region for all patients.

in prior planning and *in-vivo* studies suggesting the potential for increased skin and/or air sinus toxicities, but no unexplained toxicities were observed in this cohort (27, 28). Clinically, the treatments were well tolerated with only 2 patients reporting grade 2 acute headaches, nausea and/or fatigue, and 1 patient reporting acute grade 1 symptoms. No acute grade 3 or higher toxicities were observed in this series.

Whether or not tumor- and/or treatment-related temporal changes within the target volume during radiotherapy occur, and if they can lead to geographical misses and compromise patient outcomes, has been an unanswered question. In GBM patients undergoing concurrent chemoradiation over 6 to 6.5 weeks, studies have shown meaningful changes in target dynamics which can occur early in the treatment course (17, 29). Stewart et al. reported a migration distance greater than 5 mm in 46% and 54% of patients for the GTV and CTV, respectively, at fraction 10. Morphologic changes were observed wherein 40% of patients demonstrated a decreased GTV yet with a migration distance of > 5 mm. These data suggest that the majority of target changes occur between time of planning and fraction 10 (17). Bernchou et al. showed similar findings, noting a median maximum distance of > 5 mm between the GTVs at fractions 10, 20, and 30, compared to the original planning GTV (29). These studies provide support for treatment and evaluation of HGG patients with daily MRI guidance with adaptive re-planning as a strategy to account for tumor dynamics. Inter-fraction dynamics may be of critical importance in trials evaluating the safety of CTV margin reduction, as opposed to treatments based on current and historical practices of including 1.5 to 3.0 cm of normal brain tissue in the radiotherapy volume (29).

The present study demonstrated that FHR dynamics can be captured on the MRL, and at least 30% of patients in the study cohort at some point during the treatment course showed a change in FHR volume by 20% or more relative to the 1st fraction. Since gadolinium was not routinely given during the ATP treatment workflow, GTV dynamics could not be assessed in a similar fashion as the prior report by Stewart et al. (17) Importantly, findings noted on daily MRL FLAIR imaging triggered adaptive re-planning in three (30%) patients between fractions 9 to 12, which also led to adjustment in clinical management with respect to steroid dosing as the patients were symptomatic. The relatively early timing of the observed changes was in line with the prior prospective imaging studies. Furthermore, large inter-patient variability in FLAIR hyperintensity dynamics can be observed during the treatment course, and very few patients' temporal dynamics were closely approximated by that of the mean relative change across the cohort. In one patient (Patient 10), a rapid change in the relative volume of the FHR by nearly 100% was observed between fractions 10 to 20. Hence, the data highlights the benefit of per-fraction daily MR imaging on the MRL in this patient population.

Recent reports from our institution demonstrated feasibility of CEST MRI and DWI acquisition on the MRL for CNS tumors (21, 23), and the current study reporting our initial clinical experience confirms successful acquisition of other multi-parametric image sequences including MT and BOLD resting-state fMRI during routine treatment workflow. ADC parameter changes could be reliably tracked during radiotherapy, and correlation was observed between the median ADC and FHR volumes across all patients and time points. GBM is known to

extend beyond the T_1-weighted contrast-enhancing region on MRI, and outcomes have been correlated with FLAIR abnormalities (30–32). Studies have established an inverse relationship between ADC and glioma cellularity (33–35), therefore, high ADC regions may indicate less cellular tumor within the FHR; however, it is acknowledged that as ADC is not specific to tumor cellularity, elevated ADC may also represent regions of increased edema (36). Therefore, the mixed positive and negative correlation observed between the median ADC and FHR volumes in this series may reflect a combination of tumor cellularity/density and the presence of edema, but a larger sample size is needed to better characterize in future studies. Similarly, association between ADC changes and survival outcomes in HGG have been previously reported (25, 37, 38). This was the first clinical series with daily FLAIR imaging throughout the entire course of radiation as part of the standard treatment workflow. In those patients who developed progressive or recurrent disease, the PPV (corresponding to the fraction of the low-ADC region contained within the region of recurrence) was greater than 68% by the final MRL fraction. Low sensitivity, nonetheless, was observed indicating that tumor recurrence was not confined to only areas of low-ADC. These preliminary findings underscore the importance of further evaluation pending mature clinical outcomes data to better define the role of multi-parametric functional imaging.

The most common pattern of recurrence for HGG post radiation is within or adjacent to the original tumor bed (39, 40). Although the dominant pattern of failure is within the GTV, causes of marginal failures may include positional mis-registration between the volume intended to receive the prescription dose and the actual treated volume, anatomical deformations, and unrecognized tumor progression due to lack of MR guidance at time of treatment delivery. These potential errors could compound over several weeks of treatment. Azoulay et al. reported a 5-fraction course of stereotactic radiation concurrent with TMZ in GBM patients using a 5 mm CTV margin as opposed to the standard 1.5 – 2.0 cm CTV margin approach, which represented a novel approach (41). With a reported marginal failure rate of 11%, the data lent support for possible CTV margin reduction. Patients on this study were treated with standard margins and the intent of the MRL adaptive radiotherapy was to reduce the normal tissue irradiated by compensating for tumor dynamics. An ATP treatment workflow for HGG patients on the MRL enables improved image guidance over that of conventional cone-beam CT-based Linac, but discernment of tumor progression remains challenging in the absence of intravenous contrast. Our ongoing MRL adaptive radiotherapy trial known as UNITED (UNIty-Based MR-Linac Guided AdapTive RadiothErapy for High GraDe Glioma: A phase 2 Trial, NCT04726397), investigates adaptive ATS MRI-guided radiation treatment. The trial is fundamentally based on applying a reduced CTV margin of 5 mm with the option of encompassing adjacent FLAIR signal as a part of the CTV as a personalized approach, and weekly fully re-contoured and re-optimized ATS treatment plans using the on-line gadolinium enhanced T_1-weighted MRI sequence. Therefore, personalized adapted treatment plans are generated which assures safety of this strategy with the primary endpoint being the patterns of failure.

Our first report of treating HGG patients on the MRL is encouraging with no unexpected grade 3 or higher acute toxicities, and three out of the ten patients were re-planned due to significant changes that would have otherwise resulted in geographical miss. A notable strength of the study is the rigorous follow-up of all patients on the MOMENTUM registry study, with prospective collection of clinical outcomes data including toxicities. Unlike prior studies using a sampling of time points during treatment, temporal variations and functional parameter values from quantitative imaging were successfully evaluated on daily online imaging. Nevertheless, we acknowledge several limitations. The sample size is small and the cohort comprises mixed tumor histological and molecular diagnoses and, therefore, conclusions cannot yet be drawn regarding oncological outcomes. Selection bias could have been present in those patients selected for treatment on the MRL versus those who were ineligible due to contraindications to MRI or other reasons. Finally, significant variability was observed in the temporal trends of the median functional parameter values across the cohort, which can be attributed to the small number of patients and the mixed WHO tumor types and grades. However, we established the feasibility of multi-parametric imaging acquisition on the MRL which will be used in future work to determine if these functional maps can lead to more precise targets for dose escalation or de-escalation.

In conclusion, we report the first clinical series of HGG patients treated with radiotherapy on the Unity 1.5 T high field strength MRL. The ATP workflow and treatment times were clinically acceptable, and daily online MRL imaging triggered adaptive re-planning for selected patients. Acquisition of multi-parametric imaging sequences was feasible on the MRL during routine treatment workflow. ADC parameter changes could be reliably tracked during radiotherapy. Prospective clinical outcomes data based on personalized adapted treatment plans is anticipated from the ongoing UNITED phase 2 trial to further refine the role of MR-guided adaptive radiotherapy on the MRL.

Data availability statement

The raw data supporting the conclusions of this article will be made available by the authors, without undue reservation.

Ethics statement

The studies involving human participants were reviewed and approved by the institutional ethics review board at Sunnybrook Health Sciences Centre and all patients provided written consent

to be enrolled on the MOMENTUM trial, an international prospective registry designed to facilitate evidence-based implementation of the first MRL and collect outcomes data. The patients/participants provided their written informed consent to participate in this study. Written informed consent was obtained from the individual(s) for the publication of any potentially identifiable images or data included in this article.

Author contributions

Study concept and design: C-LT, AS. Data collection: C-LT, HC, JS, AL, RC, LL. Data analysis and interpretation: C-LT, HC, JS, AL, RC, LL, AS. Initial draft: C-LT, JS, LL, BK, AS. Revision and approval: All authors contributed to the final writing and revision of the manuscript.

Conflict of interest

C-LT has received travel accommodations/expenses & honoraria for past educational seminars by Elekta and belongs to the Elekta MR-Linac Research Consortium. JS is employed at Sunnybrook Health Sciences Centre, Toronto, Ontario, Canada. SM has received research support from Novartis AG, honoraria from Novartis AG and Ipsen and travel support from Elekta, none related to this work. SD serves as the Provincial Lead for CNS Oncology at Ontario Health, Cancer Care Ontario; he receives laboratory research support from Alkermes; he serves on the advisory board of the Subcortical Surgery Group and Xpan Medical; he is a speaker for the Congress of Neurological Surgeons. MR is a co-inventor of and owns associated intellectual property specific to the image-guidance system on the Gamma Knife Icon, none related to this work. AS has been a consultant for Varian, Elekta Gamma Knife Icon, BrainLAB, Merck, Abbvie, Roche; Vice President of the International Stereotactic Radiosurgery Society ISRS; Co-Chair of the AO Spine Knowledge Forum Tumor; received honorarium for past educational seminars for AstraZeneca, Elekta AB, Varian, BrainLAB, Accuray, Seagen Inc.; research grant with Elekta AB, Varian, Seagen Inc., BrainLAB; and travel accommodations/expenses with Elekta, Varian and BrainLAB. AS also belongs to the Elekta MR Linac Research Consortium and is a Clinical Steering Committee Member, and chairs the Elekta Oligometastases Group and the Elekta Gamma Knife Icon Group.

The remaining authors declare that the research was conducted in the absence of any commercial or financial relationships that could be construed as a potential conflict of interest.

Publisher's note

Supplementary material

The Supplementary Material for this article can be found online at: https://www.frontiersin.org/articles/10.3389/fonc.2022.1060098/full#supplementary-material

References

1. Lagendijk JJW, Raaymakers BW, Van Den Berg CAT, Moerland MA, Philippens ME, Van Vulpen M. MR guidance in radiotherapy. *Phys Med Biol* (2014) 59(21):R349–69. doi: 10.1088/0031-9155/59/21/R349

2. Raaymakers BW, Lagendijk JJW, Overweg J, Kok JGM, Raaijmakers AJE, Kerkhof EM, et al. Integrating a 1.5 T MRI scanner with a 6 MV accelerator: Proof of concept. *Phys Med Biol* (2009) 54(12):N229–37. doi: 10.1088/0031-9155/54/12/N01

3. Winkel D, Bol GH, Kroon PS, van Asselen B, Hackett SS, Werensteijn-Honingh AM, et al. Adaptive radiotherapy: The elekta unity MR-linac concept. *Clin Transl Radiat Oncol* (2019) 18:54–9. doi: 10.1016/j.ctro.2019.04.001

4. Mehrabian H, Myrehaug S, Soliman H, Sahgal A, Stanisz GJ. Evaluation of glioblastoma response to therapy with chemical exchange saturation transfer. *Int J Radiat Oncol Biol Phys* (2018) 101(3):713–23. doi: 10.1016/j.ijrobp.2018.03.057

5. Mehrabian H, Myrehaug S, Soliman H, Sahgal A, Stanisz GJ. Quantitative magnetization transfer in monitoring glioblastoma (GBM) response to therapy. *Sci Rep* (2018) 8(1):1–11. doi: 10.1038/s41598-018-20624-6

6. Mehrabian H, Desmond KL, Soliman H, Sahgal A, Stanisz GJ. Differentiation between radiation necrosis and tumor progression using chemical exchange saturation transfer. *Clin Cancer Res* (2017) 23(14):3667–75. doi: 10.1158/1078-0432.CCR-16-2265

7. Karami E, Soliman H, Ruschin M, Sahgal A, Myrehaug S, Tseng CL, et al. Quantitative MRI biomarkers of stereotactic radiotherapy outcome in brain metastasis. *Sci Rep* (2019) 9(1):19830. doi: 10.1038/s41598-019-56185-5

8. Detsky JS, Keith J, Conklin J, Symons S, Myrehaug S, Sahgal A, et al. Differentiating radiation necrosis from tumor progression in brain metastases treated with stereotactic radiotherapy: utility of intravoxel incoherent motion perfusion MRI and correlation with histopathology. *J Neurooncol* (2017) 134 (2):433–41. doi: 10.1007/s11060-017-2545-2

9. Desmond KL, Mehrabian H, Chavez S, Sahgal A, Soliman H, Rola R, et al. Chemical exchange saturation transfer for predicting response to stereotactic radiosurgery in human brain metastasis. *Magn Reson Med* (2017) 78(3):1110–20. doi: 10.1002/mrm.26470

10. Chan RW, Chen H, Myrehaug S, Atenafu EG, Stanisz GJ, Stewart J, et al. Quantitative CEST and MT at 1.5T for monitoring treatment response in glioblastoma: early and late tumor progression during chemoradiation. *J Neurooncol* (2021) 151(2):267–78. doi: 10.1007/s11060-020-03661-y

11. Kerkmeijer LGW, Fuller CD, Verkooijen HM, Verheij M, Choudhury A, Harrington KJ, et al. The MRI-linear accelerator consortium: Evidence-based clinical introduction of an innovation in radiation oncology connecting

researchers, methodology, data collection, quality assurance, and technical development. *Front Oncol* (2016) 6:215. doi: 10.3389/fonc.2016.00215

12. Perry JR, Laperriere N, O'Callaghan CJ, Brandes AA, Menten J, Phillips C, et al. Short-course radiation plus temozolomide in elderly patients with glioblastoma. *N Engl J Med* (2017) 376(11):1027–37. doi: 10.1056/nejmoa1611977

13. Van Den Bent MJ, Brandes AA, Taphoorn MJB, Kros JM, Kouwenhoven MCM, Delattre JY, et al. Adjuvant procarbazine, lomustine, and vincristine chemotherapy in newly diagnosed anaplastic oligodendroglioma: Long-term follow-up of EORTC brain tumor group study 26951. *J Clin Oncol* (2013) 31 (3):344–50. doi: 10.1200/JCO.2012.43.2229

14. van den Bent MJ, Tesileanu CMS, Wick W, Sanson M, Brandes AA, Clement PM, et al. Adjuvant and concurrent temozolomide for 1p/19q non-co-deleted anaplastic glioma (CATNON; EORTC study 26053-22054): second interim analysis of a randomised, open-label, phase 3 study. *Lancet Oncol* (2021) 22 (6):813–23. doi: 10.1016/S1470-2045(21)00090-5

15. Cairncross G, Wang M, Shaw E, Jenkins R, Brachman D, Buckner J, et al. Phase III trial of chemoradiotherapy for anaplastic oligodendroglioma: Long-term results of RTOG 9402. *J Clin Oncol* (2013) 31(3):337–43. doi: 10.1200/JCO.2012.43.2674

16. Stupp R, Mason WP, van den Bent MJ, Weller M, Fisher B, Taphoorn MJB, et al. Radiotherapy plus concomitant and adjuvant temozolomide for glioblastoma. *N Engl J Med* (2005) 352(10):987–96. doi: 10.1056/NEJMoa043330

17. Stewart J, Sahgal A, Lee Y, Soliman H, Tseng CL, Detsky J, et al. Quantitating interfraction target dynamics during concurrent chemoradiation for glioblastoma: A prospective serial imaging study. *Int J Radiat Oncol Biol Phys* (2021) 109(3):736–46. doi: 10.1016/j.ijrobp.2020.10.002

18. Tseng CL, Stewart J, Whitfield G, Verhoeff JJC, Bovi J, Soliman H, et al. Glioma consensus contouring recommendations from a MR-linac international consortium research group and evaluation of a CT-MRI and MRI-only workflow. *J Neurooncol* (2020) 149(2):305–14. doi: 10.1007/s11060-020-03605-6

19. de Mol van Otterloo SR, Christodouleas JP, Blezer ELA, Akhiat H, Brown K, Choudhury A, et al. Patterns of care, tolerability, and safety of the first cohort of patients treated on a novel high-field MR-linac within the MOMENTUM study: Initial results from a prospective multi-institutional registry. *Int J Radiat Oncol Biol Phys* (2021) 111(4):867–75. doi: 10.1016/j.ijrobp.2021.07.003

20. Ahmad SB, Sarfehnia A, Paudel MR, Kim A, Hissoiny S, Sahgal A, et al. Evaluation of a commercial MRI linac based Monte Carlo dose calculation algorithm with geant 4. *Med Phys* (2016) 43(2):894–907. doi: 10.1118/1.4939808

21. Lawrence LSP, Chan RW, Chen H, Keller B, Stewart J, Ruschin M, et al. Accuracy and precision of apparent diffusion coefficient measurements on a 1.5 T MR-linac in central nervous system tumour patients. *Radiother Oncol* (2021) 164:155–62. doi: 10.1016/j.radonc.2021.09.020

22. Veraart J, Sijbers J, Sunaert S, Leemans A, Jeurissen B. Weighted linear least squares estimation of diffusion MRI parameters: Strengths, limitations, and pitfalls. *Neuroimage* (2013) 81:335–46. doi: 10.1016/j.neuroimage.2013.05.028

23. Chan RW, Lawrence LSP, Oglesby RT, Chen H, Stewart J, Theriault A, et al. Chemical exchange saturation transfer MRI in central nervous system tumours on a 1.5 T MR-linac. *Radiother Oncol* (2021) 162:140–9. doi: 10.1016/j.radonc.2021.07.010

24. Liberman G, Louzoun Y, Ben Bashat D. T1 mapping using variable flip angle SPGR data with flip angle correction. *J Magn Reson Imaging* (2014) 40(1):171–80. doi: 10.1002/jmri.24373

25. Chenevert TL, Malyarenko DI, Galbán CJ, Gomez-Hassan DM, Sundgren PC, Tsien CI, et al. Comparison of voxel-wise and histogram analyses of glioma ADC maps for prediction of early therapeutic change. *Tomogr (Ann Arbor Mich)* (2019) 5(1):7–14. doi: 10.18383/j.tom.2018.00049

26. Wen PY, Macdonald DR, Reardon DA, Cloughesy TF, Sorensen AG, Galanis E, et al. Updated response assessment criteria for high-grade gliomas: Response assessment in neuro-oncology working group. *J Clin Oncol* (2010) 28 (11):1963–72. doi: 10.1200/JCO.2009.26.3541

27. Tseng C-L, Eppinga W, Seravalli E, Hackett S, Brand E, Ruschin M, et al. Dosimetric feasibility of the hybrid magnetic resonance imaging (MRI)-linac system (MRL) for brain metastases: The impact of the magnetic field. *Radiother Oncol* (2017) 125(2):273–9. doi: 10.1016/j.radonc.2017.09.036

28. Wang MH, Kim A, Ruschin M, Tan H, Soliman H, Myrehaug S, et al. Comparison of prospectively generated glioma treatment plans clinically delivered on magnetic resonance imaging (MRI) -linear accelerator (MR-linac) versus conventional Linac: Predicted and measured skin dose. *Technol Cancer Res Treat* (2022) 21:1–10. doi: 10.1177/15330338221124695

29. Bernchou U, Arnold TST, Axelsen B, Klüver-Kristensen M, Mahmood F, Harbo FSG, et al. Evolution of the gross tumour volume extent during radiotherapy for glioblastomas. *Radiother Oncol* (2021) 160:40–6. doi: 10.1016/j.radonc.2021.04.001

30. Kim EY, Yechieli R, Kim JK, Mikkelsen T, Kalkanis SN, Rock J, et al. Patterns of failure after radiosurgery to two different target volumes of enhancing lesions with and without FLAIR abnormalities in recurrent glioblastoma multiforme. *J Neurooncol* (2014) 116(2):291–7. doi: 10.1007/s11060-013-1290-4

31. Elson A, Bovi J, Siker M, Schultz C, Paulson E. Evaluation of absolute and normalized apparent diffusion coefficient (ADC) values within the post-operative T2/FLAIR volume as adverse prognostic indicators in glioblastoma. *J Neurooncol* (2015) 122(3):549–58. doi: 10.1007/s11060-015-1743-z

32. Marko NF, Weil RJ, Schroeder JL, Lang FF, Suki D, Sawaya RE. Extent of resection of glioblastoma revisited: Personalized survival modeling facilitates more accurate survival prediction and supports a maximum-safe-resection approach to surgery. *J Clin Oncol* (2014) 32(8):774–82. doi: 10.1200/JCO.2013.51.8886

33. Sugahara T, Korogi Y, Kochi M, Ikushima I, Shigematu Y, Hirai T, et al. Usefulness of diffusion-weighted MRI with echo-planar technique in the evaluation of cellularity in gliomas. *J Magn Reson Imaging* (1999) 9(1):53–60. doi: 10.1002/(SICI)1522-2586(199901)9:1<53::AID-JMRI7>3.0.CO;2-2

34. Ellingson BM, Malkin MG, Rand SD, Connelly JM, Quinsey C, LaViolette PS, et al. Validation of functional diffusion maps (fDMs) as a biomarker for human glioma cellularity. *J Magn Reson Imaging* (2010) 31(3):538–48. doi: 10.1002/jmri.22068

35. Chenevert TL, Lauren D, Taylor JMG, Robertson PL, Greenberg HS, Rehemtulla A, et al. Resonance Imaging: an early surrogate marker of brain tumors Background: A surrogate marker for treatment response that can be observed earlier than comparison of se- quential magnetic resonance imaging (MRI) scans , which depends on rela- tively sl. (2000) 92(24):2029–36. doi: 10.1093/jnci/92.24.2029

36. Muti M, Aprile I, Principi M, Italiani M, Guiducci A, Giulianelli G, et al. Study on the variations of the apparent diffusion coefficient in areas of solid tumor in high grade gliomas. *Magn Reson Imaging* (2002) 20(9):635–41. doi: 10.1016/S0730-725X(02)00594-5

37. Moffat BA, Chenevert TL, Lawrence TS, Meyer CR, Johnson TD, Dong Q, et al. Functional diffusion map: A noninvasive MRI biomarker for early stratification of clinical brain tumor response. *Proc Natl Acad Sci U S A.* (2005) 102(15):5524–9. doi: 10.1073/pnas.0501532102

38. Hamstra DA, Galbán CJ, Meyer CR, Johnson TD, Sundgren PC, Tsien C, et al. Functional diffusion map as an early imaging biomarker for high-grade glioma: Correlation with conventional radiologic response and overall survival. *J Clin Oncol* (2008) 26(20):3387–94. doi: 10.1200/JCO.2007.15.2363

39. Bette S, Barz M, Huber T, Straube C, Schmidt-Graf F, Combs SE, et al. Retrospective analysis of radiological recurrence patterns in glioblastoma, their prognostic value and association to postoperative infarct volume. *Sci Rep* (2018) 8 (1):1–12. doi: 10.1038/s41598-018-22697-9

40. Gebhardt BJ, Dobelbower MC, Ennis WH, Bag AK, Markert JM, Fiveash JB. Patterns of failure for glioblastoma multiforme following limited-margin radiation and concurrent temozolomide. *Radiat Oncol* (2014) 9(1):1–6. doi: 10.1186/1748-717X-9-130

41. Azoulay M, Chang SD, Gibbs IC, Hancock SL, Pollom EL, Harsh GR, et al. A phase I/II trial of 5-fraction stereotactic radiosurgery with 5-mm margins with concurrent temozolomide in newly diagnosed glioblastoma: Primary outcomes. *Neuro Oncol* (2020) 22(8):1182–9. doi: 10.1093/neuonc/noaa019

frontiers | Frontiers in Oncology

TYPE Original Research
PUBLISHED 29 November 2022
DOI 10.3389/fonc.2022.867792

OPEN ACCESS

EDITED BY
Enis Ozyar,
Acıbadem University, Turkey

REVIEWED BY
Charlotte Robert,
Institut Gustave Roussy, France
Raphael Pfeffer,
Assuta Medical Center, Israel

*CORRESPONDENCE
Amedeo Capotosti
amedeo.capotosti@policlinicogemelli.it

SPECIALTY SECTION
This article was submitted to Radiation Oncology, a section of the journal Frontiers in Oncology

RECEIVED 01 February 2022
ACCEPTED 07 November 2022
PUBLISHED 29 November 2022

CITATION
Nardini M, Capotosti A, Mazzoni LN, Cusumano D, Boldrini L, Chiloiro G, Romano A, Valentini V, Indovina L and Placidi L (2022) Tuning the optimal diffusion-weighted MRI parameters on a 0.35-T MR-Linac for clinical implementation: A phantom study. *Front. Oncol.* 12:867792. doi: 10.3389/fonc.2022.867792

Tuning the optimal diffusion-weighted MRI parameters on a 0.35-T MR-Linac for clinical implementation: A phantom study

Matteo Nardini[1], Amedeo Capotosti[1]*, Lorenzo Nicola Mazzoni[2], Davide Cusumano[1,3], Luca Boldrini[1], Giuditta Chiloiro[1], Angela Romano[1], Vincenzo Valentini[1], Luca Indovina[1] and Lorenzo Placidi[1]

[1]Fondazione Policlinico Universitario "Agostino Gemelli" Istituto di Ricovero e Cura a Carattere Scientifico (IRCCS), Rome, Italy, [2]Azienda Unità Sanitaria Locale (AUSL) Toscana Centro, Medical Physics Unit, Prato-Pistoia, Italy, [3]Mater Olbia Hospital, UOS Fisica Medica, Olbia, Italy

Purpose: This study aims to assess the quality of a new diffusion-weighted imaging (DWI) sequence implemented on an MR-Linac MRIdian system, evaluating and optimizing the acquisition parameters to explore the possibility of clinically implementing a DWI acquisition protocol in a 0.35-T MR-Linac.

Materials and methods: All the performed analyses have been carried out on two types of phantoms: a homogeneous 24-cm diameter polymethylmethacrylate (PMMA) sphere (SP) and a homemade phantom (HMP) constating in a PMMA cylinder filled with distilled water with empty sockets into which five cylindrical vials filled with five different concentrations of methylcellulose water solutions have been inserted. SP was used to evaluate the dependence of diffusion gradient inhomogeneity artifacts on gantry position. Four diffusion sequences with *b*-values of 500 s/mm^2 and 3 averages have been acquired: three with diffusion gradients in the three main directions (phase direction, read direction, slice direction) and one with the diffusion gradients switched off. The dependence of diffusion image uniformity and SNR on the number of averages in the MR sequences was also investigated to determine the optimal number of averages. Finally, the ADC values of HMP have been computed and then compared between images acquired in the scanners at 0.35 and 1.5 T.

Results: In order to acquire high-quality artifact-free DWI images, the "slice" gradient direction has been identified to be the optimal one and 0° to be the best gradient angle. Both the SNR ratio and the uniformity increase with the number of averages. A threshold value of 80 for SNR and 85% for uniformity was adopted to choose the best number of averages. By making a compromise between time and quality and limiting the number of *b*-values, it is possible to

reduce the acquisition time to 78 s. The Passing–Bablok test showed that the two methods, with 0.35 and 1.5 T scanners, led to similar results.

Conclusion: The quality of the DWI has been accurately evaluated in relation to different sequence parameters, and optimal parameters have been identified to select a clinical protocol for the acquisition of ADC maps sustainable in the workflow of a hybrid radiotherapy system with a 0.35-T MRI scanner.

KEYWORDS

MRI, DWI, MR-linac, diffusion, ADC, MRgRT

Introduction

Magnetic resonance (MR) diffusion-weighted imaging (DWI) is a very versatile technique widely used for the diagnosis of many types of malignancy (1–5). DWI signal is sensitive to the Brownian incoherent motion of water molecules due to thermal kinetic energy and to multiple-scale microscopic physiological motions, by applying diffusion-sensitizing gradients (6). It provides a quantitative measurement of the diffusivity of water molecules by means of the apparent diffusion coefficient (ADC). Moreover, DWI is also a very valued technique for assessing the response to chemo and radiotherapy of many different types of tumor because of its sensitivity to early detection of response to therapy, even in conjunction with other MR-based imaging biomarkers (7–9). Furthermore, DWI is also used in radiotherapy for the prediction of toxicity in healthy tissues and for the construction of normal tissue complication probability models (10). Also, radiomics analyses showed promising results when applied to DW images: the extracted features have been used to train predictive models in many recent studies (11–13). In the era of magnetic resonance-guided radiotherapy (MRgRT), DWI is a perfect candidate to be included in an adaptive radiotherapy protocol (14), providing quantitative information to better adapt the daily dose distribution, considering not only the anatomical variation but also the quantitative ADC variation of the target's tissue. Such an upgrade would greatly increase the value of the treatment in terms of personalization of the therapy. Nevertheless, DWI is still not implemented to clinically support MRgRT: in fact, up to date, few studies have been carried out on low-field MR systems to assess the reliability of DWI sequences (15–17). It is known that there are many sources of biases that influence the precision of DW images and, consequently, the reliability of the ADC estimation even in high-field MR systems devoted to medical imaging. Many of these depend on the MR system and on the acquisition sequence. The main ones are as follows:

- the signal-to-noise ratio (SNR), which decreases as the *b*-value increases (i.e., when the intensity of the diffusion gradients increases, producing a loss of phase coherence of the spins in the transverse plane and therefore a loss of SNR) (18);
- the image distortions, which strongly depend on the echo-planar readout of the most common DWI sequences and which are strongly affected by local non-uniformities of the static field (19);
- the gradient fields linearity along the three orthogonal spatial directions, which generates different effective *b*-values and image distortions (20).

Many optimization and correction strategies, as well as QA protocols, have been defined to monitor these effects and control the uncertainty of ADC measurements and possible related biases on high-field clinical MR systems (21–25). The same should be done for MR-Linacs, taking into account the peculiarities of these hybrid systems. In fact, the MR-Linac system is extremely complex: the integration of a linear accelerator and a magnetic resonance scanner in a single Faraday cage leads to several difficulties in obtaining good-quality images (26). The Linac is arranged on a circular crown arranged between two superconducting magnets that generate the field (27). Particular attention must be paid to the static field uniformity during the acquisition of images. In fact, field uniformity can be significantly affected by the movement of the ferromagnetic structure of the Linac, and image quality can be therefore dependent on the position of the Linac gantry head. For these reasons, it is necessary to characterize the MR-Linac system and optimize the DWI acquisition sequence considering the construction characteristics of the hybrid systems under examination, to obtain the desired results in terms of image quality (22). This work must be carried out by means of phantom measurements before translating the results onto the patient and also to separate the sources of uncertainty that depend on the patient (movement, breath, physiological

microscopic motions, etc.) from those that depend on the MR system and on the acquisition sequence. Given this background, this study aims to assess the quality of a new DWI sequence implemented on an MR-Linac MRIdian system, evaluating and optimizing the acquisition parameters to explore the possibility of clinically implementing a DWI acquisition protocol in a 0.35-T MR-Linac.

Materials and methods

Sequences

All measurements were conducted in a 0.35-T MR-Linac system (MRIdian, ViewRay Inc., Mountain View, CA, USA). Since the DWI sequence is still not available clinically, all the measurements were performed in the MRI mode, disconnecting the MR scanner from the Linac and using the onboard scanner software (Syngo MR B19 DHHS, Siemens). In this modality, the MR software allowed the acquisition of DWI sequences with different types of fields of view (FOV), square or rectangular, and a slice thickness ranging from 6 to 10 mm. All the sequences used a twice-refocused spin echo (TRSE) diffusion scheme (28) with a ratio between the repetition time (TR) and echo time (TE) of 2000/5.4 and a bandwidth of 298 Hz/px. The possible choices of *b*-values for such sequences ranged continuously from 0 to 900 s/mm^2. Moreover, an acquisition matrix of 128 × 109 pixels (pixel dimension is 2.734 × 2.734 mm^2) was used. All images were acquired using anterior and posterior surface torso coil, considering the phantoms described in the following section.

Phantoms

All the analyses in this work were carried out on two types of phantoms. The first was a homogeneous 24-cm diameter polymethylmethacrylate (PMMA) sphere containing a 2-mM aqueous solution of nickel chloride hexahydrate salt ($NiCl_2$*$6H_2O$) (Siemens Healthcare GmbH, Germany). The second was a homemade phantom (HMP) and consisted of a PMMA cylinder (183 mm diameter and 150 mm height) filled with distilled water with empty sockets into which five cylindrical vials (23 mm diameter and 100 mm height) filled with different concentrations (30, 20, 10, 5, and 1 w/w %.) of methylcellulose water solutions have been inserted.

Diffusion gradient homogeneity

A preliminary analysis was performed to study the dependence of diffusion gradient inhomogeneity artifacts on gantry position in order to determine the best gantry angle (BGA) for DWI. For this particular analysis, SP was used and four diffusion sequences with *b*-values of 500 s/mm^2 and 3 averages were acquired: three with diffusion gradients in the three main directions (phase direction, read direction, slice direction) and one with the diffusion gradients switched off. Measurements were repeated at four different gantry head angles of 0°, 90°, 180°, and 270°. All images were exported in DICOM format and analyzed with ImageJ software (29) (ver. 1.53f51). Image quality was evaluated by measuring the following:

- uniformity (U) calculated as:

$$U\,(\%) = 1 - ((P_{max} - P_{min})/(P_{max} + P_{min})) * 100$$

- where P_{max} and P_{min} are the values of the maximum and minimum of the diffusion signal within the SP, the largest radius of the sphere concentric to the SP that did not include artifacts (r_{MAX}). The latter was determined by performing visual analysis.

Analysis of the number of averages

The dependence of diffusion image uniformity and SNR on the number of averages in the MR sequences was investigated in order to determine the best average number (BAN). This analysis was repeated for the images obtained according to four different *b*-values, i.e., 0, 300, 500, and 800 s/mm^2, and for sequences with 1, 5, 10, and 15 averages. All measurements were carried out with the gantry head positioned at 0°. The uniformity was calculated as described before, while SNR was calculated according to AAPM guidelines (30) as follows:

$$SNR = \sqrt{2}\quad S/N$$

where S is the mean value of the signal and N is the standard deviation of the background.

Secondly, an analysis of the geometric distortion as a function of the number of averages was carried out by appropriately measuring the outer diameter of the HMP in the anterior–posterior (AP) and right–left (RL) directions using images acquired with the *b*-value 500 s/mm^2. Values have been compared to the real dimension of the phantom in order to evaluate the geometric distortion. In addition, an analysis of the dependence of the calculated ADC values on the number of averages used was carried out. Diffusion sequences were acquired on the HMP with four *b*-values (0, 300, 500, and 800 s/mm^2), and the corresponding ADC maps were calculated using the single exponential fit of the *MRIAnalysisPak* plugin available on ImageJ software (29, 31). The distributions of the ADC values for the different methylcellulose concentrations were plotted using OriginPro "Version 2018b" (OriginLab Corporation, Northampton, MA, USA) and compared according to the number of averages in terms of mean value and standard deviation. Once the optimal parameters for the realization of a sequence applicable in

clinical practice were established, diffusion images were acquired and the relative ADC maps of the HMP were calculated. These values were compared with those obtained by scanning the same HMP in a 1.5-T tomograph GE Signa HDxt (GE Healthcare, Waukesha, WI, USA) using a standard clinical sequence for diffusion imaging and the same *b*-values. The comparison was evaluated through statistical analysis using Passing–Bablok regression.

Other analysis

The dependence of uniformity and SNR as a function of slice thickness was investigated acquiring five different diffusion sequences (BGA, BAN, 500 s/mm^2), and slice thickness was set to 6 (minimum value allowed in the MRI protocol system for such a particular sequence), 7, 8, 9, and 10 mm, respectively.

Results

Diffusion gradient homogeneity

Figure 1 shows the DWI acquisitions at different gantry angles. Both for the images acquired with the gradients turned off and the gradients turned on in the "slice" direction, there is an almost total absence of artifacts except for the 90° angle that presents a barely perceptible artifact in the center of the sphere. With regard to the images acquired with the gradients turned on in the "read" and "phase" directions, the copious presence of inhomogeneous gradient artifacts can be noted in all gantry angles. These visual considerations are reinforced by the data in Table 1 which shows the results of the computed uniformity (U) and the r_{MAX} value at different gantry angles for the SP DWI. In this table, we can see that the uniformity reaches its maximum values (93.2, 84.8, 91.4, and 88.0 with gantry angle at 0°, 90°, 180°, and 270°, respectively) with the gradients off and with the gradients on in the "slice" direction (90.3, 76.3, 90.0, and 83.8 with gantry angle at 0°, 90°, 180°, and 270°, respectively). For the images acquired with the gradients in the "read" and "phase" directions, the uniformity has almost always the lowest values. Concerning the r_{MAX} value, expressed in millimeters, Table 1 reports its value related to the images with the gradients off and in those with the gradients turned on in the "slice" direction; the maximum value is reached at 120 mm (the SP has in fact a diameter of 240 mm). On the other hand, for images acquired with the gradients in the "read" and "phase" directions, r_{MAX} minimum values are between 0 and 73 mm. The worst situation was observed with the gantry angle at 180° where r_{MAX} for the "read" and "phase" gradients are zero because of the evident artifacts that cross the image right in the middle of the FOV. The overall result of this analysis identifies "slice" as the optimal gradient direction and 0° as the best gradient angle, to acquire high-quality artifact-free DWI images.

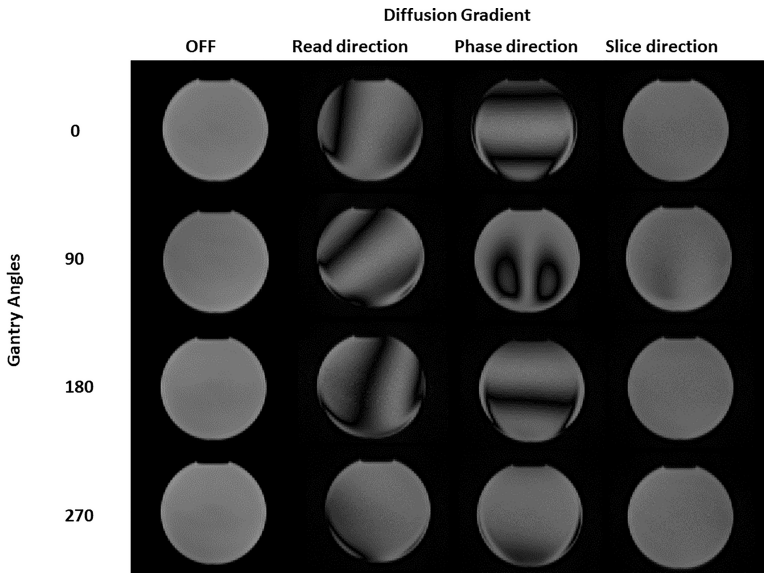

FIGURE 1
Diffusion images of the spherical phantom obtained for different gantry head positions (0, 90, 180, 270 degrees) and with different diffusion gradients (turned OFF, b-value 500 s/mm^2 "read", "phase" and "slice" direction).

TABLE 1 Values of uniformity (U) and maximum radius of artifact-free ROI for the images in Figure 1.

Gantry angle	Gradient	U (%)	r_{MAX} (mm)
0	OFF	93.2	120
	b500 read	0.0	48
	b500 phase	0.0	42
	b500 slice	90.3	120
90	OFF	84.8	120
	b500 read	0.0	31
	b500 phase	0.0	20
	b500 slice	76.3	31
180	OFF	91.4	120
	b500 read	0.0	0
	b500 phase	0.0	0
	b500 slice	90.0	120
270	OFF	88.0	120
	b500 read	0.0	83
	b500 phase	39.4	73
	b500 slice	83.8	120

Values are calculated and measured for different gantry angles and different diffusion gradient directions (gradients OFF, b-value of 500 s/mm^2 "read," phase," and "slice" directions, 3 averages).

Analysis of the number of averages

Figure 2 depicts the SNR (panel **A**) and the uniformity (panel **B**) as a function of the number of averages when varying the *b*-values. Both the SNR ratio and the uniformity increase with the number of averages. For the *b*-value 0 s/mm^2, SNR has the minimum value of 100 (1 average) and assumes the maximum value (118) at 10 averages. For the *b*-value 300 s/mm^2, SNR varies continuously from 64 (1 average) to 117 (15 averages). Similarly, for the *b*-value 500 s/mm^2, SNR varies continuously from 74 (1 average) to 112 (15 averages). The *b*-value 800 s/mm^2 shows obviously lower values than the others, ranging from a minimum of 29 (1 average) to a maximum of 93 for 15 averages, reaching a value of 86 for 10 averages. For the lowest *b*-values (0 and 300 s/mm^2), we find a high value of uniformity and SNR (as observed with 15 averages) even using few averages (1 or 5), while for the highest ones (500 and 800 s/mm^2), optimal values are reached starting from 10 averages. On the basis of these considerations, a threshold value of 80 for SNR and 85% for uniformity was adopted to choose the best BAN, which is dependent on the *b*-value: a smaller number of averages (3) can be used for the lowest *b*-values and a larger number of averages (10) must be used for the highest *b*-values. Table 2 reports the times taken by the sequences for the acquisition of a single slice and for a stack of 6 slices, according to the number of averages. The time reported is relative to the acquisition of an image with only one *b*-value; to obtain the total duration of a sequence used to generate an ADC map, the times necessary to obtain all the single *b*-values involved must be added together.

Figure 3 shows the section of the HMP used to calculate the two diameters in the AP (in yellow) and RL (in red) directions. Table 3 shows the results of the measurements and the deviations from the expected value (Δ) as a function of the number of averages. It can be seen that the distance from the expected value is always below 1 mm except for the values for images with only one mean. In this case, in fact, there is a difference of 2.9 mm for the AP direction and 1.36 mm for the RL direction.

In the fourth and fifth columns, differences with the expected values are shown. All images are acquired using the TRSE sequences with TR/TE = 2000/5.4 and a *b*-value of 500 s/mm^2 in the slice direction.

Gaussian fits of the distributions of the ADC values of the different concentrations of methylcellulose in the HMP obtained for different numbers of averages are shown in Figure 4. The ADC values are given in 10^{-3} mm^2/s, and we can see in solid black line the values obtained for 1 average, in red those for 5 averages, in blue those for 10 averages, and in green those for 15 averages.

In Table 4, we can see the parameters of the Gaussian fits for ADC value distribution. Mean value (x_m) and standard deviation (σ) are reported in 10^{-3} mm^2/s for all methylcellulose concentrations and for all numbers of averages considered in the analysis. It can be seen that the value of the ADCs remains constant except for the values obtained for 1 average which are significantly lower. On the other hand, the standard deviation decreases its value as the number of averages increases except for the 1% concentration which shows similar but slightly higher values from 5 to 10 averages.

Table 5 reports the SNR and uniformity values as a function of the slice thickness: both values do not vary significantly. The increase in slice thickness results in an increase in SNR (from 93.8 to 96.1) and uniformity (from 89% to 92%).

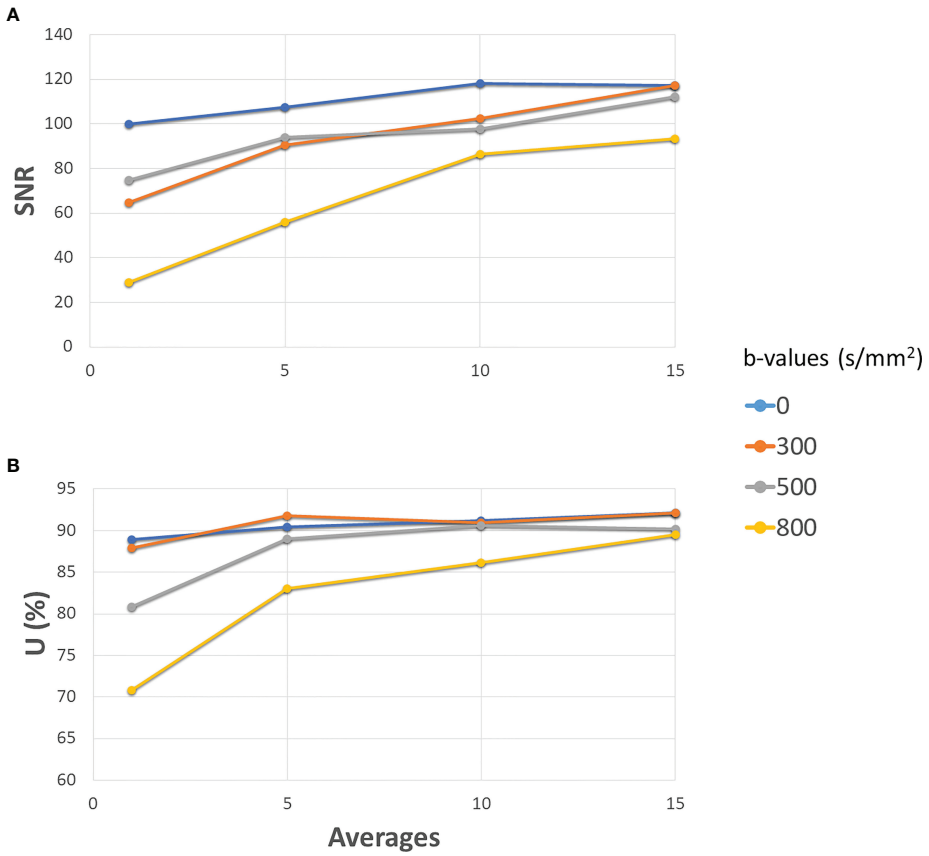

FIGURE 2
Development of SNR **(A)** and Uniformity **(B)** as the number of averages increases for different b-values. The solid blue line is for 0 s/mm^2 (gradients off), orange for 300 s/mm^2, grey for 500 s/mm^2 and yellow for 800 s/mm^2. All the gradients have been set to slice direction.

As shown in Figure 5, DWI was then acquired on HMP, and the corresponding ADC map was calculated using two *b*-values (0 and 800 s/mm^2), with the number of averages set to 3 and 10, respectively, while slice thickness was maintained to 6 mm. These settings allow to acquire a single slice in 26 s and a stack of 6 slices, which would give a volume of 350 × 294 × 36 mm^3, in 78 s (3 averages in 21 s for *b*-value at 0 s/mm^2 and 10 averages in 57 s for *b*-value at 800 s/mm^2). All sequences were acquired at the BGA.

TABLE 2 Time required to collect images with 1 (first column) or 6 (second column) slices varying the number of averages of the sequence.

Averages	Time/1 slice (s)	Time/6 slices (s)
1	4	10
5	12	31
10	22	57
15	32	83

Figure 6 reports the boxplots of the ADC coefficient values computed from the images acquired on the scanner at 0.35 T (cyan box) and on a diagnostic scanner at 1.5 T (orange box), for the various concentrations of the methylcellulose solutions present in the HMP.

Figure 7 reports the Passing–Bablok regression for comparison of ADC values of methylcellulose concentrations for 1.5 and 0.35 T scanners: the comparison showed a slope value of 1.01 (95% CI: 0.96 to 1.05) and an intercept value of −0.03 (95% CI: −0.11 to 0.04).

In Table 6, the ADC mean values and relative standard deviations for the various concentrations of methylcellulose and distilled water are reported. As it would be desirable, no significant differences between the ADC coefficient distributions obtained on the two different scanners have been noticed: the most significative variation is 0.03 10^{-3} mm^2/s for 10% of methylcellulose concentration, while it shows no difference for the 1% concentration. The agreement between couples of relative ADC mean values can be appreciated by reading the *p*-values in the fifth column which are all above the

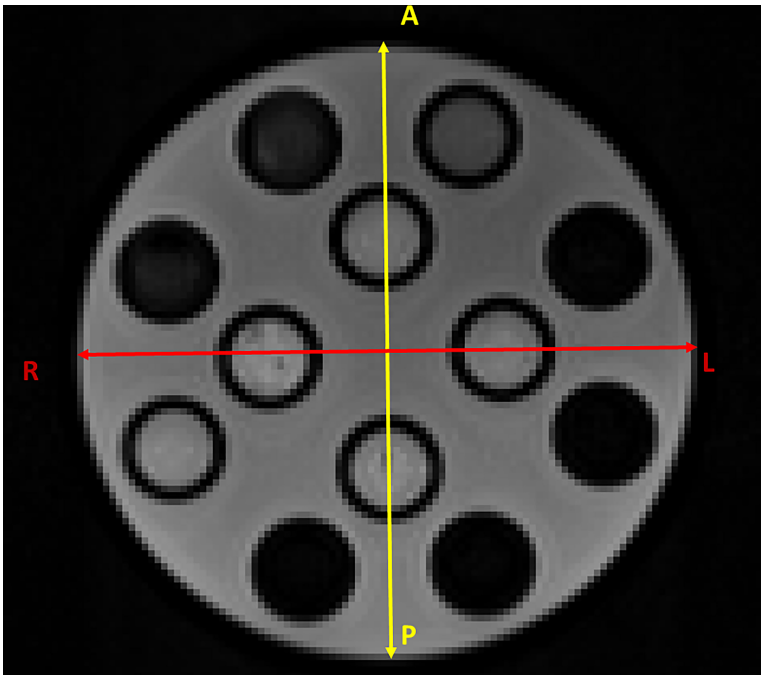

FIGURE 3
Section of the HMP used to calculate the two diameters in the AP (in yellow) and RL (in red) directions.

TABLE 3 Value of the diameter measurements in the two directions (AP second column and RL third column) expressed in millimetres.

Averages	AP diameter (mm)	RL diameter (mm)	ΔAP (mm)	ΔRL (mm)
1	180.1	181.64	2.90	1.36
5	183.21	182.94	−0.21	0.06
10	183.25	182.82	−0.25	0.18
15	183.77	183.51	−0.77	−0.51

In the fourth and fifth column the difference with the expected value. All images are acquired using TRSE sequences with TR/TE = 2000/5.4 and a b-value of 500 s/mm^2 in slice direction.

significance level. In Table 7, we summarize the optimal acquisition parameters for our center.

Discussion

In this study, the quality of DWI was evaluated in relation to different sequence parameters to identify the optimal parameters and create a clinical protocol for the acquisition of ADC maps sustainable in the workflow of a hybrid radiotherapy system with a 0.35-T MRI scanner. Initially, the dependence of the image quality on the position gantry angle was studied, observing the use of diffusion gradients in the "read" and "phase" directions which produced images with a large number of artifacts; however, they could not be used for the calculation of ADC maps. As regards the "slice" direction, good-quality images were obtained for most of the gantry angles investigated in this study (except for 90°). A similar behavior was also found in Pieniazek et al. (32) who used a 0.2-T MR scanner and only slice direction due to system limitations. In previous studies investigating the DWI acquisition on a 0.35-T MR-Linac system, there is no mention of the gradients' direction and the gantry angle used (33, 34). Although is not clearly visible in Figure 1, the quantitative analysis in Table 1 shows the differences in acquisitions with diffusion gradients in the "slice" direction for the four gantry angles (0°, 90°, 180°, and 270°) that led to the choice of 0° as the best gantry angle. Based on these findings, a clinical protocol will be designed using 0° as the best gantry angle and slice as the diffusion gradient direction. Regarding the analysis of the number of averages, it was confirmed that there was also an increase in both SNR and uniformity when the number of averages is increased: based on

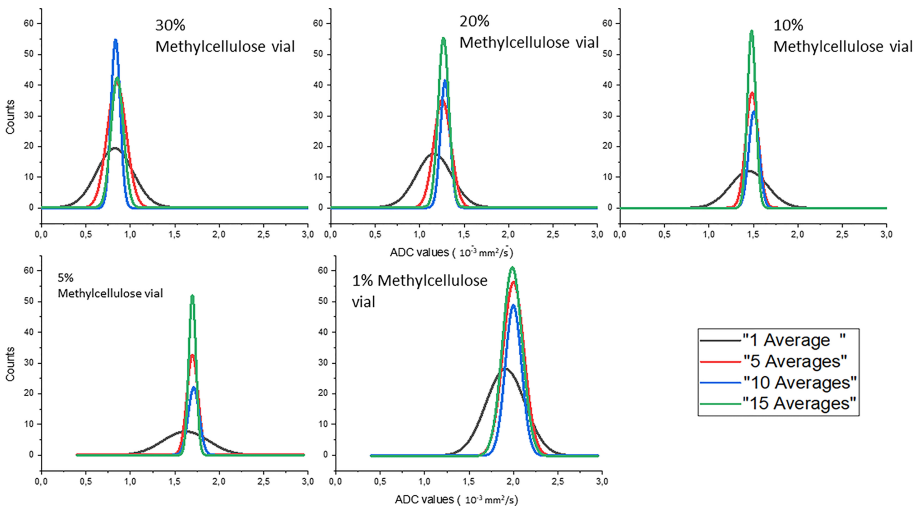

FIGURE 4
Gaussian fits of the distributions of the ADC values of the different concentrations of methylcellulose in the HMP obtained for different numbers of averages.

TABLE 4 Parameters of Gaussian fits for ADC value distributions for all methylcellulose concentrations and all averages analyzed.

Methylcellulose %		1 average	5 averages	10 averages	15 averages
30	x_m	0.88 ± 0.02	0.90 ± 0.01	0.89 ± 0.01	0.91 ± 0.01
	σ	0.41 ± 0.03	0.22 ± 0.01	0.10 ± 0.01	0.10 ± 0.01
20	x_m	1.22 ± 0.02	1.31 ± 0.01	1.32 ± 0.01	1.33 ± 0.01
	σ	0.40 ± 0.02	0.19 ± 0.01	0.11 ± 0.01	0.11 ± 0.01
10	x_m	1.48 ± 0.02	1.52 ± 0.01	1.52 ± 0.01	1.51 ± 0.01
	σ	0.42 ± 0.03	0.14 ± 0.01	0.12 ± 0.01	0.10 ± 0.01
5	x_m	1.66 ± 0.02	1.73 ± 0.01	1.74 ± 0.01	1.73 ± 0.01
	σ	0.50 ± 0.03	0.12 ± 0.01	0.12 ± 0.01	0.10 ± 0.01
1	x_m	1.91 ± 0.02	1.99 ± 0.01	1.99 ± 0.01	1.99 ± 0.01
	σ	0.44 ± 0.03	0.18 ± 0.01	0.19 ± 0.01	0.15 ± 0.01

Mean values and standard deviations are reported in 10^{-3} mm^2/s.

this, the different numbers of averages depending on the *b*-value acquired were considered. By making a compromise between time and quality and limiting the number of *b*-values used for the calculation of the ADC maps to 2, it is possible to reduce the acquisition time to 78 s. This time reduction can be considered a satisfactory result since the duration of the typical diagnostic scanner sequences ranges from 40 s to 3–4 min depending on the need (35) and patient compliance (36). Our results in terms of stability analysis of ADC values as a function of averages are in line with those reported in a previous experience recently published (37, 38). Since the results obtained for the variation of SNR and uniformity showed insignificance to minor deviations when varying slice thickness, we did not find it useful to proceed with an analysis of the stability of ADC coefficient values as a function of slice thickness. The optimal sequence designed was finally tested acquiring DWI on the HMP and calculating ADC values. Such maps were compared with those obtained with acquisitions on a 1.5-T diagnostic scanner on the same phantom, obtaining good agreement which is desirable. As can be seen in Figure 6, there is a certain difference in the standard

TABLE 5 SNR and uniformity as a function of the slice thickness.

Slice thickness (mm)	SNR	*U* (%)
6	93.8	89
7	94.1	89
8	94.7	90
9	95.4	91
10	96.1	92

Values are calculated on the images of the SP acquired with a sequence at BGA, with gradient in the "slice" direction and a b-value of 500 s/mm^2.

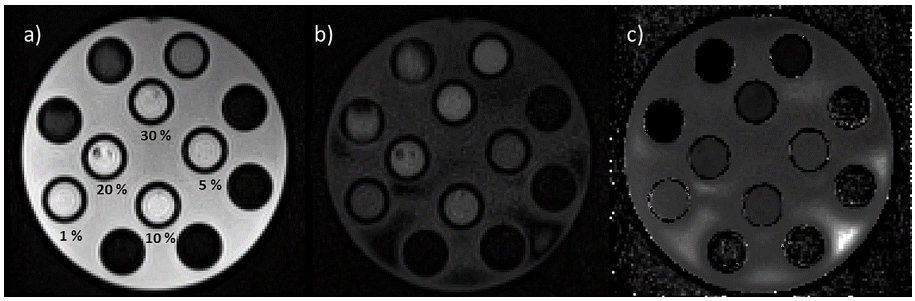

FIGURE 5
Images of the HMP acquired using diffusion sequences with b-values set to 0 s/mm^2, 3 averages (a) and 800 s/mm2, 10 averages (b). In panel "c" is reported the calculated ADC map. In panel "a" are also reported the values of the concentrations of methylcellulose solution below the relative vial.

deviations of the values obtained using the two different scanners: a probable explanation can be found in the inhomogeneity of the methylcellulose solutions since some vials contain more inhomogeneous solution than the others due to small lumps or small air bubbles. These are detected, when present, by the higher resolution of a 1.5-T scanner leading to a higher standard deviation. This is a limitation of this study and can be overcome by using a different polymer in the solution [like polyvinylphenol (PVP)] to make it more homogenous. As far as the authors know, this represents one of the first studies on diffusion sequences carried out on a 0.35-T system using a phantom. A comparable study was proposed by Lewis et al., who investigated the geometric distortion as a function of gantry angles (38). The substantial differences mainly involved two aspects: the first merely concerns the parameters used for the sequence. Lewis et al. used an EPI diffusion scheme and made no mention of using particular gradient directions. The other aspect concerns the phantom: Lewis et al. made use of a commercial NIST phantom for DWI, while our measurements were carried out using a homemade phantom that is easily replicable and cheap. Lewis et al. found a difference in ADC values when comparing the scanners at 0.35 T with those at 1.5 and 3 T, while in our study, there is a good agreement in ADC values calculated with images acquired in the 0.35- and 1.5-T scanners as shown by the Passing–Bablok regression analysis. A possible reason for this discordance lies in the different diffusion schemes used and probably in the choice of the different *b*-values chosen for the sequences. In addition, a similar study was

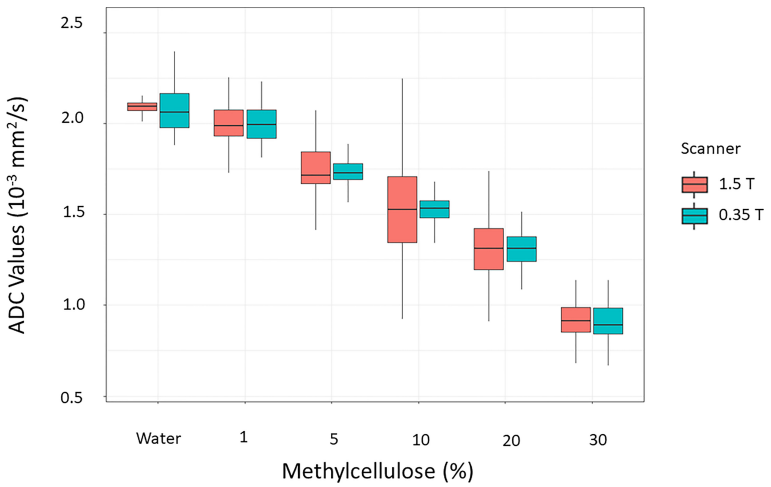

FIGURE 6
Distributions of the values of the ADC coefficients calculated from the images acquired on the scanner at 0.35 T (cyan box) in comparison with those acquired with a homologous sequence on a diagnostic scanner at 1.5 T (orange box) for the various concentrations of the methylcellulose solutions present in the HMP.

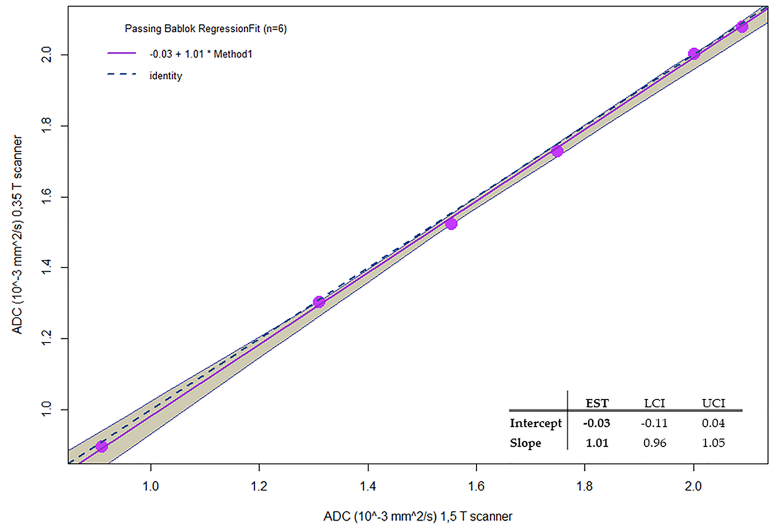

FIGURE 7
Passing-Bablok regression for comparison of ADC values of Methylcellulose concentrations for 1.5 T and 0.35 T scanners.

TABLE 6 Mean values of ADC (10^{-3} mm^2/s) obtained for different methylcellulose concentrations and distilled water.

% Methylcellulose	Scanner	Mean ADC Value	St.Dev.
30	1.5 T	0.91	0.10
	0.35 T	0.90	0.11
20	1.5 T	1.31	0.19
	0.35 T	1.30	0.10
10	1.5 T	1.55	0.29
	0.35 T	1.52	0.08
5	1.5 T	1.75	0.16
	0.35 T	1.73	0.07
1	1.5 T	2.00	0.13
	0.35 T	2.00	0.11
Distilled water	1.5 T	2.09	0.03
	0.35 T	2.08	0.13

Results are reported for both scanners used to acquire images: 1.5 T diagnostic scanner and 0.35 T MRIdian integrated scanner.

TABLE 7 Acquisition parameters for ADC measurements.

Topic	Parameters
Diffusion scheme	TRSE
Diffusion gradient direction	Slice
TR/TE	2000/5.4
Gantry angle	0
Number of averages	At least 3 (*b*-value-dependent)
Max *b*-values	800 s/mm^2
Slice thickness	6 mm (lower possible)

published on an MR-Linac system with a static magnetic field at 1.5 T by Kooreman et al. (39). In this multicenter study (6 MR-Linac system scanners), the spatial dependence of the ADCs was evaluated using a cylindrical phantom. Similar to the present work, Kooreman et al. also found images affected by artifacts for acquisitions with diffusion gradients that were not in the z-direction (our "slice" direction). Although they found the presence of these artifacts, they did not render the images unusable but only forced them to define a confidence zone around the isocenter (7 cm radius) for the calculation of ADC values. In our case, however, if we had to calculate the same kind of confidence zone, we would have found a null surface. This study obviously has all the limitations of a single-

center study. This calls for a multicenter evaluation study, involving other MR-Linac systems with a static magnetic field at 0.35 T, to characterize the gradient inhomogeneities in a machine-independent manner to understand their nature and make the necessary corrections.

In conclusion, the present study identified the optimal parameters to obtain high-quality diffusion-weighted MR images on a 0.35-T MR-Linac system.

Data availability statement

The original contributions presented in the study are included in the article/supplementary material. Further inquiries can be directed to the corresponding author.

Author contributions

MN provided writing (draft), data curation and formal analysis. MN, LNM provided methodology. MN, LNM, LP provided conceptualization. LB, GC, AR provided resources and writing (review). AC, LNM, DC, LP provided supervision, validation and writing (review). LP, LI, VV provided project administration and funding acquisition.

Conflict of interest

LB, LP, and DC received research grants and personal fees from ViewRay.

The remaining authors declare that the research was conducted in the absence of any commercial or financial relationships that could be construed as a potential conflict of interest.

Publisher's note

References

1. Kim JY, Kim JJ, Hwangbo L, Kang T, Park H. Diffusion-weighted imaging of invasive breast cancer: relationship to distant metastasis–free survival. *Radiol* (2019) 291(2):300–7. doi: 10.1148/radiol.2019181706

2. Woo S, Suh CH, Kim SY, Cho JY, Kim SH. Head-to-head comparison between high-and standard-b-value DWI for detecting prostate cancer: A systematic review and meta-analysis. *Am J Roentgenol* (2018) 210(1):91–100. doi: 10.2214/AJR.17.18480

3. Park JE, Kim HS, Park SY, Jung SC, Kim JH, Heo HY. Identification of early response to anti-angiogenic therapy in recurrent glioblastoma: Amide proton transfer–weighted and perfusion-weighted MRI compared with diffusion-weighted MRI. *Radiol* (2020) 295(2):397–406. doi: 10.1148/radiol.2020191376

4. Granata V, Grassi R, Fusco R, Setola SV, Palaia R, Belli A, et al. Assessment of ablation therapy in pancreatic cancer: The radiologist's challenge. *Front Oncol* (2020) 10:2666. doi: 10.3389/fonc.2020.560952

5. Blackledge MD, Tunariu N, Zugni F, Holbrey R, Orton MR, Ribeiro A, et al. Noise-corrected, exponentially weighted, diffusion-weighted MRI (niceDWI) improves image signal uniformity in whole-body imaging of metastatic prostate cancer. *Front Oncol* (2020) 10:704. doi: 10.3389/fonc.2020.00704

6. Stejskal EO. Use of spin echoes in a pulsed magnetic-field gradient to study anisotropic, restricted diffusion and flow. *J Chem Phys 19 maggio* (2004) 43(10):3597. doi: 10.1063/1.1696526

7. Cusumano D, Boldrini L, Yadav P, Yu G, Musurunu B, Chiloiro G, et al. Delta radiomics for rectal cancer response prediction using low field magnetic resonance guided radiotherapy: An external validation. *Phys Med* (2021) 84:186–91. doi: 10.1016/j.ejmp.2021.03.038

8. Russo L, Gui B, Miccò M, Panico C, De Vincenzo R, Fanfani F, et al. The role of MRI in cervical cancer> 2 cm (FIGO stage IB2-IIA1) conservatively treated with neoadjuvant chemotherapy followed by conization: a pilot study. *Radiol Med* (La Radiologia Medica) (2021) 126(8):1055–63. doi: 10.1007/s11547-021-01377-1

9. Sun NN, Ge XL, Liu XS, Xu LL. Histogram analysis of DCE-MRI for chemoradiotherapy response evaluation in locally advanced esophageal squamous cell carcinoma. *Radiol Med (Torino)* (2020) 125(2):165–76. doi: 10.1007/s11547-019-01081-1

10. Buizza G, Zampini MA, Riva G, Molinelli S, Fontana G, Imparato S, et al. Investigating DWI changes in white matter of meningioma patients treated with proton therapy. *Phys Med* (2021) 84:72–9. doi: 10.1016/j.ejmp.2021.03.027

11. Tsarouchi MI, Vlachopoulos GF, Karahaliou AN, Vassiou KG, Costaridou LI. Multi-parametric MRI lesion heterogeneity biomarkers for breast cancer diagnosis. *Phys Med* (2020) 80:101–10. doi: 10.1016/j.ejmp.2020.10.007

12. Li C, Yin J. Radiomics based on T2-weighted imaging and apparent diffusion coefficient images for preoperative evaluation of lymph node metastasis in rectal cancer patients. *Front Oncol* (2021) 11:1506. doi: 10.3389/fonc.2021.671354

13. Yu XY. Multiparameter MRI radiomics model predicts preoperative peritoneal carcinomatosis in ovarian cancer. *Front Oncol* (2021) 4348. doi: 10.3389/fonc.2021.765652

14. Placidi L, Romano A, Chiloiro G, Cusumano D, Boldrini L, Cellini F, et al. On-line adaptive MR guided radiotherapy for locally advanced pancreatic cancer: Clinical and dosimetric considerations. *Tech Innov Patient Support Radiat Oncol settembre* (2020) 15:15–21. doi: 10.1016/j.tipsro.2020.06.001

15. Zhuang Y, Potchen MJ, Kampondeni SD, Tivarus M, Birbeck GL, Zhong J. Validation of diffusion measurements obtained on a 0.35 T MR in Malawi: important insights for radiologists in low income settings with low field MRI. *Magn Reson Imaging* (2018) 45:120–8. doi: 10.1016/j.mri.2017.10.001

16. Chandarana H, Bagga B, Huang C, Dane B, Petrocelli R, Bruno M, et al. Diagnostic abdominal MR imaging on a prototype low-field 0.55 T scanner operating at two different gradient strengths. *Abdom Radiol* (2021) 46(12):5772–80. doi: 10.1007/s00261-021-03234-1

17. Mehdizade A, Somon T, Wetzel S, Kelekis A, Martin JB, Scheidegger JR, et al. Diffusion weighted MR imaging on a low-field open magnet. comparison with findings at 1.5 T in 18 patients with cerebral ischemia. *J Neuroradiol J Neuroradiol* (2003) 30(1):25–30. doi: JNR-01-2003-30-1-632735-101019-ART04

18. Zhang H, Sun A, Li H, Saiviroonporn P, Wu EX, Guo H. Stimulated echo diffusion weighted imaging of the liver at 3 Tesla. *Magn Reson Med* (2017) 77 (1):300–9. doi: 10.1002/mrm.26128

19. Stocker D, Manoliu A, Becker AS, Barth BK, Nanz D, Klarhöfer M, et al. Image quality and geometric distortion of modern diffusion-weighted imaging sequences in magnetic resonance imaging of the prostate. *Invest Radiol* (2018) 53 (4):200–6. doi: 10.1097/RLI.0000000000000429

20. Pang Y, Malyarenko DI, Amouzandeh G, Barberi E, Cole M, Vom Endt A, et al. Empirical validation of gradient field models for an accurate ADC measured on clinical 3T MR systems in body oncologic applications. *Phys Med* (2021) 86:113–20. doi: 10.1016/j.ejmp.2021.05.030

21. Fedeli L, Benelli M, Busoni S, Belli G, Ciccarone A, Coniglio A, et al. On the dependence of quantitative diffusion-weighted imaging on scanner system characteristics and acquisition parameters: A large multicenter and multiparametric phantom study with unsupervised clustering analysis. *Phys Med* (2021) 85:98–106. doi: 10.1016/j.ejmp.2021.04.020

22. McGee KP, Hwang KP, Sullivan DC, Kurhanewicz J, Hu Y, Wang J, et al. Magnetic resonance biomarkers in radiation oncology: The report of AAPM task group 294. *Med Phys* (2021) 48(7):e697–732. doi: 10.1002/mp.14884

23. Taouli B, Beer AJ, Chenevert T, Collins D, Lehman C, Matos C, et al. Diffusion-weighted imaging outside the brain: consensus statement from an ISMRM-sponsored workshop. *J Magn Reson Imaging* (2016) 44(3):521–40. doi: 10.1002/jmri.25196

24. Shukla-Dave A, Obuchowski NA, Chenevert TL, Jambawalikar S, Schwartz LH, Malyarenko D, et al. Quantitative imaging biomarkers alliance (QIBA) recommendations for improved precision of DWI and DCE-MRI derived biomarkers in multicenter oncology trials. *J Magn Reson Imaging* (2019) 49(7): e101–21. doi: 10.1002/jmri.26518

25. Stanescu T, Mousavi SH, Cole M, Barberi E, Wachowicz K. Quantification of magnetic susceptibility fingerprint of a 3D linearity medical device. *Phys Med* (2021) 87:39–48. doi: 10.1016/j.ejmp.2021.05.023

26. Steinmann A, Alvarez P, Lee H, Court L, Stafford R, Sawakuchi G, et al. MRIgRT head and neck anthropomorphic QA phantom: design, development, reproducibility, and feasibility study. *Med Phys* (2020) 47(2):604–13. doi: 10.1002/mp.13951

27. Cusumano D, Boldrini L, Dhont J, Fiorino C, Green O, Güngör G, et al. Artificial intelligence in magnetic resonance guided radiotherapy: Medical and physical considerations on state of art and future perspectives. *Phys Med* (2021) 85:175–91. doi: 10.1016/j.ejmp.2021.05.010

28. Nagy Z, Thomas DL, Weiskopf N. Orthogonalizing crusher and diffusion-encoding gradients to suppress undesired echo pathways in the twice-refocused spin echo diffusion sequence. *Magn Reson Med* (2014) 71(2):506–15. doi: 10.1002/mrm.24676

29. Schindelin J, Arganda-Carreras I, Frise E, Kaynig V, Longair M, Pietzsch T, et al. Fiji: an open-source platform for biological-image analysis. *Nat Methods luglio* (2012) 9(7):676–82. doi: 10.1038/nmeth.2019

30. Price RR, Axel L, Morgan T, Newman R, Perman W, Schneiders N, et al. Quality assurance methods and phantoms for magnetic resonance imaging: Report of AAPM nuclear magnetic resonance task group no. *1 Med Phys* (1990) 17(2):287–95. doi: 10.1118/1.596566

31. Rasband WS. *ImageJ*. Bethesda, Maryland, US: U. S. National Institutes of Health (1997-2020).

32. Pieniazek P, Wojtek P, Konopka M, Jasinski A, Walecki J, Hartel M, et al. Diffusion weighted imaging (DWI) EPI on low field MR system (0.2T). In: *Comparison with 1.5T and preliminary report on clinical use in brain ischemia*. European Congress of Radiology (2004). Available at: https://epos.myesr.org/poster/esr/ecr2004/C-746.

33. Yang Y, Cao M, Sheng K, Gao Y, Chen A, Kamrava M, et al. Longitudinal diffusion MRI for treatment response assessment: Preliminary experience using an MRI-guided tri-cobalt 60 radiotherapy system. *Med Phys* (2016) 43(3):1369–73. doi: 10.1118/1.4942381

34. Shaverdian N, Yang Y, Hu P, Hart S, Sheng K, Lamb J, et al. Feasibility evaluation of diffusion-weighted imaging using an integrated MRI-radiotherapy system for response assessment to neoadjuvant therapy in rectal cancer. *Br J Radiol* (2017) 90(1071):20160739. doi: 10.1259/bjr.20160739

35. Taron J, Martirosian P, Erb M, Kuestner T, Schwenzer NF, Schmidt H. Simultaneous multislice diffusion-weighted MRI of the liver: Analysis of different breathing schemes in comparison to standard sequences. *J Magn Reson Imaging* (2016) 44(4):865–79. doi: 10.1002/jmri.25204

36. Cuccia F, Alongi F, Belka C, Boldrini L, Hörner-Rieber J, McNair H, et al. Patient positioning and immobilization procedures for hybrid MR-linac systems. *Radiat Oncol 20 settembre* (2021) 16(1):183. doi: 10.1186/s13014-021-01910-6

37. Celik A. Effect of imaging parameters on the accuracy of apparent diffusion coefficient and optimization strategies. *Diagn Interv Radiol gennaio* (2016) 22 (1):101–7. doi: 10.5152/dir.2015.14440

38. Lewis B, Guta A, Mackey S, Gach HM, Mutic S, Green O, et al. Evaluation of diffusion-weighted MRI and geometric distortion on a 0.35T MR-LINAC at multiple gantry angles. *J Appl Clin Med Phys* (2021) 22(2):118–25. doi: 10.1002/acm2.13135

39. Kooreman ES, van Houdt PJ, Keesman R, Pos FJ, van Pelt VWJ, Nowee ME, et al. ADC Measurements on the unity MR-linac – a recommendation on behalf of the elekta unity MR-linac consortium. *Radiother Oncol J Eur Soc Ther Radiol Oncol* (2020) 153:106–13. doi: 10.1016/j.radonc.2020.09.046

frontiers | Frontiers in Oncology

TYPE Original Research
PUBLISHED 11 January 2023
DOI 10.3389/fonc.2022.1037674

OPEN ACCESS

EDITED BY
Merav Ben-David,
Assuta Medical Center, Ramat-Hahayal, Israel

REVIEWED BY
Toshiyuki Toshito,
Nagoya City University, Japan
James Chow,
University of Toronto, Canada
John Baines,
Townsville University Hospital, Australia

*CORRESPONDENCE
Matthew D. Hall
matthewha@baptisthealth.edu

SPECIALTY SECTION
This article was submitted to Radiation Oncology, a section of the journal Frontiers in Oncology

RECEIVED 06 September 2022
ACCEPTED 20 December 2022
PUBLISHED 11 January 2023

CITATION
Hall MD, Mittauer KE, Herrera R, Von Werne K, Kotecha R, Kalman NS, McCulloch J, Alvarez D, McAllister NC, Doty DG, Rzepczynski AE, Deere W, Gutierrez AN and Chuong MD (2023) Initial clinical experience with magnetic resonance-guided radiotherapy in pediatric patients: Lessons learned from a single institution with proton therapy. *Front. Oncol.* 12:1037674. doi: 10.3389/fonc.2022.1037674

Initial clinical experience with magnetic resonance-guided radiotherapy in pediatric patients: Lessons learned from a single institution with proton therapy

Matthew D. Hall[1,2]*, Kathryn E. Mittauer[1,2], Roberto Herrera[1], Katherine Von Werne[1], Rupesh Kotecha[1,2], Noah S. Kalman[1,2], James McCulloch[1], Diane Alvarez[1,2], Nicole C. McAllister[1], Delia G. Doty[1], Amy E. Rzepczynski[1], Will Deere[1], Alonso N. Gutierrez[1,2] and Michael D. Chuong[1,2]

[1]Department of Radiation Oncology, Miami Cancer Institute, Baptist Health South Florida, Miami, FL, United States, [2]Herbert Wertheim College of Medicine, Department of Radiation Oncology, Florida International University, Miami, FL, United States

Purpose/Objectives: Magnetic resonance-guided radiotherapy (MRgRT) is increasingly used in a variety of adult cancers. To date, published experience regarding the use of MRgRT in pediatric patients is limited to two case reports. We report on the use of MRgRT for pediatric patients at our institution during a four-year period and describe important considerations in the selection and application of this technology in children.

Materials/Methods: All patients treated with MRgRT since inception at our institution between 4/2018 and 4/2022 were retrospectively reviewed. We also evaluated all pediatric patients treated at our institution during the same period who received either imaging or treatment using our magnetic resonance-guided linear accelerator (MR Linac). We summarize four clinical cases where MRgRT was selected for treatment in our clinic, including disease outcomes and toxicities and describe our experience using the MR Linac for imaging before and during treatment for image fusion and tumor assessments.

Results: Between 4/2018 and 4/2022, 535 patients received MRgRT at our center, including 405 (75.7%) with stereotactic ablative radiotherapy (SABR). During this period, 347 distinct radiotherapy courses were delivered to pediatric patients, including 217 (62.5%) with proton therapy. Four pediatric patients received MRgRT. One received SABR for lung metastasis with daily adaptive replanning and a second was treated for liver metastasis using a non-adaptive workflow. Two patients received fractionated MRgRT for an ALK-rearranged non-small cell lung cancer and neuroblastoma. No Grade 2 or higher toxicities were observed or reported during MRgRT or subsequent

follow-up. Twelve patients underwent MR imaging without contrast during treatment for brain tumors to assess for tumor/cystic changes. Two patients treated with other modalities underwent MR simulation for target volume delineation and organ at risk sparing due to anatomic changes during treatment or unexpected delays in obtaining diagnostic MR appointments.

Conclusions: In four pediatric patients treated with MRgRT, treatment was well tolerated with no severe acute effects. At our center, most pediatric patients are treated with proton therapy, but the cases selected for MRgRT demonstrated significant organ at risk sparing compared to alternative modalities. In particular, MRgRT may provide advantages for thoracic/abdominal/pelvic targets using gated delivery and adaptive replanning, but selected patients treated with fractionated radiotherapy may also benefit MRgRT through superior organ at risk sparing.

KEYWORDS

stereotactic body radiation therapy, SBRT, SABR, MR Linac, motion management, anesthesia, proton therapy, adaptive replanning

Introduction

Magnetic resonance-guided radiotherapy (MRgRT) provides enhanced soft tissue visualization compared to computed tomography (CT) and the potential for an online adaptive workflow, which may enable safer dose escalation for tumors adjacent to dose-limiting organs at risk (OAR) without increasing toxicity. Additional benefits include improvements in daily setup accuracy, the ability to reduce planning target volume (PTV) margins for some disease sites, use of continuous cine tumor motion tracking and beam gating, and application of respiratory breath-hold techniques to abrogate tumor motion. In adults, MRgRT has been applied in stereotactic ablative radiotherapy (SABR) for inoperable pancreatic carcinoma and oligometastatic lesions in the abdomen, pelvis, liver, and adrenal glands with favorable early outcomes (1, 2).

In children (defined as < 21 years of age in this study), MRgRT may provide similar opportunities to improve the therapeutic ratio with a potentially greater emphasis on reducing late adverse effects of radiotherapy. In 2020, a survey of twelve current and future users of MRgRT systems in International Society of Paediatric Oncology (SIOP) and Children's Oncology Group (COG) radiotherapy centers examined the potential benefits of MRgRT in pediatric patients (3). While the survey identified several clinical scenarios and tumor sites where MRgRT was expected to improve clinical outcomes and toxicities, experience with MRgRT in children remains limited. To date, the published experience for the use of MRgRT in pediatric patients is limited to two case reports (4, 5), which is likely influenced by the low number of MRgRT facilities and prioritization of other modalities, such as proton therapy (PT), in this population. The purpose of this investigation is to report on the use of MRgRT for treatment and imaging purposes at our institution during a four-year period, discuss potential applications for this technology at a large center with varied radiotherapy modalities, and describe lessons learned from treating pediatric patients with MRgRT.

Materials and methods

After obtaining institutional review board (IRB) approval, we retrospectively reviewed all patients treated with MRgRT on the MRIdian (ViewRay, Oakwood Village, OH) linear accelerator (MR Linac) at a single institution between 4/2018 and 4/2022. We also reviewed all pediatric and young adult patients (< 21 years of age) treated at our institution during the same time interval and identified all who received either imaging or treatment using the MR Linac.

All patients underwent simulation and treatment in the supine position. Every simulation comprised both a 0.35 T balanced steady-state free precession sequence (TrueFISP) MR scan acquired over 17-25 seconds on the MR Linac followed by a CT simulation. Patients treated with conventional fractionation using a non-adaptive workflow were simulated arms up or arms down based on the disease site and at the discretion of the radiation oncologist. For abdominal and thoracic tumors

undergoing SABR, simulation was performed either with both arms down or one arm raised above the head for comfort and reproducibility; this was important particularly for patients undergoing daily online adaptive replanning and treatment in breath hold. For SABR, our treatment planning and delivery approach were previously described (6). Fiducial markers and oral/intravenous contrast were not used given that gross disease and OARs were well visualized during simulation and treatment. Target volume and OAR delineation and treatment planning were performed on the MR simulation scan. When appropriate, and based on the disease site treated, a clinical target volume (CTV) was added surrounding the gross tumor volume (GTV) at the discretion of the radiation oncologist. The PTV margin consisted of an isotropic 3 mm expansion of GTV or CTV (if present).

Prior to each daily treatment, GTV was used to define the tracking region of interest in the sagittal plane. Continuous cine imaging and real-time tumor tracking were applied, and treatment was automatically held if > 3-5% of the tracking region of interest was displaced by > 3 mm from its original location (e.g. outside of the tracking boundary). In SABR cases, mid-inspiration breath hold was preferred over deep inspiration breath hold respiratory gating and free breathing to improve treatment efficiency and decrease the time the patient was required to be in the MR Linac. On-table adaptive replanning was performed in SABR cases where OAR anatomy was expected to change from day to day and dose constraints would be exceeded. The target volumes and critical OARs within 2 cm of the PTV were recontoured every day and replanning was performed if deemed medically necessary based on predicted dose from the initial plan recalculated on the anatomy of the day. The highest priority for all delivered treatments was to ensure that OAR constraints were met, even if target coverage was compromised. During planning, treatment plans were optimized to deliver 95% of the prescription dose to 100% of the PTV. In the event that organ at risk constraints could not be met with this dose coverage, OAR constraint priorities were met and undercoverage was accepted. During daily online adaptive replanning, we employed an isotoxicity planning approach, where treatment plans were normalized to the nearest OAR dose constraint, typically for the nearest gastrointestinal (GI) OAR. Pretreatment patient-specific quality assurance was performed before delivery of the first planned fraction in all cases and was performed prior to each daily fraction in all plans that underwent online adaptive replanning.

Clinical and radiographic data from baseline and routine follow-up, including patient and tumor characteristics, treatment details, acute and chronic toxicities, and disease response, were collected (by MDH, RH, and KVW) and entered into a coded electronic database. Electronic medical records were also reviewed from the primary pediatric oncology teams for assessment of toxicities. Patients were seen 3 months after MRgRT and then every 3-4 months for routine care in our clinic. Treatment response was evaluated with Response Evaluation Criteria in Solid Tumors (RECIST) version 1.1 criteria. Early and late toxicities were prospectively recorded weekly during MRgRT and then at each radiation oncology follow-up visit using Common Terminology Criteria for Adverse Events (CTCAE) version 5. Acute toxicity was defined as any toxicity occurring during or within 90 days after completing MRgRT.

Descriptive statistics were used to illustrate patient allocation between various treatment modalities in our department and patient-specific outcomes. Local control (LC) was defined as the absence of in-field treatment failure. Overall survival (OS) was determined by the time to death from any cause with censorship at the date of last follow-up. The data presented here comprise all follow-up data up to the close-out date of September 5, 2022.

Results

Between 4/2018 and 4/2022, 535 patients received MRgRT in at our center. Of this total, 405 patients (75.7%) received SABR, defined as doses ≥ 6 Gy delivered in ≤ 10 fractions. Within the SABR cohort, 370 patients were treated with ablative dosing using 5 or fewer fractions while 35 received 6-8 fractions. The two reasons patients did not receive ≤ 5 fractions were if insurance did not approve five-fraction SABR (in this event, patients most often received 40-50 Gy in 6 fractions) or if the radiation oncologist selected a more gently fractionated ablative regimen, such as 60 Gy in 8 fractions for central lung tumors. The most common sites treated in this cohort using SABR were inoperable pancreatic cancer (26.5%), lymph node metastases (16.1%), hepatobiliary tumors (10.3%), and adrenal metastases (9.0%). In this dataset, 69 MRgRT patients (12.9%) received conventional fractionation, most commonly for lung and GI tumor sites treated with definitive intent.

During this four-year period, 347 distinct courses of external beam radiotherapy were delivered to pediatric and young adult patients who were < 21 years of age. This included 28 patients treated with cranial stereotactic radiosurgery (8.1%) and 29 who received total body irradiation as part of the conditioning regimen for hematopoietic cell transplantation. As a result, a total of 290 courses of fractionated external beam radiotherapy were delivered during this interval, including 217 (74.8%) with proton therapy.

In this same period, four pediatric patients received MRgRT. One patient with metastatic Ewing sarcoma received SABR for a lung metastasis in the left lower lobe abutting the diaphragm. For this patient daily adaptive replanning was adopted to meet OAR constraints to the adjacent stomach. For this patient daily adaptive replanning was adopted to meet OAR constraints to the adjacent stomach. A second patient received non-adaptive SABR for a single liver metastasis with gated beam delivery. Two

patients received MRgRT to 30 Gy in 10 fractions for metastatic ALK-rearranged non-small cell lung cancer and neuroblastoma. Fourteen other patients had imaging alone performed on the MR Linac for either image fusion or quality assurance during treatment. Twelve underwent MR imaging without contrast for brain tumors to assess for tumor/cystic changes during treatment. Two additional patients who were subsequently treated using other radiotherapy modalities underwent MR simulation for target volume delineation and organ at risk sparing due to observed anatomic changes or unexpected delays in obtaining diagnostic MR appointments.

Below, we describe four clinical cases from this cohort that illustrate the potential clinical applications for MRgRT in pediatric cancer patients. In addition, we illustrate one example patient in which the MR Linac was used for image fusion and offline adaptive replanning in a patient treated with proton therapy.

Clinical cases and outcomes

Case 1. Lung metastasis near the diaphragm

The patient is an 18-year-old female with recurrent Stage IV Ewing sarcoma with three oligoprogressive lung metastases. Prior therapy included systemic chemotherapy with vincristine, doxorubicin and cyclophosphamide (VDC) alternating with ifosfamide and etoposide (IE) according to Children's Oncology Group (COG) study AEWS1031. She also received surgery and postoperative radiotherapy for a primary tumor in the sacrum and comprehensive metastatic site radiotherapy, including whole lung irradiation to 15 Gy in 10 fractions. The patient relapsed 18 months following completion of primary treatment with metastatic disease in the lungs and recurrence of the primary tumor in the Lumbar spine. She received vincristine, irinotecan, and temozolomide (VIT) chemotherapy with partial response. After chemotherapy, three residual lung metastases remained. Due to prior whole lung irradiation, stereotactic ablative radiotherapy was recommended to 35 Gy in 5 fractions (7, 8).

The patient underwent four-dimensional CT simulation for radiation treatment planning. Two metastases were peripherally located, including one in the anterior left lower lobe (LLL) as illustrated in Figure 1. On CT simulation, tumor excursion was < 8 mm for these lesions. Based on the scoring system proposed by Seravalli and colleagues for the use of MRgRT in pediatric patients, these two lesions were assessed to have a modest potential benefit with MRgRT (3). Based on modest benefit in terms of reduction of total lung dose, these two lesions were treated with SABR using volumetric-modulated arc therapy (VMAT) stereotactic delivery.

In comparison, the third lung metastasis was in the posterior LLL and was near the heart, esophagus, and stomach. This lesion had a maximal tumor excursion of 15 mm during breathing with abdominal compression. Based on proximity to radiosensitive OARs and tumor motion > 10 mm, a strong benefit from MRgRT was predicted. MR simulation was performed with the left (ipsilateral) arm above the head to enable left-sided beams during treatment; the right arm was positioned at the patient's side. This third metastatic lesion was treated with MRgRT in mid-inspiration breath hold with daily online adaptive replanning. OAR dose objectives were set to keep the stomach $D_{0.03cc}$ < 32 Gy. This constraint included the dose contribution from SABR to the anterior LLL delivered using VMAT. Figure 1 illustrates the large magnitude interfraction change observed in the stomach between simulation and the 5th treatment fraction and the resulting dose constraint violation to the stomach based on the anatomy of the day. Online adaptive replanning was performed for all 5 fractions due to predicted dose constraint violations to the stomach.

No adverse toxicities were observed during or after SABR to these metastatic lesions through 11 months of follow-up. The patient had a radiographic complete response of all three treated

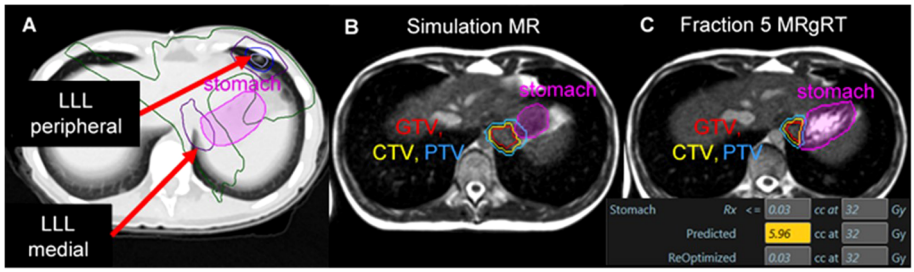

FIGURE 1
A patient with metastatic Ewing sarcoma with two left lower lobe lesions where two SABR plans resulted in dose overlap within the stomach. Isodose lines: Yellow = 40 Gy, Blue = 33 Gy, Green = 20 Gy, Purple = 10 Gy all over 5 fractions **(A)**. A significant change in stomach anatomy was observed during daily cine imaging between simulation **(B)** and each treatment fraction **(C)**. Online adaptive replanning was performed to enable the plan of the day to meet dose constraints for the stomach; in this example, the predicted dose on the anatomy of the day would have exposed 5.96 cc of the stomach to ≥ 32 Gy, while the re-optimized plan improved GTV/PTV coverage and met dose constraints.

lesions on last imaging 10 months after SABR. The patient developed further disease progression at the site of the primary tumor and was treated with chemotherapy and palliative reirradiation 3 months after SABR. At last follow-up, she had active disease at other non-lung sites and continued palliative chemotherapy.

Case 2. Liver metastasis

The patient is a 7-year-old female with a history of rhabdomyosarcoma who presented with a solitary site of metastatic disease in the caudate lobe of the liver. The patient was diagnosed at age 5 with a primary tumor in the distal lower extremity with biopsy-proven popliteal nodal involvement. The patient received systemic chemotherapy according to COG ARST0431 with vincristine and irinotecan (VI), followed by VDC alternating with IE, and then vincristine, dactinomycin, and cyclophosphamide (VAC) alternating with VI. Local therapy included surgery for the primary tumor in the distal calf followed by adjuvant radiotherapy due to nodal involvement. At relapse, she presented with a solitary site of metastatic disease in segment IV of the liver. She received VIT chemotherapy with partial response and no new evidence of metastatic disease. She was referred for consideration of consolidative radiotherapy.

Based on the tumor location and the anticipated tumor excursion during breathing, SABR using MRgRT was recommended. During MR simulation, both arms were placed at the patient's side for comfort and treatment compliance. On CT simulation, the estimated tumor excursion during breathing was between 15 to 20 mm. The patient was treated with SABR to 40 Gy in 5 fractions using MRgRT for margin reduction and improved soft tissue visualization. Figure 2 illustrates that the 0.35 T MRI clearly distinguished tumor from the normal liver without contrast. The patient was planned for treatment with gated delivery in mid-inspiration breath hold using continuous cine MR imaging for tumor tracking in the sagittal plane at 4 frames per second. No internal target volume (ITV) expansion was added. During treatment, the patient proved largely unable to adhere to mid-inspiration breath hold as instructed by the radiation therapists. The patient was coached during treatment with suboptimal compliance. Treatment was still delivered on MRgRT with gated beam delivery when the tumor was in position. The patient tolerated MRgRT with no adverse effects during treatment apart from poor compliance.

At three months, the treated lesion in the caudate lobe of the liver demonstrated a complete radiographic response on imaging. However, 6 additional lesions were identified in the liver in addition to disease in the pancreatic head. Additional salvage therapies, included pazopanib and nivolumab, were given. The patient died with disease 7 months after completion of SABR. No adverse events were observed or reported during this follow up interval. Final CT-based imaging performed within one week of the patient's death demonstrated no clear evidence of disease recurrence in the caudate lobe of the liver.

Case 3. Metastatic neuroblastoma of the mandible

The patient is a 7-year-old male with high-risk neuroblastoma with a painful metastasis involving the right mandible. He was initially diagnosed with Stage IV disease and received high-risk chemotherapy according to COG ANBL0532. He received consolidative proton therapy to 21.6 Gy RBE in 12 fractions to the abdomen and a metastasis in the left temporal bone of the skull that remained positive on functional imaging before high dose chemotherapy with stem

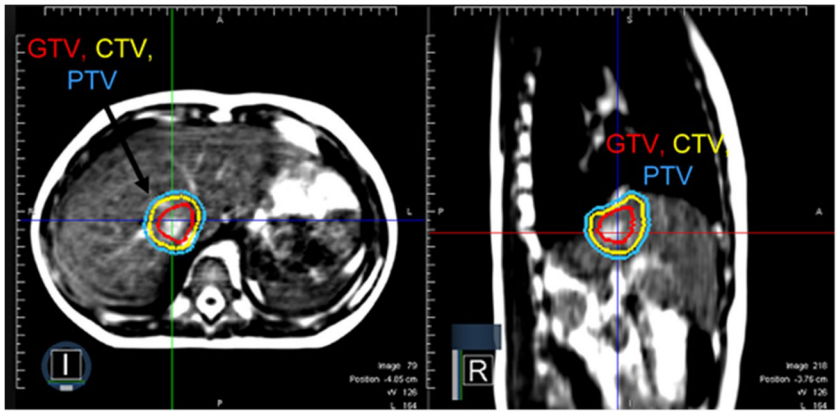

FIGURE 2
A patient with metastatic rhabdomyosarcoma with a solitary liver metastasis who received SABR using MRgRT. Continuous cine imaging and gated delivery during mid-inspiration breath hold enabled treatment with PTV expansion of 3 mm. No ITV was used.

cell rescue. At first recurrence, he developed metastatic disease in multiple bones and was treated with salvage chemotherapy and dinutuximab. He was referred for radiotherapy for a painful mass involving the mandible. Based on limited volume disease, palliative radiotherapy to 30 Gy in 10 fractions was recommended. Based on the scoring system by Seravalli and colleagues, we estimated that MRgRT would provide limited potential benefit in terms of tumor control for this dose regimen but anticipated a modest benefit may be derived from sparing the oral cavity compared to conventional linear accelerator (3).

The patient underwent MR and CT simulation with a thermoplastic mask and moldcare pillow. Figure 3 demonstrates that the MR Linac significantly improved soft tissue visualization and permitted differentiation between the tumor and the adjacent masseter and pterygoid muscles. As a result, MRgRT enabled more precise target volume delineation than would be feasible with CT-based planning, where GTV would have been overestimated. The patient was treated with a 3D conformal MRgRT plan using 9 fields that delivered a mean dose of 18.5 and 17.5 Gy to the ipsilateral parotid and submandibular glands, 9.0 Gy to the oral cavity, and < 5 Gy to the contralateral parotid and submandibular glands. The MRgRT plan enabled significant reduction in OAR dosing, particularly to the oral cavity, compared to 3D conformal plan on a conventional linear accelerator. Due to the treatment planning process for MRgRT, the MR Linac 3D conformal plan was similar in quality to an IMRT plan without excess cost to the healthcare system. At follow up visits at 3 and 6 months, the patient denied xerostomia, dysgeusia, oral mucositis, and pain, which are commonly experienced by patients following palliative radiotherapy to this region.

Case 4. Metastatic non-small cell lung adenocarcinoma in a lifelong non-smoker

The patient is a 19-year-old non-smoker with Stage IV ALK-rearranged non-small cell lung cancer, who presented with right neck and chest pain and Horner's syndrome. Imaging demonstrated a 10 cm soft tissue mass abutting the right mediastinum and displacing the right heart border, multiple pleural-based soft tissue masses, enlarged mediastinal and right supraclavicular nodes, and bone metastases in C5, C7, T1, T3, and T4 with involvement of the neural foramina at T3-T4. Due to pain, she was referred for radiotherapy and received 30 Gy in 10 fractions with MRgRT using step-and-shoot IMRT. Figure 4 depicts the MRgRT plan, which delivered a mean dose of 7.77 Gy to the heart, 7.92 Gy to the lungs, and 16.78 Gy to the esophagus. The volume of esophagus receiving prescription dose was 18%.

Following treatment, the patient developed Grade 1 esophagitis, managed with dietary changes and increased fluid

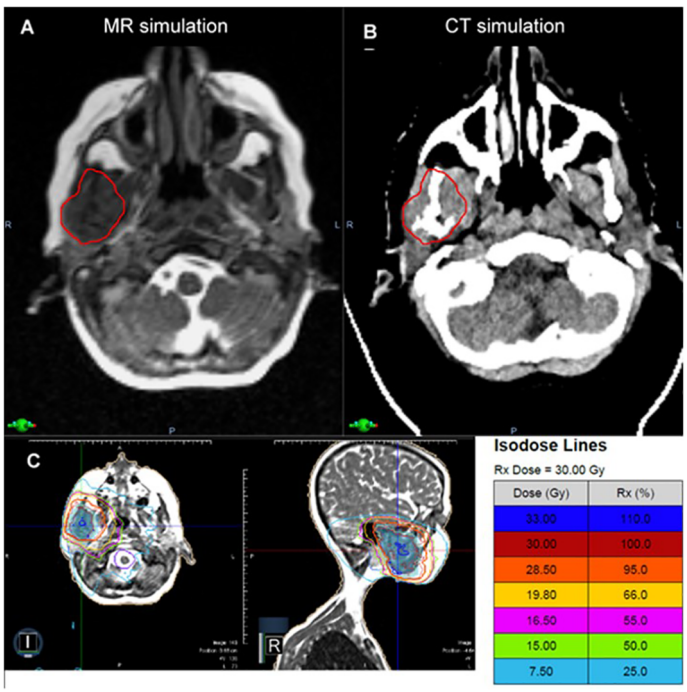

FIGURE 3
In a patient with metastatic neuroblastoma involving the mandible, the MR simulation **(A)** provided superior visualization of the tumor relative to the adjacent masseter and pterygoid muscles compared to CT **(B)**. The patient was treated with a 3D conformal MRgRT plan **(C)**, which provided favorable sparing of the oral cavity and the ipsilateral and contralateral salivary glands with similar plan quality to IMRT.

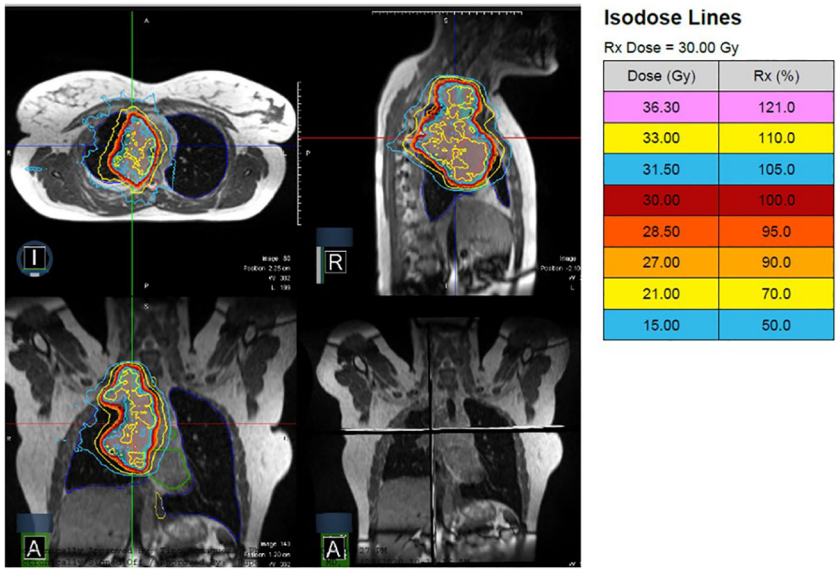

FIGURE 4
A patient with Stage IV ALK-rearranged non-small cell lung cancer and a 10 cm primary tumor received 30 Gy in 10 fractions with MRgRT. Continuous cine imaging and gated delivery during mid-inspiration breath hold enabled treatment with PTV expansion of 3mm. No ITV was used.

intake. No pain medications were needed. She initiated alectinib for systemic therapy. At two months following radiotherapy, a partial response was documented on imaging with a 50% volumetric reduction in the dominant mass. Last clinic and imaging follow up was 2 years and 3 months following MRgRT, when the patient had no clear evidence of residual tumors in the lung and sclerotic bone lesions, consistent with treated tumor.

Weekly imaging on the MR Linac and offline adaptive replanning in a craniopharyngioma patient receiving proton therapy

The patient is a 10-year-old male with craniopharyngioma who received intensity-modulated proton therapy to 54 Gy RBE in 30 fractions. Proton therapy was recommended based on the favorable prognosis and significant reduction in total integral dose and hippocampus and temporal lobe sparing. Weekly on-treatment MR imaging was obtained on the MR Linac to evaluate changes in the tumor/cyst and the need for offline adaptive replanning. Figure 5 demonstrates the CT simulation and the MR acquired on the MR Linac during week 1 of proton therapy (22 days following simulation), which demonstrated that the tumor/cyst had increased in size and now abutted the original CTV contour. Offline adaptive replanning was performed. The patient received two additional fractions using the initial proton therapy plan and then began the new plan three days after MR imaging.

In our center, weekly MR is feasible on the MR Linac either before or after proton therapy and eliminates the need for a separate appointment in radiology for a diagnostic MRI without contrast. This is a more efficient use of patient time and cancer center resources, given that the weekly appointments on the MR Linac last approximately 10 minutes and are more easily coordinated with proton therapy treatment times. This provides significant time savings for the patient and family compared to an appointment in radiology and still permits excellent tumor differentiation for adaptive replanning (9).

Discussion

MRgRT is a relatively new modality in radiation oncology, which is growing in utilization as more systems are brought online. Early results suggest that MRgRT may lead to clinical benefits in selected adults across several disease sites, including inoperable pancreatic cancer treated with SABR with survival rates that compared favorably to historical controls (1) and prostate SABR with improved toxicity rates compared to cone-beam CT-based delivery (10). The current experience for pediatric cancers, however, remains particularly limited (4, 5). To our knowledge, this is the largest published experience of MRgRT in pediatric and young adult patients, amounting to only four patients during the first four years of utilization at our institution.

The MOMENTUM academic industrial collaborative group recently reported early outcomes of MRgRT patients treated on a

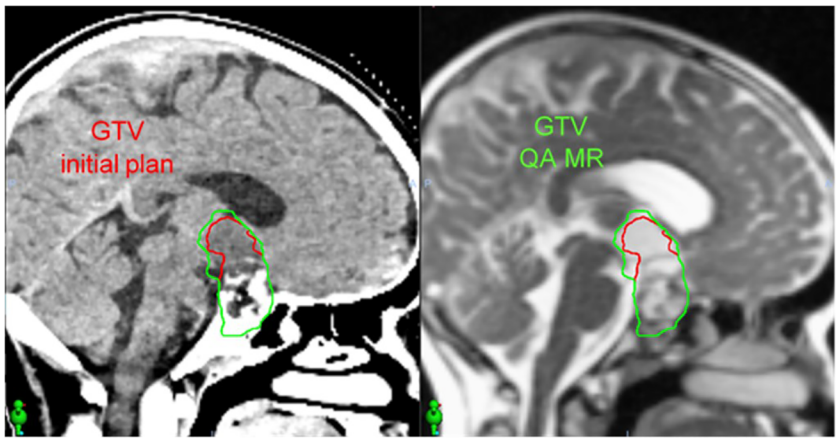

FIGURE 5
In a patient with craniopharyngioma, an on-treatment MR acquired using the MR Linac (right) 22 days after CT simulation (left) demonstrated increased size of the tumor/cyst. This MR image set was used to perform offline adaptive replanning.

prospective registry between February, 2019 and October, 2020. In this first report, 943 adult patients (age 21-93) were treated at 7 institutions in Europe, Canada, and the United States, and 415 (44.0%) had acute toxicity data at 3-month follow-up. The observed rate of grade 3 toxicity was 4% in patients treated for a wide range of indications including prostate cancer, oligometastatic lymph nodes, brain tumors, and rectal cancer; the majority of patients received ≤ 5 fractions (11). While clinical experience with MRgRT is growing in adult tumors, greater effort and planning is needed to bridge the gap on clinical development in pediatrics.

Due to the rarity and diversity of pediatric tumors, multi-institutional collaboration by all centers treating pediatric patients with MRgRT is a significant unmet need. To this end, a pediatric MRgRT working group of twelve members across SIOPE and COG-affiliated radiotherapy departments, including three ViewRay MRIdian and nine Elekta Unity (Elekta, Crawley, UK) users, was established in June, 2021 (3). Given the small number of pediatric patients who will receive MRgRT at each center, enrolling all patients into a registry and prospectively tracking outcomes will be important to build clinical expertise.

While the experience presented here only adds five scenarios where the MR Linac was applied in clinic, we observed three important findings. First, MRgRT can be applied in varied clinical scenarios, but the same advantages identified in adult patients also exist in children, including improved soft tissue visualization, gated delivery plus real-time tumor tracking, and online adaptive replanning to meet critical OAR constraints. Cases 1 and 2 in this report describe tumors treated with SABR that were characterized by significant motion and proximity to luminal GI OARs where gated delivery and online adaptive replanning enabled superior target coverage without an ITV. Second, patient selection must be carefully considered both for MRgRT utilization and based on the relative benefits of other available modalities in the department. At our center, SABR, most commonly with online adaptive replanning, comprises approximately 75% of MRgRT cases. Given that each treatment fraction generally lasts 50-60 minutes with online adaptive replanning, limited slots remain for treatment of patients with more modest benefits from MRgRT. This is also illustrated in Case 1 of this report. While the metastatic lesion near the stomach received MR-guided SABR, two other lesions with more limited respiratory excursion and without the need for online adaptive replanning were treated with CBCT-based SABR. Further, most pediatric patients at our center receive proton therapy for curative intent tumors in order to reduce late effects following treatment. If proton therapy were not accessible to patients at our center, the utilization of MRgRT may have been different than observed here, but the authors find that MRgRT is unlikely to replace proton therapy in the vast majority of cases at our institution. At our institution, patient selection is largely driven by the treating physician. Cases 3 and 4 present two patients who could have received equally efficacious treatment without MRgRT but may have potentially benefited from OAR sparing and resulting reduction in acute toxicities with this approach.

Many challenges with MRgRT utilization are similar in adults and children. One potential barrier is longer treatment times, particularly when using an online adaptive workflow. Patients should be selected who will be able to hold still for the requisite amount of time to complete treatment. Careful patient positioning and immobilization at simulation should also be enacted to improve patient comfort and compliance. Future improvements, including automatic contouring and planning capabilities may reduce treatment times and minimize this challenge with MRgRT (12). Similarly, technological improvements in MRgRT such as volumetric arc delivery may also reduce delivery times and improve plan quality (13). Real-

time respiratory gating is currently available only in a subset of MRgRT units, which may reduce plan quality and the ability to deliver ablative dosing for some tumor locations. In the future, the integration of respiratory gating capabilities in all MRgRT systems may enable greater utilization in abdominal and pelvic tumors near GI OARs. Patient selection is critical to identify patients who will gain the most from MRgRT. Clinicians should consider the importance of (1) soft tissue visualization, (2) respiratory motion management, and (3) proximity to OARs and the ability to spare them using MRgRT with or without online adaptive replanning compared to other radiotherapy modalities.

Other barriers to the use of MRgRT in pediatric patients are more exclusive to children. For example, pediatric patients more commonly use anesthesia during radiotherapy than adults. Potential users should consider anesthesia needs if planning to treat such patients with MRgRT, including the use of MR-compatible anesthesia and patient monitoring equipment within the vault. Supportive care resources, such as an audiovisual entertainment system and a certified child life specialist can also assist with treatment compliance and emotional adjustment for patients who will undergo MRgRT (14, 15). Finally, staff should ensure that all equipment and devices used are compatible with MRgRT. For example, the patient treated in Case 3 had to be re-simulated prior to treatment because metallic paint was applied to the thermoplastic mask to create a superhero image at the request of the patient. Figure 6 illustrates both the decorated mask and the new one that was ultimately used for treatment. Metallic paint can induce heating in the MR Linac vault and could potentially result in skin burns. This case example provides and important opportunity to stress the importance of MR safety education and awareness in developing a MRgRT program.

We acknowledge several limitations in this published work. First, due to its retrospective design and the patient population treated, the duration of follow-up was generally short and was often limited due to death from disease. Retrospective studies can potentially underreport treatment-related toxicities. We strived to mitigate this limitation by prospectively evaluating toxicities at each patient visit during and after treatment as a matter of routine care. In addition, our study period included several years during the COVID-19 pandemic. While this reality certainly altered healthcare delivery, patient follow-up arguably was not adversely impacted by the pandemic, due in large part to the incorporation of telehealth conferences with patients during follow-up. Distance from our facility and appointments with other physicians represent common barriers for patients to attend follow-up clinic in person. In contrast to disruption, the typically short courses delivered on MRgRT may have been more practical for patients compared to longer courses of radiation that may have been given without MR Linac and follow-up was maintained or may have been arguably improved with patients using telehealth services to make some of their appointments in our clinic. Second, patient-reported outcomes are important measures of treatment tolerance and toxicity and were not collected in this analysis. The future prospective pediatric MRgRT registry should consider including such metrics to better understand patient quality-of-life following MRgRT. Finally, the small incidence of pediatric tumors overall and the scarcity of pediatric patients who will receive MRgRT

FIGURE 6
This image illustrates a mask used to treat a pediatric patient for metastatic neuroblastoma that has been decorated with paint that contained metallic components. All devices used during MRgRT must be MR compatible. In this case, the patient was re-simulated before treatment with an unpainted mask.

will lead to limited patient numbers and considerable heterogeneity in clinical outcomes. This underscores the importance of prospective registries to build clinical knowledge and technical skill in the application of MRgRT in new patient populations, including children.

In summary, we report four clinical cases treated with MRgRT at a single institution and an example patient where MR Linac was used for mid-treatment imaging and offline adaptive replanning during treatment. The four patients treated with MRgRT tolerated treatment well and without any Grade 2 or higher toxicities following treatment. Our manuscript adds to the body of literature on the use of MRgRT in pediatric patients, illustrates several clinical scenarios where MRgRT may be used, and describes several lessons learned that are pertinent to future users of this novel radiotherapy treatment strategy.

Data availability statement

The raw data supporting the conclusions of this article will be made available by the authors, without undue reservation.

Ethics statement

The studies involving human participants were reviewed and approved by Miami Cancer Institute IRB. Written informed consent from the participants' legal guardian/next of kin was not required to participate in this study in accordance with the national legislation and the institutional requirements.

Author contributions

The authors affirm their contributions to the paper as follows: Study conceptualization: MH, KM, and MC. Data curation: MH, RH, KM, and KV. Data analysis: MH and KM. Writing – original draft: MH, KV, KM, and MC, Manuscript editing and review: All authors. All authors contributed to the article and approved the submitted version.

Funding

No external funding was received for this study. Internal departmental funding was used to submit the article for publication, but had not role in the study design, data analysis, or decision to submit the article for publication.

Conflict of interest

Author MH reports grants from the Florida Department of Health Live Like Bella Pediatric Cancer Research Initiative, personal fees from Ion Beam Associates (IBA), outside the submitted work. Author KM reports personal fees and nonfinancial support from ViewRay, other from MR Guidance, LLC, outside the submitted work. Author RK reports personal fees and non-financial support from Elekta, grants from Novocure, personal fees from Accuray, grants from Blue Earth Diagnostics, grants from Medtronic, grants from AstraZeneca, grants from Exelixis, personal fees from ViewRay, outside the submitted work. Author AG reports personal fees and non-financial support from ViewRay, outside the submitted work. Author MC reports grants, personal fees and non-financial support from ViewRay, personal fees from Sirtex, grants from Novocure, personal fees from Advanced Accelerator Applications, outside the submitted work.

The remaining authors declare that the research was conducted in the absence of any commercial or financial relationships that could be construed as a potential conflict of interest.

Publisher's note

References

1. Chuong MD, Herrera R, Kaiser A, Rubens M, Romaguera T, Alvarez D, et al. Induction chemotherapy and ablative stereotactic magnetic resonance image-guided adaptive radiation therapy for inoperable pancreas cancer. *Front Oncol* (2022) 12:888462. doi: 10.3389/fonc.2022.888462

2. Kutuk T, Herrera R, Mustafayev TZ, Gungor G, Ugurluer G, Atalar B, et al. Multi-institutional outcomes of stereotactic magnetic resonance image guided adaptive radiation therapy with a median biologically effective dose of 100 Gy10 for non-bone oligometastases. *Adv Radiat Oncol* (2022) 7(6):100978. doi: 10.1016/j.adro.2022.100978

3. Seravalli E, Kroon PS, Buatti JM, Hall MD, Mandeville HC, Marcus KJ, et al. The potential role of MR-guided adaptive radiotherapy in pediatric oncology: Results from a SIOPE-COG survey. *Clin Transl Radiat Oncol* (2021) 29:71–8. doi: 10.1016/j.ctro.2021.05.008

4. Henke LE, Green OL, Schiff J, Rodriguez VL, Mutic S, Michalski J, et al. First reported case of pediatric radiation treatment with magnetic resonance image guided radiation therapy. *Adv Radiat Oncol* (2019) 4(2):233–6. doi: 10.1016/j.adro.2019.01.008

5. Egriboyun S, Ugurluer G, Corapcioglu FV, Celik L, Gungor G, Atalar B, et al. Magnetic resonance image-guided stereotactic body radiation therapy for liver rhabdoid tumor in infancy: A case report. *J Med Imaging Radiat Sci* (2021) 52 (2):305–11. doi: 10.1016/j.jmir.2021.02.006

6. Chuong MD, Bryant J, Mittauer KE, Hall M, Kotecha R, Alvarez D, et al. Ablative 5-fraction stereotactic magnetic resonance-guided radiation therapy with on-table adaptive replanning and elective nodal irradiation for inoperable pancreas cancer. *Pract Radiat Oncol* (2021) 11(2):134–47. doi: 10.1016/j.prro.2020.09.005

7. Brown LC, Lester RA, Grams MP, Haddock MG, Olivier KR, Arndt CA, et al. Stereotactic body radiotherapy for metastatic and recurrent ewing sarcoma and osteosarcoma. *Sarcoma* (2014) 2014:418270. doi: 10.1155/2014/418270

8. Deck J, Eastwick G, Sima J, Raymond A, Bogart J, Aridgides P. Efficacy and tolerability of stereotactic body radiotherapy for lung metastases in three patients with pediatric malignancies. *Onco Targets Ther* (2019) 12:3723–7. doi: 10.2147/OTT.S194812

9. Kumar RS, Rotondo RL, Bradley JA, Vern-Gross T, Huh S, Indelicato DJ. Mid-treatment magnetic resonance imaging in pediatric intracranial low-grade gliomas treated with proton beam therapy. *Acta Oncol* (2017) 56(9):1243–7. doi: 10.1080/0284186X.2017.1306105

10. Kishan AU, Lamb J, Casado M, Wang X, Ma TM, Low D, et al. Magnetic resonance imaging-guided versus computed tomography-guided stereotactic body radiotherapy for prostate cancer (MIRAGE): Interim analysis of a phase III randomized trial. *J Clin Oncol* (2022) 40:6(suppl):255. doi: 10.1200/JCO.2022.40.6_suppl.255

11. de Mol van Otterloo SR, Christodouleas JP, Blezer ELA, Akhiat H, Brown K, Choudhury A, et al. Patterns of care, tolerability, and safety of the first cohort of patients treated on a novel high-field MR-linac within the MOMENTUM study: Initial results from a prospective multi-institutional registry. *Int J Radiat Oncol Biol Phys* (2021) 111(4):867–75. doi: 10.1016/j.ijrobp.2021.07.003

12. Mittauer K, Paliwal B, Hill P, Bayouth JE, Geurts MW, Baschnagel AM, et al. A new era of image guidance with magnetic resonance-guided radiation therapy for abdominal and thoracic malignancies. *Cureus* (2018) 10(4):e2422. doi: 10.7759/cureus.2422

13. Hoeben BA, Carrie C, Timmermann B, Mandeville HC, Gandola L, Dieckmann K, et al. Management of vertebral radiotherapy dose in pediatric patients with cancer: Consensus recommendations from the SIOPE radiotherapy working group. *Lancet Oncol* (2019) 20(3):e155–66. doi: 10.1016/S1470-2045(19)30034-8

14. Prasad RN, Baliga S, Banner J, Cadieux C, Cetnar A, Degnan M, et al. Radiation therapy without anesthesia for a 2-Year-Old child using audio-visual assisted therapeutic ambience in radiation therapy (AVATAR). *Pract Radiat Oncol* (2021) 12(3):e216–20. doi: 10.1016/j.prro.2021.12.009

15. Boik N, Hall MD. Psychosocial support for pediatric patients at proton therapy institutions. *Int J Part Ther* (2020) 7(1):28–33. doi: 10.14338/IJPT-20-00015.1

frontiers | Frontiers in Oncology

TYPE Original Research
PUBLISHED 16 January 2023
DOI 10.3389/fonc.2022.1095633

OPEN ACCESS

EDITED BY
Claudio Fiorino,
San Raffaele Hospital (IRCCS), Italy

REVIEWED BY
Francesco Ricchetti,
Sacro Cuore Don Calabria Hospital (IRCCS), Italy
Enis Ozyar,
Acıbadem University, Turkey

*CORRESPONDENCE
Laura Uder
laura.uder@med.uni-tuebingen.de

SPECIALTY SECTION
This article was submitted to Radiation Oncology, a section of the journal Frontiers in Oncology

RECEIVED 11 November 2022
ACCEPTED 14 December 2022
PUBLISHED 16 January 2023

CITATION
Uder L, Nachbar M, Butzer S, Boldt J, Baumeister S, Bitzer M, Königsrainer A, Seufferlein T, Hoffmann R, Gatidis S, Nikolaou K, Zips D, Thorwarth D, Gani C and Boeke S (2023) Local control and patient reported outcomes after online MR guided stereotactic body radiotherapy of liver metastases. *Front. Oncol.* 12:1095633. doi: 10.3389/fonc.2022.1095633

Local control and patient reported outcomes after online MR guided stereotactic body radiotherapy of liver metastases

Laura Uder[1]*, Marcel Nachbar[2], Sarah Butzer[1], Jessica Boldt[1], Sabrina Baumeister[1], Michael Bitzer[3], Alfred Königsrainer[4], Thomas Seufferlein[5], Rüdiger Hoffmann[6], Sergios Gatidis[6], Konstantin Nikolaou[6], Daniel Zips[1,7,8], Daniela Thorwarth[2,7], Cihan Gani[1,7] and Simon Boeke[1,7]

[1]Department of Radiation Oncology, University Hospital and Medical Faculty, Eberhard Karls University Tübingen, Tübingen, Germany, [2]Section for Biomedical Physics, Department of Radiation Oncology, University Hospital and Medical Faculty, Eberhard Karls University Tübingen, Tübingen, Germany, [3]Department of Internal Medicine I, University Hospital Tübingen, Tübingen, Germany, [4]Department of General, Visceral and Transplant Surgery, University Hospital Tübingen, Tübingen, Germany, [5]Department of Internal Medicine I, Ulm University Hospital Medical Center, Ulm, Germany, [6] Department of Diagnostic and Interventional Radiology , University of Tübingen, Tübingen, Germany, [7]German Cancer Consortium (DKTK), partner site Tübingen; and German Cancer Research Center (DKFZ), Heidelberg, Germany, [8]Department of Radiation Oncology, Berlin Institute of Health, Charité - Universitätsmedizin Berlin, Corporate Member of Freie Universität Berlin, Humboldt-Universität zu Berlin, Berlin, Germany

Introduction: Stereotactic body radiotherapy (SBRT) is used to treat liver metastases with the intention of ablation. High local control rates were shown. Magnetic resonance imaging guided radiotherapy (MRgRT) provides the opportunity of a marker-less liver SBRT treatment due to the high soft tissue contrast. We report herein on one of the largest cohorts of patients treated with online MRgRT of liver metastases focusing on oncological outcome, toxicity, patient reported outcome measures (PROMs), quality of life.

Material and methods: Patients treated for liver metastases with online MR-guided SBRT at a 1,5 T MR-Linac (Unity, Elekta, Crawley, UK) between March 2019 and December 2021 were included in this prospective study. UK SABR guidelines were used for organs at risk constraints. Oncological endpoints such as survival parameters (overall survival, progression-free survival) and local control as well as patient reported acceptance and quality of life data (EORTC QLQ-C30 questionnaire) were assessed. For toxicity scoring the Common Toxicity Criteria Version 5 were used.

Results: A total of 51 patients with 74 metastases were treated with a median of five fractions. The median applied BED GTV D98 was 84,1 Gy. Median follow-up was 15 months. Local control of the irradiated liver metastasis after 12 months was 89,6%, local control of the liver was 40,3%. Overall survival (OS) after 12 months was 85.1%. Progression free survival (PFS) after 12 months was 22,4%. Local control of the irradiated liver lesion was 100% after three years when a BED ≥100 Gy was reached. The number of treated lesions did not impact local control

neither of the treated or of the hepatic control. Patient acceptance of online MRgSBRT was high. There were no acute grade ≥ 3 toxicities. Quality of life data showed no significant difference comparing baseline and follow-up data.

Conclusion: Online MR guided radiotherapy is a noninvasive, well-tolerated and effective treatment for liver metastases. Further prospective trials with the goal to define patients who actually benefit most from an online adaptive workflow are currently ongoing.

KEYWORDS

magnetic resonance guided radiotherapy, stereotactic body radiation therapy, image guided radiation therapy, liver metastases, online adaptive radiation therapy

Introduction

With the advent of oligometastatic disease as a third disease state between "metastatic" and "non-metastatic", there is in growing interest in effective local treatment options such as microwave ablation, surgery or radiofrequency ablation (1, 2). Stereotactic body radiotherapy (SBRT) in particular has recently been shown to prolong overall survival in patients with oligometastatic disease (3, 4). However using SBRT in the abdominal compartment and in specifically in the liver is challenging due to the very limited soft tissue contrast of cone-beam computed tomography (CBCT) based linear accelerators. For this reason fiducial markers are often used as surrogate markers. Recently online adaptive magnetic resonance tomography guided radiotherapy (MRgRT) was introduced into the clinical routine (5–9). MRgRT provides higher soft tissue contrast of MR imaging than cone-beam computed tomography (CBCT). It also allows online plan adaptation for each radiotherapy fraction (10). Especially for treatment of tumors in the abdomen the better soft tissue contrast of MR imaging allows to visualize tumors and organs at risk (OAR) at the timepoint of treatment (11). MRgRT also offers the opportunity of a marker-less SBRT without the possible complications due to the invasive fiducial placement potentially increasing patient acceptance compared to invasive procedures (12). In this study we report the largest cohorts of patients treated with online MRgRT of liver metastases focusing on oncological outcome, toxicity, patient reported outcome measures (PROMs) and quality of life.

Materials and methods

Patient selection

In this study consecutive patients with liver metastases receiving online MR-guided SBRT with a fraction size above 5 Gy at a 1,5 T MR-Linac (Unity, Elekta, Crawley, UK) were included. The MR-01 study (NCT04172753) is a prospective phase 2 basket trial primarily assessing the feasibility of online adaptive MR guided radiotherapy but also oncological endpoints such as survival parameters and patient-reported outcomes (PROMs). Written informed consent of all patients was provided. Prior to radiotherapy therapeutic alternatives were debated in a multidisciplinary tumor board. The institutional review board of the medical faculty Tübingen (IRB 659/2017BO1) approved the study.

Treatment planning and radiotherapy workflow

Detailed report of the treatment planning and online workflow has been published (11). For treatment simulation and for every fraction patients had to feast for 3 hours. Patients received a four dimensional CT simulation scan in treatment position with indexed patient positioning aids. On the same day an MR simulation scan was performed on the 1.5T MR-Linac. Three MR simulation scans were performed: A triggered T2 (voxel size 2 mm × 2 mm × 2.4 mm, TE 206 ms, TR 2100 ms) and T2 spair (voxel size 2 mm × 2 mm × 2.4 mm, TE 248 ms, TR 2100 ms), both in exhale position and non– triggered T2 (voxel size 2 mm × 2 mm × 2.4 mm, TE 206 ms, TR 2100 ms).

For delineation and treatment planning Monaco ® V.5.4 was used. Combining information of all available images an internal target volume was created. Information of the 4D CT as well as the cine MR images was used to determine the respiratory motion of the metastases. To account for intrafractional variablity a planning target volume (PTV) margin of three to six millimeters was added on the discretion of the treating physician. UK SABR guidelines were used for organs at risk constraints (10, 13). In case OARs constraints could not be met the encompassing dose to the PTV was lowered. BED was calculated as reported previously (12).

Depending on target localisation eight to eleven individual beam angles have been used, avoiding high-density couch structures. Plan calculation was done on the exhale phase of the four dimensional planning CT.

The workflow for SBRT application was as the following: a free breathing T2 scan (voxel size 2 mm × 2 mm × 2.4 mm, TE 206 ms, TR 2100 ms) was performed after patient positioning. A rigid registration of the daily MR to the planning CT to the was performed in the online treatment system (Monaco ®, Elekta AB, Stockholm, Sweden) by the attending physician. Adaptation was done by the "adapt to position" workflow to account for internal shifts and a new plan was optimized online (14). After evaluation of the adapted plan by the treating physician and after a secondary dose calculation as an online quality assurance (QA)-check, plan was approved and the treatment was initiated. Cine MR imaging with a predefined structure (usually the PTV) at a frequency of 5 Hz was performed during beam on to ensure target coverage. For QA another free breathing T2 scan was acquired post-treatment. Additional images such as diffusion weighted imaging for research purposes could be taken hereafter (15).

Beam on time and in room time (in minutes) were assessed by radiotherapy therapists. For scoring acute and late toxicity Common Toxicity Criteria Version 5 have been used. During follow- up patients were contacted by phone or seen in person. In general, the first follow-up was three months after radiotherapy and included an MRI using contrast agent, blood test, PROMs and assessment of toxicity. Afterwards follow up was repeated every 3 month.

Prior to radiotherapy blood work with liver function tests and a clinical assessment for cirrhotic liver disease (Child-Pugh score) was done. Time to event data was calculated according to the Kaplan-Meier method. For group comparisons the log-rank test was performed. Local control was calculated from the day of the last radiotherapy fraction until the first report of disease progression on imaging or histological confirmation of disease recurrence or persistence. Progression-free survival was calculated from the last radiotherapy fraction until local or distant disease progression or death of any cause. Overall survival was calculated from the last radiotherapy fraction until death of any cause. Statistics were performed using SPSS, Version 28, IBM, Armonk, New York, and Graphpad Prism 5. A p-value of less than 0.05 was considered statistically significant.

Patient reported acceptance of online MRgSBRT was assessed by a previously published questionnaire (13, 14). For radiation induced liver disease (RILD) the definition of Lawrence et al. was used (16).

Results

Patient and treatment characteristics

Between March 2019 and December 2021 a total of 51 consecutive patients have been treated with online MR-guided SBRT for liver metastases. Patient characteristics are shown in Table 1.

Median patient age was 67 years (range 42 – 90 years). Of the 51 patients, 24 patients (47%) had received liver directed local treatment prior to SBRT and 42 (82,4%) of the patients had received chemotherapy. In 45 patients a single lesion was treated, 12 patients received treatment of more than one liver lesion using separate treatment plans.

Dosimetric parameters are summarized in Table 2.

A median of five fractions were applied (range three to eight fractions). Median beam-on time was 7,4 min (4 -12 range). The median in room time was 35,56 min (22,2 – 44,8).

The median applied BED GTV D98 was 84,1 Gy (26,7 – 135,5 Gy). The median applied BED ITV D98 was 81,4 Gy (29,1 – 132,9 Gy).

There were no acute grade ≥ 3 toxicities. No change in Child-Pugh Score was observed during follow-up.

Oncological outcome

Median follow-up was 15 months (3 – 39 months). Median chemotherapy-free interval after completion of SBRT was 4.9 months (0 – 24 months) after SBRT.

Local control of the irradiated liver metastasis after 12 months was 89,6%; after 24 months 67,7% and after 36 months 67,7% (Figure 1A). Local control of the liver, outside of the irradiated liver lesion was 40,3% after 12 months, 16,8% after 24 months and 8,4% after 36 months as shown in Figure 1B. Overall survival after 12 months, 24 months and 36 months were 85.1%, 76.2% and 66.7%. Median OS was not reached (Figure 1C). Progression free survival (PFS) after 12 months was 22,4% and 4.7% after 24 months. Median PFS was 5 months (Figure 1D).

No difference in local control regarding the irradiated lesion was observed between metastasis originating from colorectal vs non-colorectal primary sites (p=0.64), Supplementary figure 1.

Local control of the irradiated liver lesion was 100% after three years when a BED ≥100 Gy was reached and 85.7%, 53.6% and 53.6% after 12, 24 and 36 months respectively, when a BED < 100 Gy was applied (p=0,02) as shown in Figure 2A. The number of treated lesions did not impact local control neither of the treated lesions (66,7% vs 66,7% after 24 months) or of the hepatic control (16,7% vs 16,7% after 24 months) as shown in Figures 2B, C. Local control when a single lesion was treated was 77,4% after 12 months (24 months: 37,1%, 36 months: 37,1%). After treatment of multiple liver lesions local control was 55,0% after 12 months (24 months: 55,0%, 36 months: 55,0%).

Patient acceptance of online MRgSBRT was high as shown in Figure 3.

Quality of life data assessed by the EORTC QLQ-C30 questionnaire is shown in Figures 4A, B.

Quality of life data was available before the start of radiotherapy (26 patients), at last radiotherapy (29 patients), at

10.3389/fonc.2022.1095633

TABLE 1 Patient and treatment characteristics.

	n (%)
Patients	51
Sex	
Male	32 (62,7)
Female	19 (37,3)
Median age (range)	67 (42 – 90)
Irradiated metastases	74
Treated metastases	
n=1	45 (78,9)
n>1	12 (21,1)
Number of hepatic metastasis prior to RT	
n=1	31 (54,4)
n>1	26 (45,6)
maximum	4
median	1,7
Indication	
Oligometastatic disease	43 (75,4)
Oligoprogression	14 (24,6)
Extrahepatic tumour	
Yes	26 (45,6)
No	31 (54,4)
Median fractions (range)	5 (3 – 8)
Primary tumor	
Cholangiocarcinoma	7 (13,7)
Colorectal	23 (45,1)
Breast	2 (3,9)
Choroidal melanoma	4 (7,8)
Other*	15 (29,4)
Chemotherapy prior to RT	
Yes	42 (82,4)
No	9 (17,6)
Previous liver directed therapy (treated lesion)	
No	39 (68,4)
Yes	18 (31,6)
Surgery	13
TACE	0
RFA	1
SIRT	0
Chemosaturation	4
Previous hepatic therapy (other lesions)	
No	33 (57,9)
Yes	24 (42,1)
Surgery	17
TACE	0
RFA	4
Radiotherapy	2
SIRT	2
Chemosaturation	3
Liver cirrhosis prior to RT	
No	51 (89,5)
Child Pugh A	5 (8,8)
Child Pugh B	1 (1,8)
Child Pugh C	0 (0)
Median chemotherapy-free time after RT (range)	4,9 (0 – 24) months
Median in room time (range)	35,7 (22,2 – 44,8) minutes
Median beam on time (range)	7,4 (4 – 12) minutes

*Esophageal cancer (n=2), gastrointestinal stromal tumor (GIST, n=2), pancreas (adenocarcinoma) (n=2), n=1 for esophagus, adenoidcystic carcinoma of the head and neck, renal cell carcinoma, epipharyngeal cancer, ovarial cancer, yolk sac tumor, neuroendocrine tumor (NET) of the pancreas, NET of the small bowel, adenocarcinoma of unknown primary site.
TACE (Transcatheter arterial chemoembolization), RFA (Radiofrequency ablation), SIRT (Selective internal radiation therapy).

three months follow-up (20 patients) and at six months follow-up (19 patients). All comparisons between baseline and "last radiotherapy fraction", "3 months follow-up" and "6 months follow-up" showed no significant difference, apart from "appetite loss" being significantly lower at six months follow-up compared with baseline (11.5 vs. 1.8, p=0.04).

Discussion

With the "introduction" of the oligometastatic disease state as a third state between non-metastastic and diffusely metastatic and the associated paradigm shift towards local metastases directed therapies there is growing need for effective and non-invasive local treatments for patients presenting with oligometastases (3, 4).

The present study reports the largest cohort of liver metastases treated on a 1.5 T MR-Linac. We had previously published data on the feasibility of the online workflow and the imaging quality with an excellent visibility of the majority of the lesions treated (11). As in our previous report patient acceptance of the treatment was excellent and no treatment had to be discontinued due to patient request. This is reassuring as there had been concerns initially whether patients could manage to remain still in an MRI with arms above head for the duration of treatment. Data on treatment outcomes after online-MR guided radiotherapy for liver metastases is still sparse.

A selection of studies on MR guided stereotactic body radiotherapy of liver metastases is shown in Table 3.

For instance Weykamp and colleagues report a one year local control rate of 88% in twenty patients treated for liver tumors (18 metastases, two HCCs) on a 0.35 T MR-Linac (17). Van Dams et al. also report data of a mixed cohort (n=20) of

TABLE 2 Dosimetric parameters. GTV-Gross tumor volume, IQR-Inter quartile range.

	median	minimal	maximal	25% quartile	75% quartile	IQR
ITV volume (cc)	23,4	0,5	201,4	4,5	27,8	23,3
PTV volume (cc)	48,9	3,0	260,5	13,0	71,7	58,7
Liver volume (cc)	1432,8	852,7	3011,1	1129,1	1633,3	504,2
Liver minus GTV volume (cc)	1451,1	873,6	3056,7	1156,6	1642,9	486,3
Mean dose liver minus GTV (Gy)	7,1	0,6	12,9	4,8	9,9	5,1
Mean dose GTV (Gy)	47,1	22,2	62,1	40,5	53,1	12,7
Maximum dose GTV (Gy)	50,3	26,4	67,8	42,2	57,7	15,5
GTV D98% (Gy)	43,7	19,3	55,7	38,6	49,8	11,2

GTV, Gross Tumor Volume; ITV, Internal Target Volume; PTV, Planning Target Volume; IQR, inter-quartile range.

eight patients with primary and 12 patients with secondary liver tumors (18). In that study, one and two year local were 94.7% and 79.6%, respectively. Ugurluer et al. reported an intra- and extrahepatic progression-free survival of 89.7% and 73.5% after one year in 21 oligometastatic patients and a 1-year overall survival of 93.3% (19). Yoon et al. retrospectively analyzed SBRT of Primary and metastatic tumors and reported a local control after 1 year of 87% an after 2 years 71%. In case of lesions treated with BED >=100 a local control after 2 years of 96% was shown (20).

While the actual adaptive workflow in the treatment with adaptive radiotherapy is the same independent of the underlying histology, the indication for treatment, comorbidities, competing risks and radiosensitivity are different between primary and secondary liver tumors. We have therefore opted to report outcomes for liver metastases exclusively. With a one year and three local control rate of approximately 90% and 70% respectively our results are favorable in particular since lower local control rates have been reported for liver metastases compared with primary liver tumors before (21). Local control rates for liver metastases after treatment on cone-beam CT based linear accelerators vary in the literature (22–24). Using MR guidance we were able to omit the placement of fiducial markers and facilitate a fully non-invasive workflow. Furthermore as in

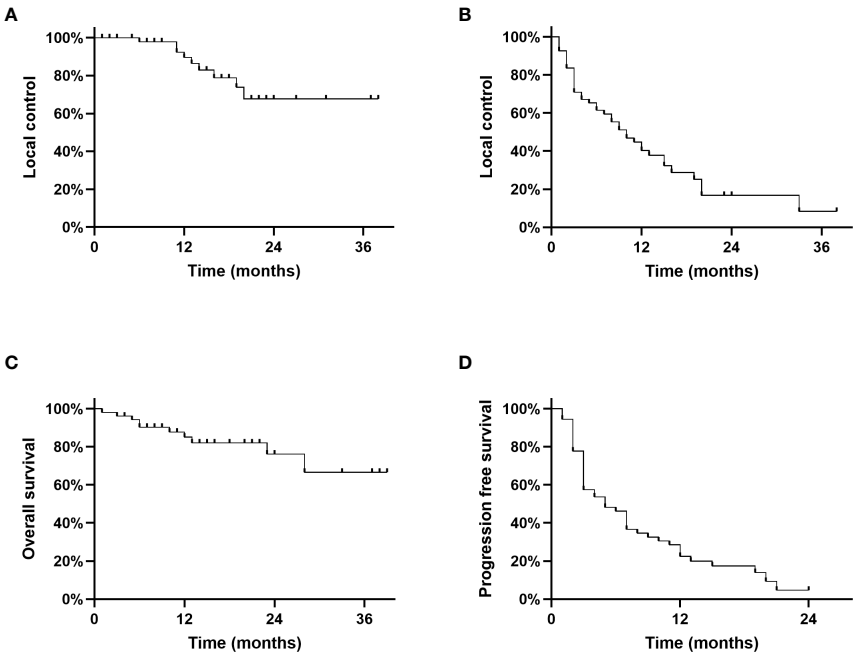

FIGURE 1
(A): Local control of the irradiated liver lesion, **(B)**: Local control rate of the liver, **(C)**: Overall survival, **(D)**: Progression free survival.

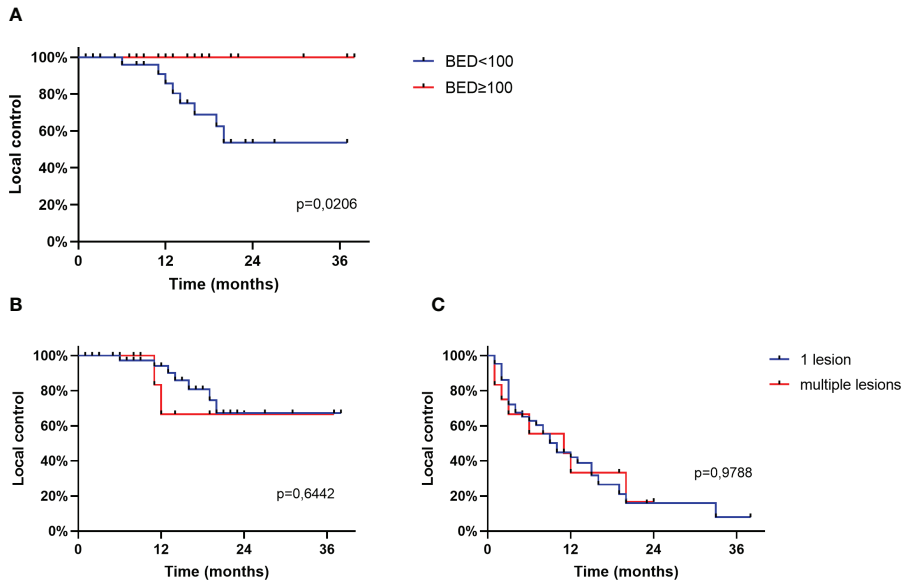

FIGURE 2
(A): Local control of the irradiated liver lesion based on BED, **(B)**: Local control of the irradiated liver lesion based on number of treated lesions, **(C)**: Local control of the liver based on number of treated lesions.

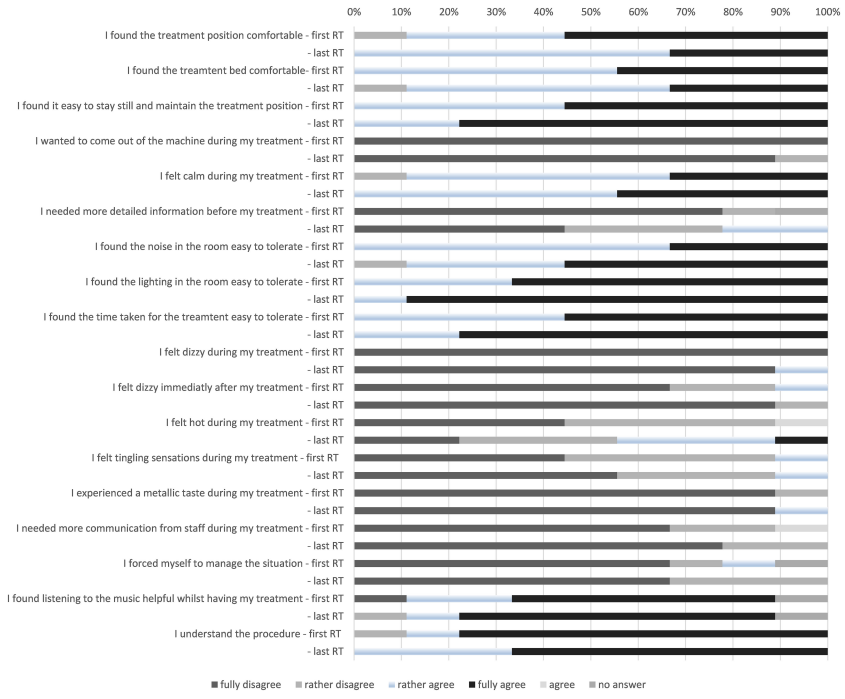

FIGURE 3
Patient acceptance of various aspects of online MRgSBRT. RT (radiotherapy).

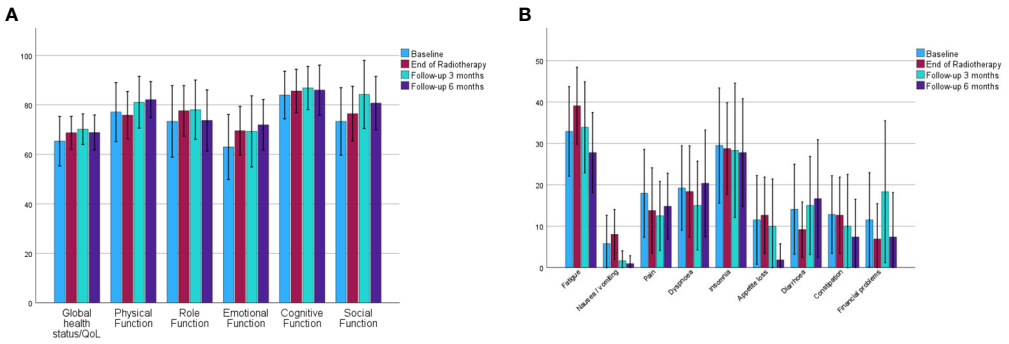

FIGURE 4
Mean values and 95% confidence intervals for EORTC QLQ-C30 data for global health status and function subscales **(A)** and symptom subscales **(B)**. (EORTC QLQ-C30, European Organisation for Research and Treatment of Cancer core questionnaire).

our previous report, we were able to visualize almost all tumors and therefore ensure adequate tumor coverage (11). When interpreting our results it has to be considered that most patients were heavily pretreated systemically and often have had other local liver directed treatments before being referred for radiotherapy. We observed the strong impact of the biological effective dose on the local control of the treated metastases with 100% local control in lesions that were treated with a BED of 100 Gy or more. This is in line with results from previous reports (18, 25). The question may arise while patients are treated with a BED of less than 100 Gy. The decision to prescribe a BED below or higher than 100 Gy is always driven by the present clinical scenario. Patients with oligometastatic disease are more likely to receive higher doses potentially accepting a higher likelihood for normal tissue complications than patients to were treated for oligoprogressive disease when the sole goal of treatment is to prolong the interval without systemic treatment or maintenance of the systemic treatment that is well-tolerated (26). Very few reports have longitudinally assessed quality of life and symptom scores in patients who have received stereotactic radiotherapy for liver metastases (27). In our cohort using the EORTC QLQ-C30 questionnaire we observed widely stable scores for quality of life and symptom scales holding true comparing both the time from baseline to the last fraction of radiotherapy and also during a six-month follow-up. This can likely be explained by the precise treatment and the median chemotherapy free interval

TABLE 3 Studies on MR guided stereotactic body radiotherapy of liver metastases reporting local control and survival data. (OS – Overall survival, LC – local control, PFS – progression free survival).

Author	Year	Primary or secondary tumors	Patients (n)	Patients with liver metas-tases (n)	Patients with primary tumors (n)	Median Dose	Median fraction	OS	LC
Van Dams et al.	2022	Primary liver tumors, liver metastases	20	12	8	54 Gy (11,5-60)	3 (1-5)	2 year: 50,7%	1 year: 94,7% 2 year: 79,6%
Ugurluer et al.	2021	Liver metastases	21	21	0	50 Gy (40-60)	5 (3-8)	1 year: 93% 2 year: 93%	1 year: 89,7%, 2 year: 64,6% (intrahepatic PFS)
Yoon et al.	2021	Primary and metastatic tumors (abdomen, pelvis)	106	46	60	40 Gy (24-60)	5 (3-5)	1 year: 79%2 year: 57%	1 year: 87% 2 year: 71%
Weykamp et al.	2021	Liver metastases, HCC	20	18	2	50 Gy (45-60)	8 (3-12)	1 year: 84%	1 year: 88,1%
Rosenberg et al.	2019	Primary liver tumors, liver metastases	26	18	8	50 Gy	5	2 year: 60%	21,2 months: 80,4%
Henke et al.	2017	Primary liver tumors, liver metastases, other abdominal sites	20	5	10	50 Gy	5	1 year: 75%	15 months: 90%

of five months observed over all patients. The strength of our study lies in its sample size and prospective character assuring stringent follow-up using regular imaging studies and the standardized assessment of quality of life and toxicity. Despite including only patients who were treated for metastases, there is a heterogeneity in terms of the underlying primary tumors which is a limitation. When we conducted this trial the 1.5 Tesla MR-Linac did not support a gated treatment. Using a gated workflow tumors can be irradiated in a predefined position during the respiratory cycle resulting in the smallest possible volume to be treated at the price of a longer treatment time per fraction (17). However, motion management strategies have recently been announced also for the 1.5 Tesla MR-Linac.

Conclusion

Online MR guided radiotherapy is a noninvasive, well-tolerated and effective treatment for liver metastases. Further prospective trials with the goal to define patients who actually benefit most from an online adaptive workflow are currently ongoing (28).

Data availability statement

The raw data supporting the conclusions of this article will be made available by the authors, without undue reservation.

Ethics statement

The studies involving human participants were reviewed and approved by the institutional review board of the medical faculty Tübingen (IRB 659/2017BO1). The patients/participants provided their written informed consent to participate in this study.

Author contributions

Conceptualization: LU, CG, SBo, DZ. Data analysis: LU, CG, SBo. Writing original draft preparation: LU, CG, SBo, DZ. Writing, review and editing: LU, CG, SBo. All authors contributed to the article and approved the submitted version

Funding

The MRgRT program in Tübingen is funded by the German Research Council (DFG ZI 736/2-1; PAK 997/1: GA 2996/1-1, ZI 736/4-1), the University Hospital Tübingen and the Medical Faculty Tübingen. CG, DZ, SG and DT received funding by the German Research Council (DFG ZI 736/2-1; PAK 997/1: GA 2996/1-1, ZI 736/4-1). We acknowledge support by Open Access Publishing Fund of University of Tübingen.

Conflict of interest

The Department of Radiation Oncology Tübingen receives within the frame of research agreements financial and technical support as well as sponsoring for travels and scientific symposia from: Elekta AB Stockholm, Sweden, Philips, Siemens, Dr. Sennewald Medizintechnik, Kaiku Health, TheraPanacea, PTW, ITV. CG, SB: Travel costs by Elekta AB.

The remaining authors declare that the research was conducted in the absence of any commercial or financial relationships that could be construed as a potential conflict of interest.

Publisher's note

Supplementary material

The Supplementary Material for this article can be found online at: https://www.frontiersin.org/articles/10.3389/fonc.2022.1095633/full#supplementary-material

References

1. Al Bandar MH, Kim NK. Current status and future perspectives on treatment of liver metastasis in colorectal cancer (Review). *Oncol Rep* (2017) 37(5):2553–64. doi: 10.3892/or.2017.5531

2. Jackson WC, Tao Y, Mendiratta-Lala M, Bazzi L, Wahl DR, Schipper MJ, et al. Comparison of stereotactic body radiation therapy and radiofrequency ablation in the treatment of intrahepatic metastases. *Int J Radiat Oncol Biol Phys* (2018) 100(4):950–8. doi: 10.1016/j.ijrobp.2017.12.014

3. Gomez DR, Blumenschein GRJr., Lee JJ, Hernandez M, Ye R, Camidge DR, et al. Local consolidative therapy versus maintenance therapy or observation for patients with oligometastatic non-small-cell lung cancer without progression after first-line systemic therapy: A multicentre, randomised, controlled, phase 2 study. *Lancet Oncol* (2016) 17(12):1672–82. doi: 10.1016/S1470-2045(16)30532-0

4. Palma DA, Olson R, Harrow S, Gaede S, Louie AV, Haasbeek C, et al. Stereotactic ablative radiotherapy versus standard of care palliative treatment in

patients with oligometastatic cancers (SABR-COMET): A randomised, phase 2, open-label trial. *Lancet* (2019) 393(10185):2051–8. doi: 10.1016/S0140-6736(18)32487-5

5. Kluter S. Technical design and concept of a 0.35 T MR-linac. *Clin Transl Radiat Oncol* (2019) 18:98–101. doi: 10.1016/j.ctro.2019.04.007

6. Winkel D, Bol GH, Kroon PS, van Asselen B, Hackett SS, Werensteijn-Honingh AM, et al. Adaptive radiotherapy: The elekta unity MR-linac concept. *Clin Transl Radiat Oncol* (2019) 18:54–9. doi: 10.1016/j.ctro.2019.04.001

7. Boldrini L, Corradini S, Gani C, Henke L, Hosni A, Romano A, et al. MR-guided radiotherapy for liver malignancies. *Front Oncol* (2021) 11:616027. doi: 10.3389/fonc.2021.616027

8. Nachbar M, Monnich D, Kalwa P, Zips D, Thorwarth D, Gani C. Comparison of treatment plans for a high-field MRI-linac and a conventional linac for esophageal cancer. *Strahlenther Onkol* (2019) 195(4):327–34. doi: 10.1007/s00066-018-1386-z

9. Nachbar M, Monnich D, Boeke S, Gani C, Weidner N, Heinrich V, et al. Partial breast irradiation with the 1.5 T MR-linac: First patient treatment and analysis of electron return and stream effects. *Radiother Oncol* (2020) 145:30–5. doi: 10.1016/j.radonc.2019.11.025

10. Hanna GG, Murray L, Patel R, Jain S, Aitken KL, Franks KN, et al. UK Consensus on normal tissue dose constraints for stereotactic radiotherapy. *Clin Oncol (R Coll Radiol)* (2018) 30(1):5–14. doi: 10.1016/j.clon.2017.09.007

11. Gani C, Boeke S, McNair H, Ehlers J, Nachbar M, Mönnich D, et al. Marker-less online MR-guided stereotactic body radiotherapy of liver metastases at a 1.5 T MR-linac - feasibility, workflow data and patient acceptance. *Clin Transl Radiat Oncol* (2021) 26:55–61. doi: 10.1016/j.ctro.2020.11.014

12. Fowler JF. 21 years of biologically effective dose. *Br J Radiol* (2010) 83 (991):554–68. doi: 10.1259/bjr/31372149

13. Barnes H, Alexander S, Bower L, Ehlers J, Gani C, Herbert T, et al. Development and results of a patient-reported treatment experience questionnaire on a 1.5 T MR-linac. *Clin Transl Radiat Oncol* (2021) 30:31–7. doi: 10.1016/j.ctro.2021.06.003

14. Olausson K, Holst Hansson A, Zackrisson B, Edvardsson D, Östlund U, Nyholm T. Development and psychometric testing of an instrument to measure the patient's experience of external radiotherapy: The radiotherapy experience questionnaire (RTEQ). *Tech Innov Patient Support Radiat Oncol* (2017) 3-4:7–12. doi: 10.1016/j.tipsro.2017.06.003

15. Leibfarth S, Winter RM, Lyng H, Zips D, Thorwarth D. Potentials and challenges of diffusion-weighted magnetic resonance imaging in radiotherapy. *Clin Transl Radiat Oncol* (2018) 13:29–37. doi: 10.1016/j.ctro.2018.09.002

16. Lawrence TS, Robertson JM, Anscher MS, Jirtle RL, Ensminger WD, Fajardo LF. Hepatic toxicity resulting from cancer treatment. *Int J Radiat Oncol Biol Phys* (1995) 31(5):1237–48. doi: 10.1016/0360-3016(94)00418-K

17. Weykamp F, Hoegen P, Klüter S, Spindeldreier CK, König L, Seidensaal K, et al. Magnetic resonance-guided stereotactic body radiotherapy of liver tumors: Initial clinical experience and patient-reported outcomes. *Front Oncol* (2021) 11:610637. doi: 10.3389/fonc.2021.610637

18. van Dams R, Wu TC, Kishan AU, Raldow AC, Chu FI, Hernandez J, et al. Ablative radiotherapy for liver tumors using stereotactic MRI-guidance: A prospective phase I trial. *Radiother Oncol* (2022) 170:14–20. doi: 10.1016/j.radonc.2021.06.005

19. Ugurluer G, Mustafayev TZ, Gungor G, Atalar B, Abacioglu U, Sengoz M, et al. Stereotactic MR-guided online adaptive radiation therapy (SMART) for the treatment of liver metastases in oligometastatic patients: Initial clinical experience. *Radiat Oncol J* (2021) 39(1):33–40. doi: 10.3857/roj.2020.00976

20. Yoon SM, Luterstein E, Chu FI, Cao M, Lamb J, Agazaryan N, et al. Clinical outcomes of stereotactic magnetic resonance image-guided adaptive radiotherapy for primary and metastatic tumors in the abdomen and pelvis. *Cancer Med* (2021) 10(17):5897–906. doi: 10.1002/cam4.4139

21. Ohri N, Tomé WA, Méndez Romero A, Miften M, Ten Haken RK, Dawson LA, et al. Local control after stereotactic body radiation therapy for liver tumors. *Int J Radiat Oncol Biol Phys* (2021) 110(1):188–95. doi: 10.1016/j.ijrobp.2017.12.288

22. Andratschke N, Alheid H, Allgäuer M, Becker G, Blanck O, Boda-Heggemann J, et al. The SBRT database initiative of the German society for radiation oncology (DEGRO): Patterns of care and outcome analysis of stereotactic body radiotherapy (SBRT) for liver oligometastases in 474 patients with 623 metastases. *BMC Cancer* (2018) 18(1):283. doi: 10.1186/s12885-018-4191-2

23. Scorsetti M, Comito T, Clerici E, Franzese C, Tozzi A, Iftode C, et al. Phase II trial on SBRT for unresectable liver metastases: Long-term outcome and prognostic factors of survival after 5 years of follow-up. *Radiat Oncol* (2018) 13 (1):234. doi: 10.1186/s13014-018-1185-9

24. Dawood O, Mahadevan A, Goodman KA. Stereotactic body radiation therapy for liver metastases. *Eur J Cancer* (2009) 45(17):2947–59. doi: 10.1016/j.ejca.2009.08.011

25. Joo JH, Park J-h, Kim JC, Yu CS, Lim S-B, Park IJ, et al. Local control outcomes using stereotactic body radiation therapy for liver metastases from colorectal cancer. *Int J Radiat Oncol Biol Physics* (2017) 99(4):876–83. doi: 10.1016/j.ijrobp.2017.07.030

26. Guckenberger M, Lievens Y, Bouma AB, Collette L, Dekker A, deSouza NM, et al. Characterisation and classification of oligometastatic disease: A European society for radiotherapy and oncology and European organisation for research and treatment of cancer consensus recommendation. *Lancet Oncol* (2020) 21(1):e18–28. doi: 10.1016/S1470-2045(19)30718-1

27. Méndez Romero A, Wunderink W, van Os RM, Nowak PJCM, Heijmen BJM, Nuyttens JJ, et al. Quality of life after stereotactic body radiation therapy for primary and metastatic liver tumors. *Int J Radiat Oncol Biol Physics* (2008) 70 (5):1447–52. doi: 10.1016/j.ijrobp.2007.08.058

28. Regnery S, Ristau J, Weykamp F, Hoegen P, Sprengel SD, Paul KM, et al. Magnetic resonance guided adaptive stereotactic body radiotherapy for lung tumors in ultracentral location: The MAGELLAN trial (ARO 2021-3). *Radiat Oncol* (2022) 17(1):102. doi: 10.1186/s13014-022-02070-x

frontiers | Frontiers in Oncology

TYPE Original Research
PUBLISHED 19 January 2023
DOI 10.3389/fonc.2023.1039901

OPEN ACCESS

EDITED BY
Frank Lagerwaard,
Amsterdam University Medical Center,
Netherlands

REVIEWED BY
Morgan Michalet,
Institut du Cancer de Montpellier (ICM),
France
Chen-Yu Huang,
Hong Kong Sanatorium and Hospital,
Hong Kong SAR, China

*CORRESPONDENCE
Ning-Ning Lu
Ning-Ning.Lu@hotmail.com
Ye-Xiong Li
yexiong12@163.com
Nian-Zeng Xing
xingnianzeng@126.com

†These authors have contributed equally to this work and share first authorship

SPECIALTY SECTION
This article was submitted to Radiation Oncology, a section of the journal Frontiers in Oncology

RECEIVED 08 September 2022
ACCEPTED 03 January 2023
PUBLISHED 19 January 2023

CITATION
Gao L-R, Tian Y, Wang M-S, Xia W-L, Qin S-R, Song Y-W, Wang S-L, Tang Y, Fang H, Tang Y, Qi S-N, Yan L-L, Liu Y-P, Jing H, Chen B, Xing N-Z, Li Y-X and Lu N-N (2023) Assessment of delivered dose in prostate cancer patients treated with ultra-hypofractionated radiotherapy on 1.5-Tesla MR-Linac. *Front. Oncol.* 13:1039901. doi: 10.3389/fonc.2023.1039901

Assessment of delivered dose in prostate cancer patients treated with ultra-hypofractionated radiotherapy on 1.5-Tesla MR-Linac

Lin-Rui Gao[1†], Yuan Tian[1†], Ming-Shuai Wang[2†], Wen-Long Xia[1], Shi-Rui Qin[1], Yong-Wen Song[1], Shu-Lian Wang[1], Yu Tang[3], Hui Fang[1], Yuan Tang[1], Shu-Nan Qi[1], Ling-Ling Yan[1], Yue-Ping Liu[1], Hao Jing[1], Bo Chen[1], Nian-Zeng Xing[4*], Ye-Xiong Li[1*] and Ning-Ning Lu[1*]

[1]Department of Radiation Oncology, National Cancer Center/National Clinical Research Center for Cancer/Cancer Hospital, Chinese Academy of Medical Sciences and Peking Union Medical College, Beijing, China, [2]Department of Urology, National Cancer Center/National Clinical Research Center for Cancer/Cancer Hospital, Chinese Academy of Medical Sciences and Peking Union Medical College, Beijing, China, [3]GCP Center/Clinical Research Center, National Cancer Center/National Clinical Research Center for Cancer/Cancer Hospital, Chinese Academy of Medical Sciences and Peking Union Medical College, Beijing, China, [4]Department of Urology and State Key Laboratory of Molecular Oncology, National Cancer Center/National Clinical Research Center for Cancer/Cancer Hospital, Chinese Academy of Medical Sciences and Peking Union Medical College, Beijing, China

Objective: To quantitatively characterize the dosimetric effects of long on-couch time in prostate cancer patients treated with adaptive ultra-hypofractionated radiotherapy (UHF-RT) on 1.5-Tesla magnetic resonance (MR)-linac.

Materials and methods: Seventeen patients consecutively treated with UHF-RT on a 1.5-T MR-linac were recruited. A 36.25 Gy dose in five fractions was delivered every other day with a boost of 40 Gy to the whole prostate. We collected data for the following stages: pre-MR, position verification-MR (PV-MR) in the Adapt-To-Shape (ATS) workflow, and 3D-MR during the beam-on phase (Bn-MR) and at the end of RT (post-MR). The target and organ-at-risk contours in the PV-MR, Bn-MR, and post-MR stages were projected from the pre-MR data by deformable image registration and manually adapted by the physician, followed by dose recalculation for the ATS plan.

Results: Overall, 290 MR scans were collected (85 pre-MR, 85 PV-MR, 49 Bn-MR and 71 post-MR scans). With a median on-couch time of 49 minutes, the mean planning target volume (PTV)-$V_{95\%}$ of all scans was 97.83 ± 0.13%. The corresponding mean clinical target volume (CTV)-$V_{100\%}$ was 99.93 ± 0.30%, 99.32 ± 1.20%, 98.59 ± 1.84%, and 98.69 ± 1.85%. With excellent prostate-$V_{100\%}$ dose coverage, the main reason for lower CTV-$V_{100\%}$ was slight underdosing of seminal vesicles (SVs). The median $V_{29\ Gy}$ change in the rectal wall was -1% (-20%–17%). The $V_{29\ Gy}$ of the rectal wall increased by >15% was observed in one scan. A slight increase in the high dose of bladder wall was noted due to gradual bladder growth during the workflow.

Conclusions: This 3D-MR–based dosimetry analysis demonstrated clinically acceptable estimated dose coverage of target volumes during the beam-on period with adaptive ATS workflow on 1.5-T MR-linac, albeit with a relatively long on-couch time. The 3-mm CTV-PTV margin was adequate for prostate irradiation but occasionally insufficient for SVs. More attention should be paid to restricting high-dose RT to the rectal wall when optimizing the ATS plan.

KEYWORDS

prostate cancer, ultra-hypofractionated radiotherapy, MR-guided adaptive radiotherapy, beam-on, dosimetry analysis

Introduction

External beam radiotherapy (EBRT) is one of the recommended treatment modality for localized prostate cancer (PCa). With the evolution of RT technique and radiobiological progress, the EBRT course had decreased from nearly 2 months with conventional fractionation to within 1–2 weeks with ultra-hypofractionated RT (UHF-RT). Although the PACE-B trial (administration of 36.25 Gy in five fractions over 1–2 weeks) did not demonstrate any difference in acute toxicities (1), another randomized controlled trial, HYPO-RT-PC (administration of 42.7 Gy in seven fractions over 2.5 weeks) identified more severe urinary side-effects at 1 year in the UHF-RT group (2).

Inter- and intra-fractional variability of target volumes and organs at risk (OARs) deformation and shifting called into question the safety of further dose escalation and UHF-RT for PCa. Contrary to the commonly used volumetric modulated arc therapy (VMAT), and intra-fractional motion monitoring or repeated static imaging in the PACE-B trial, the majority (80%) of patients in the HYPO-RT-PC trial were treated by 3-dimensional conformal radiotherapy and position control was not feasible during fraction delivery (2). Even with cone-beam CT (CBCT) registration, the prostate target coverage was only 61.9-62%, which means online adaptive RT is needed for approximately one-third of the treatment fractions (3, 4). In addition, the resolution of CBCT images was generally low for prostate registration (4). Moreover, a fiducial marker or electromagnetic transponder insertion can improve the registration accuracy (4), but is inconvenient to patients due to invasiveness, potential pain, bleeding, and marker shifting. Furthermore, neither of the above-mentioned registration steps could compensate for the prostate (5–7) and seminal vesicle (SV) (8) deformations, nor the OARs (mainly bladder and rectum) motion.

Magnetic resonance (MR)-guided radiotherapy (MRgRT) is a milestone in the progress of RT technique. It not only affords improved soft-tissue resolution for registration but also brings online adaptive RT into clinical practice. With the integration of 1.5-Tesla MR into 7-MV linac, the Elekta 1.5-T MR-linac provided online Adapt-To-Position (ATP) and Adapt-to-Shape (ATS) workflows. The ATS workflow can meet all the above requirements of PCa UHF-RT by online target editing and optimizing plan from fluence optimization (9). Furthermore, real-time 2D cine MR can be used to monitor the motion, and 3D high-resolution magnetic resonance imaging (MRI) can be acquired during the beam-on period. Both these approaches allow for motion control and help to achieve high-precision RT delivery (10). However, the current online adaptive procedure is time-consuming, which makes many researchers concerned about the accuracy of the delivered dose, especially the dosimetric effects on the target and OARs due to intra-fractional motion.

De Muinck Keizer et al. firstly reported prostate intra-fraction motions during each ATS session and dose reconstruction using cine MR dynamics, which was determined with a previously validated soft-tissue contrast–based tracking algorithm (11, 12). For each fraction, the treatment delivery record was generated by proportionally splitting the plan into 11s intervals based on the delivered monitor units (13), which could possibly affect the actual delivered dose. Hence, the purpose of this study was to estimate the delivered dose for targets and OARs by dosimetry analysis based on high resolution 3D-MR aquisitions, including pre-, position verification (PV-), beam-on (Bn-), and post-3D-MR scans, of each adaptive RT session for PCa patients treated on 1.5-T MR-linac.

Materials and methods

Patient eligibility

A prospective observational study with regular follow-up was initiated for PCa in 2019 to investigate the feasibility, tolerability, and toxicity profiles of UHF-RT on 1.5-T MR-linac (NCT05183074, ChiCTR2000033382). The risk group was defined per the National Comprehensive Cancer Network (NCCN) v.1.2019 edition. For this study, dosimetry data were collected from 17 consecutive patients with localized low-, intermediate- to selective high-risk PCa (Table S1).

Abbreviations: ATP, Adapt-To-Position; ATS, Adapt-To-Shape; Bn-MR, Beam-on MR; CTV, Clinical target volume; CBCT, Cone-beam CT; CI, Confidence interval; EBRT, External beam radiotherapy; MR, Magnetic resonance; MRI, Magnetic resonance imaging; MRgRT, Magnetic resonance-guided radiotherapy; NCCN, National Comprehensive Cancer Network; OAR, Organ at risk; PTV, Planning target volume; PV-MR, Position verification-MR; PCa, Prostate cancer; PSA, Prostate-specific antigen; ROI, Region of interest; SVs, Seminal vesicles; UHF-RT, Ultra-hypofractionated radiotherapy; VMAT, Volumetric modulated arc therapy.

Target volume delineation and reference plan

Simulation CT (slice thickness = 3 mm) and MR scans (Contrast enhanced T1-weighted imaging, Fast spin echo T2-weighted imaging and diffusion weighted imaging, slice thickness = 3 mm) were acquired and registered for contouring and reference planning. About 1 hour before simulation and each RT session, the patients were instructed to empty the rectum and bladder and asked to drink 300 to 500 ml of water in 15 to 20 minutes to ensure slow filling of the bladder, in consideration of the long on-couch time of the ATS workflow. Target delineation was defined as per EORTC-ACROP contouring guidelines (14). The clinical target volume (CTV) was defined as the whole prostate for low-risk disease (N = 1) and the whole prostate with a 3-mm margin (0 mm posteriorly) for patients (N = 16) with a potential extraprostatic extension (EPE) rate of 20% or higher per the Partin tables. The proximal 1 cm SVs were included for patients with an SV involvement rate of 15% or higher (N = 11), and the whole SV was included for patients with minimal T3b (N = 1). The planning target volume (PTV) was derived from the CTV plus a uniform 3-mm margin. For intermediate- to high-risk disease (N = 16), a simultaneous boost of CTV 40 was defined as prostate with contraction of 1 mm. Rectal wall and bladder wall were defined as the 3 mm-inner rings of the rectum and bladder, respectively.

The prescription doses of PTV and CTV 40 were 36.25 Gy and 40 Gy, respectively, in five fractions delivered every other day, with a total course of 10 to 12 days. The target volume dose prescription and OARs constraints for UHF-RT are listed in Table S2. Then a reference plan was generated using the Monaco (v5.40, Elekta AB, Stockholm, Sweden) planning system, with 7 to 10 beams and less than 80 segments (<120 segments was acceptable for complicated plans).

Online ATS workflow and image acquisition

The image acquisition procedure is listed in Figure 1. During each fraction, an initial (pre-MR) scan was acquired after set-up using a T2-weighted 3D sequence with a duration of 6 minutes for the first 12 patients and that of 2 minutes thereafter. After rigidly registering the pre-MR data to simulation CT or previous pre-MR image, contours were automatically deformed to the pre-MR image and manually adapted by the physician, followed by full plan re-optimization in the Monaco system starting from fluence optimization (9). The pseudo-CT is generated using the bulk electron density assignment strategy, that is, the inside of each region of interest (ROI) on the MR image is filled with the mean relative electron density of the corresponding ROI on the reference CT image according to the user-specified layer order. Before the end of plan reoptimization, a PV-MR scan was acquired. If the CTV was still within the PTV on the PV scan and the rectum did not move ventrally, the ATS plan was accepted and treatment delivery with real-time cine MR was started.

For the first seven patients, 2D cine MR images were continuously collected during the "beam-on" period, owing to concerns about unexpected target and OAR moving. The delivery will be interrupted if the prostate moved out of the PTV or the rectum moved ventrally. From the eighth patient, if the position of all the organs was stable, 2D cine MR monitoring was stopped and a Bn-MR scan was acquired using a T2-weighted 3D sequence with a duration of 2 minutes. Directly after RT delivery, another post-MR T2-weighted 3D sequence scan was acquired. The procedure was well tolerated for the majority of sessions; however, no post-MR scan was acquired in three sessions for two patients because of their bladders being excessively full. An extended workflow was used in three sessions because of rectum motion, in another three sessions because of an overfilled bladder, and in one session because of SVs moving out of CTV (one with another ATP and six with another ATS workflow).

Image fusion and re-planning on each MR scan for dose calculation

By image registration and propagation of anatomical contours, the targets and OARs of the ATS plan for each session were transferred to the corresponding PV-, Bn-, and post-MR scans, respectively. The same radiation oncologist edited the targets and OARs manually to ensure contouring consistency if necessary. A senior radiation oncologist reviewed all the contours. The dose distribution for the online ATS plans was recalculated on each

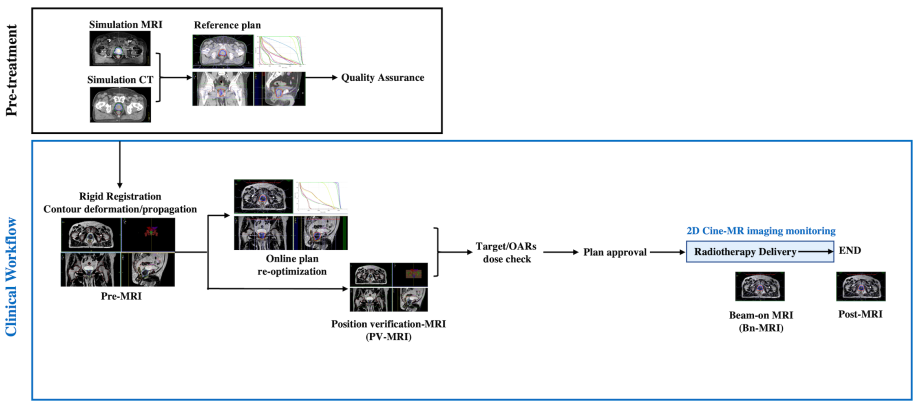

FIGURE 1
Pre-treatment and clinical workflow. Simulation MRI, MRI acquired for reference plan; usually scanned 1 to 2 weeks before treatment; Pre-MRI, MRI acquired each treatment day for adaptive plan optimization; OARs, Organs at risk; PV-MR, Position verification-MR.

pseudo-CT scan derived from each MR scan by using the "original segments" mode. The dose metrics were evaluated for the adapted ROIs. For each fraction, the volumes of the clinical targets and OARs, as well as the re-computed doses on different MR scans were compared with the corresponding parameters of the online ATS plan, instead of comparing the cumulative dose of five fractions with that of the original ATS plan.

Statistical analysis

SPSS 25.0 (IBM Corp., Armonk, NY, USA) was used for statistical analysis. Continuous variables are presented as the mean ± SD, median (range), 95% confidence interval (CI), or frequencies with percentages depending on their distribution. Generalized estimating equation was used to compare the variables on different scans for each fraction. Differences were defined as significant when the p-value was <0.05.

Results

Patients' characteristics

Patients' (N=17) characteristics are shown in Table S1. The median patient age was 75 (58–87) years. The baseline prostate-specific antigen (PSA) level was ≤10 ng/ml in five (29.4%) patients, 10–20 ng/ml in five (29.4%) patients, and ≥20 ng/ml in seven (41.2%) patients. Per the NCCN risk grouping, there were 2 (11.8%), 12 (70.6%), and 3 (17.6%) patients with low-, intermediate-, and high-risk diseases, respectively. The median prostate volume was 42.48 (28.86–64.14) cc.

MRI for analysis

In total, 290 1.5-Tesla high-resolution MRIs from 85 fractions of 17 consecutive patients were used for dosimetry analysis, including 85 pre-, 85 PV-, 49 Bn-, and 71 post-MR scans, respectively. Beam-on 3D-MR scans were collected from 49 fractions of 10 patients because for one session, we observed rectum gas bubbles and used continuous 2D cine MR for monitoring. Post-MR scans were not acquired for three sessions of two patients because of their bladders being too full, and the remaining 11 post-scans of five patients failed to transmit to the Monaco system. An example of the dose distributions on each MR scans after re-planning was shown in Figure 2.

Target dose coverage

The median on-couch time was 49 (24–78) minutes. Comparison of the target and OARs volumes and volume differences relative to those in the corresponding ATS plan (based on pre-MR scans) are shown in Table S3. For each fraction, the target volume differences of the prostate and CTV on different scans were less than 3.0 cc, indicating good consistency of target contouring.

The planning targets of all fractions, calculated by the daily ATS plan dose in PV-, Bn- and post-MR scans were shown in the Figure S1. The mean PTV-$V_{95\%}$ ($V_{34.4Gy}$) of all scans was 97.83 ± 0.13% (Figure S1B). On 27/290 (9.3%) scans, the PTV-$V_{95\%}$ was less than 95% (Figure S1B). Furthermore, the mean CTV-$V_{100\%}$ ($V_{36.25Gy}$) of all scans was 99.21 ± 0.09%, and that of the ATS plan and PV-MR, Bn-MR, and post-MR phases, respectively, was 99.93 ± 0.30%, 99.32 ± 1.20%, 98.59 ± 1.84%, and 98.69 ± 1.85% (all $p < 0.001$; Figure 3A). Interestingly, the average CTV-$V_{100\%}$ ($V_{36.25Gy}$) of each phase was all covered by 98% of the prescribe dose during treatment. With excellent

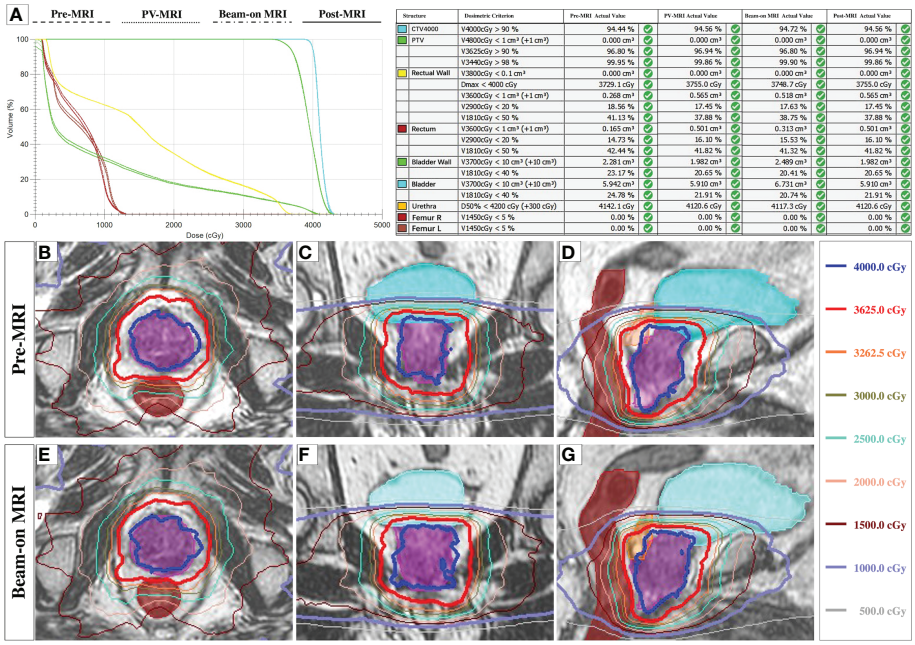

FIGURE 2
The dose distributions on each MRI scans. **(A)**: The representative DVH plot with four plans and the dose metrics on each MRI scans after re-planning in one fraction. **(B–G)**: The representative dose distributions of three planes of ATS plan on Pre-MR **(B–D)** and Beam-on MR scan **(E–G)**.

dose coverage of prostate-$V_{100\%}$ ($V_{36.25Gy}$) (Figure 3C), the main reason for lower CTV-$V_{100\%}$ ($V_{36.25Gy}$) was slight underdosing of SVs (Figure 3E).

The $V_{95\%}$ of CTV (Figure 3B), the prostate (Figure 3D), and SVs (Figure 3F) were shown in Figure 3. Among the 31 scans on which the SV-$V_{36.25Gy}$ was less than 95%, the SVs-$V_{100\%}$ (SV-$V_{36.25Gy}$) was between "=90%" and 95% on 6.3% (13/206) scans, between "=85%" and 90% on 2.4% (5/206) scans, between "=75%" and 85% on 1.9% scans (4/206), between "=60%" and 75% on 3.9% scans (8/206) and only 41% on one scan, respectively (Figure S1A). The corresponding SVs-$V_{95\%}$ (SV-$V_{34.4Gy}$) was between "=90%" and 95% on 0.5% (1/206) scans, between "=85%" and 90% on 3.0% (6/206) scans, between "=75%" and 85% on 1.0% (2/206) scans, and less than 75% on one scan (Figure S1B). Furthermore, SV-$V_{34.4Gy}$ of less than 95% was found in 6 fractions of 3 patients.

As shown in Figure 4, we also summed the CTV-$D_{99\%}$ (Figure 4A) and CTV-$D_{95\%}$ (Figure 4B) values of five fractions on a per-patient basis for pre-, PV-, Bn-, and post-MR scans, respectively. Although there were 12 patients with SV underdose, the sum of CTV-$D_{95\%}$ on each MR scan was higher than the prescription dose (36.25 Gy) for all 17 patients (Figure 4B).

OARs

The volumes of the rectum fluctuated during treatment, with mean variation of 1.59 cc, 2.37 cc, and 1.37 cc on the PV-MR, Bn-MR and post-MR scans, respectively (Table S3). In comparison to the values of ATS plan, the estimated delivered dose to the rectal wall during the whole workflow also varied (Table 1), with a mean variation V_{38Gy} of 0.23 ± 0.28 cc on PV-MR, 0.41 ± 0.51 cc on Bn-MR, and 0.39 ± 0.52 cc on post-MR, and a mean variation V_{36Gy} of 0.27 ± 0.57 cc on PV-MR, 0.39 ± 0.71 cc on Bn-MR, and 0.30 ± 0.68 cc on post-MR. There is no statistical difference between mean $V_{29\ Gy}$ or $V_{18.1\ Gy}$ in the rectal wall of ATS plan and that of PV-MR, Bn-MR, and post-MR phases, respectively (p = 0.882, 1.000 and 0.587 for $V_{29\ Gy}$; p = 0.221, 1.000 and 0.363 for $V_{18.1\ Gy}$). The changes in the V_{29Gy} and $V_{18.1Gy}$ of the rectal wall in comparison with the ATS plans are shown in Figures 5A, B. The median $V_{29\ Gy}$ change in the rectal wall was -1% (-20%–17%). An increase of >15% in V_{29Gy} was only observed in one scan (1/205, 0.5%). No fraction showed an increase of >15% in the $V_{18.1Gy}$ of the rectal wall. The V_{29Gy} of the rectal wall (Figure 5A) showed an increase of 5%–15% in 21.2% (18/85), 16.3% (8/49), and 18.3% (13/71) of the PV-, Bn-, and post-MR scans,

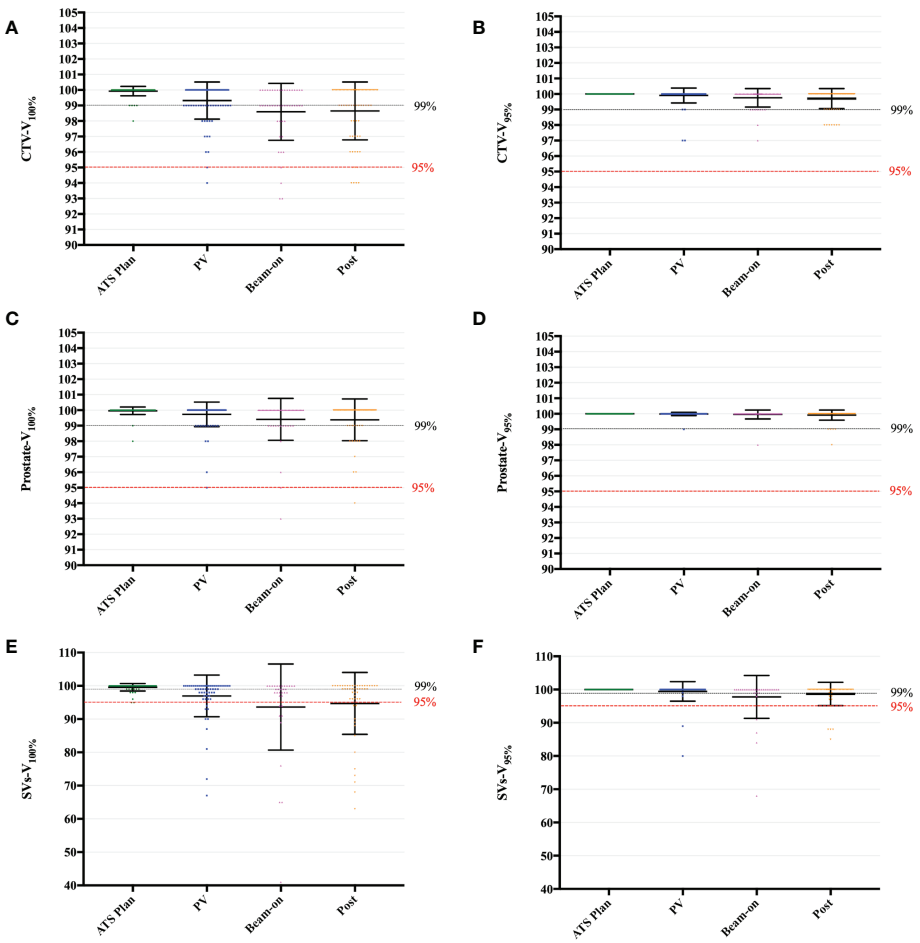

FIGURE 3
Boxplot of $V_{100\%}$ and $V_{95\%}$ values to the CTV **(A, B)**, Prostate **(C, D)** and SVs **(E, F)**, calculated by the daily ATS plan dose on the PV-, Bn- and post-MR scan for each session and patient. Individual data points are shown as dots. The mean ± SD are shown as the error bars.

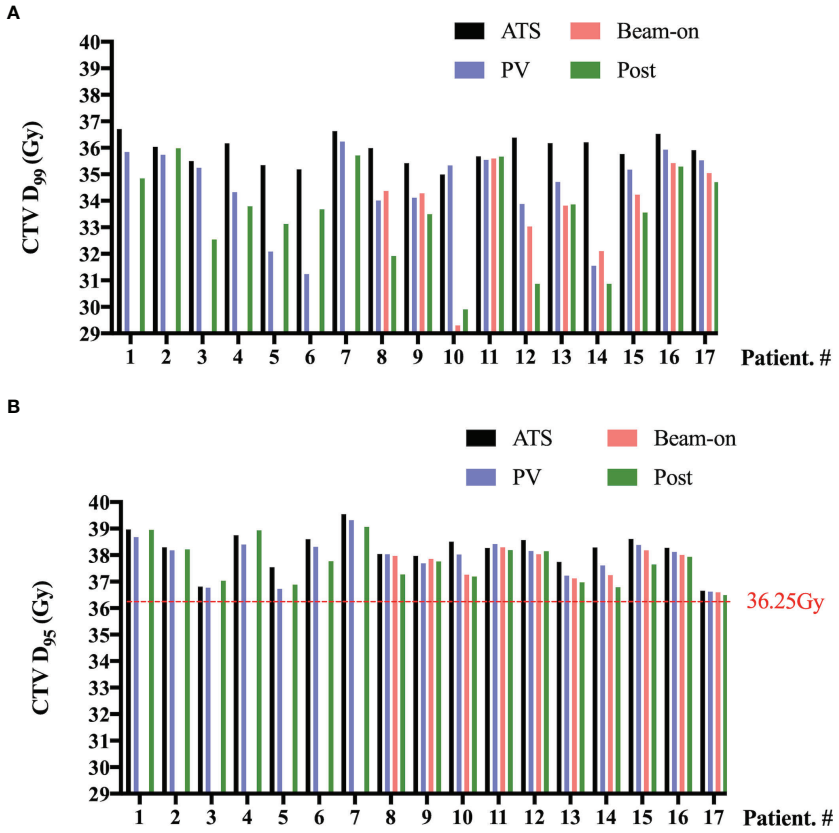

FIGURE 4
Per-patient $D_{99\%}$ **(A)** and $D_{95\%}$ **(B)** values to the clinical target volume (CTV) summed by five fractions of pre- (ATS plan), PV-, Bn- and post-MR scans. No beam-on scans were acquired for the first 7 patients due to concerns about unexpected target and OAR moving.

respectively, and the corresponding values for an increase of 5%–15% in V18.1Gy (Figure 5B) were 23.5% (20/85), 16.3% (8/49), and 19.7% (14/71), respectively.

In contrast, the bladder volume gradually increased with time, with mean variation of 83.96 cc, 136.75 cc, and 140.36 cc, respectively (Table S3). As the volume of the bladder increased, the bladder volume receiving high dose increased slightly. The mean V_{37Gy} of the ATS plan and PV-MR, Bn-MR, and post-MR phases was 2.44 ± 1.15 cc, 2.86 ± 1.50 cc, 3.09 ± 1.34 cc, 3.27 ± 1.85 cc, respectively (Table 1). The mean variation $V_{18.1Gy}$ was -0.03 ± 0.12 cc on PV-MR, -0.06 ± 0.03 cc on Bn-MR, and -0.05 ± 0.03 cc on post-MR, respectively, due to gradual growth of the bladder over the workflow. A $V_{18.1Gy}$ increase of 10% was only observed in one scan (1/205, 0.5%), while an increase of >5% was only observed in 4.7% (4/85), 0%, and 4.2% (3/71) of the PV-, Bn- and post-MR scans, respectively (Figure 5C).

The dose metrics are summarized in Table 1. The D_{max} of the colon and intestine and the $V_{14.5Gy}$ of femur L/R were also evaluated.

Discussion

To our knowledge, this is the first study assessing the delivered dose to targets and OARs of online adaptive UHF-RT for PCa patients based on high resolution 3D beam-on and post-treatment MRIs on a 1.5 T MR-linac. Our study demonstrated clinically acceptable estimated dose coverage of target volumes during the beam-on period with an adaptive ATS workflow, with a slight increase of rectal wall volume receiving high dose and a gradual reduction of the bladder dose. The 3-mm CTV-PTV margin applied in our study has been shown to be sufficient for the prostate and may be insufficient for a small portion of SVs.

The potential effects of inaccurate delivery of radiotherapy doses due to inter- and intra-fractions on treatment efficacy and/or toxicity of normal tissues has long been a concern associated with radical radiotherapy. Several strategies have been adopted to decrease these potential effects, with CBCT w/o fiducial markers being the most widely used approach. Peng et al. observed target underdosing in approximately one-third of the treatment fractions with CBCT using prostate alignment, with the Prostate-$V_{100\%}$ decreasing by >15% in 4.3% of the fractions and by 3%–15% in 18.0% of the fractions (3). CBCT with insertion of fiducial markers or Calypso with electromagnetic transponder tracking will improve the treatment accuracy to levels comparable to those of MRgRT (4, 7, 15), but the invasiveness of the insertion procedures has made them difficult to be widely used in clinical practice. Moreover, none of the non-adaptive radiotherapies can offset the prostate volume changes during the treatment course (16), which would be more significant with extreme hypo-fractionation schedules, and could be associated with the prostate continuous swelling during the whole course observed by Gunlaugsson et al. (17). With the online ATS workflow, we re-contoured and re-optimized the plan for each session. The mean dose coverage of Prostate-$V_{100\%}$ was 99.66 ± 0.06%, and the Prostate-

10.3389/fonc.2023.1039901

TABLE 1 Dose metrics for the original ATS plan and re-computed plans on PV-MR, beam-on MR and post-MR scans.

Dose metrics		ATS Plan (Mean±SD)	PV (Mean±SD)	Beam-on (Mean±SD)	Post (Mean±SD)
Target coverage					
CTV4000					
	$V_{100\%\ (40\ Gy)}$	95.90±0.26	93.46±0.44	92.14±0.58	91.70±0.61
	$V_{42.5Gy}$ (cc)	4.26±5.38	4.55±5.68	3.58±4.45	4.34±5.61
PTV					
	$V_{100\%\ (36.25Gy)}$	95.27±1.67	92.60±3.14	91.53±3.23	91.47±3.80
	$V_{95\%\ (34.4\ Gy)}$	99.27±0.75	97.69±2.03	97.04±2.29	96.87±2.57
OAR metrics					
Rectal wall					
	D_{max}	38.35±1.09	38.71±2.22	38.77±2.27	38.71±2.59
	$V_{38\ Gy\ (cc)}$	0.05±0.08	0.28±0.49	0.36±0.56	0.40±0.80
	$V_{36\ Gy\ (cc)}$	0.59±0.39	0.86±1.00	0.94±1.03	0.92±1.15
	$V_{29\ Gy}$	16.45±4.99	15.25±6.96	16.33±6.44	15.47±8.26
	$V_{18.1\ Gy}$	34.92±6.72	33.32±8.61	35.12±7.29	34.20±8.91
Bladder wall					
	V_{37Gy} (cc)	2.44±1.15	2.86±1.50	3.09±1.34	3.27±1.85
	$V_{18.1\ Gy}$	23.80±8.98	20.53±9.41	19.49±8.05	18.84±7.43
Intestine	D_{max}	2.32±2.30	1.81±1.86	1.75±1.92	1.93±2.23
Colon	D_{max}	5.10±4.37	3.87±3.19	4.11±3.32	3.78±3.00
Femur L	$V_{14.5\ Gy}$	0.94±2.57	0.99±2.67	1.41±3.28	1.10±2.85
Femur R	$V_{14.5\ Gy}$	0.73±1.48	0.73±1.30	0.63±1.22	0.71±1.60

$V_{100\%}$ did not decrease by >10% on any scan in our study, demonstrating greater accuracy of dose delivery of adaptive RT.

The adaptive workflow provided by MRgRT offers the potential to characterize and track anatomy variations, and ultimately realize real-time plan adaptation. This could offer the opportunity for reducing CTV-PTV margins, and particularly suitable to prostate reirradiation with the need to deliver high doses in a small volume with maximum sparing of pelvic OARs (18, 19). Although both ATP and ATS workflow available for adaptation, the study investigating dosimetry analysis of 100 fractions of 20 PCa patients by our team showed that the ATP strategy could only meet the clinical requirements (relatively lower dose requirements with PTV-V90% achieving prescribed dose as goal) for 23 (23%) fractions, compared with 100 (100%) fractions by ATS strategy (20). Furthermore, some data also showed that only the optimization from fluence and segment could fit all requirements for prostate cancer (9).

The online adaptive workflow solved the problems with the inter-fraction motion, but accentuated the intra-fraction motion, especially with the obvious long on-couch time. Usually, 30–40 and 50–60 minutes were needed with the 2-minute and 6-minute MR scans (12, 21), respectively. Intra-fraction prostate motion assessed by Calypso electromagnetic beacons (22, 23), fluoroscopy (24) or 4D ultrasound (25) has previously been characterized as different categories, while more recent studies focusing on MRgRT which have monitored prostate motion over longer time periods have concluded differently (12).

Although the prostate motion was reported as different categories intra-fractionally with a larger range, it seems different as per studies aiming for adaptive RT in the MRgRT era. With a median of 49 (24–78) min of on-couch time in our study, we did observe a slight CTV dose reduction with time (Figures 3A, B). Similar findings had been reported by other studies based on dose reconstruction algorithms using beam-on 2D-cine MR (26) or cine MR dynamics (11), both of which adopted moderate fractionation schedules (60 Gy/20 fr or 62 Gy/20 fr). Menten et al. analyzed prostate intra-fraction motion and extrapolated the dose changes by processing MR-linac treatment log files and online 2D-cine MR, and concluded that the mean CTV-$D_{98\%}$ decreased by 1.1 Gy ± 1.6 Gy (26). The UMC Utrecht constructed a soft tissue tracking algorithm with cine MR dynamics, with a mean processing time of 10.7 ± 2.5 s per dynamic (11). By extracting the treatment log files and assigning them to the appropriate cine MR dynamic volumes, they deduced that the CTV-$D_{99\%}$ underwent a dose

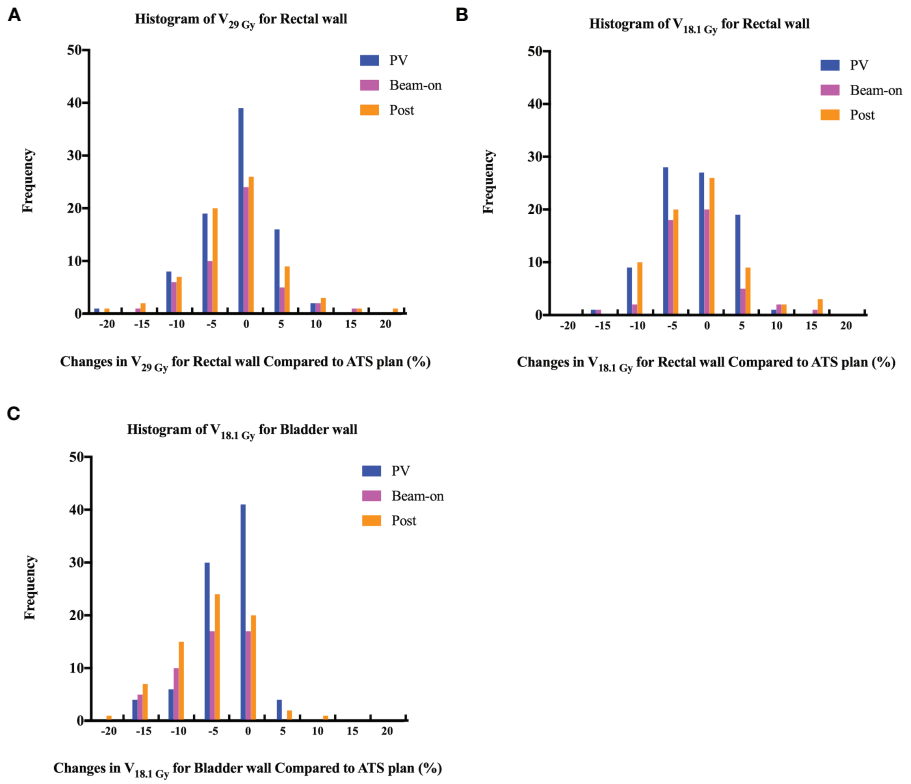

FIGURE 5
Histogram of changes in volume receiving 29 Gy (**A**, $V_{29\ Gy}$) or 18.1 Gy (**B**, $V_{18.1\ Gy}$) dose for rectal wall and 18.1 Gy **(C)** dose ($V_{18.1\ Gy}$) for bladder wall among PV-, Bn- and post-MR scans compared to ATS plans.

reduction of 2.2% ± 2.9% (11). Although a slight dose reduction was observed during the beam-on period in comparison with the ATS plan, the estimated dose delivered is still clinically acceptable. Research on prostate intra-fraction motion also demonstrated that the 95% CI of translation was within clinically applied margins of 5 mm by using cine MR dynamics (12), which was smaller than the data reported previously in the CBCT era (6–9 mm) (1, 2, 27). The main reasons for the small prostate motion and relatively stable dose coverage are as follows: first, the patients had been positioned on the couch for a relatively long time (27 minutes in de Muinck Keizer's study (12) and 33 minutes in our study) before cine MR and treatment delivery in these adaptive MRgRT series, compared to usually less than 5 minutes in studies investigating motion with CBCT and VMAT. It was reported previously that the prostate intra-fraction motion reached saturation after approximately 30 min of on-couch time (12), which could probably explain the non-significant beam-on dose reduction with long on-couch time. Second, we advised patients to drink water more slowly during preparation to avoid quick bladder volume changes during on-couch, which could also account for the dose findings of acceptable target coverage.

Although a 3-mm margin from CTV to PTV seems to be adequate for the prostate, with prostate $V_{36.25Gy} \geq 95\%$ for the 99% (204/206) scan (Figure 3C), it is not the case for SVs. The underdose (less than 95% of SVs-$V_{100\%}$) of SVs was observed on 31 scans collected from 18 fractions of 8 patients, which indicated that the intra-fractional SVs motion was a general problem. However, we also noticed that except for two patients, the SV-$V_{95\%}$ (SV-$V_{34.4Gy}$) of the remaining 10 patients reached more than 95%, which indicated that the significant SV motion caused by long on-couch time is also patient-specific. Furthermore, one patient had some urine leakage after delivery due to too full bladder for two sessions, which caused worse underdose of SVs on Bn-scan compared with Post-scan (Figures 3, 4A, Patient. #10 and Figure S2). The prostate and SVs have been shown to reveal independent motion characteristics, and SVs' movement has been shown to correlate more with the movement of the bladder and rectum (28). The slow filling of the bladder and adequate preparation of the rectum in our study could mitigate the prostate motion due to bladder volume changes, but might not compensate for all SV motion. The maximal range (3.6-7.2 mm) of SV motion has been reported to occur in the superior-inferior dimension (8, 28, 29), and the range increases with treatment time (29). An intra-fractional SVs motion analysis of 15 PCa patients reported that the 5-mm margins provided 95% intra-fractional SV coverage in over 90% of fractions (8). De Muinck Keizer also reported that intra-fraction coverage probability of 99% can be achieved with 5 mm isometric expansion for the left and right SV on MR-linac (30).

The rectum volumes slightly fluctuated during the ATS workflow, although we asked all patients to empty the rectum with an enema before each session. The estimated delivered dose to the rectal wall was clinically acceptable (Table 1), which were similar or a little bit higher than the dose metrics of ATS plan (Table S2). Nevertheless, a rectal wall V_{29Gy} increase of >15% was only observed on one post-MR scan and a $V_{18.1Gy}$ increase of >15% was not observed on any fractions (Figures 5A, B). In comparison with the data obtained using

conventionally fractionated RT with CBCT, which reported 5.6% fractions of the rectum-V_{45Gy} increased by >15% (3), the online adaptive UHF-RT is safe for the rectum and delivers a more accurate dose. Moreover, during the treatment, gas pockets in the rectum were observed on 12.9% (11/85) of the scans, which were also reported in some studies (4, 10). The gas bubbles always occurred between the acquisition of the PV scan and the start of the cine MR acquisition and remained in place during dose delivery in most cases (11.8%, 10/85 scans). Only in one fraction, a gas bubble was observed on Bn-scan but disappeared on the post-scan. Nevertheless, the $V_{36.25Gy}$ of CTV, prostate, and SVs for this patient were all 100% on each scan. Thus, continuous monitoring of target and rectum motion by cine MR is quite important for accurate dose delivery. Simultaneously, the continuous bladder volume increase caused a slight increase in bladder wall-mean variation V_{37Gy} (0.52 ± 0.58 cc) in a comparison with the ATS plan, and a reduction in bladder wall-mean variation $V_{18.1Gy}$ (-0.05 ± 0.03 cc) conversely. The clinical findings also confirmed the estimated dose delivered to normal tissues. The rates of worst acute RTOG grade 2 or more severe genitourinary and gastrointestinal toxicities were 25% and 0% (unpublished data), as reported in our preliminary results.

This study had several limitations. The sample size was still small with only 17 patients. However, we collected dosimetry data on the PV-, Bn-, and post-MR scans, providing comprehensive data that can indicate the dose changes in all organs. Furthermore, it was still difficult to conclude the estimated delivered dose during the beam-on period by using the PV-, Bn-, and post-MR scans. In our study, we included 10 patients with beam-on 3D MR and recalculated the dose based on the beam-on 3D MR, which can provide a more accurate 3D representation of the prostate volume and position compared to that used by dose reconstruction approaches based on cine MR that collected MR images on certain slices. There are merits to using large field-of-view, high-resolution 3D MR acquisitions for dose estimation, however, the slow acquisition of 3D-MR images (approximately 3 min needed for the 2-min T2 MR), the low temporal resolution of the MR datasets, collecting data at certain time point instead of whole beam-on period and reliance on a bulk electron density assignment strategy would be a concern for the dose inaccuracy, and maybe tempo-wise less accurate than using continuous cine-MR dynamics (11, 12). Nevertheless, using similar high-resolution 3D-MR acquisitions with the adaptive ATS plan, our estimated dose should be reliable. In addition, we stopped the cine MR acquisition and collected beam-on 3D MR only when the target and rectum were stable on cine MR, therefore biasing the results towards good agreement with the planned doses. However, it seems that due to the low incidence of such cases, the impact of this limitation in practice is minimal. Furthermore, the dosimetry results demonstrated the reliability of our methods, which involved monitoring motion by cine MR and pausing delivery if necessary.

In conclusion, our study investigating the dose on beam-on 3D-MR scans for each session demonstrated that clinically acceptable estimated dose coverage of target volumes was achieved during the beam-on period with an adaptive ATS workflow on a 1.5-T MR-linac, despite the relatively long on-couch time. The 3-mm CTV-PTV margin applied in our study is sufficient for the prostate and may be inadequate for a very small portion of SVs. More attention should be paid to restricting the rectal wall high dose when optimizing the ATS plan.

Data availability statement

The corresponding author has full access to all the data in the study and final responsibility for the decision to submit for publication. The data that support the findings of this study are available from H6WORLD platform (https://h6world.cn/signin) but restrictions apply to the availability of these data, which were used under license for the current study, and so are not publicly available. Data are however available from the authors upon reasonable request and with permission of H6WORLD platform. Requests to access the datasets should be directed to Ning-Ning Lu, Ning-Ning.Lu@hotmail.com.

Ethics statement

The studies involving human participants were reviewed and approved by Independent Ethics Committee of Chinese Academy of Medicine Sciences (NCT05183074, ChiCTR2000033382). The patients/participants provided their written informed consent to participate in this study.

Author contributions

N-NL, L-RG, YTian, M-SW, N-ZX, and Y-XL designed the study, analyzed the data and wrote the manuscript. N-NL, YTian, N-ZX, and Y-XL contributed to the study concept. N-NL, L-RG, YTian, M-SW, N-ZX, and Y-XL contributed to the study coordination. L-RG, N-NL, M-SW, and Y-XL performed the statistical analysis. All authors contributed to the article and approved the submitted version.

Funding

Supported by the Non-profit Central Research Institute Fund of Chinese Academy of Medical Sciences, Longevity and Health Project, 2021-JKCS-003. The funder of this study had no role in study design, data collection, data analysis, data interpretation, or writing of this manuscript.

Conflict of interest

The authors declare that the research was conducted in the absence of any commercial or financial relationships that could be construed as a potential conflict of interest.

Publisher's note

Supplementary material

The Supplementary Material for this article can be found online at: https://www.frontiersin.org/articles/10.3389/fonc.2023.1039901/full#supplementary-material

SUPPLEMENTARY FIGURE 1
Overviews of planning targets of all fractions, calculated by the daily ATS plan dose in PV-, Bn- and post-MR scans. 100% prescription dose **(A)** and 95% prescription dose **(B)**. Individual data points are shown as dots. The mean ± SD are shown as the error bars.

SUPPLEMENTARY FIGURE 2
Per-patient SVs-$V_{100\%}$ **(A)** and SVs-$V_{95\%}$ **(B)** mean values to the clinical target volume (CTV) summed by five fractions of pre- (ATS plan), PV-, Bn- and post-MR scans. Scar bars present the standard deviation (SD). No beam-on scans were acquired for the first 7 patients due to concerns about unexpected target and OAR moving. No SVs irradiation for Patient. #6, #7, #15 to #17.

References

1. Brand DH, Tree AC, Ostler P, van der Voet H, Loblaw A, Chu W, et al. Intensity-modulated fractionated radiotherapy versus stereotactic body radiotherapy for prostate cancer (PACE-b): Acute toxicity findings from an international, randomised, open-label, phase 3, non-inferiority trial. *Lancet Oncol* (2019) 20(11):1531–43. doi: 10.1016/S1470-2045(19)30569-8

2. Widmark A, Gunnlaugsson A, Beckman L, Thellenberg-Karlsson C, Hoyer M, Lagerlund M, et al. Ultra-hypofractionated versus conventionally fractionated radiotherapy for prostate cancer: 5-year outcomes of the HYPO-RT-PC randomised, non-inferiority, phase 3 trial. *Lancet* (2019) 394(10196):385–95. doi: 10.1016/S0140-6736(19)31131-6

3. Peng C, Ahunbay E, Chen G, Anderson S, Lawton C, Li XA. Characterizing interfraction variations and their dosimetric effects in prostate cancer radiotherapy. *Int J Radiat Oncol Biol Phys* (2011) 79(3):909–14. doi: 10.1016/j.ijrobp.2010.05.008

4. Nicosia L, Sicignano G, Rigo M, Figlia V, Cuccia F, De Simone A, et al. Daily dosimetric variation between image-guided volumetric modulated arc radiotherapy and MR-guided daily adaptive radiotherapy for prostate cancer stereotactic body radiotherapy. *Acta Oncol* (2021) 60(2):215–21. doi: 10.1080/0284186X.2020.1821090

5. Moteabbed M, Trofimov A, Khan FH, Wang Y, Sharp GC, Zietman AL, et al. Impact of interfractional motion on hypofractionated pencil beam scanning proton therapy and VMAT delivery for prostate cancer. *Med Phys* (2018) 45(9):4011–19. doi: 10.1002/mp.13091

6. McPartlin AJ, Li XA, Kershaw LE, Heide U, Kerkmeijer L, Lawton C, et al. MRI-Guided prostate adaptive radiotherapy - a systematic review. *Radiother Oncol* (2016) 119 (3):371–80. doi: 10.1016/j.radonc.2016.04.014

7. Tanyi JA, He T, Summers PA, Mburu RG, Kato CM, Rhodes SM, et al. Assessment of planning target volume margins for intensity-modulated radiotherapy of the prostate gland: role of daily inter- and intrafraction motion. *Int J Radiat Oncol Biol Phys* (2010) 78 (5):1579–85. doi: 10.1016/j.ijrobp.2010.02.001

8. Sheng Y, Li T, Lee WR, Yin FF, Wu QJ. Exploring the margin recipe for online adaptive radiation therapy for intermediate-risk prostate cancer: An intrafractional seminal vesicles motion analysis. *Int J Radiat Oncol Biol Phys* (2017) 98(2):473–80. doi: 10.1016/j.ijrobp.2017.02.089

9. Winkel D, Bol GH, Kroon PS, van Asselen B, Hackett SS, Werensteijn-Honingh AM, et al. Adaptive radiotherapy: The elekta unity MR-linac concept. *Clin Transl Radiat Oncol* (2019) 18:54–9. doi: 10.1016/j.ctro.2019.04.001

10. Vargas C, Saito AI, Hsi WC, Indelicato D, Falchook A, Zengm Q, et al. Cine-magnetic resonance imaging assessment of intrafraction motion for prostate cancer patients supine or prone with and without a rectal balloon. *Am J Clin Oncol* (2010) 33 (1):11–6. doi: 10.1097/COC.0b013e31819fdf7c

11. Kontaxis C, de Muinck Keizer DM, Kerkmeijer LGW, Willigenburg T, den Hartogh MD, van der Voort van Zyp JRN, et al. Delivered dose quantification in prostate radiotherapy using online 3D cine imaging and treatment log files on a combined 1.5T magnetic resonance imaging and linear accelerator system. *Phys Imaging In Radiat Oncol* (2020) 15:23–9. doi: 10.1016/j.phro.2020.06.005

12. de Muinck Keizer DM, Kerkmeijer LGW, Willigenburg T, van Lier ALHMW, MDd H, van der Voort van Zyp JRN, et al. Prostate intrafraction motion during the preparation and delivery of MR-guided radiotherapy sessions on a 1.5T MR-linac. *Radiotherapy Oncol J Eur Soc For Ther Radiol Oncol* (2020) 151:88–94. doi: 10.1016/j.radonc.2020.06.044

13. de Muinck Keizer DM, Kontaxis C, Kerkmeijer LGW, van der Voort van Zyp JRN, van den Berg CAT, Raaymakers BW, et al. Dosimetric impact of soft-tissue based intrafraction motion from 3D cine-MR in prostate SBRT. *Phys Med Biol* (2020) 65 (2):025012. doi: 10.1088/1361-6560/ab6241

14. Salembier C, Villeirs G, De Bari B, Hoskin P, Pieters BR, Van Vulpen M, et al. ESTRO ACROP consensus guideline on CT- and MRI-based target volume delineation for primary radiation therapy of localized prostate cancer. *Radiother Oncol* (2018) 127 (1):49–61. doi: 10.1016/j.radonc.2018.01.014

15. Lovelock DM, Messineo AP, Cox BW, Kollmeier MA, Zelefsky MJ. Continuous monitoring and intrafraction target position correction during treatment improves target coverage for patients undergoing SBRT prostate therapy. *Int J Radiat Oncol Biol Phys* (2015) 91(3):588–94. doi: 10.1016/j.ijrobp.2014.10.049

16. King BL, Butler WM, Merrick GS, Kurko BS, Reed JL, Murray BC, et al. Electromagnetic transponders indicate prostate size increase followed by decrease during the course of external beam radiation therapy. *Int J Radiat Oncol Biol Phys* (2011) 79(5):1350–7. doi: 10.1016/j.ijrobp.2009.12.053

17. Gunnlaugsson A, Kjellén E, Hagberg O, Thellenberg-Karlsson C, Widmark A, Nilsson P. Change in prostate volume during extreme hypo-fractionation analysed with MRI. *Radiat Oncol (London England)* (2014) 9:22. doi: 10.1186/1748-717X-9-22

18. Michalet M, Riou O, Cottet-Moine J, Castan F, Gourgou S, Valdenaire S, et al. Magnetic resonance-guided reirradiation for local recurrence within the prostate or in the prostate bed: One-year clinical results of a prospective registry study. *Cancers (Basel)* (2022), 14(8):1943. doi: 10.3390/cancers14081943

19. Michalet M, Riou O, Valdenaire S, Debuire P, Ailleres N, Draghici R, et al. Magnetic resonance-guided reirradiation for local recurrence within the prostate or in the prostate bed: Preliminary results of a prospective registry study. *Adv Radiat Oncol* (2021) 6(5):100748. doi: 10.1016/j.adro.2021.100748

20. Xia WL, Liang B, Men K, Zhang K, Tian Y, Li MH, et al. Prediction of adaptive strategies based on deformation vector field features for MR-guided adaptive radiotherapy of prostate cancer. *Med Phys* (2022). doi: 10.1002/mp.16192

21. Alongi F, Rigo M, Figlia V, Cuccia F, Giaj-Levra N, Nicosia L, et al. 1.5 T MR-guided and daily adapted SBRT for prostate cancer: Feasibility, preliminary clinical tolerability, quality of life and patient-reported outcomes during treatment. *Radiat Oncol (London England)* (2020) 15(1):69. doi: 10.1186/s13014-020-01510-w

22. Kupelian P, Willoughby T, Mahadevan A, Djemil T, Weinstein G, Jani S, et al. Multi-institutional clinical experience with the calypso system in localization and continuous, real-time monitoring of the prostate gland during external radiotherapy. *Int J Radiat Oncol Biol Phys* (2007) 67(4):1088–98. doi: 10.1016/j.ijrobp.2006.10.026

23. Pommer T, Oh JH, Munck Af Rosenschold P, Deasy JO. Simulating intrafraction prostate motion with a random walk model. *Adv Radiat Oncol* (2017) 2(3):429–36. doi: 10.1016/j.adro.2017.03.005

24. Ng JA, Booth JT, Poulsen PR, Fledelius W, Worm ES, Eade T, et al. Kilovoltage intrafraction monitoring for prostate intensity modulated arc therapy: First clinical results. *Int J Radiat Oncol Biol Phys* (2012) 84(5):e655–661. doi: 10.1016/j.ijrobp.2012.07.2367

25. Ballhausen H, Li M, Hegemann NS, Ganswindt U, Parodi K, Belka C. Intra-fraction motion of the prostate is a random walk. *Strahlenther Onkol* (2015) 191:S7–8. doi: 10.1088/0031-9155/60/2/549

26. Menten MJ, Mohajer JK, Nilawar R, Bertholet J, Dunlop A, Pathmanathan AU, et al. Automatic reconstruction of the delivered dose of the day using MR-linac treatment log files and online MR imaging. *Radiotherapy Oncol J Eur Soc For Ther Radiol Oncol* (2020) 145:88–94. doi: 10.1016/j.radonc.2019.12.010

27. Ghadjar P, Fiorino C, Munck Af Rosenschold P, Pinkawa M, Zilli T, van der Heide UA. ESTRO ACROP consensus guideline on the use of image guided radiation therapy for localized prostate cancer. *Radiother Oncol* (2019) 141:5–13. doi: 10.1016/j.radonc.2019.08.027

28. Mak D, Gill S, Paul R, Stillie A, Haworth A, Kron T, et al. Seminal vesicle interfraction displacement and margins in image guided radiotherapy for prostate cancer. *Radiat Oncol* (2012) 7:139. doi: 10.1186/1748-717X-7-139

29. Gill S, Dang K, Fox C, Bressel M, Kron T, Bergen N, et al. Seminal vesicle intrafraction motion analysed with cinematic magnetic resonance imaging. *Radiat Oncol* (2014) 9:174. doi: 10.1186/1748-717X-9-174

30. Muinck Keizer D, Willigenburg T, der Voort van Zyp J, Raaymakers BW, Lagendijk JJW, Boer J. Seminal vesicle intrafraction motion during the delivery of radiotherapy sessions on a 1.5 T MR-linac. *Radiother Oncol* (2021) 162:162–9. doi: 10.1016/j.radonc.2021.07.014

frontiers | Frontiers in Oncology

TYPE Review
PUBLISHED 27 January 2023
DOI 10.3389/fonc.2023.1117874

OPEN ACCESS

EDITED BY
Feng Liu,
The University of Queensland, Australia

REVIEWED BY
David Waddington,
The University of Sydney, Australia
Francesco Cuccia,
ARNAS Ospedali Civico Di Cristina Benfratelli, Italy
Brendan Whelan,
The University of Sydney, Australia

*CORRESPONDENCE
John Ng
jon9024@med.cornell.edu

SPECIALTY SECTION
This article was submitted to Radiation Oncology, a section of the journal Frontiers in Oncology

RECEIVED 07 December 2022
ACCEPTED 16 January 2023
PUBLISHED 27 January 2023

CITATION
Ng J, Gregucci F, Pennell RT, Nagar H, Golden EB, Knisely JPS, Sanfilippo NJ and Formenti SC (2023) MRI-LINAC: A transformative technology in radiation oncology. *Front. Oncol.* 13:1117874. doi: 10.3389/fonc.2023.1117874

MRI-LINAC: A transformative technology in radiation oncology

John Ng[1]*, Fabiana Gregucci[1,2], Ryan T. Pennell[1], Himanshu Nagar[1], Encouse B. Golden[1], Jonathan P. S. Knisely[1], Nicholas J. Sanfilippo[1] and Silvia C. Formenti[1]

[1]Department of Radiation Oncology, Weill Cornell Medicine, New York, NY, United States, [2]Department of Radiation Oncology, Miulli General Regional Hospital, Acquaviva delle Fonti, Bari, Italy

Advances in radiotherapy technologies have enabled more precise target guidance, improved treatment verification, and greater control and versatility in radiation delivery. Amongst the recent novel technologies, Magnetic Resonance Imaging (MRI) guided radiotherapy (MRgRT) may hold the greatest potential to improve the therapeutic gains of image-guided delivery of radiation dose. The ability of the MRI linear accelerator (LINAC) to image tumors and organs with on-table MRI, to manage organ motion and dose delivery in real-time, and to adapt the radiotherapy plan on the day of treatment while the patient is on the table are major advances relative to current conventional radiation treatments. These advanced techniques demand efficient coordination and communication between members of the treatment team. MRgRT could fundamentally transform the radiotherapy delivery process within radiation oncology centers through the reorganization of the patient and treatment team workflow process. However, the MRgRT technology currently is limited by accessibility due to the cost of capital investment and the time and personnel allocation needed for each fractional treatment and the unclear clinical benefit compared to conventional radiotherapy platforms. As the technology evolves and becomes more widely available, we present the case that MRgRT has the potential to become a widely utilized treatment platform and transform the radiation oncology treatment process just as earlier disruptive radiation therapy technologies have done.

KEYWORDS

MRI, external beam radiotherapy, radiation therapy technology, image-guided radiation therapy, MR-guided radiation therapy, medical physics

1 Introduction

The development of a linear accelerator (LINAC) system with an integrated Magnetic Resonance Imaging (MRI) scanner is a major advance in image guided radiation technology (1, 2). Previously, image guided radiation therapy would rely on on-board portal film imaging or planar kV radiographs or cone-beam computed tomography (CT) scanning during patient setup for image verification before radiation dose delivery. With the integration of an on-board MR scanner within the LINAC radiation therapy system, real time image guidance throughout tumor and organ motion and during radiation delivery became feasible.

In the field of external beam photon radiation oncology, several earlier technical and technological improvements - including intensity-modulated radiotherapy (IMRT), volumetric arc radiotherapy (VMAT) and stereotactic radiotherapy (SRT) - have been implemented in daily clinical practice. A point of crucial interest with these new technologies has been the faculty to control, verify, and eventually modify the treatment planning and delivery process with high accuracy and precision. This power to achieve a more homogeneous better target volume coverage is coupled with the ability to significantly reduce the volume of healthy tissue irradiated to high doses (3).

These great efforts to push the boundaries of a safe and effective radiotherapy plan have raised a central question - "how can we know during treatment delivery whether what we have so carefully measured and calculated in the planning process is the actually delivered treatment?" In fact, the central challenge of precision radiotherapy remains the intra-fraction variability of the target, i.e., controlling for the individual physiological body movements at the precise moment of dose delivery.

To address this key challenge, several solutions have been brought forth, leading to the revolutionary concepts of tumor tracking and adaptive radiotherapy (ART). Real time motion management and ART reduces the uncertainties related to imaging, treatment planning, and treatment delivery due to daily organ variability and motion, tumor delineation (including microscopic disease) and inter- and intra- fraction setup error and variability. Historically, the generation of significant planning target volume (PTV) margins around the target was introduced to compensate for these uncertainties, with the drawback of irradiating more healthy tissue and increasing the toxicity to organs at risk (OaRs) (4). The development of 4-dimensional CT (4D-CT) allowed tracking of the tumor through the study and control of respiratory motion (5). 4D-CT was a major advance allowing the radiation oncologist and treatment team to reduce PTV margins related to motion during the respiratory cycle. However, organ motion control and verification remain complex problems requiring different solutions. Target uncertainty not only depends on breathing but it is also associated with motion/changes in other organs such as bowel peristalsis, bladder filling, and day-to-day anatomic variation. Hence, 4D-CT can neither resolve the issue of correct target definition nor account for inter- and intra-fractional anatomic changes.

In this era of highly customized and personalized therapy, a broader concept of adaptive image-guided and biology-guided RT has arisen (6–8). The field of image-guided radiation therapy interfaces thus intersects with the fields of radiomics and bioinformatics, including machine learning and artificial intelligence (AI) (9). We summarize three seminal applications of adaptive image-guided RT: i) therapy guidance (target and OaRs definition); ii) treatment plan verification (inter-fraction management); and iii) real-time delivery control (intra-fraction management).

1.1 Therapy guidance

The starting point of the care pathway in RT is represented by target volume and OaRs definition within the individual patient. The clinical team must accurately evaluate the area to be treated with a curative radiation dose and its relative anatomic relationships with the surrounding healthy tissue, to plan for a dose delivery that spares normal tissue as much as possible from irradiation. Kilovoltage CT imaging acquired at simulation is the standard basis for the construction of the treatment plan. It allows for morphological mapping of the anatomy based upon the distribution of differing electronic densities of various tissues. Today, highly sophisticated and complementary imaging modalities, such as MRI and positron emission tomography (PET) are merged with the CT simulation images. Fusion with these additional imaging modalities lead to a better morphological and structural definition of the area being treated as well as the integration of metabolic and functional information (10–12). Fusion occurs in the planning phase but lack of advanced on-board imaging within the standard linear accelerator precludes a precise application for each dose delivered.

1.2 Treatment verification

Another critical aspect of radiation delivery which relies upon image guidance is treatment verification and the possibility of real-time re-planning in case of anatomical variations related to disease response or to human physiology that may occur during the course of RT. In the past, the best available on board imaging technique was 2D radiological imaging obtained using low contrast MV or kV x-rays which permitted visualization of bony landmarks or suitably positioned radiopaque markers to verify target coverage (13).

Daily transabdominal ultrasonic spatial localization of the prostate is an example of a non-invasive approach that avoided radio-opaque fiducial markers implantation's expense, discomfort, and risks (14). The introduction of cone beam CT (CBCT) technology has permitted volumetric visualization of the anatomical treatment field, improving accuracy in management of inter-fraction variations. In some clinical sites such as brain, abdomen and pelvis, however, CBCT imaging does not allow sufficient definition of the soft tissue, often burdened by significant artifacts from the presence of air and scattered photons that limit imaging accuracy of cone beam CT reconstruction algorithms (15).

Surface matching algorithms are another approach that has recently been used for guiding radiotherapy treatments. Surface matching, however, does not contain direction information about the location of the target volume or organs at risk that are not immediately correlated to the surface markers.

These treatment verification strategies were developed for treatment courses where a radiotherapy treatment was planned once. Every effort would be exerted to provide reproducible geometries and additional margins would be introduced during planning to assure that the treatment would not miss the target. Fractionation schemes were selected to permit normal tissue included in the high dose volume to not exceed established acute or long-term tolerances.

As technologies improved to precisely deliver highly conformal intensity modulated treatments and technologies emerged to assess the relationships of target organs to organs at risk, it was realized that a radiation plan generated from a remotely acquired imaging study may not reflect the optimal treatment plan on the day of delivery. The ability to acquire imaging, plan treatment, and deliver treatment using real-time image guidance, which an MR-guided linear accelerator is capable of, breaks through multiple barriers to providing better care.

1.3 Delivery control

A major goal of image guided radiotherapy is the possibility to see in *real time* what happens at the treatment site during the delivery phase and to intervene/adjust if there is a significant shift on the target. This challenge is the latest frontier of adaptive guided-RT application, and reinforces the need for technologies which can address intra-fraction motion management and pave the way for safe dose escalation and de-escalation therapy (6).

A current standard for accounting for real time tumor and organ motion is four-dimensional computed tomography (4D-CT). 4D-CT utilizes a set of CT images acquired throughout different phases of the patient's respiratory cycle and combines them with tracking of external respiratory markers during patient setup and delivery. The uncertainties associated with 4D-CT are accounted for by the expansion of internal target volume (ITV) and planning target volume (PTV) margins, theoretically compensating for intra-fractional tumor and organ motion. The individual breathing cycle is studied during simulation and dose delivery is planned consistently.

However, 4D-CT is inherently limited by the daily reproducibility of the breathing cycles and does not control for changes in daily tumor and organ motion (16). In other words, 4D-CT informs a plan to improve delivery control and motion management through images acquired during CT simulation, but it cannot represent real-time, daily motion management. Ultimately, representative delivery control is possible only with real-time motion visualization through on-board intra-fraction imaging, target structure tracking, and gated treatment delivery.

We present the case that MRgRT is the most promising disruptive radiation oncology technology to overcome the challenges of intra-fraction motion. Through improving upon contemporary image-guided radiation technology, MRgRT is transforming the radiotherapy delivery process within radiation oncology centers, reorganizing patient flow and how treatment team members interact. In this review, we describe some of the advantages that MRgRT provides and the remaining major barriers to its routine adoption. We summarize the original data in disease sites where MRgRT has already had an impact. Finally, we introduce some emerging developments involving MRgRT.

2 MRI-Linac systems and other platforms

In recent years, several radiotherapy platforms have become commercially available in clinical radiation oncology to meet the challenges of adaptive image-guided RT. Similar to the earlier technical advances described above, these newer technologies are starting off as resource intensive approaches with specialized clinical applications. With continuous stepwise improvements, the reduced toxicity and other clinical advantages made possible by IMRT, VMAT, and stereotactic RT overcame the initial barriers of cost and resource investment (6, 17). It is expected that over time, incremental improvements and broader indications will enable these newer technologies to be widely disseminated into standard radiation oncology practice.

There are currently two main MRgRT platforms commercially available – the ViewRay MRIdian system (Viewray Inc., Oakwood, OH) which uses a 0.35 Tesla MRI scanner and the Elekta Unity (Elekta AB, Stockholm, Sweden) system which uses a 1.5 Tesla MRI scanner. The ViewRay system initially used cobalt-60 as its radiation source and received FDA approval in 2012 (18). ViewRay then developed a platform where the MRI scanner was integrated within a linear accelerator, receiving FDA clearance in 2017 (19). The Elekta Unity system was approved in 2019 by the FDA as the second MRI-linear accelerator system (20).

More recently, other hybrid linear accelerator systems with adaptive capabilities have also gained FDA clearance and are treating patients in the clinic. Varian's Ethos system (Varian, Palo Alto, CA), FDA cleared in 2020, enables adaptive radiotherapy utilizing on-board fan-beam CT imaging (21). The most recent is the Reflexion system (RefleXion, Hayward, CA), a radiotherapy system that the FDA approved in 2021 with future plans to utilize an on-board PET scanner as the integrated imaging modality used for guidance while treating patients on a linear accelerator (22). The Ethos and the Reflexion systems join the earlier Cyberknife system (Accuray, Sunnyvale, CA) and Radixact system (Accuray, Sunnyvale, CA) as non-MRgRT based adaptive radiotherapy systems. All these radiotherapy technologies revolve around the idea that future radiation oncology practices will leverage the ability to acquire imaging while the patient is on the table to account for motion management and adapt treatment planning on the day of delivery. The Viewray MRIdian has the faculty of real time intrafraction modulation of dose delivery by imaging during treatment delivery, and the Elekta Unity scanner introduced support for motion management during radiation delivery in October of 2022.

Table 1 summarizes the features of some of the most common commercially available IGRT platforms that have received FDA regulatory clearance for radiation delivery in patients.

3 Main differences between the MRI-Linac-based systems

Between the two widely utilized MRI-Linac systems, there are key differences in design and treatment features. We summarize them here and in Table 2:

3.1 Construction

MRIdian: The split superconductor 0.35 Tesla magnet design allows for a smaller source-to-axis distance (SAD). The integration of the linear accelerator and the magnet allows for robust integration of imaging registration with treatment planning capabilities.

Unity: A single magnet design with the LINAC components placed outside the 1.5 Tesla MR scanner. Due to its greater magnet field strength with this design allows for greater imaging capability compared to a lower-field imaging system.

3.2 Treatment delivery

MRIdian: The MRIdian utilizes coplanar static IMRT fields and can deliver radiation dose at a 650MU/min dose rate. The gantry rotation speed is 0.5 rpm with no collimator rotation.

TABLE 1 Commercially available radiotherapy platforms specializing in adaptive image-guided and biology-guided radiation therapy.

System	Image guided modality	Real-timeinter-fraction management	Real-timeintra-fraction management	Strengths	Weaknesses
MRIdian	MR (0.35 Tesla)	Yes	Yes, automatically	No ionizing radiations for imaging	Time
				Target visualization during treatment	Coplanar beam fields
				High soft tissue discrimination	No electronic density data
				Functional imaging data	
Unity	MR (1.5 Tesla)	Yes	Yes, not automatically	No ionizing radiations for imaging	Time
				Target visualization during treatment	Coplanar beam fields
				High soft tissue discrimination	No electronic density data
				Functional imaging data	
Ethos	Artificial Intelligence CT based	Yes	No	Time	Use of ionizing radiations for imaging
					Coplanar beam fields
				Electronic density data	No target visualization during treatment
					Low soft tissue discrimination
					Functional imaging data
RefleXion	PET-CT	Yes	No	Time	Use of ionizing radiations for imaging
				Electronic density data	Coplanar beam fields
				Functional imaging data	No target visualization during treatment
					Low soft tissue discrimination

Unity: The Unity utilizes coplanar static IMRT fields and can deliver radiation dose at a 500MU/min dose rate. The gantry rotation speed is 6.0 rpm gantry with no collimator rotation.

3.3 Imaging

MRIdian: The MRIdian utilizes a balanced steady state free precession (SSFP) MRI pulse sequence for planning, setup, and treatment delivery. Other MRI pulse sequences, such as T2/T1 and DWI sequences, can only be used as registered images alongside the balanced SSFP sequence.

Unity: The Unity has a broad range of pulse sequences available for planning and treatment. MR imaging is available during the treatment. Up to recently, if the clinical team chooses to image with the MRI host during treatment, they would lose the ability to track the target during delivery. Very recently, Elekta has introduced a motion management package that overcomes this limitation.

TABLE 2 Comparison of the MRIdian and Unity MRI-Linac radiotherapy platforms.

Feature	MRIdian	Unity
Construction	Split Magnet Design	Single Magnet Design
Imaging	Trufi Sequence Imaging based	Range of Imaging sequences available
Gating	Real time tracking and automatic gating	Real time tracking without automatic gating
Treatment	Gantry rotation maximum speed of 0.5 rpm	Gantry rotation maximum speed of 6.0 rpm

3.4 Gating

MRIdian: The MRIdian is able to automatically gate on one sagittal slice delineated from the 3D volumetric scan at 8 frames per second. Its newer A3I features allow for tracking capabilities on all three planes (sagittal, coronal, and axial) simultaneously or on multiple planes in the same orientation. The beam will automatically gate itself once the target migrates too far beyond the defined boundary expansion.

Unity: The Unity has the ability to track targets in real time on three planes (sagittal, coronal and axial). If the target moves outside the pre-specified envelope, the treatment beam will be automatically gated by the machine (currently pending FDA approval, CE Marked in the European Union).

4 Advantages of the MRI-Linac Technology

To address the challenges posed by image guided radiation therapy at the present, we will review three key advances in adaptive image-guided RT made possible by the MRI-Linac technology: 1) imaging for therapy guidance (Figure 1); 2) adaptive treatment planning for inter-fractional management (Figure 2); and 3) real time imaging and gating for intra-fractional management (Figure 3).

4.1 MRgRT: Imaging for therapy guidance

MR imaging is an imaging technique based on nuclear magnetic resonance which maps the spatial concentration of signal bearing spins of the tissue environment. The imaging is also dependent on differing signal intensities between the tissues. These properties permit MR images to have higher resolution relative to CT imaging, even without the administration of contrast. A range of possible MR pulse sequences that can be used clinically can allow the acquisition of different forms of images, most commonly T1-weighted, T2-weighted or proton density based imaging sequences, each characterized by a different signal intensity that creates contrast between the various tissues. In T1-weighted images, fluid is hypointense and fat is hyperintense while in T2-weighted images the fluid is hyperintense and the fat is mildly hypointense (23). The features of T1- and T2-weighted imaging are often used in RT for the anatomical definition of the target and the OaRs due to their signal contrast in soft tissue (24). There is further promise that combining different MR pulse sequences, such as combining different functional spin echo-based and/or gradient echo-based sequences, can allow MR imaging to obtain different functional information that could help characterize the tumor microenvironment. These sequences could include fluid-attenuation inversion recovery (FLAIR), short tau inversion recovery (STIR), diffusion-weighted imaging (DWI) and dynamic contrast-enhanced (DCE) (25). As MR image voxels can measure quantitative properties over time, they allow measurements of parameters that are indicators of tumor cell density (with DWI), vascularity (with perfusion), stiffness/stroma (with elastography) and hypoxia (with relaxometry), biologic factors that are known to drive radiosensitivity and radioresistance (26, 27). Overall, MR imaging is more versatile and can potentially unlock addition clinical information complementary to conventional CT imaging.

4.2 MRgRT: Adaptive treatment planning for inter-fractional management

The anatomic changes that occur from the time of simulation to when daily treatments are initiated, and in between daily treatments have been a problem in treatment verification, often necessitating wider target margins to ensure the target received full dose radiation delivery. This is often counterbalanced by limiting the total prescription dose and coverage to limit the risk of toxicity. The current standard 4D-CT involving CT imaging, sometimes with the placement of fiducial markers, at the simulation and in the treatment room throughout the respiratory cycle before delivery was a major advance in the field, but there remained the persistent issue of adjusting for these day-to-day positional changes in the tumor target and OaRs (28). For example, several studies of abdominal

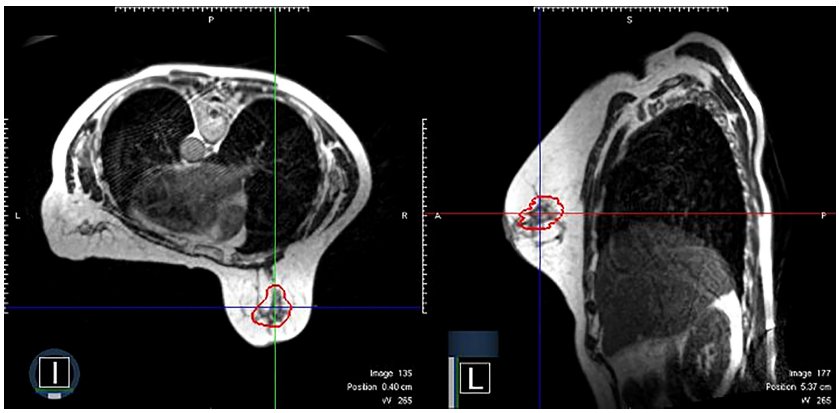

FIGURE 1
An example of clinical MRI-Linac images utilized for therapy guidance. The panel on the left shows a patient receiving prone breast irradiation with an MRI image in the axial plane. The same patient with a sagittal plane image. The red contour depicts the lumpectomy surgical cavity which serves as the clinical target volume.

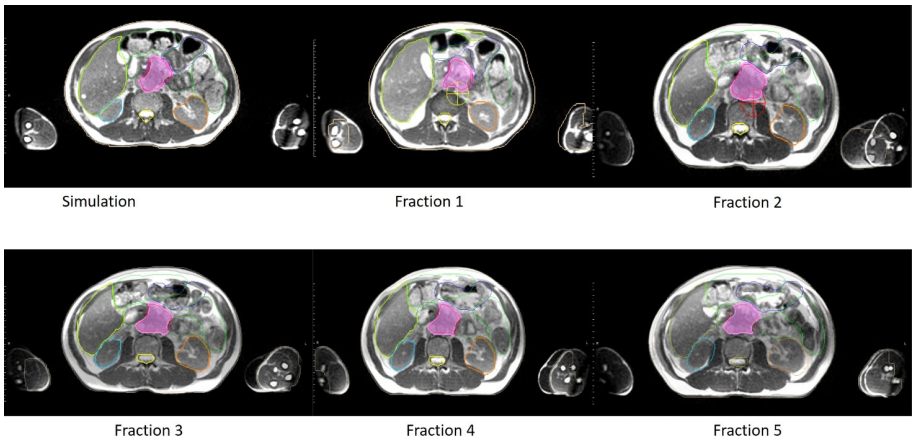

FIGURE 2
An example of clinical MRI-Linac images utilized for inter-fractional management. Comparison of anatomy seen on the day of simulation (upper left panel) and days of treatment (panels labeled Fractions 1 to 5 respectively) for a pancreatic cancer patient treated at our institution. In each panel, the target volume, stomach, and bowel anatomy are contoured.

tumors and organs showed that the daily variation of the pancreas position could exceed 1 cm in each direction (29, 30).

Adaptive radiation treatment planning (ART) is an approach that allows for daily adjustments of the radiation treatment plan based on re-determining spatial parameters for the treatment targets and nearby tissues. While this can be occasionally done on acquired images with the patient off the table, a significant step forward would be performing the same tasks while the patient is on the treatment table. Conventional linear accelerators are not capable of such an approach.

The advent of the hybrid MRI-Linac systems make routine clinical implementation of on table ART possible. The MRI-Linac systems feature full integration of the treatment planning software with the radiation delivery unit and also feature newer rapid dose calculation algorithms. Adaptive re-planning of radiation treatments with MRI guidance have now been shown to be feasible and to offer comparable plan qualities to their respective reference treatment plans (31). The ability to acquire an updated MRI scan while the patient is on the treatment table, to adjust for anatomic changes prior to radiation delivery, and to adapt the treatment plan could allow for tighter margins on treatment volumes and enable dose escalation with favorable toxicity when compared to non-adaptive radiation planning, but prospective clinical data will be necessary to establish these benefits.

4.3 MRgRT: Real time imaging and gating for intra-fractional management

As discussed above, current motion management strategies such as 4D-CT are passive, utilizing patterned or expected motion to determine additional safety margins such as an ITV. An improved intra-fractional management strategy would be active, such as beam gating, whereby a pre-specified target is monitored in motion and the beam is turned on only when that target is within a pre-defined window.

For beam gating, the hybrid MRI-Linac systems have the distinct advantage of real-time imaging of soft tissues (32). This major technical advance enables the clinical team to visualize with high accuracy the target during overall treatment course and provides the ability to monitor in real time the physiologic moments of internal organs that impact on intra-fraction reproducibility of dose delivery.

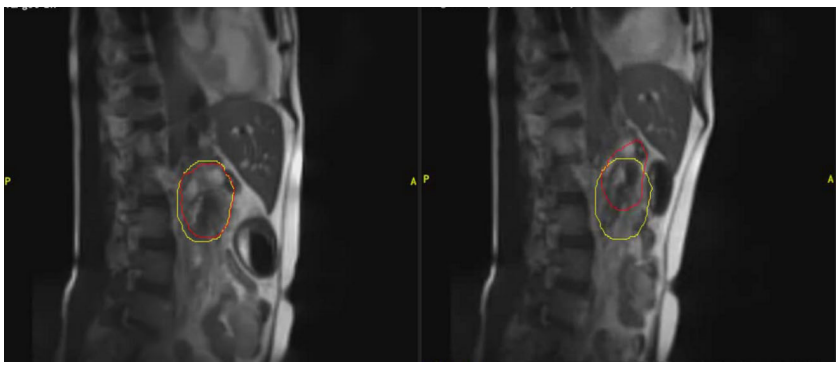

FIGURE 3
An example of clinical MRI-Linac images utilized for intra-fractional management. The panel on the left shows a patient receiving pancreatic radiotherapy while imaged with a deep inspiratory breathe hold. The panel of the right shows the same patient breathing freely. The red contour depicts the tracking contour and the yellow contour depicts the treatment envelope boundary.

With recent upgrades on the Unity, both MRI-Linac systems are now capable of *automatic*, active intra-fractional beam gating. With the MRIdian system, two-dimensional cine MRI images are acquired in the sagittal plane (can also be done in the axial and coronal planes) at 8 frames per second. A gating tracking target is contoured during a breath-hold MR scan, and a gating envelope is generated off a margin expansion from that contoured gating target. As radiation treatment is being delivered, if a pre-specified volume (for example, 5%) of the gating target is outside the gating envelope, the beam is automatically turned off. If the total volume of the gating target falls within the gating envelope by a defined threshold, the beam automatically turns on. Later in this review, we will describe several disease sites where automatic real-time gating may have powerful clinical applications.

MRgRT permits the clinical team to set threshold boundaries on the maximum safe displacement of the treatment target (33). In turn, real time intra-fractional imaging and active gating provide the possibility of reducing treatment margins, of increasing target dose, and of sparing dose to organs at risk (OARs) (34). The approach is applicable to many clinical scenarios including thoracic, abdominal and pelvic disease. In those anatomic regions, the proximity and movement of OaRs limit target dose, and dose escalation may improve oncologic outcomes and dose avoidance may reduce toxicity (35).

Compared to conventional on-board imaging of a CT-based linear accelerator, MRgRT does not use ionizing radiation to obtain real-time images. This is a great advantage in terms of patient protection, but it has fostered a new argument relative to the effect on human body of long exposure to radiofrequency energy emitted by a MR scanner (28). This energy causes heating of the body in a proportional way to the square of the magnetic field strength and it may be a future challenge to understand its potential implications, particularly for individuals with implanted devices that may be more susceptible to localized heating (36).

5 Limitations of the MRI-LINAC technology

5.1 Capital costs

The most immediate barrier to wide implementation of the MRI-LINAC technology in radiation oncology centers are the capital costs associated with acquiring and maintaining the system. The current estimates are that initial acquisition price would be greater than $7.5 million for a MRI-Linac (37, 38). In addition, the annual maintenance costs are estimated to be greater than $500,000 per year.

Further initial expenses include construction and installation costs for a dedicated vault for a MRI-Linac with the necessary shielding and increased needed capacity for a superconducting magnet with helium, estimated to be greater than $14,000 per square meter (37).

5.2 Duration of treatment and throughput

A second major limitation is the time allocation needed for MRgRT treatments. A typical MRI-guided treatment requires daily patient checks to ensure MRI-capability. The patient then has to be set up according to simulation with appropriate MR coils placement. An MRI sequence is needed to be acquired for patient setup verification with physician approval. Finally, a tracking contour and a tracking cine has to be generated for treatment verification. In summary, the dedicated time to apply a real time treatment management workflow is a process that requires around 30-60 minutes for each treatment session (19, 39, 40). Two prospective phase I trials that included adaptive treatments in the thorax and in the abdomen on the MRI-Linac failed to meet their initially allotted fixed time constraint endpoints (41, 42).

For an adaptive treatment, further time must be allocated for each treatment. While the patient is on the table, the MRI image acquired is then utilized to predict the coverage and OAR doses from the pre-set treatment plan. If the predicted dosimetry is considered inadequate, the physician can re-contour the target volumes and the proximate OaRs. The treatment planning team with the physician, therapists, dosimetrist, and physicist at the planning console then creates a day of treatment plan. An optimized plan created on the day of treatment is approved and then delivered. The dedicated time for patients receiving an MRgRT treatment with ART would be around 90-120 minutes with all clinical team members present at the console and completing their individual tasks in close coordination (40) (Figure 4). There is further time complexity involved in the latency between the image acquisition and consequent action decision (43). Several algorithms have been proposed to mitigate this issue. Recently, Jöhl and colleagues elaborated a linear methods approach to predict the target displacement and proposed that hereafter artificial neural networks could be implemented (43, 44).

Given these time and resources allocated for MRgRT, the patient throughput with this technology is slower than that of a conventional linear accelerator (37, 39). Implementing a MRgRT program requires high quality imaging and an efficient workflow process to acquire the MRI scan, adapt the radiation plan, perform quality assurance, and deliver the radiation while the patient is set up for treatment. Wider practical applicability of MRgRT will be limited by the intense utilization of personnel and time to safely and properly deliver adaptive treatments, but exciting future developments are expected in the coming years which we will describe later.

5.3 Lack of non-coplanar beam delivery and other delivery limitations

While treatment delivery is more versatile in terms of intra-fractional and inter-fractional management with the MRI-Linac system, radiation delivery is also limited by the hybrid integration of the MR scanner within the linear accelerator. For example, it currently is not possible to deliver arc therapy or non-coplanar beam therapy with a MRI-Linac system (27). The current MRI-Linac systems also cannot deliver electron beam therapy (27).

Other delivery limitations are due to the design of the current MRI-Linac systems. When a patient is lying within the treatment bore, the ability to shift the table position or to rotate the couch is limited. Finally the size of the MRI bore limits its use to patients with an appropriate body habitus.

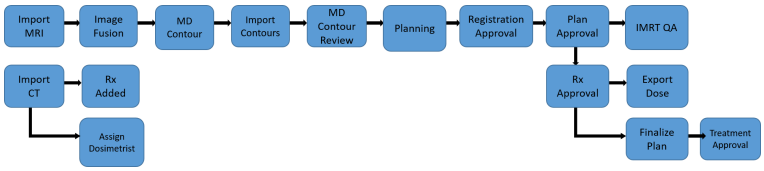

FIGURE 4
A representative example of the care pathway implemented during a MRgRT treatment. Each blue box represents a distinct task that a clinical treatment team member must complete before triggering the next task to be done, demonstrated by the arrow diagram.

5.4 Contraindications to MR imaging

The MRI technology also has other established practical limitations and patient contraindications. Claustrophobia in MRI scanners are common in the general population. Some studies estimate that 10-15% of patients would require some level of sedation to be able to be able to complete an MRI scan (45). Hospitals and clinics have established safety policies and standards in place for MRI safety, and the clinical team must maintain vigilance to ensure that the patient does not have MRI-incompatible material in their body or on their person (46). Implanted medical devices such as pacemakers and defibrillators have to be interrogated before and after approaching an MRI scanner (47).

6 Disease sites and clinical applications

Despite the challenges just described that counterbalance wide adoption of MRgRT, acquisition of the technology and its utilization in the clinic has been steadily increasing. We will describe several disease sites where current clinical evidence justify their utilization and reinforce their unrealized potential.

6.1 Prostate cancer

MRI is routinely employed for prostate cancer diagnosis, staging, and management (48, 49), enabling identification of malignant portions within the prostate, as well as enhanced discrimination of the adjacent bowel, rectum and bladder (50). MRI is used as an adjunct imaging modality to CT-based radiotherapy planning to further delineate soft tissues (51). Additionally, MRI can aid with sparing the neurovascular structures associated with erectile dysfunction (52). However, static imaging acquired prior to treatment fails to capture changes in target volumes after the initial planning, as well physiological movement of internal organs (53–55). In contrast, MRgRT allows monitoring of both tumor changes and daily positional changes of internal organs for each treatment to achieve a more accurate estimation of a treatment plan's dose distribution (i.e. inter-fraction adaptive planning), as well as real-time motion monitoring during treatment (i.e. intra-fraction gating) (56).

Adaptive planning utilizes day-of-treatment imaging and re-contouring of target volumes and/or organs at risk based on changes in their size or relative position. This can improve the therapeutic index in rapidly changing tumors, or in regions where there are dramatic changes in organ position during each fraction, such as the rectum for prostate treatment. Gating refers to synchronizing the radiation beam with a predetermined parameter. In respiratory gating, radiation is delivered within a specified range of respiratory motion so that the beam is turned off when there are deviations outside set inspiratory and expiratory parameters. An inherent benefit of MR is that there is no additional radiation exposure as a consequence of real-time imaging, and thus can be performed continuously during treatment delivery. In MR-guided therapy where real-time imaging is employed, gating of the target volume within a user-specified boundary is typically performed, in which the beam is only on if the PTV falls within the pre-defined boundary (see Figure 5).

In prostate radiotherapy, image gating is useful to account for organ movement resulting from bowel gas, stool passage and bladder filling as well as contracting of the muscles of the pelvic floor (57). Adaptive planning and gating are complementary techniques, in which adaptive planning corrects for inter-fraction anatomic variation and gating accounts for real-time, intra-fraction physiologic motion. Other potential roles for the MR-Linac in prostate cancer treatment include its applications for dominant lesion boosting and prostate re-irradiation (58, 59). Furthermore, intra-fractional motion management with MRgRT now enables enhanced ability to observe intra-fraction prostate motion during prostate SBRT (60, 61).

6.2 Lung cancer

Recent advances in lung cancer radiation therapy include stereotactic body radiation therapy (SBRT) for early-stage disease and IMRT for locally advanced cases (62). In either clinical situation, precise dose delivery is paramount to maximize local control and avoid toxicity.

While SBRT and IMRT have improved the therapeutic ratio, challenges still exist. In patients treated with SBRT, chest wall toxicity, including rib fracture, has been reported in the range of 6-46% (63). Tumors abutting central mediastinal structures are even more problematic. Haseltine reported 12% grade >3 toxicity in central or ultra-central tumors which rose to 30.7% when the tumor was <1cm from the proximal bronchial tree (64). Toxicities of concurrent chemo-radiation therapy (CRT) in locally advanced disease are similarly well described. In a meta-analysis of radiation toxicities in non-small cell lung cancer, Or and colleagues reported Grade >3 esophagitis and pneumonitis 22% and 11%, respectively, when concurrent chemotherapy was employed (65).

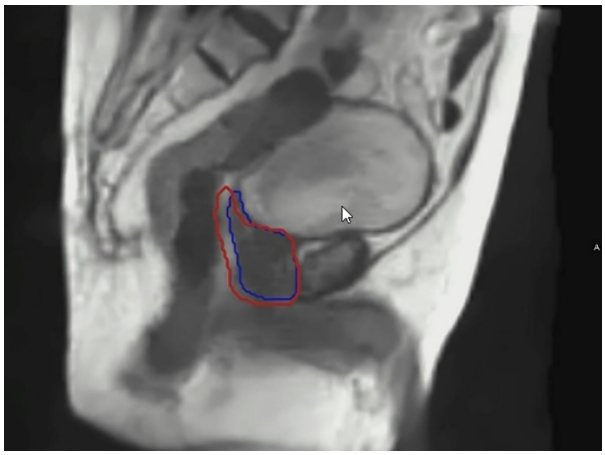

FIGURE 5
An example of real time imaging during a prostate MRgRT treatment. The blue contour depicts the prostate target tracking contour. The red contour depicts the gated treatment envelope boundary.

Management of tumor motion offers the potential to improve tumor control and reduce toxicity. Seppenwoolde and colleagues reported average amplitude of tumor motion was the greatest in the cranial-caudal direction for tumors located in the lower lobe and not attached to rigid structures (such as chest wall and vertebrae) compared to upper lobe and attached to rigid structures [12 ± 6 mm (SD) versus 2 ± 2 mm (SD)] (66).

Giaj-Levra and colleagues have suggested improved dose to cardiac structures resulting this motion management (67). Some have expressed concern over magnetic-field induced deviation of electron trajectories, creating hot or cold spots in relation to air-tissue interfaces. However, Raajimakers illustrated that with multiple and opposing beams, this concern is mitigated (68). Bainbridge and colleagues came to similar conclusions in a dosimetric study examining 10 plans in patients with locally advanced NSCLC and also suggested superior dose distributions could be achieved when MRI treatment employed smaller PTV margins which can be more easily achieved with real time tumor visualization (69).

6.3 Liver malignancies

Over the past four decades, the accumulated data collected from liver resections for patients with metastatic cancer demonstrated that the risk-benefit profile for hepatic resection shifted in favor of benefit (with long-term curative potential) for selected patients with primary colorectal tumors (70–72). This finding led to the proposed clinical state of oligometastases, whereby the anatomy and physiology may limit or concentrate metastases to a single or a limited number of organs that should be amenable to a curative therapeutic strategy (73). Interestingly, recent results from the randomized phase II SABR-COMET trial corroborated the idea that aggressive treatment of oligometastatic disease may improve overall survival (74). Although surgery remains the gold standard for patients diagnosed with primary or secondary liver tumors, not all patients are deemed to be surgical candidates. For nonsurgical candidates, radiofrequency ablation (RFA), trans-arterial chemoembolization (TACE), cryotherapy, trans-arterial radioembolization (TARE), and radiotherapy are frequently utilized alternative local treatment options, where the proper treatment selection relies on a multidisciplinary approach (75). The use of SBRT has increasingly been used in the management of liver metastasis and hepatic malignancies where many studies have reported their 2-year local control rates of ≥ 90%, comparable to other locoregional therapies (76). The control rates and survival for primary and secondary malignancies have somewhat shown to correlate with radiation dose (for example, cholangiocarcinoma [$BED_{10} \leq 80.5$ Gy vs > 80.5 Gy], liver metastases [$BED_{10} \leq 100$ Gy vs > 100Gy] (77, 78). Unfortunately, the liver, stomach, duodenum, bowel, and kidneys are radiosensitive organs and the radiation doses to these organs must be constrained (and the target dose reduced by proxy) to limit treatment related toxicities while treating liver lesions to ablative doses (79).

The use of stereotactic MR guided online adaptive radiation therapy for the treatment of primary and secondary liver malignancies represents a promising approach to improve the therapeutic ratio. This technique allows for better visualization of soft tissue, real-time tumor tracking, motion management (during the breathing cycle) *via* deep inspiration breath holding techniques (to allow for smaller target volumes), and adaptive planning (to improve target dosing while limiting dose to radiosensitive organs [that move with the respiratory cycle and change their juxtaposition daily] in line with recommended dose constraint guidelines) (74, 80). Although the normal organ constraints come from retrospective series, CT based planning (that assumes mobile structures remain in the same position throughout treatment), and animal studies, some have posited that radiation toxicity risks may be overestimated, the dose constraints too conservative, and the tumor unnecessarily underdosed (to meet the dose constraints) in patients treated with MRI guided adaptive radiotherapy (81). Thus, through a combination of raising the tolerance for normal organs at risk and reducing the margins delivered through MRI guidance, the overall dose to the tumor could be substantially increased or improved (82).

Recent and ongoing studies are working towards validating this hypothesis. In a phase I trial of MRI guided online adaptive radiation therapy (50Gy in 5 fractions, BED_{10} = 100Gy) for abdominal malignancies (20 patients with oligometastatic or unresectable primary liver cancers), Henke et al. demonstrated that adaptive planning allows for PTV dose escalation and/or simultaneous normal organ sparing compared to a non-adaptive SBRT approach (42, 83). Similarly, Rogowski et al. reported their early clinical experience of online adaptive MRI guided radiation therapy for liver tumors (84). Their retrospective series included treated patients with cholangiocarcinoma and various metastases (neuroendocrine tumors, colorectal carcinoma, sarcomas, and gastrointestinal stromal tumors). The median prescribed dose of BED_{10} = 84.4 Gy was delivered in 3 to 5 fractions. Adaptive planning was performed in 98% of fractions to improve PTV coverage and to reduce organ at risk constraint violations. After a median follow up of five months neither local failures nor ≥ grade 2 toxicities were observed. Ugurluer et al. reported their early experience in 21 patients with oligometastatic liver disease (85). The median dose delivered was 50 Gy in 5 fractions with 93 out of 111 fractions requiring re-optimization. All patients had either

complete or partial response at their irradiated sites with an estimated 1-year overall survival of 93.3%. No ≥ grade 3 acute or late toxicities were observed. Padgett et al. reported their experience of 10 patients treated with MRI guided online adaptive SBRT for liver tumors (86). With a prescription dose range between 27-50 gray in 3-5 fractions and the daily utilization of adaptive planning, they observed significantly reduced PTV coverage for 32 out of 47 (68%) fractions and organ at risk constraint violations in 5 out of 23 (22%) fractions prior re-optimization. They concluded that online adaptive MR guided SBRT of liver tumors using daily re-optimization resulted in better target conformality, coverage, and organ at risk sparing compared with non-adaptive SBRT. Finally, in a prospective phase I trial van Dams et al. reported their outcomes after MRI-guided SBRT treatment of 20 patients with a mix of primary (8) and secondary (12) liver tumors (87). With a median follow-up of 18.9 months, they reported a 2-year local control rate of 79.6% utilizing a median dose of 54Gy in 3 fractions. Interestingly, they observed a local control difference between single vs multiple lesions and a BED_{10} < 100Gy vs BED_{10} ≥ 100Gy.

The ongoing MAESTRO randomized controlled phase 2 trial is testing the non-inferiority of MRI guided adaptive radiation versus ITV-based SBRT for hepatic metastases for hepatobiliary and gastrointestinal ≥ grade 3 toxicities (88). The secondary outcomes include local regional and distant tumor control, progression free-survival, overall survival, and the possibility of increase of BED using MRI guided radiotherapy if the BED is limited with ITV base SBRT. The results of this trial will further define whether MRI guided adaptive radiotherapy provides for an improved therapeutic ratio as compared to standard ITV-based SBRT for liver lesions.

6.4 Pancreatic cancer

The role of radiation therapy for pancreatic ductal adenocarcinoma (PDAC) remains unclear. Recently reported clinical trials have not shown any significant improvement in overall survival in the localized setting (89, 90). It has been hypothesized that one of the reasons for the limited efficacy seen in the recent trials with pancreatic radiotherapy has been the delivery of non-ablative radiation doses to the pancreatic tumor target. A role for radiation dose escalation in PDAC is supported by other studies which use higher ablative doses, showing improved local control and potentially survival (91–93).

The major challenge in pancreatic radiotherapy is delivering significant radiation doses to the pancreatic target without causing significant toxicity. In particular, the stomach, the duodenum, bowel, and other nearby radiosensitive organs often receive significant collateral radiation doses. The significant toxicities attributable to pancreatic radiation treatments highlight the limitations of conventional techniques (94–97). Applying MRgRT shows great promise in overcoming the clinical challenges of organ motion and daily anatomic changes particular to pancreatic radiotherapy.

Stereotactic MR-guided on-table Adaptive Radiation Therapy (SMART) is an MRgRT application designed to account for inter-fractional anatomic changes. It utilizes the MRI scans acquired both before and continuously during treatment delivery to account for intra-fractional motion management to deliver ablative radiation doses. A retrospective study of 5-fraction SMART in locally advanced PDAC showed promising efficacy and safety (92). More recently, a multi-institutional prospective Phase 2 trial of SMART in localized pancreatic cancer completed accrual and presented early results, showing promising efficacy and toxicity outcomes (98). Pancreatic cancer treatment may be one of the most apparent direct applications of MRgRT with several Phase 3 clinical trials in the development phase that plan to test whether ablative pancreatic radiotherapy may improve overall survival in the locally advanced PDAC setting. There is eager anticipation to gather further prospective clinical data on the role of ablative pancreatic radiotherapy made feasible by adaptive image guided radiotherapy.

6.5 Breast cancer

In early-stage breast cancer management, there is significant momentum towards de-escalating intensity of treatment. Local recurrence rates in early stage disease have decreased over time and are reported to be less than 5% over 10 years of follow up in recent clinical trials (99–101). Nevertheless, fear of recurrence after treatment and long-term toxicities associated with treatment remain primary issues in survivorship, and local and distal breast cancer recurrence risk remains a concern for patients even 20 years or more after treatment for early stage breast cancer (102).

De-escalation in breast radiotherapy has emphasized treating smaller target volumes and prioritizing avoiding the nearby heart and lungs, based on the improvements in image-guided radiotherapy technologies. Several large Phase 3 trials have demonstrated good efficacy and toxicity of external beam partial breast irradiation (PBI) when compared with whole breast radiotherapy (99, 101). For external beam PBI, a current standard is daily CT-based image guidance. The capability of on-table MRI guidance, adaptive planning, and delivery with the prone technique has several particular potential advantages over CT-based imaging.

MR imaging is superior in delineating soft tissue contrast in the breast, allowing for more accurate surgical cavity and target volume delineation. Intra-fractional MR-guided imaging and decreased chest wall excursion with the prone breast setup can further account for organ motion and decrease targeting uncertainty (103). MRI guidance would potentially allow CTV and PTV margins to be reduced. With potentially smaller treatment volumes, MRgRT may decrease toxicities associated with breast radiotherapy (104).

The versatility of daily adaptive imaging, contouring, planning, and radiation delivery process can help mitigate the challenges of daily setup uncertainties for breast radiotherapy. The surgical cavity can be difficult to delineate even with surgical clip or marker placement within the surgical bed, a practice not universally followed by breast surgeons. When surgical clips are placed to mark the cavity, they can migrate from their initial position within the breast over time. It is known that the surgical cavity can change over the time it takes to deliver a course of breast radiotherapy (105). Significant topological and volume changes in the breast can occur during the course of radiation treatment (106). Nearby organs at risk can also change in relative position on a day-by-day basis. Of particularly clinical concern, cardiac positioning can vary considerably relative to the bony anatomy and other anatomic

landmarks used for patient positioning (107). Even with prone positioning, the left anterior descending coronary artery can receive significant radiation dose if daily imaging guidance is not utilized (108). For those patients where positional setup uncertainty is significant, similar to the standard for PBI, it is recommended that more frequent image-guidance be utilized during breast radiotherapy, such as daily cone-beam CTs (109). A technique of combining MRgRT with prone breast irradiation, which we coin Precision Prone Irradiation (PPI) enables greater flexibility and potentially more accurate treatment delivery (110).

As explained above, CT-based breast treatment planning often requires frequent or daily cone beam CT imaging for setup verification. For patients with high aversion to the radiation exposure from daily CT scans or tattoo marking, MRgRT offers the opportunity to potentially bypass the CT simulation, permanent skin tattooing, or regular cone beam CT image verifications which have become standard. The potential promise of smaller radiation treatment volumes through the PPI technique and the significance of any such advantages will have to be established through prospective clinical trials.

6.6 Central nervous system tumors

In the CNS, for both primary parenchymal brain tumors and for brain metastases, identifying post-planning changes in target volumes that have occurred since their delineation permits more accurate delineation of target volumes at the time that treatment is actually being delivered. Changes in the position of both target volumes and normal tissues at risk of injury from irradiation have been documented to be increasingly likely to occur with longer elapsed time since a dedicated planning study (111, 112).

For patients with intrinsic brain tumors where the operative bed is part of the target volume, the gradual resolution of mass effect after craniotomy will present a very different substrate for contouring (and planning) depending on when the imaging for planning irradiation is performed. Changes resulting from the craniotomy may continue to occur during a several month period after surgery is performed—during the time that fractionated radiotherapy will be delivered.

Unfortunately, the competing capabilities of a hybrid MR-Linac hinder both the imaging and treatment delivery capabilities relative to dedicated machines. Specialized imaging assessments such as chemical exchange saturation transfer imaging and diffusion weighted imaging have been performed on a 1.5T MRI-Linac (113, 114). Many specialized pulse sequences have not yet been demonstrated on an MRI-Linac, and lower field strength scanners may never be able to perform many specialized sequences.

Also, it may not be cost-effective to use the MRI capabilities of a MRI-Linac to perform specialized assessments when treatment throughput is an important criterion of successful implementation of this technology. Magnetic resonance fingerprinting, still in its relative infancy, allows the simultaneous measurement of multiple tissue properties in a single, time-efficient manner, and may permit serial assessments of responses to radiation treatment to be gathered during the re-planning guided by anatomic information (115, 116). It remains to be confirmed if serial short acquisitions during daily treatment can provide oncologically important information to help with guiding treatment recommendations for patients with CNS malignancies.

It may be argued that for radiosurgical treatments, the short duration of treatment delivery (1-5 sessions) will prevent significant shifts in the location and conformation of target volumes and contiguously located critical normal tissues. A single adaptation on the first day of treatment may be all that is needed, but it is also possible that changes in the target volumes consequent to the treatments already delivered will require changes in one or more additional fractions (117). There is no prospectively acquired data from daily MR imaging during a course of hypofractionated radiosurgery that might adapt current treatment recommendations for brain metastasis or benign tumor (meningioma, schwannoma, etc.) treatments, where a single treatment plan generated and checked before the start of therapy is used for all delivered fractions.

Investigators at Sunnybrook Medical Center in Toronto have conducted a prospective study of sequential MRI scans on a 1.5T MR-LINAC that were done on the first day, 11th day, and 21st day of partial brain radiotherapy in a 6 week course of treatment. Both the locations and sizes of the target volume locations were evaluated. The gross target volume decreased over the course of therapy in most patients with a median volume decrease from 18.4 cm^3 on day 1 to 14.7 cm^3 on day 11, and 13.7 cm^3 on day 21. The intracranial position of the target volume changed during the course of therapy as well. Migrations of >0.5 cm in the target volumes were seen in 54% of patients by the beginning of the 3rd week of radiotherapy (day 11 imaging), and 58% of patients by the beginning of the 5th week of radiotherapy (day 21 imaging) (118). The large margins used for radiotherapy of malignant gliomas may lower the probability of a complete geographic miss, but being able to decrease target volume margins while avoiding geographic misses would potentially benefit many patients receiving partial brain radiotherapy by exposing less brain to high-dose irradiation.

Over a multiple-week course of radiation therapy, as is commonly delivered for an intrinsic low- or high-grade glioma, or for a pituitary neuroendocrine tumor, craniopharyngioma, or meningioma located close to the anterior visual pathways, there also may be changes in the locations of the target volume and normal tissues at risk for morbidity when compared to an MRI scan performed 1-2 weeks or more prior to initiation of radiotherapy. Indeed, for craniopharyngioma treatments, it is advised to have an MRI scan done part-way through treatment to ensure that there has been no change in the target volume that would necessitate re-planning to reflect the new anatomic realities (119). Finally, there are relatively mobile targets within the CNS (optic nerve sheath meningioma) where a patient's eye position on the treatment planning MRI and simulation CT scan may not be matched for any of the 5+ weeks of daily radiotherapy. Having a daily confirmation of the position of the target would perhaps improve the therapeutic ratio for this particular tumor.

MRgRT may be particularly valuable for soft-tissue imaging in the presence of surgically implanted devices such as spinal fixation hardware in patients who have had surgical stabilization of their spines and require irradiation for control of metastatic cancer. The low field strength permits visualization of the bony and soft-tissue anatomy in the area where the radiation is required. Conventional 1.5 or 3T imaging introduces artifact from the surgical stabilization devices, and the presence of artifact from the hardware also

degrades CT imaging so that the spinal cord's exact position may only be determined by a CT myelogram (120). Dosimetric studies suggest a potential impact for the MRI-Linac in spinal irradiation or re-irradiation (121–123).

7 Future developments

In this section, we will highlight what are some of the most exciting and evident developments emerging in MRgRT. As we described above, adaptive MRgRT treatment currently require significant time dedicated by the clinical team members. One development which has emerged in the past year is an upgrade to the MRI-Linac system that allows for parallel workflow processes in the treatment planning process. These upgrades should allow multiple users to work on the plan simultaneously, thereby reducing the total time needed for adapted fractions. Two other potential high impact developments that we will describe in more detail are the intense ongoing research in generating synthetic CT (sCT) images and in radiomics.

7.1 Synthetic CT

The workflow for treatment on a MRI-Linac is a two-step process: one based on MR imaging acquisition and other based on CT imaging acquisition. The disadvantage of the MRI simulation is the lack of electronic density tissue information that are fundamental in RT planning to calculate the dose distribution. These essential data are typically derived from CT based on Hounsfield Units (HU) and cannot be obtained directly from MR images. Moreover, this crucial aspect is necessary both to start treatment planning and during treatment to evaluate adaptive re-planning. To overcome this limit, several solutions have been proposed to convert MR intensities in HU, generating synthetic-CT images (Figure 6) (124).

Three main domains summarize these solutions: bulk density, atlas-based, and machine learning (ML) methods. Bulk density is the least sophisticated and time consuming method. It consists of grouping structures with similar density and attributing a homogeneous electronic value without taking into account the tissue heterogeneity. The atlas-based methods require co-registration of CT with MR images based on library collections. Although it is possible to evaluate tissue heterogeneity, the co-registration and the different position/anatomy of the patient is an important limitation of the method. Finally, ML and deep learning approaches are the most promising and most recently investigated methods that allow fast and accurate sCT (125). In 2017, Han proposed a novel deep convolutional neural network method for sCT generation, showing that it is able to produce accurate sCT in real time and opening the way for future developments (126). The main DL architectures used for sCT generation are the U-Net and the Generative Adversarial Networks (GAN) (127). A narrow restriction is represented by the ability of these models to adequately respond to considerable anatomical variations. While the central nervous system is easily reproducible and predictable, anatomic regions such as the head and neck, the pelvis, and the abdomen are examples of extreme variability due to physiological changes. Today, the search for a standardized, reliable, and applicable model for various anatomical and clinical scenarios remains a great challenge.

7.2 Radiomics

Radiomics is often defined as the application of quantitative imaging analysis to convert images to higher dimensional data and the subsequent mining of these data for improved decision support when integrated with clinical data (128). Radiomics analysis could potentially predict tumor response based not just on morphological criteria, according to Response Evaluation Criteria in Solid Tumor (RECIST), but also through integration of biological and functional data to implement predictive-prognostic models of survival (129–131). In this field, MRI has potential beyond other imaging modalities (e.g. CT and PET) by providing morphological and functional data together (132, 133). In particular, dynamic-contrast enhanced (DCE) images can describe vascularization and apparent diffusion coefficients (ADC) derived by diffusion weighted imaging (DWI) can quantify cellularity, applications with great potential if contrast is administered before MRgRT treatments. These biologically relevant data have a potential key role to predict treatment response while taking into account the ability to quantitatively describe cell metabolism and death. Furthermore, combination with

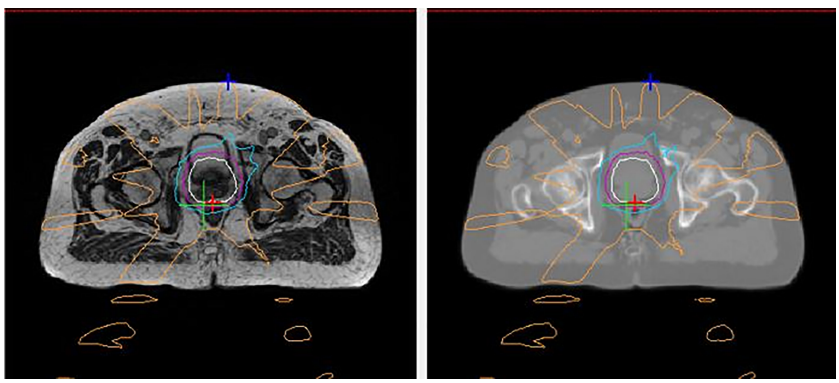

FIGURE 6
An example of a generated synthetic-CT (sCT) for prostate radiotherapy. The left panel shows an axial MR image acquired with a MRI-Linac during a MRI simulation. The right panel shows the corresponding sCT generated based on that MRI image by converting MR intensities into Hounsfield Units.

morphological and structural data could lead to an accurate description of the tumor microenvironment (134). The versatility of the MRI-Linac technology opens the possibility to collect this biologic data while imaging and treating the patient.

The availability of repeat MRI imaging during treatment also opens the possibility of another promising treatment response analysis: delta radiomics. The rationale behind delta radiomics is that the combined analysis of images acquired before, during and after treatment can provide a more complete description of tumor behavior, including sensitivity of the individual patient to a specific treatment (135). Considering the clinical impact of immunotherapy and precision medicine, a current challenge is the ability to evaluate changes in the microenvironment induced by the immune response or targeted therapy, which may be possible by combining multiparametric MR images (136–138).

8 Conclusion

MRgRT is a transformative radiotherapy technology that is having significant impact in clinical radiation oncology. This novel technology allows the clinical team to improve on three staples of the radiation treatment process: therapy guidance, treatment verification, and delivery control. In inter-fractional and intra-fractional management, MRgRT offers several advantages over current standard radiotherapy technologies. However, these advantages are counterbalanced by increased costs, increased resource and time allocation, and other practical limitations. This pattern is similar to previous disruptive radiotherapy technologies where further refinements and clearer clinical roles enabled widespread adoption. The utilization and capabilities of the MRI-Linac are already expanding in a wide range of clinical disease sites. Future advances will smoothen the MRgRT treatment planning and delivery process. Advances in MR imaging, radiomics, and advances in artificial learning/machine learning will further leverage this technology's clinical potential. We expect the utilization of the MRgRT platform to grow and reshape the radiation oncology clinic in the coming decades.

Author contributions

All authors listed have made a substantial, direct, and intellectual contribution to the work, and approved it for publication.

Conflict of interest

The authors declare that the research was conducted in the absence of any commercial or financial relationships that could be construed as a potential conflict of interest.

Publisher's note

References

1. Lagendijk JJ, Raaymakers BW, Raaijmakers AJ, Overweg J, Brown KJ, Kerkhof EM, et al. MRI/linac integration. *Radiother Oncol* (2008) 86(1):25–9. doi: 10.1016/j.radonc.2007.10.034

2. Jaffray DA. Image-guided radiotherapy: from current concept to future perspectives. *Nat Rev Clin Oncol* (2012) 9(12):688–99. doi: 10.1038/nrclinonc.2012.194

3. Meduri B, Gregucci F, D'Angelo E, Alitto AR, Ciurlia E, Desideri I, et al. Volume de-escalation in radiation therapy: state of the art and new perspectives. *J Cancer Res Clin Oncol* (2020) 146(4):909–24. doi: 10.1007/s00432-020-03152-7

4. Zou W, Dong L, Kevin Teo BK. Current state of image guidance in radiation oncology: Implications for PTV margin expansion and adaptive therapy. *Semin Radiat Oncol* (2018) 28(3):238–47. doi: 10.1016/j.semradonc.2018.02.008

5. Keall P. 4-dimensional computed tomography imaging and treatment planning. *Semin Radiat Oncol* (2004) 14(1):81–90. doi: 10.1053/j.semradonc.2003.10.006

6. Dawson LA, Sharpe MB. Image-guided radiotherapy: rationale, benefits, and limitations. *Lancet Oncol* (2006) 7(10):848–58. doi: 10.1016/S1470-2045(06)70904-4

7. Dawson LA, Jaffray DA. Advances in image-guided radiation therapy. *J Clin Oncol* (2007) 25(8):938–46. doi: 10.1200/JCO.2006.09.9515

8. Zhang Z, Liu X, Chen D, Yu J. Radiotherapy combined with immunotherapy: the dawn of cancer treatment. *Signal Transduct Target Ther* (2022) 7(1):258. doi: 10.1038/s41392-022-01102-y

9. Huynh E, Hosny A, Guthier C, Bitterman DS, Petit SF, Haas-Kogan DA, et al. Artificial intelligence in radiation oncology. *Nat Rev Clin Oncol* (2020) 17(12):771–81. doi: 10.1038/s41571-020-0417-8

10. Lapa C, Nestle U, Albert NL, Baues C, Beer A, Buck A, et al. Value of PET imaging for radiation therapy. *Strahlenther Onkol* (2021) 197(9):1–23. doi: 10.1007/s00066-021-01812-2

11. Mazzola R, Fersino S, Alongi P, Di Paola G, Gregucci F, Aiello D, et al. Stereotactic body radiation therapy for liver oligometastases: predictive factors of local response by 18F-FDG-PET/CT. *Br J Radiol* (2018) 91(1088):20180058. doi: 10.1259/bjr.20180058

12. Hörner-Rieber J, Klüter S, Debus J, Adema G, Ansems M, Verheij M. MR-guided radiotherapy: The perfect partner for immunotherapy? *Front Oncol* (2021) 10:615697. doi: 10.3389/fonc.2020.615697

13. Killoran JH, Allen AM, Kann BH, Lyatskaya Y. Inter fractional variability of breathing phase definition as determined by fiducial location. *Med Phys* (2008) 35(2):753–63. doi: 10.1118/1.2828197

14. Mohan DS, Kupelian PA, Willoughby TR. Short-course intensity-modulated radiotherapy for localized prostate cancer with daily transabdominal ultrasound localization of the prostate gland. *Int J Radiat Oncol Biol Phys* (2000) 46(3):575–80. doi: 10.1016/S0360-3016(99)00454-X

15. Ali I, Ahmad S, Alsbou N, Lovelock DM, Kriminski S, Amols H. Correction of image artifacts from treatment couch in cone-beam CT from kV on-board imaging. *J Xray Sci Technol* (2011) 19(3):321–32. doi: 10.3233/XST-2011-0296

16. Ge J, Santanam L, Noel C, Parikh PJ. Planning 4-dimensional computed tomography (4DCT) cannot adequately represent daily intrafractional motion of abdominal tumors. *Int J Radiat Oncol Biol Phys* (2013) 85(4):999–1005. doi: 10.1016/j.ijrobp.2012.09.014

17. Intensity Modulated Radiation Therapy Collaborative Working Group. Intensity-modulated radiotherapy: current status and issues of interest. *Int J Radiat Oncol Biol Phys* (2001) 51(4):880–914. doi: 10.1016/S0360-3016(01)01749-7

18. Mutic S, Dempsey JF. The ViewRay system: magnetic resonance-guided and controlled radiotherapy. *Semin Radiat Oncol* (2014) 24(3):196–9. doi: 10.1016/j.semradonc.2014.02.008

19. Acharya S, Fischer-Valuck BW, Kashani R, Parikh P, Yang D, Zhao T, et al. Online magnetic resonance image guided adaptive radiation therapy: First clinical applications. *Int J Radiat Oncol Biol Phys* (2016) 94:394–403. doi: 10.1016/j.ijrobp.2015.10.015

20. Raaymakers BW, Jürgenliemk-Schulz IM, Bol GH, Glitzner M, Kotte ANTJ, van Asselen B, et al. First patients treated with a 1.5 T MRI-linac: clinical proof of concept of a high-precision, high-field MRI guided radiotherapy treatment. *Phys Med Biol* (2017) 62(23):L41–50. doi: 10.1088/1361-6560/aa9517

21. Yoon SW, Lin H, Alonso-Basanta M, Anderson N, Apinorasethkul O, Cooper K, et al. Initial evaluation of a novel cone-beam CT-based semi-automated online adaptive radiotherapy system for head and neck cancer treatment - a timing and automation quality study. *Cureus.* (2020) 12(8):e9660. doi: 10.7759/cureus.9660

22. Oderinde OM, Shirvani SM, Olcott PD, Kuduvalli G, Mazin S, Larkin D. The technical design and concept of a PET/CT linac for biology-guided radiotherapy. *Clin Transl Radiat Oncol* (2021) 29:106–12. doi: 10.1016/j.ctro.2021.04.003

23. Dirix P, Haustermans K, Vandecaveye V. The value of magnetic resonance imaging for radiotherapy planning. *Semin Radiat Oncol* (2014) 24(3):151–9. doi: 10.1016/j.semradonc.2014.02.003

24. Schmidt MA, Payne GS. Radiotherapy planning using MRI. *Phys Med Biol* (2015) 60(22):R323–61. doi: 10.1088/0031-9155/60/22/R323

25. Matsuo M, Matsumoto S, Mitchell JB, Krishna MC, Camphausen K. Magnetic resonance imaging of the tumor microenvironment in radiotherapy: perfusion, hypoxia, and metabolism. *Semin Radiat Oncol* (2014) 24(3):210–7. doi: 10.1016/j.semradonc.2014.02.002

26. Gurney-Champion OJ, Mahmood F, van Schie M, Julian R, George B, Philippens MEP, et al. Quantitative imaging for radiotherapy purposes. *Radiother Oncol* (2020) 146:66–75. doi: 10.1016/j.radonc.2020.01.026

27. Surov A, Meyer HJ, Wienke A. Correlation between apparent diffusion coefficient (ADC) and cellularity is different in several tumors: a meta-analysis. *Oncotarget* (2017) 8 (35):59492–9. doi: 10.18632/oncotarget.17752

28. Thorwarth D, Low DA. Technical challenges of real-time adaptive MR-guided radiotherapy. *Front Oncol* (2021) 11:634507. doi: 10.3389/fonc.2021.634507

29. Shiinoki T, Shibuya K, Nakamura M, Nakamura A, Matsuo Y, Nakata M, et al. Interfractional reproducibility in pancreatic position based on four-dimensional computed tomography. *Int J Radiat Oncol Biol Phys* (2011) 80(5):1567–72. doi: 10.1016/j.ijrobp.2010.10.020

30. Liu F, Erickson B, Peng C, Li XA. Characterization and management of interfractional anatomic changes for pancreatic cancer radiotherapy. *Int J Radiat Oncol Biol Phys* (2012) 83(3):e423–9. doi: 10.1016/j.ijrobp.2011.12.073

31. van Timmeren JE, Chamberlain M, Krayenbuehl J, Wilke L, Ehrbar S, Bogowicz M, et al. Treatment plan quality during online adaptive re-planning. *Radiat Oncol* (2020) 15 (1):203. doi: 10.1186/s13014-020-01641-0

32. Hall WA, Paulson ES, van der Heide UA, Fuller CD, Raaymakers BW, Lagendijk JJW, et al. The transformation of radiation oncology using real-time magnetic resonance guidance: A review. *Eur J Cancer* (2019) 122:42–52. doi: 10.1016/j.ejca.2019.07.021

33. Winkel D, Bol GH, Kroon PS, et al. Adaptive radiotherapy: The elekta unity MR-linac concept. *Clin Transl Radiat Oncol* (2019) 18:54–9. doi: 10.1016/j.ctro.2019.04.001

34. Kerkmeijer LGW, Valentini V, Fuller CDD, Slotman BJ. Editorial: Online adaptive MR-guided radiotherapy. *Front Oncol* (2021) 11:748685. doi: 10.3389/fonc.2021.748685

35. Rammohan N, Randall JW, Yadav P. History of technological advancements towards MR-Linac:The future of image-guided radiotherapy. *J Clin Med* (2022) 11 (16):4730. doi: 10.3390/jcm11164730

36. Bottomley PA. Turning up the heat on MRI. *J Am Coll Radiol* (2008) 5(7):853–5. doi: 10.1016/j.jacr.2008.04.003

37. Parikh NR, Lee PP, Raman SS, Cao M, Lamb J, Tyran M, et al. Time-driven activity-based costing comparison of CT-guided versus MR-guided SBRT. *JCO Oncol Pract* (2020) 16(11):e1378–85. doi: 10.1200/JOP.19.00605

38. Castelluccia A, Mincarone P, Tumolo MR, Sabina S, Colella R, Bodini A, et al. Economic evaluations of magnetic resonance image-guided radiotherapy (MRIgRT): A systematic review. *Int J Environ Res Public Health* (2022) 19(17):10800. doi: 10.3390/ijerph191710800

39. Palacios MA, Verheijen S, Schneiders FL, Bohoudi O, Slotman BJ, Lagerwaard FJ, et al. Same-day consultation, simulation and lung stereotactic ablative radiotherapy delivery on a magnetic resonance-linac. *Phys Imaging Radiat Oncol* (2022) 24:76–81. doi: 10.1016/j.phro.2022.09.010

40. Johnstone PAS, Kerstiens J, Wasserman S, Rosenberg SA. MRI-Linac economics II: Rationalizing schedules. *J Clin Med* (2022) 11(3):869. doi: 10.3390/jcm11030869

41. Henke L, Kashani R, Robinson CG, Curcuru A, DeWees T, Bradley J, et al. Phase I trial of stereotactic MR-guided online adaptive radiation therapy (SMART) for the treatment of oligometastatic or unresectable primary malignancies of the abdomen. *Radiother Oncol* (2018) 126:519–26. doi: 10.1016/j.radonc.2017.11.032

42. Henke LE, Olsen JR, Contreras JA, Curcuru A, DeWees TA, Green OL, et al. Stereotactic MR-guided online adaptive radiation therapy (SMART) for ultracentral thorax malignancies: Results of a phase 1 trial. *Adv Radiat Oncol* (2018) 4(1):201–9. doi: 10.1016/j.adro.2018.10.003

43. Poulsen PR, Cho B, Sawant A, Ruan D, Keall PJ. Detailed analysis of latencies in image-based dynamic MLC tracking. *Med Phys* (2010) 37(9):4998–5005. doi: 10.1118/1.3480504

44. Jöhl A, Ehrbar S, Guckenberger M, Klöck S, Meboldt M, Zeilinger M, et al. Performance comparison of prediction filters for respiratory motion tracking in radiotherapy. *Med Phys* (2020) 47(2):643–50. doi: 10.1002/mp.13929

45. Lombardo E, Rabe M, Xiong Y, Nierer L, Cusumano D, Placidi L, et al. Offline and online LSTM networks for respiratory motion prediction in MR-guided radiotherapy. *Phys Med Biol* (2022) 67(9). doi: 10.1088/1361-6560/ac60b7

46. Murphy KJ, Brunberg JA. Adult claustrophobia, anxiety and sedation in MRI. *Magn Reson Imaging* (1997) 15(1):51–4. doi: 10.1016/S0730-725X(96)00351-7

47. Russo RJ, Costa HS, Silva PD, Anderson JL, Arshad A, Biederman RW, et al. Assessing the risks associated with MRI in patients with a pacemaker or defibrillator. *N Engl J Med* (2017) 376(8):755–64. doi: 10.1056/NEJMoa1603265

48. Nyenhuis JA, Park S-M, Kamondetdacha R, Amjad A, Shellock FG, Rezai AR. MRI And implanted medical devices: basic interactions with an emphasis on heating. *IEEE Trans Device Mater Rel* (2005) 5(3):467–80. doi: 10.1109/TDMR.2005.859033

49. Kasivisvanathan V, Rannikko AS, Borghi M, Panebianco V, Mynderse LA, Vaarala MH, et al. MRI-Targeted or standard biopsy for prostate-cancer diagnosis. *N Engl J Med* (2018) 378(19):1767–77. doi: 10.1056/NEJMoa1801993

50. Sidaway P. MRI Improves diagnosis. *Nat Rev Clin Oncol* (2018) 15(6):345. doi: 10.1038/s41571-018-0013-3

51. Thompson J, Lawrentschuk N, Frydenberg M, Thompson L, Stricker P. The role of magnetic resonance imaging in the diagnosis and management of prostate cancer. *BJU Int* (2013) 112 Suppl;2:6–20. doi: 10.1111/bju.12381

52. Metcalfe P, Liney GP, Holloway L, Walker A, Barton M, Delaney GP, et al. The potential for an enhanced role for MRI in radiation-therapy treatment planning. *Technol Cancer Res Treat* (2013) 12(5):429–46. doi: 10.7785/tcrt.2012.500342

53. Cassidy RJ, Yang X, Liu T, Thomas M, Nour SG, Jani AB, et al. Neurovascular bundle-sparing radiotherapy for prostate cancer using MRI-CT registration: A dosimetric feasibility study. *Med Dosim* (2016) 41(4):339–43. doi: 10.1016/j.meddos.2016.08.003

54. Nonaka H, Onishi H, Watanabe M, Nam VH. Assessment of abdominal organ motion using cine magnetic resonance imaging in different gastric motilities: a comparison between fasting and postprandial states. *J Radiat Res* (2019) 60(6):837–43. doi: 10.1093/jrr/rrz054

55. Keall PJ, Mageras GS, Balter JM, Emery RS, Forster KM, Jiang SB, et al. The management of respiratory motion in radiation oncology report of AAPM task group 76. *Med Phys* (2006) 33(10):3874–900. doi: 10.1118/1.2349696

56. Abbas H, Chang B, Chen ZJ. Motion management in gastrointestinal cancers. *J Gastroint Oncol* (2014) 5(3):223–35. doi: 10.3978/j.issn.2078-6891.2014.028

57. Tocco BR, Kishan AU, Ma TM, Kerkmeijer LGW, Tree AC. MR-guided radiotherapy for prostate cancer. *Front Oncol* (2020) 10:616291. doi: 10.3389/fonc.2020.616291

58. Cuccia F, Corradini S, Mazzola R, Spiazzi L, Rigo M, Bonù ML, et al. MR-guided hypofractionated radiotherapy: Current emerging data and promising perspectives for localized prostate cancer. *Cancers (Basel)* (2021) 13(8):1791. doi: 10.3390/cancers13081791

59. Cuccia F, Rigo M, Figlia V, Giaj-Levra N, Mazzola R, Nicosia L, et al. 1.5T MR-guided daily adaptive stereotactic body radiotherapy for prostate re-irradiation: A preliminary report of toxicity and clinical outcomes. *Front Oncol* (2022) 12:858740. doi: 10.3389/fonc.2022.858740

60. Cuccia F, Mazzola R, Nicosia L, Figlia V, Giaj-Levra N, Ricchetti F, et al. Impact of hydrogel peri-rectal spacer insertion on prostate gland intra-fraction motion during 1.5 T MR-guided stereotactic body radiotherapy. *Radiat Oncol* (2020) 15(1):178. doi: 10.1186/s13014-020-01622-3

61. de Muinck Keizer DM, Kontaxis C, Kerkmeijer LGW, van der Voort van Zyp JRN, van den Berg CAT, Raaymakers BW, et al. Dosimetric impact of soft-tissue based intrafraction motion from 3D cine-MR in prostate SBRT. *Phys Med Biol* (2020) 65 (2):025012. doi: 10.1088/1361-6560/ab6241

62. Timmerman R, Paulus R, Galvin J, Michalski J, Straube W, Bradley J, et al. Stereotactic body radiation therapy for inoperable early stage lung cancer. *JAMA* (2010) 303(11):1070–6. doi: 10.1001/jama.2010.261

63. Thibault I, Chiang A, Erler D, Yeung L, Poon I, Kim A, et al. Predictors of chest wall toxicity after lung stereotactic ablative radiotherapy. *Clin Oncol (R Coll Radiol)* (2016) 28:28–35. doi: 10.1016/j.clon.2015.06.009

64. Haseltine JM, Rimner A, Gelblum DY, Modh A, Rosenzweig KE, Jackson A, et al. Fatal complications after stereotactic body radiation therapy for central lung tumors abutting the proximal bronchial tree. *Pract Radiat Oncol* (2016) 6:E27–33. doi: 10.1016/j.prro.2015.09.012

65. Or M, Liu B, Lam J, Vinod S, Xuan W, Yeghiaian-Alvandi R, et al. A systematic review and meta-analysis of treatment-related toxicities of curative and palliative radiation therapy in non-small cell lung cancer. *Sci Rep* (2021) 11(1):5939. doi: 10.1038/s41598-021-85131-7

66. Seppenwoolde Y, Shirato H, Kitamura K, Shimizu S, van Herk M, Lebesque JV, et al. Precise and real-time measurement of 3D tumor motion in lung due to breathing and heartbeat, measured during radiotherapy. *Int J Radiat Oncol Biol Phys* (2002) 53:822–34. doi: 10.1016/S0360-3016(02)02803-1

67. Giaj-Levra N, Borghetti P, Bruni A, Ciammella P, Cuccia F, Fozza A, et al. Current radiotherapy techniques in NSCLC: challenges and potential solutions. *Expert Rev Anticancer Ther* (2020) 20(5):387–402. doi: 10.1080/14737140.2020.1760094

68. Raaijmakers AJE, Raaymakers BW, Lagendijk JJW. Integrating a MRI scanner with a 6 MV radiotherapy accelerator: Dose increase at tissue–air interfaces in a lateral magnetic field due to returning electrons. *Phys Med Biol* (2005) 50.7:1363–376. doi: 10.1088/0031-9155/50/7/002

69. Bainbridge HE, Menten MJ, Fast MF, Nill S, Oelfke U, McDonald F. Treating locally advanced lung cancer with a 1.5 T MR-linac – effects of the magnetic field and irradiation geometry on conventionally fractionated and isotoxic dose-escalated radiotherapy. *Radiothe Oncol* (2017) 125.2:280–85. doi: 10.1016/j.radonc.2017.09.009

70. Foster JH. Survival after liver resection for secondary tumors. *Am J Surg* (1978) 135 (3):389–94. doi: 10.1016/0002-9610(78)90072-7

71. Fong Y, Cohen AM, Fortner JG, Enker WE, Turnbull AD, Coit DG, et al. Liver resection for colorectal metastases. *J Clin Oncol* (1997) 15(3):938–46. doi: 10.1200/JCO.1997.15.3.938

72. Tomlinson JS, Jarnagin WR, DeMatteo RP, Fong Y, Kornprat P, Gonen M, et al. Actual 10-year survival after resection of colorectal liver metastases defines cure. *J Clin Oncol* (2007) 25(29):4575–80. doi: 10.1200/JCO.2007.11.0833

73. Hellman S, Weichselbaum RR. Oligometastases. *J Clin Oncol* (1995) 13(1):8–10. doi: 10.1200/JCO.1995.13.1.8

74. Palma DA, Olson R, Harrow S, Gaede S, Louie AV, Haasbeek C, et al. Stereotactic ablative radiotherapy versus standard of care palliative treatment in patients with oligometastatic cancers (SABR-COMET): a randomised, phase 2, open-label trial. *Lancet* (2019) 393(10185):2051–8. doi: 10.1016/S0140-6736(18)32487-5

75. Apisarnthanarax S, Barry A, Cao M, Czito B, DeMatteo R, Drinane M, et al. External beam radiation therapy for primary liver cancers: An ASTRO clinical practice guideline. *Pract Radiat Oncol* (2022) 12(1):28–51. doi: 10.1016/j.prro.2021.09.004

76. Feng M, Suresh K, Schipper MJ, Bazzi L, Ben-Josef E, Matuszak MM, et al. Individualized adaptive stereotactic body radiotherapy for liver tumors in patients at high risk for liver damage: A phase 2 clinical trial. *JAMA Oncol* (2018) 4(1):40–7. doi: 10.1001/jamaoncol.2017.2303

77. Mendez Romero A, Wunderink W, Hussain SM, De Pooter JA, Heijmen BJ, Nowak PC, et al. Stereotactic body radiation therapy for primary and metastatic liver tumors: A single institution phase i-ii study. *Acta Oncol* (2006) 45(7):831–7. doi: 10.1080/02841860600897934

78. Cardenes HR, Price TR, Perkins SM, Maluccio M, Kwo P, Breen TE, et al. Phase I feasibility trial of stereotactic body radiation therapy for primary hepatocellular carcinoma. *Clin Transl Oncol* (2010) 12(3):218–25. doi: 10.1007/s12094-010-0492-x

79. Ohri N, Tomé WA, Méndez Romero A, Miften M, Ten Haken RK, Dawson LA, et al. Local control after stereotactic body radiation therapy for liver tumors. *Int J Radiat Oncol Biol Phys* (2021) 110(1):188–95. doi: 10.1016/j.ijrobp.2017.12.288

80. Tao R, Krishnan S, Bhosale PR, Javle MM, Aloia TA, Shroff RT, et al. Ablative radiotherapy doses lead to a substantial prolongation of survival in patients with inoperable intrahepatic cholangiocarcinoma: A retrospective dose response analysis. *J Clin Oncol* (2016) 34(3):219–26. doi: 10.1200/JCO.2015.61.3778

81. Romesser PB, Tyagi N, Crane CH. Magnetic resonance imaging-guided adaptive radiotherapy for colorectal liver metastases. *Cancers (Basel)* (2021) 13(7):1636. doi: 10.3390/cancers13071636

82. Witt JS, Rosenberg SA, Bassetti MF. MRI-Guided adaptive radiotherapy for liver tumours: visualising the future. *Lancet Oncol* (2020) 21(2):e74–82. doi: 10.1016/S1470-2045(20)30034-6

83. Henke LE, Contreras JA, Green OL, Cai B, Kim H, Roach MC, et al. Magnetic resonance image-guided radiotherapy (MRIgRT): A 4.5-year clinical experience. *Clin Oncol (R Coll Radiol)* (2018) 30(11):720–7. doi: 10.1016/j.clon.2018.08.010

84. Rogowski P, von Bestenbostel R, Walter F, Straub K, Nierer L, Kurz C, et al. Feasibility and early clinical experience of online adaptive MR-guided radiotherapy of liver tumors. *Cancers (Basel)* (2021) 13(7):1523. doi: 10.3390/cancers13071523

85. Ugurluer G, Mustafayev TZ, Gungor G, Atalar B, Abacioglu U, Sengoz M, et al. Stereotactic MR-guided online adaptive radiation therapy (SMART) for the treatment of liver metastases in oligometastatic patients: initial clinical experience. *Radiat Oncol J* (2021) 39(1):33–40. doi: 10.3857/roj.2020.00976

86. Padgett KR, Mustafayev Gungor TZ, Atalar G, Abacioglu B, Sengoz U, M, et al. Assessment of online adaptive MR-guided stereotactic body radiotherapy of liver cancers. *Phys Med* (2020) 77:54–63. doi: 10.1016/j.ejmp.2020.07.027

87. van Dams R, Wu TC, Kishan AU, Raldow AC, Chu FI, Hernandez J, et al. Ablative radiotherapy for liver tumors using stereotactic MRI-guidance: A prospective phase I trial. *Radiother Oncol* (2022) 170:14–20. doi: 10.1016/j.radonc.2021.06.005

88. Hoegen P, Zhang KS, Tonndorf-Martini E, Weykamp F, Regnery S, Naumann P, et al. MR-guided adaptive versus ITV-based stereotactic body radiotherapy for hepatic metastases (MAESTRO): a randomized controlled phase II trial. *Radiat Oncol* (2022) 17 (1):59. doi: 10.1186/s13014-022-02033-2

89. Hammel P, Huguet F, van Laethem JL, Huguet F, van Laethem JL, Goldstein D, Glimelius B, Artru P, et al. Effect of chemoradiotherapy vs chemotherapy on survival in patients with locally advanced pancreatic cancer controlled after 4 months of gemcitabine with or without erlotinib: The lap07 randomized clinical trial. *JAMA* (2016) 315:1844–53. doi: 10.1001/jama.2016.4324

90. Katz MHG, Shi Q, Meyers J, Herman JM, Chuong M, Wolpin BM, et al. Efficacy of preoperative mFOLFIRINOX vs mFOLFIRINOX plus hypofractionated radiotherapy for borderline resectable adenocarcinoma of the pancreas: The A021501 phase 2 randomized clinical trial. *JAMA Oncol* (2022) 8(9):1263–70. doi: 10.1001/jamaoncol.2022.2319

91. Krishnan S, Chadha AS, Suh Y, Chen HC, Rao A, Das P, et al. Focal radiation therapy dose escalation improves overall survival in locally advanced pancreatic cancer patients receiving induction chemotherapy and consolidative chemoradiation. *Int J Radiat Oncol Biol Phys* (2016) 94(4):755–65. doi: 10.1016/j.ijrobp.2015.12.003

92. Rudra S, Jiang N, Rosenberg SA, Olsen JR, Roach MC, Wan L, et al. Using adaptive magnetic resonance image-guided radiation therapy for treatment of inoperable pancreatic cancer. *Cancer Med* (2019) 8(5):2123–32. doi: 10.1002/cam4.2100

93. Reyngold M, O'Reilly EM, Varghese AM, Fiasconaro M, Zinovoy M, Romesser PB, et al. Association of ablative radiation therapy with survival among patients with inoperable pancreatic cancer. *JAMA Oncol* (2021) 7(5):735–8. doi: 10.1001/jamaoncol.2021.0057

94. Schellenberg D, Kim J, Christman-Skieller C, Chun CL, Columbo LA, Ford JM, et al. Single-fraction stereotactic body radiation therapy and sequential gemcitabine for the treatment of locally advanced pancreatic cancer. *Int J Radiat Oncol Biol Phys* (2011) 81 (1):181–8. doi: 10.1016/j.ijrobp.2010.05.006

95. Hoyer M, Roed H, Sengelov L, Traberg A, Ohlhuis L, Pedersen J, et al. Phase-II study on stereotactic radiotherapy of locally advanced pancreatic carcinoma. *Radiother Oncol* (2005) 76(1):48–53. doi: 10.1016/j.radonc.2004.12.022

96. Herman JM, Wild AT, Wang H, Tran PT, Chang KJ, Taylor GE, et al. Randomized phase III multi-institutional study of TNFerade biologic with fluorouracil and radiotherapy for locally advanced pancreatic cancer: final results. *J Clin Oncol* (2013) 31(7):886–94. doi: 10.1200/JCO.2012.44.7516

97. Huguet F, Andre T, Hammel P, Artru P, Balosso J, Selle F, et al. Impact of chemoradiotherapy after disease control with chemotherapy in locally advanced pancreatic adenocarcinoma in gercor phase ii and iii studies. *J Clin Oncol* (2007) 25:326–31. doi: 10.1200/JCO.2006.07.5663

98. *ClinicalTrials.gov identifier: NCT03621644*.

99. Vicini FA, Cecchini RS, White JR, Arthur DW, Julian TB, Rabinovitch RA, et al. Long-term primary results of accelerated partial breast irradiation after breast-conserving surgery for early-stage breast cancer: a randomised, phase 3, equivalence trial. *Lancet* (2019) 394(10215):2155–64. doi: 10.1016/S0140-6736(19)32514-0

100. Formenti SC, Truong MT, Goldberg JD, Mukhi V, Rosenstein B, Roses D, et al. Prone accelerated partial breast irradiation after breast-conserving surgery: preliminary clinical results and dose-volume histogram analysis. *Int J Radiat Oncol Biol Phys* (2004) 60 (2):493–504. doi: 10.1016/j.ijrobp.2004.04.036

101. Meattini I, Marrazzo L, Saieva C, Desideri I, Scotti V, Simontacchi G, et al. Accelerated partial-breast irradiation compared with whole-breast irradiation for early breast cancer: Long-term results of the randomized phase III APBI-IMRT-Florence trial. *J Clin Oncol* (2020) 38(35):4175–83. doi: 10.1200/JCO.20.00650

102. Pan H, Gray R, Braybrooke J, Davies C, Taylor C, McGale P, et al. EBCTCG. 20-year risks of breast-cancer recurrence after stopping endocrine therapy at 5 years. *N Engl J Med* (2017) 377(19):1836–46. doi: 10.1056/NEJMoa1701830

103. Merfeld EC, Blitzer GC, Kuczmarska-Haas A, Witt JS, Wojcieszynski AP, Mittauer KM, et al. Considering lumpectomy cavity PTV expansions: Characterization of intrafraction lumpectomy cavity motion. *Pract Radiat Oncol* (2022), S1879–8500(22) 00266-1. doi: 10.1016/j.prro.2022.08.011

104. Reddy JP, Lei X, Bloom ES, Reed VK, Schlembach PJ, Arzu I, et al. OPAL trial investigators. optimizing preventive adjuvant linac-based (OPAL) radiation: A phase II tial of daily partial breast irradiation. *Int J Radiat Oncol Biol Phys* (2022), S0360–3016(22) 03419-8. doi: 10.1016/j.ijrobp.2022.09.083

105. Lee G, Parmar H, Li W, Shessel A. The effect of lumpectomy cavity changes on planning dose in breast radiotherapy boost. *J Med Imaging Radiat Sci* (2019) 50(2):317–22. doi: 10.1016/j.jmir.2019.02.002

106. Seppälä J, Vuolukka K, Virén T, Heikkilä J, Honkanen JTJ, Pandey A, et al. Breast deformation during the course of radiotherapy: The need for an additional outer margin. *Phys Med* (2019) 65:1–5. doi: 10.1016/j.ejmp.2019.07.021

107. Topolnjak R, Borst GR, Nijkamp J, Sonke JJ. Image-guided radiotherapy for left-sided breast cancer patients: geometrical uncertainty of the heart. *Int J Radiat Oncol Biol Phys* (2012) 82(4):e647–55. doi: 10.1016/j.ijrobp.2011.08.024

108. Yao S, Zhang Y, Nie K, Liu B, Haffty BG, Ohri N, et al. Setup uncertainties and the optimal imaging schedule in the prone position whole breast radiotherapy. *Radiat Oncol* (2019) 14(1):76. doi: 10.1186/s13014-019-1282-4

109. Yang DS, Yoon WS, Chung SY, Lee JA, Lee S, Park YJ, et al. Set-up uncertainty during breast radiotherapy. image-guided radiotherapy for patients with initial extensive variation. *Strahlenther Onkol* (2013) 189(4):315–20. doi: 10.1007/s00066-012-0271-4

110. Ng J, Pennell R, Formenti SC. The initial experience of MRI-guided precision prone breast irradiation with daily adaptive planning in treating early stage breast cancer patients. *Front Oncol* (2022) 12:1048512. doi: 10.3389/fonc.2022.1048512

111. Champ CE, Siglin J, Mishra MV, Shen X, Werner-Wasik M, Andrews DW, et al. Evaluating changes in radiation treatment volumes from post-operative to same-day planning MRI in high-grade gliomas. *Radiat Oncol* (2012) 7:220. doi: 10.1186/1748-717X-7-220

112. Salkeld AL, Hau EKC, Nahar N, Sykes JR, Wang W, Thwaites DI. Changes in brain metastasis during radiosurgical planning. *Int J Radiat Oncol Biol Phys* (2018) 102 (4):727–33. doi: 10.1016/j.ijrobp.2018.06.021

113. Chan RW, Lawrence LSP, Oglesby RT, Chen H, Stewart J, Theriault A, et al. Chemical exchange saturation transfer MRI in central nervous system tumours on a 1.5 T MR-linac. *Radiother Oncol* (2021) 162:140–9. doi: 10.1016/j.radonc.2021.07.010

114. Lawrence LSP, Chan RW, Chen H, Keller B, Stewart J, Ruschin M, et al. Accuracy and precision of apparent diffusion coefficient measurements on a 1.5 T MR-linac in central nervous system tumour patients. *Radiother Oncol* (2021) 164:155–62. doi: 10.1016/j.radonc.2021.09.020

115. Chen Y, Lu L, Zhu T, Ma D. Technical overview of magnetic resonance fingerprinting and its applications in radiation therapy. *Med Phys* (2022) 49(4):2846–60. doi: 10.1002/mp.15254

116. Panda A, Mehta BB, Coppo S, Jiang Y, Ma D, Seiberlich N, et al. Magnetic resonance fingerprinting-an overview. *Curr Opin BioMed Eng* (2017) 3:56–66. doi: 10.1016/j.cobme.2017.11.001

117. Han EY, Wang H, Briere TM, Yeboa DN, Boursianis T, Kalaitzakis G, et al. Brain stereotactic radiosurgery using MR-guided online adaptive planning for daily setup

variation: An end-to-end test. *J Appl Clin Med Phys* (2022) 23(3):e13518. doi: 10.1002/acm2.13518

118. Stewart J, Sahgal A, Lee Y, Soliman H, Tseng CL, Detsky J, et al. Quantitating interfraction target dynamics during concurrent chemoradiation for glioblastoma: a prospective serial imaging study. *Int J Radiat Oncol Biol Phys* (2021) 109(3):736–46. doi: 10.1016/j.ijrobp.2020.10.002

119. (2022). Available at: https://www.uptodate.com/contents/craniopharyngioma.

120. Marciscano AE, Knisely JP, Nagar H. Leveraging an MRI-guided linear accelerator platform for post-operative stereotactic body radiation therapy (SBRT) of spinal metastases. *Neuro-oncol Adv* (2022) 4(Suppl 1):i11. doi: 10.1093/noajnl/vdac078.043

121. Han EY, Yeboa DN, Briere TM, Yang J, Wang H. Dosimetric analysis of MR-LINAC treatment plans for salvage spine SBRT re-irradiation. *J Appl Clin Med Phys* (2022) 23(10):e13752. doi: 10.1002/acm2.13752

122. Redler G, Stevens T, Cammin J, Malin M, Green O, Mutic S, et al. Dosimetric feasibility of utilizing the ViewRay magnetic resonance guided linac system for image-guided spine stereotactic body radiation therapy. *Cureus.* (2019) 11(12):e6364. doi: 10.7759/cureus.6364

123. Yadav P, Musunuru HB, Witt JS, Bassetti M, Bayouth J, Baschnagel AM. Dosimetric study for spine stereotactic body radiation therapy: magnetic resonance guided linear accelerator versus volumetric modulated arc therapy. *Radiol Oncol* (2019) 53(3):362–8. doi: 10.2478/raon-2019-0042

124. Gurney-Champion OJ, Landry G, Redalen KR, Thorwarth D. Potential of deep learning in quantitative magnetic resonance imaging for personalized radiotherapy. *Semin Radiat Oncol* (2022) 32(4):377–88. doi: 10.1016/j.semradonc.2022.06.007

125. Boulanger M, Nunes JC, Chourak H, Largent A, Tahri S, Acosta O, et al. Deep learning methods to generate synthetic CT from MRI in radiotherapy: A literature review. *Phys Med* (2021) 89:265–81. doi: 10.1016/j.ejmp.2021.07.027

126. Han X. MR-based synthetic CT generation using a deep convolutional neural network method. *Med Phys* (2017) 44:1408–19. doi: 10.1002/mp.12155

127. Cusumano D, Boldrini L, Dhont J, Fiorino C, Green O, Güngör G, et al. Artificial intelligence in magnetic resonance guided radiotherapy: Medical and physical considerations on state of art and future perspectives. *Phys Med* (2021) 85:175–91. doi: 10.1016/j.ejmp.2021.05.010

128. Gillies RJ, Kinahan PE, Hricak H. Radiomics: Images are more than pictures, they are data. *Radiology* (2016) 278(2):563–77. doi: 10.1148/radiol.2015151169

129. Lambin P, Leijenaar RTH, Deist TM, Peerlings J, de Jong EEC, van Timmeren J, et al. Radiomics: the bridge between medical imaging and personalized medicine. *Nat Rev Clin Oncol* (2017) 14(12):749–62. doi: 10.1038/nrclinonc.2017.141

130. Gregucci F, Fiorentino A, Mazzola R, Ricchetti F, Bonaparte I, Surgo A, et al. Radiomic analysis to predict local response in locally advanced pancreatic cancer treated with stereotactic body radiation therapy. *Radiol Med* (2022) 127(1):100–7. doi: 10.1007/s11547-021-01422-z

131. Bera K, Braman N, Gupta A, Velcheti V, Madabhushi A. Predicting cancer outcomes with radiomics and artificial intelligence in radiology. *Nat Rev Clin Oncol* (2022) 19(2):132–46. doi: 10.1038/s41571-021-00560-7

132. Michalet M, Riou O, Azria D, Decoene C, Crop F. News in magnetic resonance imaging use for radiation oncology. *Cancer Radiother* (2022) 26(6-7):784–8. doi: 10.1016/j.canrad.2022.06.028

133. Mazurowski MA, Buda M, Saha A, Bashir MR. Deep learning in radiology: An overview of the concepts and a survey of the state of the art with focus on MRI. *J Magn Reson Imaging* (2019) 49(4):939–54. doi: 10.1002/jmri.26534

134. Das IJ, McGee KP, Tyagi N, Wang H. Role and future of MRI in radiation oncology. *Br J Radiol* (2019) 92(1094):20180505. doi: 10.1259/bjr.20180505

135. Cusumano D, Boldrini L, Yadav P, Yu G, Musurunu B, Chiloiro G, et al. Delta radiomics for rectal cancer response prediction using low field magnetic resonance guided radiotherapy: an external validation. *Phys Med* (2021) 84:186–91. doi: 10.1016/j.ejmp.2021.03.038

136. Lau D, McLean MA, Priest AN, Gill AB, Scott F, Patterson I, et al. Multiparametric MRI of early tumor response to immune checkpoint blockade in metastatic melanoma. *J Immunother Cancer* (2021) 9(9):e003125. doi: 10.1136/jitc-2021-003125

137. Ramlee S, Hulse D, Bernatowicz K, Pérez-López R, Sala E, Aloj L. Radiomic signatures associated with CD8+ tumour-infiltrating lymphocytes: A systematic review and quality assessment study. *Cancers (Basel)* (2022) 14(15):3656. doi: 10.3390/cancers14153656

138. Wang JH, Wahid KA, van Dijk LV, Farahani K, Thompson RF, Fuller CD. Radiomic biomarkers of tumor immune biology and immunotherapy response. *Clin Transl Radiat Oncol* (2021) 28:97–115. doi: 10.1016/j.ctro.2021.03.006

frontiers | Frontiers in Oncology

TYPE Methods
PUBLISHED 27 January 2023
DOI 10.3389/fonc.2023.1061854

OPEN ACCESS

EDITED BY
Frank Lagerwaard,
Amsterdam University Medical Center,
Netherlands

REVIEWED BY
Miguel A. Palacios,
VU Medical Center, Netherlands
Joachim Widder,
Medical University of Vienna, Austria

*CORRESPONDENCE
Stephen A. Rosenberg
Stephen.Rosenberg@moffitt.org

†These authors share first authorship

SPECIALTY SECTION
This article was submitted to
Radiation Oncology,
a section of the journal
Frontiers in Oncology

RECEIVED 05 October 2022
ACCEPTED 03 January 2023
PUBLISHED 27 January 2023

CITATION
Bryant JM, Sim AJ, Feygelman V, Latifi K and Rosenberg SA (2023) Adaptive hypofractionted and stereotactic body radiotherapy for lung tumors with real-time MRI guidance.
Front. Oncol. 13:1061854.
doi: 10.3389/fonc.2023.1061854

Adaptive hypofractionted and stereotactic body radiotherapy for lung tumors with real-time MRI guidance

John M. Bryant[1†], Austin J. Sim[1,2†], Vladimir Feygelman[1], Kujtim Latifi[1] and Stephen A. Rosenberg[1*]

[1]Department of Radiation Oncology, H. Lee Moffitt Cancer Center & Research Institute, Tampa, FL, United States, [2]Department of Radiation Oncology, Comprehensive Cancer Center – The James Cancer Hospital, Columbus, OH, United States

The treatment of central and ultracentral lung tumors with radiotherapy remains an ongoing clinical challenge. The risk of Grade 5 toxicity with ablative radiotherapy doses to these high-risk regions is significant as shown in recent prospective studies. Magnetic resonance (MR) image-guided adaptive radiotherapy (MRgART) is a new technology and may allow the delivery of ablative radiotherapy to these high-risk regions safely. MRgART is able to achieve this by utilizing small treatment margins, real-time gating/tracking and on-table plan adaptation to maintain dose to the tumor but limit dose to critical structures. The process of MRgART is complex and has nuances and challenges for the treatment of lung tumors. We outline the critical steps needed for appropriate delivery of MRgART for lung tumors safely and effectively.

KEYWORDS

lung, MRI, radiation, adaptive, radiotherapy, MRI guidance, MR-guided radiation therapy, image-guided RT

1 Introduction

Despite the widespread use of stereotactic body radiation therapy (SBRT) and image guided radiotherapy (IGRT) for the treatment of primary and metastatic lung tumors (1–6), central (7, 8) and ultra-central lesions (9, 10) remain a therapeutic challenge for safe delivery of ablative radiation doses using conventional linear accelerators. Specifically, ablative doses near central structures, such as the esophagus, proximal bronchial tree, and great vessels have generated concerning toxicity signals in prior randomized controlled trials, even with slightly lower doses per fraction (9) (Figure 1). Indeed, in the recently reported Nordic-HILUS trial, delivery of 56 Gy in eight fractions to lesions adjacent to these central structures resulted in a grade 5 toxicity rate of 15.4% (9). The toxicity in the Nordic-HILUS trial may be secondary to significant hot spots (150% of prescription), heterogeneity in organs at risk (OAR) segmentation, and not delineating the walls of critical organs (i.e. mainstem bronchi) (12).

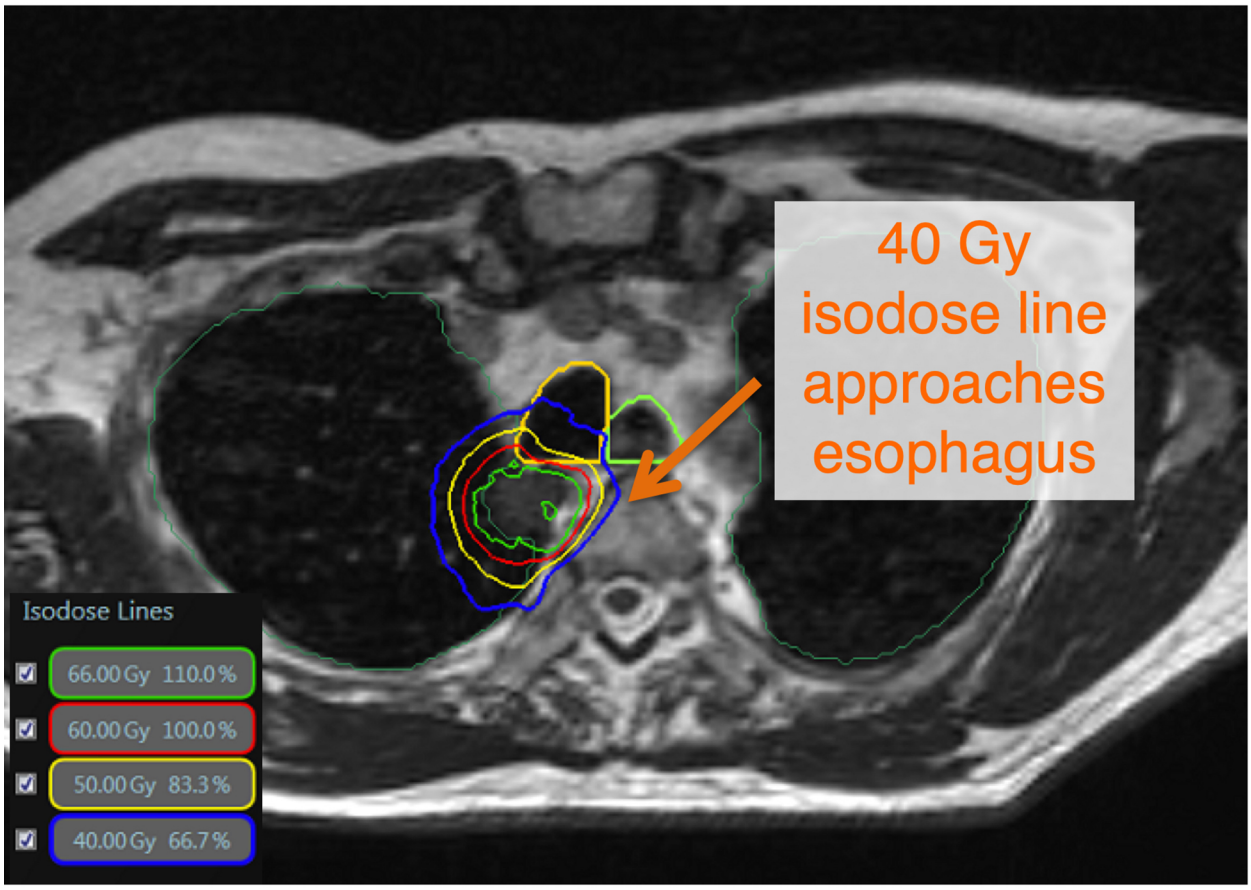

FIGURE 1
There is no consensus definition of ultracentral lung tumors. The Nordic-HILUS trial defines ultracentral targets as ≤ 1cm from the proximal bronchial tree, which is also used at our institution. These close tumors may lead to high dose to critical organs such as proximal airways and the esophagus. This is a TRUFI sequence on the MRIdian system showing an ultracentral tumor with doses approaching critical organs such as the esophagus and trachea (11).

Although there is no consensus for defining ultracentral lung tumors, our institution has adapted the Nordic-HILUS trial's definition of ≤ 1cm from the proximal bronchial tree. The highest risk patients are those with tumors within 1 cm of the trachea and mainstem bronchi (Group A in the Nordic-HILUS trial) as they had the highest risk of death from treatment.

Respiratory and cardiac motion during radiotherapy necessitates adequate motion management strategies to account for tumor movement (13–15). An example includes the use of an internal target volume (ITV) approach that results in larger treatment volumes (16). These larger volumes may increase overlap with critical OAR which may increase the rate and severity of potential toxicities. This necessitates a trade-off between toxicity and potential for local control in high-risk locations (17). These are critical considerations in the central/ultracentral locations due to the movement of OAR or slight changes in set up that alter the airway position in relation to the tumor (Figure 2). With standard IGRT, imaging and beam delivery are typically not simultaneous and must be delicately balanced for the optimization of dose placement, which represents a significant daily challenge for many clinicians (18). However, the advent of magnetic resonance (MR) image-guided adaptive radiotherapy (MRgART) has demonstrated promise in mitigating many of these impediments, leading to the best of both worlds: ensuring adequate ablative dose, while at the same time minimizing OAR doses to unprecedented levels (19, 20).

In this paper, we will review the workflow that our institution uses to perform MRgART for central and ultracentral lung tumors. This workflow incorporates the MRIdian (ViewRay Technologies Inc, Oakwood Village, Ohio), a 0.35T MR linear accelerator (MRL), that has a unique real-time tracking feature. This is important because the motion management enabled by this feature underpins this process.

2 Patient selection

Radiotherapy always requires careful patient selection, however, due to the functional design and geometry of MRgRT systems, proper patient selection requires additional considerations prior to simulation. The key aspects include (1) body habitus and (2) presence of claustrophobia, given the narrow bore (70 cm diameter) of both commercially available MRL systems (21, 22). While there are no current effective strategies to deal with body habitus, many patients can tolerate MRgRT with low-dose anxiolytics. The (3) presence of MR-incompatible devices and implants must also be considered and every institution utilizing MRgRT should implement an effective MRI safety screening protocol. Patients must also be able

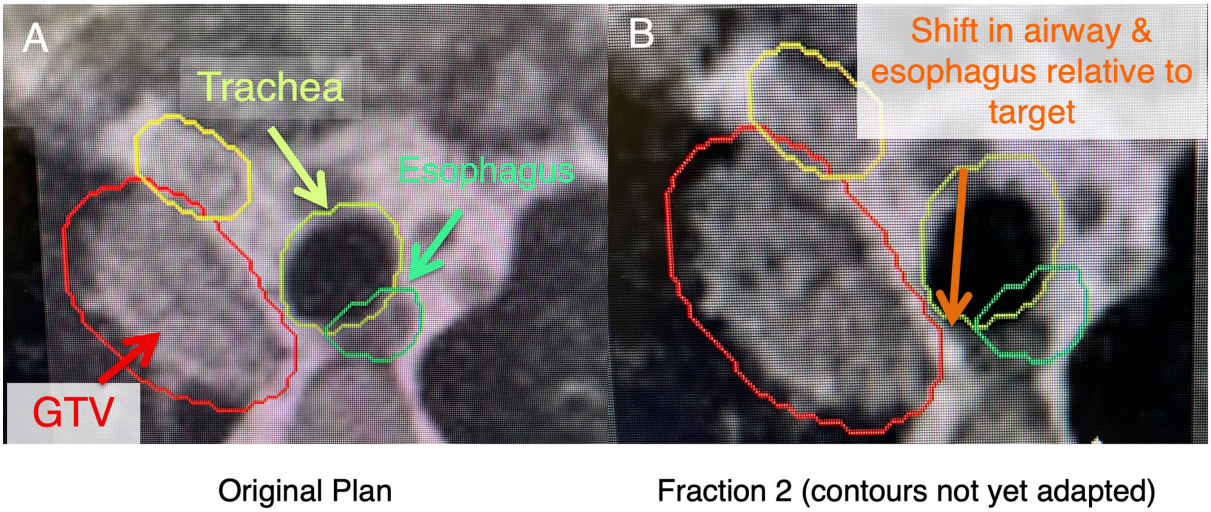

FIGURE 2
In these ultracentral locations, there may a shift of anatomy secondary to setup uncertainty and movement of nearby critical organs (i.e., esophagus), which may lead to an unacceptably high dose to these critical organs. **(A)** shows a patient with an ultracentral lung cancer at MR-simulation. **(B)** shows a shift of the esophagus and trachea relative to the tumor before contours are adapted (changed to the anatomy of the day).

to (4) lie flat and (5) hold their breath for at least 25 seconds for the simulation scan, in addition to longer time intervals for treatment delivery, particularly when respiratory gating is used for motion management. Treatment times are significantly longer when using an adaptive workflow, and therefore, patients must also (6) be able to extend their arm(s) cranially for extended periods of time, which can be more than 60 to 90 minutes.

3 Simulation

When scheduling for simulation (SIM), care must be taken to schedule both an MR simulation for target delineation, as well as a computed tomography (CT) simulation to acquire electron density data. These scans are preferably performed in immediate succession during the same patient visit to obtain the most accurate image registration for subsequent dose calculations. Patients are taken to the MRL and placed in a supine position between the flexible body coils, with their arms up on an MR-safe wing board. Although having both arms cranially extended is ideal to ensure the maximum number of possible beam angles, patients with limited mobility and/or other range of motion limitations may be simulated with one arm up (ipsilateral to the tumor), or in the worst case, with both arms by their side. No further immobilization is typically required. During simulation, a 25-second 3D balanced fast imaging with steady-state free precession (TRUFI) sequence (23) is obtained while the patient performs a deep inspiratory breath hold (DIBH). A representative sagittal slice containing the primary tumor is identified. This region of interest (ROI) is then contoured on three consecutive sagittal slices to create a tracking structure. A 3 mm isotropic expansion of the tracking structure is then created to form a "boundary structure" (i.e., gating envelope) for real time gating during treatment delivery at our institution. The gating boundary structure should be completely encompassed by the planning target volume (PTV) to ensure appropriate dosimetric coverage. A 25-30-second cine sequence is obtained while the patient is performing cycling of breath hold and free breathing maneuvers to ensure appropriate tracking and duty cycle for treatment delivery. A percentage excursion threshold of the tracking structure (i.e., primary tumor) outside of the boundary structure is typically set at <5% to trigger beam on at our center. Other institutions utilize a <5-20% trigger for beam on as long as the PTV margin is bigger than the boundary structure—for example if the gating structure is the ROI (most commonly the tumor) expanded by 3 mm and the PTV margin is say 5 mm (20). The patient is subsequently marked at the laser sites and taken to the CT simulator after MR sim.

The patient is then placed in an identical supine position as they were the MR-Linac at the CT simulator, complete with dummy coils, and undergoes a deep inspiratory breath hold scan (DIBH). It should be noted that this contrasts with a 4D CT scan that is typically done for conventional SBRT when using an ITV approach. Some centers utilize a shallow breath hold technique or a mid-respiratory cycle approach. Our center uses DIBH if it is tolerated by the patient. If this is not tolerated, we will often use a free breathing approach. There has also been increased interest across centers to utilize 2-3 L of nasal oxygen during treatment to improve tolerability and gating duty cycle for treatment. We currently use this intermittently as needed.

4 Contouring

A static breath hold MRI is used to contour the gross tumor volume (GTV) because MR guidance can utilize real-time gating. Although the MR is the primary data set for contouring, the CT can be valuable to help delineate tumor spiculations and OAR (e.g., airways). Therefore, the appropriate fusion of the CT and MR images is critical for appropriate tumor and OAR delineation. The GTV is isotropically expanded by 3 mm to create the nominal planning target volume (PTV) and is equivalent to our boundary structure.

A key aspect of contouring these structures is appropriate contouring of OAR. Most importantly, this means including the walls for tubular critical structures such as the esophagus and proximal bronchial tree. The contour of these OAR should not be only the air within these structures, as this may lead to incidental hot spots within the walls during initial planning or adaptation. The proximal bronchial tree includes the distal 1/3 of the trachea, mainstem bronchi and lobar bronchi until segmental bifurcation occurs. For simplicity, we often include the entire trachea as part of the proximal bronchial tree contour. The entire course of the esophagus should be contoured through the thorax. Again, it is critical that the wall of the esophagus is included in this contour. The great vessels are often underappreciated in contouring these cases. It is important to include the walls of these vessels to ensure hot spots are not being placed there. Although we include great vessels as part of our contours (aorta, superior vena cava and pulmonary artery), we will also contour out the brachiocephalic vessels and the azygous vein if within 2-3 cm of the target (Figure 3).

The PTV is then expanded by 2 cm sup/inf and 3 cm radially to create an "OAR eval" structure, within which the OAR will be recontoured daily for adaptive treatment. OAR that require contours within this ring are any critical structures that include the lungs, spinal cord, chest wall, heart, esophagus, proximal bronchial tree (PBT) (7), and the brachial plexus if indicated, as they are in conventional lung SBRT plans. Additionally, the great vessels (i.e., aorta, superior vena cava, and pulmonary artery) are typically contoured separately to extend at least 2 cm beyond both the cranial and caudal extent and, in addition, 3 cm beyond the radial extent of the PTV (Figure 3). At our institution, we are not typically recontouring the GTV daily for these patients. However, if there is a change in tumor volume secondary to necrosis/edema, this may necessitate adjusting the GTV contour and recreating the PTV

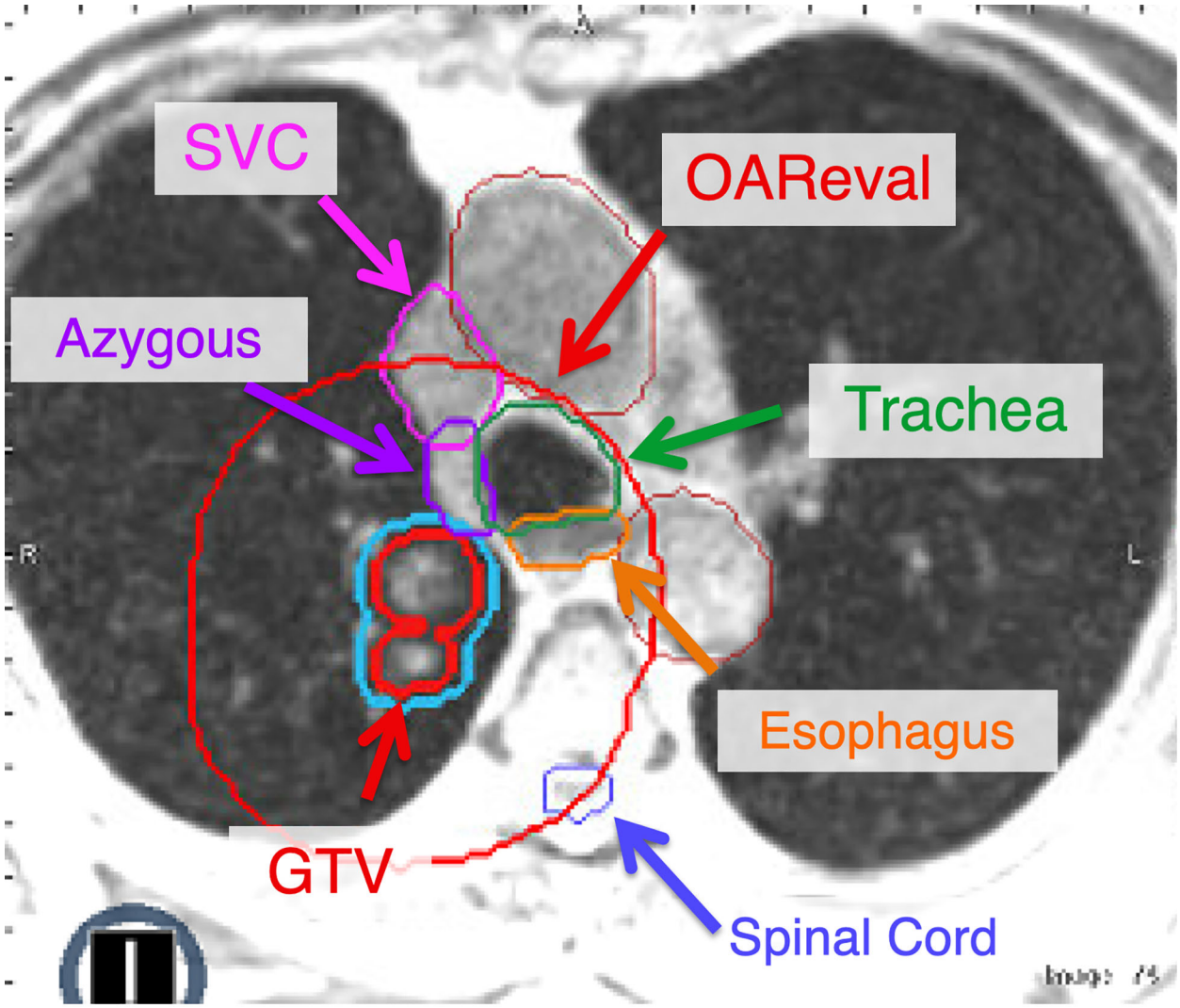

FIGURE 3
The OAReval structure is generated by taking the PTV and expanding 2 cm sup/inf and 3 cm radially. Central and ultracentral structures should be contoured to ensure inclusion of the wall of critical structures such as the esophagus and airways (i.e., trachea, mainstem). The focus of adaptive recontouring will be on OAR within the OAReval structure. However, it is critical to ensure an appropriate spinal cord contour is present. At our institution, we recommend contouring all great vessels (Aorta, SVC, etc.). However, we also include the brachiocephalic and azygous if they fall within the OAReval to ensure that they do not receive doses above 105% of the prescription.

(with the same 3 mm isotropic expansion). Of note, there are some centers that recontour the GTV daily with each fraction.

Central OAR that may trigger adaptation, including the PBT, great vessels, and esophagus are combined into a single structure and expanded by 3 mm to create an avoidance structure (OAR+3mm). This avoidance structure is then subtracted from the nominal PTV to generate a PTVopti structure that drives the optimizer and can be modified by the daily adaptation process. The Boolean logic on the structures that are expected to change daily is saved as rules that can be easily applied during adaptation. Since all structures must have placeholders prior to daily adaptations, the appropriate density control structures are always added. At our institution, we use densWater, densAir, and densOther structures as needed (Figure 4).

5 Planning

Our institutional practice is typically to treat the central and ultracentral lesions to either 50 Gy in 5-10 fractions, 60 Gy in 8 fractions, or 60 Gy in 15 fractions, depending on the histology and anatomic location. The most common dose and fractionation is 60 Gy in 8 fractions. Our goals are to ensure we approach a biological effective dose (BED) of at least 100 Gy for these regions while respecting OAR tolerances (24). We limit the Dmax (single voxel, 2 mm isotropically) within these tumors to 120-125% of the prescription dose. For critical OAR such as the great vessels and the PBT when delivering 60 Gy in 8 fractions, we try to limit the Dmax to 105% of the prescription. To be conservative, we try to limit the esophagus to 40 Gy Dmax over 8 fractions (Figure 1). Previous studies have shown that D1cc<40 Gy to the esophagus has a low risk of toxicity with 8 fraction treatment (11). The importance of low esophageal dose in central and ultracentral tumors is critical as esophagus may be associated with significant motion between fractions (Figure 2). These dose constraints are consistent (and may be more conservative in some instances) than those used in the SUNSET trial (NCT03306680). These plans typically have approximately 15-18 beams and 50 segments although there can be significant variance depending on lesion size, OAR locations, and if stricter OAR constraints are utilized by the physician due to increased concern of toxicity.

In addition to standard dose constraints for OAR dependent on the dose/fractionation and the anatomy of the day, additional pre-defined metrics are used as thresholds to trigger daily adaptation. While every effort is taken to obtain the optimal plan, the option of daily online adaptation allows for some additional flexibility in accepting suboptimal plans *a priori* with the understanding that online adaptation allows for incremental optimization based on the anatomy of the day. The goal of treatment is isotoxic dose delivery to tumor, i.e., ensuring a maximum cumulative BED during a course of treatment while minimizing toxicity.

It is a good strategy to have a standardized plan labeling strategy for the final approved base plan and each adaptive plan to minimize confusion. For example, there could be up to nine total plans for a patient if they are being treated with 60 Gy in 8 fractions. At our institution, the final approved base plan is appended with the suffix notation of "_A0." Adaptive plans will thus be labeled in iterative succession with the trailing integers representing the fraction number. It is not necessary to use this labeling system but utilizing a standardized system that is understood by all users will help minimize errors in proper plan identification.

6 Technical considerations

Although MRgART has many advantages, including tighter margins, real-time gating, and adaptive replanning, significant challenges remain to overcome central and ultracentral lung lesion treatment limitations. This includes the low proton density of the lung and artifacts secondary to air-tissue interfaces in addition to both cardiac and respiratory motion (25).

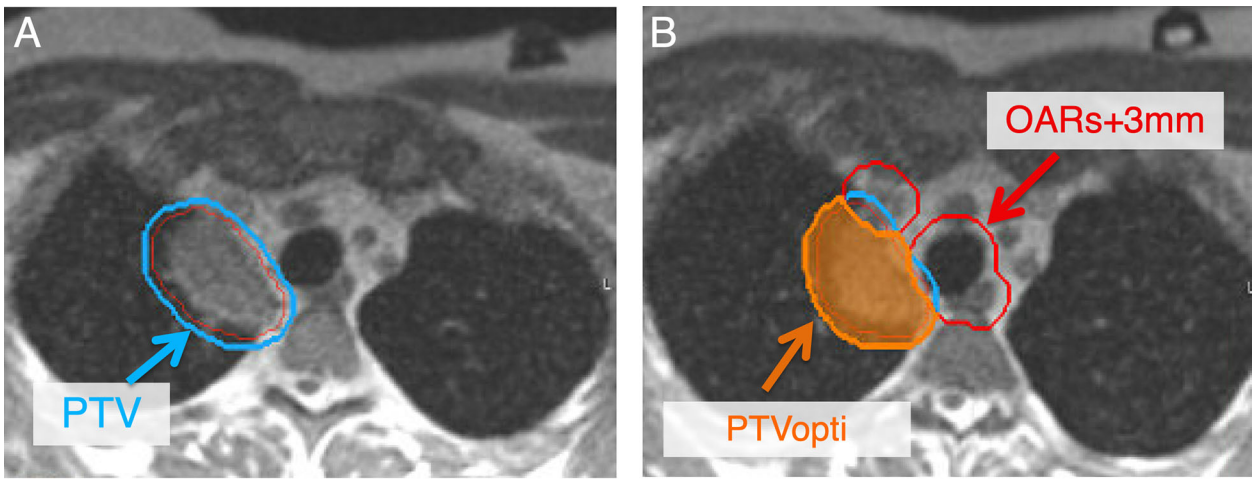

FIGURE 4
Secondary to changes in position to critical OAR, adaptive planning is pursued to decrease doses to critical OAR while maintaining high dose to the tumor. To develop an adaptive plan, a PTVopti (PTVoptimization) is generated for the optimizer to re-plan based on the anatomy of the day. The PTV at our institution is a 3 mm expansion from the GTV **(A)**. The PTVopti is generated by taking the critical OAR and expanding them by 3 mm—we then take the PTV minus the OAR+3mm to generate the PTVopti **(B)**. This allows for appropriate fall off dose toward critical OAR.

At this point, treatment planning for lung malignancies requires a CT scan in the same respiratory phase as the planning MRI (see above for simulation). MRI-only planning with a "synthetic CT" is hard to implement in lung where the density can vary significantly (i.e., between 0.02 to 0.3 g/cm^3) depending on the patient characteristics and respiratory state (26). While MRI-based segmentation could differentiate between air, lung, tissue and bone, a CT is needed to estimate the lung density, which in turn affects the tumor coverage and the normal lung dose (27). The bulk lung density assignment is definitely not dosimetrically appropriate and it remains to be seen if machine learning approaches could eventually become reliable in determining the actual lung density (28). As of now, the thorax is not a region that is believed to be feasible initially with MRI-only planning techniques (29).

Deformable image registration in MRIdian is usually sufficiently accurate to properly align the soft tissue/tumor, lung, and airways between the MRI and CT datasets. To achieve a more accurate deformable registration, the MR and CT scans should be done in the same setup and in a relatively short time from each other, preferably with MR sim being done first with CT reproducing its setup shortly after. Unlike in the abdomen, manual replacement of air density with tissue or vv. is virtually never required. The standard motion management strategy is a combination of breath hold with real time tumor gating technique with either fixed gantry angle 3D or step-and-shoot intensity-modulated RT (IMRT) beam delivery. The intrafractional MR cine of the MRIdian provides sufficient real time tumor motion visibility to accurately gate the tumor directly without relying on any indirect techniques despite magnetic interference of nearby electrical motors. This method results in the least amount of normal tissue irradiation compared to other motion-management techniques, but it is also the slowest (30, 31).

7 Daily adaptive workflow

At our institution, the steps of the MRgART workflow outlined below are embedded in formal checklists that are followed during both the initial planning and adaptive treatment phases. We encourage any new center looking to develop and implement an MRgART program to develop similar checklists to ensure each step in the adaptive processes is followed in a consistent manner.

7.1 Positioning

Daily online adaptation is performed while the patient is positioned on the table reproducing the simulation set up. A new 3D MR scan of the day is obtained with the field of view including the entirety of the target with a superior/inferior margin and the entirety of corresponding patient anatomy. Positional adjustments are limited to 3D translations only. The translational shifts are based on manual primary tumor alignment and approved by the physician. An external contour corresponding to the new patient scan/position is automatically generated. It serves as a guide for the system to determine if the shifts can be executed safely. Once confirmed, the shifts are executed. The target volumes are always rigidly translated and aligned from the simulation MR to the daily volumetric MR scan frame of reference. The OAR also need to be segmented on the daily MR. At our institution, we found that rigid registration has been the most consistent starting point in the thorax as compared to deformable registration. The electron density map from a simulation CT deformably registered to the daily MR is examined and necessary overrides, if any, could be performed using the pre-defined density control structures.

7.2 Adaptive re-contouring

The tracking structure, which is usually based on the GTV, is then evaluated, and modified if necessary by a properly trained radiation therapist. To save time, the OAR are typically edited only within the bounds of the focused OAReval ring. However, the spinal cord is always segmented, and dose verified even if it lies outside the OAReval structure. Although the rigidly translated lung contours do not need to be perfect on the daily MR, they should reasonably approximate the daily anatomy to ensure that lung dose is appropriately accounted for. At our institution, adaptive OAR contouring is a team effort, initially completed by the radiation therapist or radiation oncologist trainee, followed by a thorough review by an attending physician with experience in adaptive radiotherapy.

GTV volume edits are usually not required because plan contours are aligned to the target on the daily MR image and there are typically minimal geometric changes of the target over the course of treatment to justify edits to the GTV (i.e., the original GTV is able to encompass the target). However, GTV edits are necessary if target geometry has changed enough where the original contour no longer appropriately delineates the tumor edges or if an interface with an abutting OAR evolves over the course of treatment as such so that the GTV now overlaps with the OAR. We realize there are institutions that do edit the GTV daily for adaptive treatment. In our practice, we have found that with SBRT (8 fractions or less) there is minimal change in the tumor volume over a treatment course that necessitates daily GTV edits (exceptions do exist). If edits are made to the GTV then the PTV volumes must be regenerated as stated above. After the attending physician is satisfied with the segmentation effort, the OAR contours are cleaned up according to the pre-determined software protocol (these settings are user defined and we use them to remove holes, smooth out edges, and remove disconnected contours). Pre-set Boolean rules are then applied to generate the new PTVopti. The nominal PTV remains unchanged during this process, unless the GTV was modified. A useful check of the adaptive process is to watch the PTVopti change with application of the rules.

7.3 Dose Prediction

A prior plan, which can be the base plan or a previous adapted plan, is recalculated on the daily imaging dataset taking the isocenter shift into account. The target and recontoured OAR metrics achieved by either the base plan or a prior adapted plan on the daily MR anatomy scan are then evaluated. If any target coverage or OAR constraint violations occur, a decision is made to either pursue a simple weight optimization (i.e., changing the relative distribution of monitor units [MUs] between the beamlets without changing their shape or number)

or to immediately proceed to a full re-optimization, whereby the beamlets will change based upon whether the cost function is modified. The beam angles never change. After reoptimization, the new plan may still require manual reoptimization to meet any of the critical metrics, including target coverage or OAR constraint(s).

The original plan generated on the always remains available for treatment should it be chosen after reoptimization. Once an optimal plan is chosen based on the DVH metrics snapshot, the crucial last step is to review the isodose lines through the target level and within 2 cm superiorly and inferiorly. This is a good practice since even if the pre-defined DVH metrics are all met, unexpected hot spots away from the target or lack of coverage conformality could be easily visualized and further corrected by replanning if necessary (Figure 5).

At the end of the planning process patient-specific dosimetric quality assurance must be performed as with any inversely planned treatment. It must rely on independent dose recalculation since a pre-treatment measurement is obviously not possible with a patient on the table. To that end, the MRIdian system has a second Monte Carlo calculation engine that relies on a code completely different from the main one. The two dose distributions are compared by gamma-analysis (32). The gamma analysis is performed with 2% (local normalization) dose-error threshold, 2 mm distance-to-agreement threshold, and 10% of the maximum dose analysis cut off threshold. While 95% passing rate with 3%/2mm dose-error/distance to agreement threshold should be considered acceptable (33), in our experience 100% agreement with more stringent 2%/2mm criteria is typically achieved. Also, the total MUs for the daily online adapted plan are compared to the original plan and recorded prior to treatment delivery.

7.4 Dose delivery

A MR-compatible monitor is installed on the far wall of the vault where the bore axis intersects it, as a visual aid for coaching the patient to keep their breath held at the needed respiratory position. The monitor replicates the pertinent portions of the operator console screen, most importantly the moving tracking structure and the stationary gating envelope. The patient can see the monitor in a mirror thus receiving feedback on their efforts to hold the breath in the optimal position as instructed by the therapists.

If the anatomy at simulation was not representative (e.g., underinflated lungs) or an optimal plan was not achievable, causing the new online daily adapted plan to be clearly superior, it may be saved as the new default base plan for future fractions. If keeping the tracking structure within the boundary structure proves challenging, the team may elect to liberalize the voxel excursion percentage to above 5% to achieve a practical duty cycle depending on PTV margins and the clinical context.

7.5 After the treatment course

Patients must be closely monitored for toxicity. Per our institutional experience, the approach has been associated with excellent primary tumor control and minimal toxicity with presentations and manuscripts pending (Figure 6). However, these patients remain at risk for regional (i.e., lymph node) failure and should be followed closely with serial CT scans.

8 Conclusion

MRgART allows for ablative doses to be delivered safely to central and ultracentral lung lesions, to achieve improved local control while minimizing toxicity. However, the proper use of this technique is required to ensure that OAR remain protected from ablative doses. In this guide, we have reviewed our institution's MRgART workflow that allows us to achieve the necessary target coverage while respecting the

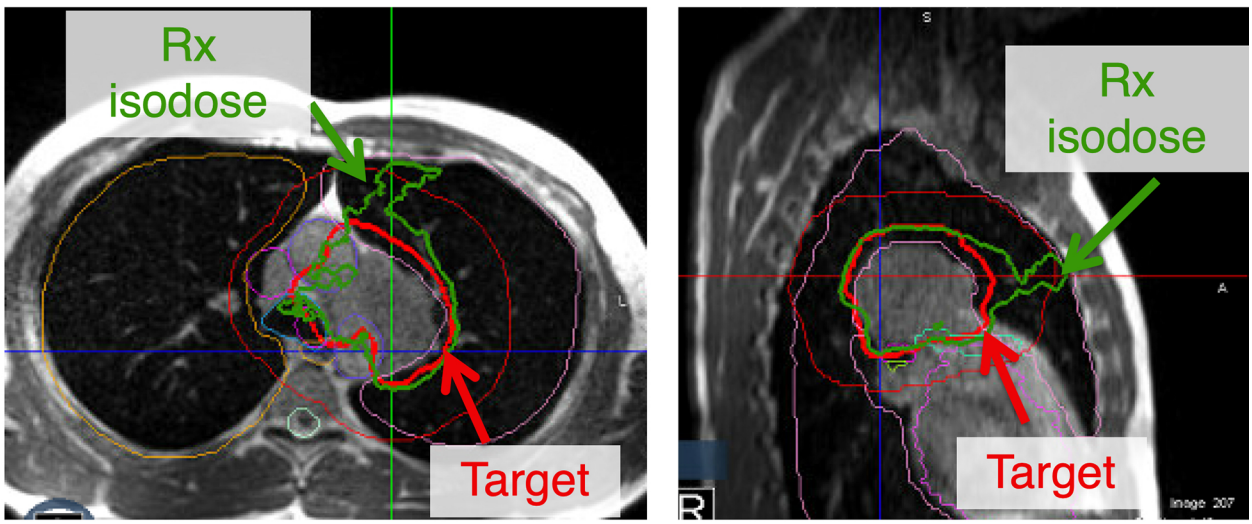

FIGURE 5
Although all the constraints for adaptive replanning may be met, a critical last step is to evaluate the isodose lines. This may be secondary to contouring errors that could be overlapping into an inappropriate location. Additionally, a lack of conformality to the plan may lead to the prescription isodose line not following the target. In this figure, all the constraints are met but the plan lacks appropriate conformality and another iteration of adaptive re-planning may be warranted.

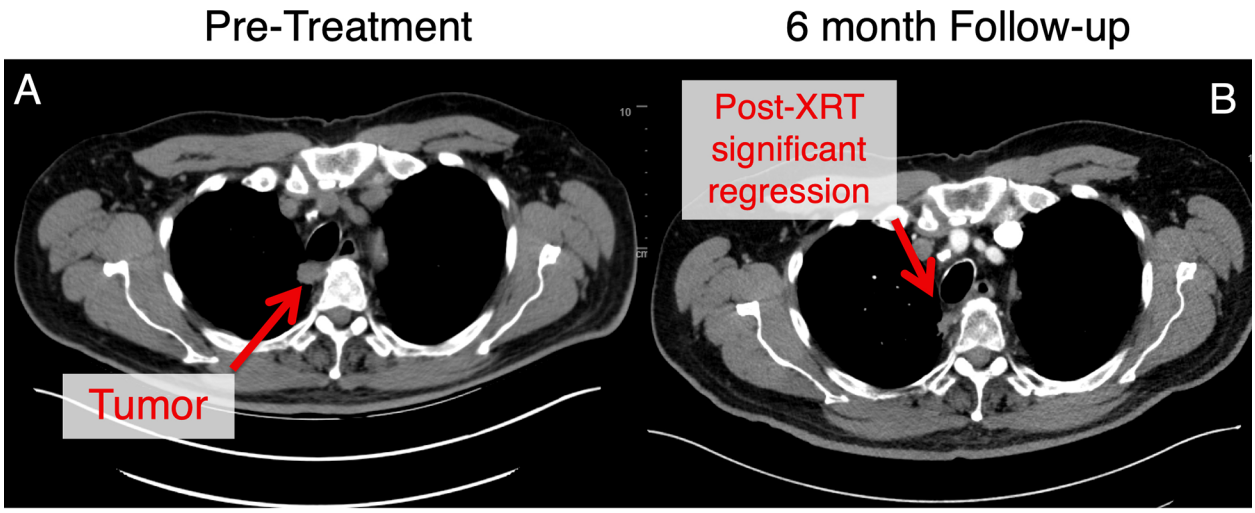

FIGURE 6
This patient with an ultracentral tumor was treated with 60 Gy in 8 fractions with daily adaptive therapy. This tumor was adjacent to the trachea and esophagus at the start of treatment **(A)**. Follow-up at approximately 6 months **(B)**, there has been significant tumor regression for this patient. This patient experienced mild gastroesophageal reflux disease at baseline that was managed with proton pump inhibitor therapy without any other toxicities noted.

OAR' tolerances. This appears to be a practical and consistent interim approach with MRgART, as we await the results of the prospective LUNG STAAR trial (NCT04917224).

Data availability statement

The original contributions presented in the study are included in the article/supplementary material. Further inquiries can be directed to the corresponding author.

Author contributions

All authors confirm contribution to the paper as follows: conception, design and drafting of the manuscript. All authors contributed to the article and approved the submitted version.

Conflict of interest

SR: Performs consulting work for Viewray and receives research funding and honorarium. VF and KL: Perform consulting work for Viewray.

The remaining authors declare that the research was conducted in the absence of any commercial or financial relationships that could be construed as a potential conflict of interest.

Publisher's note

All claims expressed in this article are solely those of the authors and do not necessarily represent those of their affiliated organizations, or those of the publisher, the editors and the reviewers. Any product that may be evaluated in this article, or claim that may be made by its manufacturer, is not guaranteed or endorsed by the publisher.

References

1. Zimmermann FB, et al. Stereotactic hypofractionated radiotherapy in stage I (T1-2 N0 M0) non-small-cell lung cancer (NSCLC). *Acta Oncol* (2006) 45(7):796–801. doi: 10.1080/02841860600913210

2. Nguyen NP, et al. Can stereotactic fractionated radiation therapy become the standard of care for early stage non-small cell lung carcinoma. *Cancer Treat Rev* (2008) 34 (8):719–27. doi: 10.1016/j.ctrv.2008.06.001

3. Xia T, et al. Promising clinical outcome of stereotactic body radiation therapy for patients with inoperable stage I/II non-small-cell lung cancer. *Int J Radiat Oncol Biol Phys* (2006) 66(1):117–25. doi: 10.1016/j.ijrobp.2006.04.013

4. Eriguchi T, et al. Suitability of metastatic lung tumors for stereotactic body radiotherapy. *Cancer Invest* (2021) p:1–9. doi: 10.1080/07357907.2021.2017950

5. Rieber J, et al. Stereotactic body radiotherapy (SBRT) for medically inoperable lung metastases-a pooled analysis of the German working group "stereotactic radiotherapy". *Lung Cancer* (2016) 97:51–8. doi: 10.1016/j.lungcan.2016.04.012

6. Siva S, MacManus M, Ball D. Stereotactic radiotherapy for pulmonary oligometastases: a systematic review. *J Thorac Oncol* (2010) 5(7):1091–9. doi: 10.1097/JTO.0b013e3181de7143

7. Bezjak A, et al. Safety and efficacy of a five-fraction stereotactic body radiotherapy schedule for centrally located non-Small-Cell lung cancer: NRG Oncology/RTOG 0813 trial. *J Clin Oncol* (2019) 37(15):1316–25. doi: 10.1200/JCO.18.00622

8. Timmerman R, et al. Excessive toxicity when treating central tumors in a phase II study of stereotactic body radiation therapy for medically inoperable early-stage lung cancer. *J Clin Oncol* (2006) 24(30):4833–9. doi: 10.1200/JCO.2006.07.5937

9. Lindberg K, et al. The HILUS-trial-a prospective Nordic multicenter phase 2 study of ultracentral lung tumors treated with stereotactic body radiotherapy. *J Thorac Oncol* (2021) 16(7):1200–10. doi: 10.1016/j.jtho.2021.03.019

10. Wang C, et al. Analysis of pneumonitis and esophageal injury after stereotactic body radiation therapy for ultra-central lung tumors. *Lung Cancer* (2020) 147:45–8. doi: 10.1016/j.lungcan.2020.07.009

11. Duijm M, et al. Predicting high-grade esophagus toxicity after treating central lung tumors with stereotactic radiation therapy using a normal tissue complication probability model. *Int J Radiat Oncol Biol Phys* (2020) 106(1):73–81. doi: 10.1016/j.ijrobp.2019.08.059

12. Rosenberg SA, et al. The Nordic-HILUS trial: Ultracentral lung stereotactic ablative radiotherapy and a narrow therapeutic window. *J Thorac Oncol* (2021) 16(10): e79–80. doi: 10.1016/j.jtho.2021.06.030

13. Tachibana H, Sawant A. Four-dimensional planning for motion synchronized dose delivery in lung stereotactic body radiation therapy. *Radiother Oncol* (2016) 119(3):467–72. doi: 10.1016/j.radonc.2016.03.028

14. Underberg RW, et al. Four-dimensional CT scans for treatment planning in stereotactic radiotherapy for stage I lung cancer. *Int J Radiat Oncol Biol Phys* (2004) 60 (4):1283–90. doi: 10.1016/j.ijrobp.2004.07.665

15. Chen T, et al. Frequency filtering based analysis on the cardiac induced lung tumor motion and its impact on the radiotherapy management. *Radiother Oncol* (2014) 112 (3):365–70. doi: 10.1016/j.radonc.2014.08.007

16. Cao J, et al. Determination of internal target volume using selective phases of a 4-dimensional computed tomography scan. *Pract Radiat Oncol* (2012) 2(3):186–92. doi: 10.1016/j.prro.2011.09.004

17. Onishi H, et al. Stereotactic hypofractionated high-dose irradiation for stage I nonsmall cell lung carcinoma: clinical outcomes in 245 subjects in a Japanese multiinstitutional study. *Cancer* (2004) 101(7):1623–31. doi: 10.1002/cncr.20539

18. Zhuang L, et al. Evaluation of image guided motion management methods in lung cancer radiotherapy. *Med Phys* (2014) 41(3):031911. doi: 10.1118/1.4866220

19. Rudra S, et al. Using adaptive magnetic resonance image-guided radiation therapy for treatment of inoperable pancreatic cancer. *Cancer Med* (2019) 8(5):2123–32. doi: 10.1002/cam4.2100

20. Finazzi T, et al. Clinical outcomes of stereotactic MR-guided adaptive radiation therapy for high-risk lung tumors. *Int J Radiat Oncol Biol Phys* (2020) 107(2):270–8. doi: 10.1016/j.ijrobp.2020.02.025

21. Menard C, van der Heide UA. Introduction: Magnetic resonance imaging comes of age in radiation oncology. *Semin Radiat Oncol* (2014) 24(3):149–50. doi: 10.1016/j.semradonc.2014.02.001

22. Lagendijk JJ, Raaymakers BW, van Vulpen M. The magnetic resonance imaging-linac system. *Semin Radiat Oncol* (2014) 24(3):207–9. doi: 10.1016/j.semradonc.2014.02.009

23. Scheffler K, Lehnhardt S. Principles and applications of balanced SSFP techniques. *Eur Radiol* (2003) 13(11):2409–18. doi: 10.1007/s00330-003-1957-x

24. Onishi H, et al. Hypofractionated stereotactic radiotherapy (HypoFXSRT) for stage I non-small cell lung cancer: updated results of 257 patients in a Japanese multi-institutional study. *J Thorac Oncol* (2007) 2(7 Suppl 3):S94–100. doi: 10.1097/JTO.0b013e318074de34

25. Sim AJ, et al. A review of the role of MRI in diagnosis and treatment of early stage lung cancer. *Clin Transl Radiat Oncol* (2020) 24:16–22. doi: 10.1016/j.ctro.2020.06.002

26. Andersson P, et al. Effects of lung tissue characterization in radiotherapy of breast cancer under deep inspiration breath hold when using Monte Carlo dosimetry. *Phys Med* (2021) 90:83–90. doi: 10.1016/j.ejmp.2021.09.009

27. Aarup LR, et al. The effect of different lung densities on the accuracy of various radiotherapy dose calculation methods: implications for tumour coverage. *Radiother Oncol* (2009) 91(3):405–14. doi: 10.1016/j.radonc.2009.01.008

28. Prior P, et al. Technical note: Is bulk electron density assignment appropriate for MRI-only based treatment planning for lung cancer? *Med Phys* (2017) 44(7):3437–43. doi: 10.1002/mp.12267

29. Owrangi AM, Greer PB, Glide-Hurst CK. MRI-Only treatment planning: benefits and challenges. *Phys Med Biol* (2018) 63(5):05TR01. doi: 10.1088/1361-6560/aaaca4

30. Keall PJ, et al. The management of respiratory motion in radiation oncology report of AAPM task group 76. *Med Phys* (2006) 33(10):3874–900. doi: 10.1118/1.2349696

31. Kontrisova K, et al. Dosimetric comparison of stereotactic body radiotherapy in different respiration conditions: a modeling study. *Radiother Oncol* (2006) 81(1):97–104. doi: 10.1016/j.radonc.2006.08.006

32. Low DA, et al. A technique for the quantitative evaluation of dose distributions. *Med Phys* (1998) 25(5):656–61. doi: 10.1118/1.598248

33. Miften M, et al. Tolerance limits and methodologies for IMRT measurement-based verification QA: Recommendations of AAPM task group no. 218. *Med Phys* (2018) 45(4): e53–83. doi: 10.1002/mp.12810

frontiers | Frontiers in Oncology

TYPE Original Research
PUBLISHED 23 March 2023
DOI 10.3389/fonc.2023.1151256

OPEN ACCESS

EDITED BY
Alan Jay Katz,
St. Francis Hospital, United States

REVIEWED BY
Hilary Bagshaw,
Stanford University, United States
Daniel Taussky,
Montreal University, Canada

*CORRESPONDENCE
Merav Akiva Ben David
meravak@assuta.co.il

†These authors have contributed equally to this work

SPECIALTY SECTION
This article was submitted to Radiation Oncology, a section of the journal Frontiers in Oncology

RECEIVED 25 January 2023
ACCEPTED 07 March 2023
PUBLISHED 23 March 2023

CITATION
Gelbart Pridan O, Ben David MA, Zalmanov S, Lipski Y, Grinberg V, Levin D, Apter S, Guindi M, Epstein D, Radus R, Arsenault O, Hod K, Tamami Q and Pfeffer R (2023) Outcome of the first 200 patients with prostate cancer treated with MRI-Linac at Assuta MC. *Front. Oncol.* 13:1151256. doi: 10.3389/fonc.2023.1151256

Outcome of the first 200 patients with prostate cancer treated with MRI-Linac at Assuta MC

Or Gelbart Pridan[1†], Merav Akiva Ben David[2,3*†], Svetlana Zalmanov[2], Yoav Lipski[2], Vladislav Grinberg[2], Daphne Levin[2], Sara Apter[2,4], Michal Guindi[3,5], Dan Epstein[2], Roman Radus[6], Orit Arsenault[2], Keren Hod[7], Qusai Tamami[2] and Raphael Pfeffer[2,3]

[1]The Adelson School of Medicine, Ariel University, Ariel, Israel, [2]Radiation Oncology Department, Assuta Medical Center, Tel Aviv, Israel, [3]Faculty of Health Sciences, Ben-Gurion University of the Negev, Beer Sheva, Israel, [4]Sackler School of Medicine, Tel Aviv University, Tel Aviv, Israel, [5]Innovation Division, Assuta Medical Center, Tel Aviv, Israel, [6]Radiation Oncology Department, Rabin Medical Center, Petah-Tikva, Israel, [7]Department of Academy and Research, Assuta Medical Center, Tel Aviv, Israel

Background: We present our experience with MR-guided stereotactic body radiotherapy (SBRT) for 200 consecutive patients with prostate cancer with minimum 3-month follow-up.

Methods: Treatment planning included fusion of the 0.35-Tesla planning MRI with multiparametric MRI and PET-PSMA for Group Grade (GG) 2 or higher and contour review with an expert MRI radiologist. No fiducials or rectal spacers were used. Prescription dose was 36.25 Gy in 5 fractions over 2 weeks to the entire prostate with 3-mm margins. Daily plan was adapted if tumor and organs at risk (OAR) doses differed significantly from the original plan. The prostate was monitored during treatment that was automatically interrupted if the target moved out of the PTV range.

Results: Mean age was 72 years. Clinical stage was T1c, 85.5%; T2, 13%; and T3, 1.5%. In addition, 20% were GG1, 50% were GG2, 14.5% were GG3, 13% were GG4, and one patient was GG5. PSA ranged from 1 to 77 (median, 6.2). Median prostate volume was 57cc, and 888/1000 (88%) fractions required plan adaptation. The most common acute GU toxicity was Grade I, 31%; dysuria and acute gastrointestinal toxicity were rare. Three patients required temporary catheterization. Prostate size of over 100cc was associated with acute fatigue, urinary hesitance, and catheter insertion. Prostate Specific Antigen (PSA) decreased in 99% of patients, and one patient had regional recurrence.

Conclusion: MR-guided prostate SBRT shows low acute toxicity and excellent short-term outcomes. Real-time MRI ensures accurate positioning and SBRT delivery.

KEYWORDS

prostate cancer, MRI-Linac, SBRT, radiation therapy, MRgRT

1 Introduction

Prostate cancer (PC) is the second most frequent cancer in men worldwide, usually in men age 50 and older. Every year, 1,400,000 new patients are diagnosed with PC and 375,000 patients die (1). The majority (91%) of PCs are diagnosed at a local or regional stage, for which the 5-year survival rate approaches 100%. The 5-year survival for disease diagnosed at metastatic stage is 30% and the 10-year survival rate for all stages combined is 98% (2). Early PC treatment options include active follow-up (active supervision/surveillance), surgery (prostate gland removal), and radiation therapy (RT; external beam radiation or brachytherapy) (3). RT is a key modality in the treatment of patients with low-, intermediate-, and high-risk PC. This non-invasive technique can be offered to many patients with PC with minimal side effects in the modern radiation era (4).

The most commonly available RT technique is external beam RT (5). The fundamental problem in treating localized PC is to provide a curative dose of radiation to the prostate while reducing the exposure to healthy surrounding organs such as the bladder, rectum, and femoral heads (5). This issue is largely overcome with modern radiation techniques, which include three-dimensional (3D) conformal radiotherapy, intensity-modulated RT, and volumetric modulated arc therapy combined with image guidance have allowed delivery of larger radiation doses with lower toxicity (6). Androgen deprivation therapy (ADT) is usually kept for clinically localized, unfavorable intermediate to high-risk PC (3)

Since August 2019, a gantry-based MR-guided linear accelerator (MRgRT) is in use at our institution (ViewRay MRIdian). This device integrates full 3D MRI target identification and radiation dose replanning before every treatment (7, 8). In our study, we collected the clinical and treatment data for the first 200 patients with PC treated with MRgRT in our institution, as well as their outcome measures. This will be one of the first reports and the largest series as of today regarding PC treated on an MR-Linac.

2 Materials and methods

This descriptive study reports 200 consecutive patients with localized PC who were treated with MRI-Linac at our institution between August 2019 and July 2021. The study was approved by the local Institutional Review Board (IRB). Inclusion criteria were histologically proven PC, localized PC by imaging, and at least 3-month follow-up. Patients treated for local recurrence following former prostatectomy or prior radiation or who had received previous pelvic RT for any cause were excluded from this analysis.

Patients underwent MRI simulation on the MRI linear accelerator (supine position, both arms on the chest, two glycerin suppositories 4 h prior to simulation and 400 cc water PO 45 min prior to scanning and before each fraction) followed by CT-based simulation in the same position. The treatment planning included fusion with pre-treatment imaging [MRI and/or positron emission tomography - prostate-specific membrane antigen (PET-PSMA)] and contouring target volume [prostate contouring target volume (CTV)] and OARs —rectum, bladder, and femoral heads, on the MR simulation imaging. The urethra was not contoured. All contours underwent an expert radiologist review prior to planning (SA). Prescription dose was 36.25 Gy in 5 fractions delivered over 2 weeks (alternate days) to the entire prostate with 3-mm margins (PTV); no regional nodes were treated. Doses to target volume and OAR were evaluated using institutional constrains as shown in Table 1. One patient received GTV boost to 40 Gy. On each fraction, MRI was performed, the OARs and prostate were re-contoured accordingly, and plan was adapted if tumor and OAR doses were significantly worse than the simulation-based plan or did not match the constrains see Figure 2. During radiation, the prostate was monitored with real-time (four frames/s) single-frame MRI, and treatment was automatically interrupted if the target volume moved out of the PTV range by 5%.

Treating physicians monitored patients' side effects both throughout and after the course of treatment. Gastrointestinal (GI) (diarrhea, proctitis, tenesmus, rectum numbness,

TABLE 1 Target volume and organs at-risk constrains for treatment plans.

Structure	Dosimetric index (volume)	Accepted criteria (Gy)
PTV	≥95%	34.4
Rectum	Max point dose	38.0
	<1.0 cc	36.25
	<3.0 cc	34.43
	<10 cc	32.62
Bladder	Max point dose	39.4
	<0.1 cc	38.0
	<1.0 cc	36.25
	<15.0 cc	32.62
Femoral heads	<10 cc	30.0

hemorrhoids, encopresis, incontinence, pain), urinal (dysuria, increased frequency of urination, nocturia, urinary jet strength, urgency, and nonspecific urination complains) and general side effects (fatigue) were monitored during radiation and physician reported in every follow-up visit thereafter. Side effects were rated according to CTCAE (version 5) (9). In addition, patients' PSA levels were tracked at baseline and every 3–6 months.

2.1 Data analysis

The primary endpoint was to evaluate GI and urinary side effects. Secondary endpoint was a short-term treatment outcome. Associations between patients' characteristics, treatment characteristics, and side effects were evaluated by Mann–Whitney test, Spearman correlation, and Chi-square test, as appropriate. A linear mixed model for repeated measure analysis was used to evaluate individual PSA levels throughout the study follow-up within the non-ADT population. In addition, four linear mixed models with adjustments for potential confounders were used. The first model adjusts for patients' age and interaction with time (i.e., age × time); the second model adjusts for prostate size and interaction with time (i.e., prostate size × time); the third model adjusts for International Society of Urological Pathology (ISUP) and interaction with time (i.e., ISUP × time); and the fourth model adjusts for ISUP, interaction with time (i.e., ISUP × time), prostate size, and interaction with time (i.e., prostate size × time). To avoid multicollinearity, we verified that there are no correlations between these independent variables that were included in each of the models; therefore, in the last model, age and its interaction with time were not included with all the rest of the independent variables (i.e., prostate size, prostate size × time, ISUP, and ISUP × time). All of these adjustments were defined as fixed effects in all models.

Level of significance used for all analyses was two tailed and set at $p < 0.05$. The SPSS statistical package (version 28, SSPS Inc., Chicago, IL) was used for all statistical analyses.

3 Results

3.1 Patients and treatment characteristics

With median follow-up of 16.4 months (range, 3–35.9 months), our first 200 consecutive patients were evaluated. Table 2 summarizes patient and treatment characteristics. Clinical stage was I, 85.5% (n = 171); II, 13.0% (n = 26); and III, 1.5% (n = 3). The average percentage of positive biopsy cores was 40.8%, and 64 (32.0%) of the patients had involvement of ≥50.0% cores. ISUP 1 accounted for 20.5% (n = 41) of patients, 50.0% (n = 100) had ISUP 2, 14.5% (n = 29) ISUP 3, 13.0% (n = 26) ISUP 4, and only 0.5% (n = 1) with ISUP 5 (three patients had missing data). Over 25% had prostate volume of 67.8cc and 23 (11.5%) had prostate larger than 80cc. Prostate size was not associated with ISUP. In this cohort, 92.0% (N = 184) had a diagnostic multiparametric MRI (1.5 or 3 Tesla) prior to radiation, and the majority (91.6%) had PIRADS 4/5 lesions, 6% had PIRADS 3, 1.8% PIRADS 2, and 0.6% PIRADS 1. MRI showed suspected extracapsular extension in 19.5% (n = 39), neuro-vascular bundle (NVB) involvement in 9.5% (n = 19), and seminal vesicles involvement in 4.3%. PET-PSMA was available for 79.0% (n = 158) of the patients before RT.

Mean treatment time (from closing doors to end of treatment: re-sim, contour check, plan evaluation, optimization and re-calculation when appropriate, on-board QA, actual treatment time) was approximately 50 min. In addition, 888/1000 (88.8%) daily treatments required plan adaptation. No correlation was found between adaptation required and time interval between simulation and RT. There was no association between age, PSA level at diagnosis, prostate volume, and body mass index (BMI) to number of adaptations.

3.2 Toxicity

We analyzed two groups of side effects: acute side effects (during and up to 30 days following the end of radiation) and subacute side effect (30–90 days following radiation). During radiation period, 0.5% (n = 1) reported fatigue, whereas 9.0% (n = 18) reported on fatigue later in the follow-up visit. The most common genitourinary (GU) symptom reported was mild dysuria (grade I) by 31.0% (n = 62) of patients, subsiding to 11% (n = 22) by 3 months. In addition, 20.5% (n = 41) reported increased nocturia (grade I) and increased frequency (grade I), subsiding to 13.0% (n = 26) and 3.0% (n = 6), respectively, by 3-month follow-up. In addition, 2.5% (n = 5) reported urgency grade I in the subacute period. Three patients (1.5%) needed a catheter insertion (grade II) (9) during radiation treatment: in one patient after 1 fraction and in two patients following 3 fractions. All catheters were removed successfully 1, 7,

TABLE 2 Patients' characteristics.

Age (years), median (range)	72.0 (53.0-90.0)
BMI (kg/m^2), median (range)	26.9 (19.8-37.7)
Prostate size (cc), median (range)	53.3 (16.5-171.8)
PSA at diagnosis (ng/ml)*,**, median (range)	6.3 (1.4-72.0)
Treatment period (days), median (range)	10.0 (7.0-29.0)
Androgen deprivation therapy, n (%)	56 (28.0)

BMI, body mass index; PSA, prostate specific antigen.
*Available for 180 patients up to 4 months prior to RT.
**PSA at diagnosis includes ADT group and non-ADT group.

and 10 days following RT. Prostate mean volume for patients with catheter was significantly higher, 105 cc (85, 89, and 141 cc) vs. 65.7 cc ($p = 0.029$). Catheter insertion was not associated with age, PSA level at diagnosis, or BMI.

Patients older than 75 years reported higher incidence of acute nocturia ($p = 0.004$). Larger prostate size was associated with acute fatigue 107.6 cc vs. 53.7 cc ($p = 0.037$) and with acute/subacute sensation of urinary hesitance of 89.0 and 109.4cc, vs. 53.3 and 52.6 cc, respectively ($p = 0.0006$ and $p = 0.014$). In addition, BMI was significantly higher among those who reported subacute penile pain [34.5 kg/m (2)], compared to those who did not (26.9 kg/m (2); $p = 0.005$).

The reported GI side effects were minor (Table 3). Maximal grade was II in this cohort. No patient reported constipation, encopresis, nausea, or any other abdominal/GI-associated symptoms.

ADT, received by 28.6% of our cohort, was not associated with acute or subacute GU or GI side effects.

3.3 Outcome

Pre-treatment PSA ranged from 1.4 to 72.0 ng/ml (Table 2) and was ≥10 ng/ml in 34 patients (17.0%). Only 28.6% (N = 57) received ADT in this cohort.

In the non-ADT group (71.4%, N = 142), mean baseline PSA was 7.4 ng/ml and decreased with time ($p<0.001$) (Figure 1). PSA decline rate was 1.0 ng/ml per 3 months on average. PSA reduction was not associated with either age, prostate size, or ISUP.

The PSA nadir in our non-ADT cohort has not been reached due to the short follow-up period; however, 6% were below 0.2 ng/ml and 41% had PSA level of <1 ng/ml at the last follow-up.

Of the 200 patients treated, 184 (92.0%) were available for follow-up of at least 6 months (3–35.9 months) following RT. One patient died because of cardiac arrest, and one (0.5%) had an isolated regional recurrence (isolated ileac lymph node) 7 months following MRgRT, treated with comprehensive pelvic irradiation, and is free of disease at the time of this analysis. A total of 192 patients (96.0%) were NED (no evidence of disease) when performing the analysis. There were missing data for seven (3.5%) patients.

4 Discussion

To the best of our knowledge, this study describes the largest series of patients with PC treated with MRgRT, reporting side effects and short-term outcomes. MRgRT with daily online plan adaption is a novel strategy for administering stereotactic body radiotherapy (SBRT) for PC but requires longer treatment time and multi-professional personnel efforts (10).

In this consecutive cohort, we found low rates of GI toxicity, and, although 31% experienced GU side effects, they were transient and mostly grade I by nature. A short-term follow-up demonstrated excellent local control and reduction in the PSA level. By using adaptive planning, real-time tracking, and particularly the use of only 3-mm CTV to PTV margins, the dose to the rectum and bladder is lower, leading to these results as described by others as well (11–13). Most CT-based prostate SBRT series use larger margins (14–16). The Magnetic resonance imaging-guided stereotactic body radiotherapy for prostate cancer (MIRAGE) study used 2-mm margins for MR-guided treatment and 4-mm margins for CT-guided treatment (13).

4.1 Acute side effects

In our series, 31% and 6.5% experienced grade I (mostly mild dysuria) or grade II GU toxicity, respectively, and three patients needed catheter insertion. For GI toxicity, very few patients experienced any side effects, with mostly grade I reported. Our excellent toxicity profile is lower when compared with other studies reporting acute GU and GI toxicity with MRgRT (11, 12).

In the early pioneer reported series of MRgRT, Alongi et al. and Tetar et al. reported very low GI and GU toxicity in their series, demonstrating the feasibility and safety of this extreme hypofractionated RT protocol (17, 18). In a study by Bruyzeel (11) et al., their group described meticulous patient-reported outcome measure and clinician reported outcome measure outcomes of 104 patients with the same radiation protocol of 36.25 Gy in 5 fractions using MRgRT, reporting ≥ grade II of any acute GU side effects of 23.8% and 5% GI. Ugurluer et al. in their series of 50 patients with a similar RT protocol reported 28% of

TABLE 3 Acute and subacute gastrointestinal toxicity.

Side-effect	Acute	Sub-acute
Hemorrhoids, n (%)	5 (2.5)	0
Anal pain, n (%)	5 (2.5)	2 (1.0)
Tenesmus, n (%)	5 (2.5)	1 (0.5)
Incontinence, n (%)	0	0
Proctitis, n (%)	2 (1.0)	0 (0.0)
Diarrhea, n (%)	1 (0.5)	0

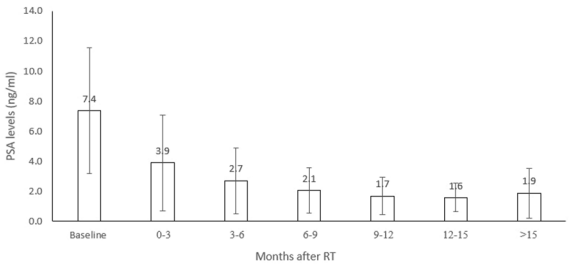

	Baseline	0-3	3-6	6-9	9-12	12-15	>15
N	132	98	90	73	57	46	28

FIGURE 1
PSA during the study follow-up in non-ADT patients.

grade I GU toxicity and 36% of grade II (12). Only 6% experienced grade I GI toxicity. The low rates of GI toxicity and the moderately low rates of GU toxicity are consistent in all studies. All these groups used 3 mm around the GTV for PTV delineation and same OAR constrains with daily adaptation. The MIRAGE study, a randomized phase 3, compared MRgRT vs. CT-based SBRT in PC with 40 Gy in 5 fractions (13). Two-millimeter margins were used for the non-adaptive MRgRT and 4-mm margins for CT-based treatment. In their study, they report significantly lower incidence of acute GI and GU side effects in the group treated with MRgRT (13).

In series using similar but non-MRgRT SBRT protocols of 36.25–40 Gy, higher acute side effects were reported. In the series of 309 patients with real-time tracking of implanted fiducials by Meier et al., 59% experienced grade I GU toxicity and 26% grade II, with 55% and 8.1% GI toxicity, respectively (19). These results resemble the findings in the study reported by Brand et al. In their study of 874 patients, half received conventional fractionated/moderately hypofractionated RT compared to SBRT (14). In 415 patients in the SBRT arm (36.25 Gy, 5 fractions), they reported that 57% of the patients experienced grade I GU toxicity and 21% grade II with 2% grade III and two patients with grade IV (14). For GI toxicity, 53% grade I and 10% grade II with one patient experience grade III.

Three patients needed catheter insertion during radiation in our series (1.5%), reported as grade II by CTACE Vr. 5. In our cohort, the urethra was not delineated and was not accounted for during dose calculation. We identified high prostate volume as risk factor for urinary retention in these patients. In the 104 patients, Bruynzeel et al. reported that the treatment was delivered to the prostate with simultaneous integrated relative sparing of the urethra, and no patient needed a catheter insertion (11). One patient (2%) in the study by Ugurluer et al. needed a catheter during RT (12). In a non-MRgRT prostate SBRT series, the need for catheterization was 1% in the acute phase period (19). Urethral sparing techniques may reduce urinary symptoms as reported from brachytherapy series (15, 20); however, daily urethral catheter insertions were uncomfortable and may increase urinary tract

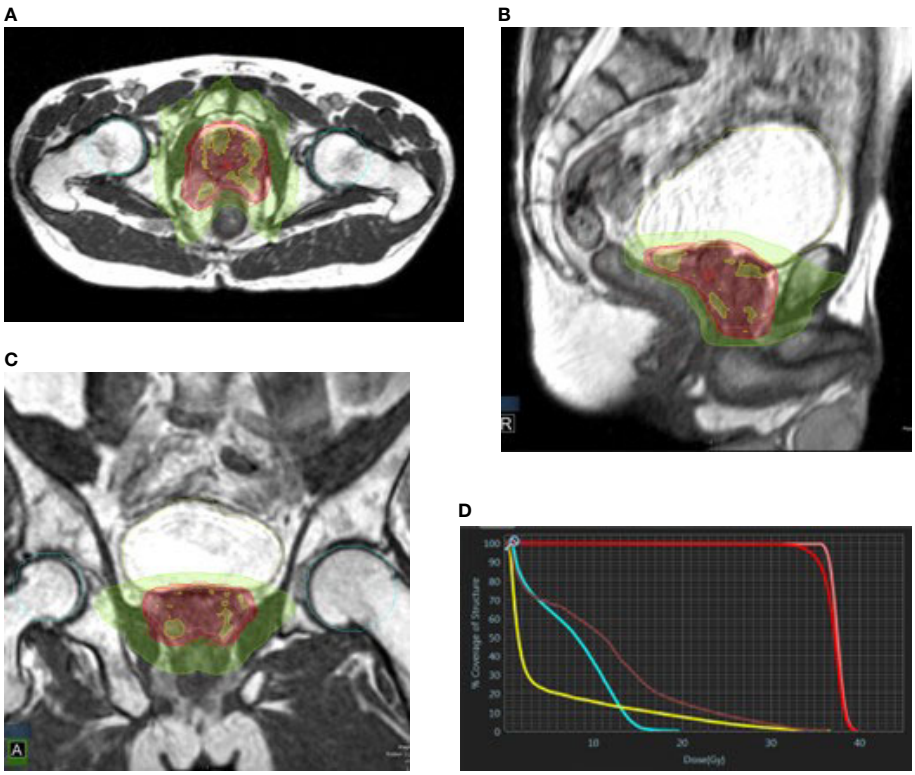

FIGURE 2
Prostate plan in axial **(A)**, sagittal **(B)**, and coronal **(C)** views. Green, 50% isodose line; red, 95% isodose line; yellow, 105% isodose line. **(D)** DVH: pink, CTV; red, PTV; yellow, bladder; brown, rectum; cyan, femoral heads.

discomfort. In addition, urethral sparing based on catheter-free MRI can be observer-dependent, time-consuming, risk-underdosing tumor close to the urethra and produce heterogeneity in the target volume (16). There are no reliable urethral contouring guidelines, and it is not consistently delineated in most series (19). Of note, the low rates of GI toxicity are comparable to the reports of external beam RT using rectal spacers, showing less than 5% grade II GI toxicity (21). Another advantage of the MRgRT is the avoidance of the need for implanted fiducials, i.e., gold markers.

Overall, the incidence of side effects was low, and the treatment was well tolerated in prior reports of prostate SBRT treated by MRgRT, leading to worldwide acceptance of extreme hypofractionated protocols for localized PC, following the road for shorter radiation protocols as HYPRO and CHHip trials (11–13, 22, 23).

With median follow-up of 16.4 months, only one patient (0.5%) experienced regional recurrence of isolated ileac lymph node and was salvaged by comprehensive pelvic irradiation. This low rate of regional recurrence, although very early, is anticipated, as most of the patients were in the low-risk group (ISUP 1 + 2, 70.5%). PSA level as a surrogate for distant metastatic disease and overall survival is well established in definitive radiation to the prostate gland (24, 25). There is a range of possible PSA level measurements in the literature as a cut-point value for nadir determination, and as reported, 41% of our cohort reached a PSA level lower than 1 ng/ml (24). Because the nadir of PSA level was not yet achieved in our series, with our reported mean decrease rate of 1 ng/ml every 3 months, a longer follow-up is necessary for evaluating this outcome.

We acknowledge the limitation of this study as this cohort is a single institution series, retrospective in nature, with a relatively short follow-up time. However, this is the largest study evaluating short-term toxicity and outcome of patients with localized PC treated with MRgRT with an ultra-hypofractionated scheme. In this homogenous group, disease baseline imaging data were very updated with 92% undergoing diagnostic prostate MRI prior to RT and PET-PSMA available for 79% of the patients. A total of 97% of the patient were available for follow-up.

5 Conclusions

MRgRT for localized PC with ultra-hypofractionated dose protocol of 36.25 Gy demonstrated low rates of acute and subacute GI and GU toxicity with excellent short-term outcomes. We anticipate that future research will add to our understanding of the tolerability and clinical outcomes of this novel technology method.

Data availability statement

The raw data supporting the conclusions of this article will be made available by the authors, without undue reservation.

Ethics statement

The studies involving human participants were reviewed and approved by the Institutional Review Board (or Ethics Committee) of ASSUTA Ramat Hahayal (ASMC-0062-21 19.12.2021). Written informed consent for participation was not required for this study in accordance with the national legislation and the institutional requirements.

Author contributions

The authors confirm the contribution to the paper as follows: OG: data collection, data analysis and interpretation of results, and draft manuscript preparation; MB: treating physician, data analysis and interpretation of results, draft manuscript preparation, design of the work, and supervision; SZ: treating physician, and writing review and editing; YL: treating physician, and writing review and editing; VG: treating physician, and writing review and editing; DL: on-board physicist and analyst, and data collection; SA: delineation quality assurance and data analysis; MG: data analysis; DE: on-board physicist and analyst, and data collection; RR: on-board physicist and analyst, and data collection; OA: on-board physicist and analyst, and data collection; QT: on-board physicist and analyst, and data collection; KH: statistician, data management, data analysis, and interpretation of results; RP: treating physicians, critical revision of the article, and supervision. All authors have read and agreed to the published version of the manuscript.

Conflict of interest

The authors declare that the research was conducted in the absence of any commercial or financial relationships that could be construed as a potential conflict of interest.

Publisher's note

All claims expressed in this article are solely those of the authors and do not necessarily represent those of their affiliated organizations, or those of the publisher, the editors and the reviewers. Any product that may be evaluated in this article, or claim that may be made by its manufacturer, is not guaranteed or endorsed by the publisher.

References

1. Sung H, Ferlay J, Siegel RL, Laversanne M, Soerjomataram I, Jemal A, et al. Global cancer statistics 2020: GLOBOCAN estimates of incidence and mortality worldwide for 36 cancers in 185 countries. *CA Cancer J Clin* (2021) 71(3):209–49. doi: 10.3322/CAAC.21660

2. Siegel RL, Miller KD, Fuchs HE, Jemal A. Cancer statistics, 2022. *CA Cancer J Clin* (2022) 72(1):7–33. doi: 10.3322/CAAC.21708

3. Schatten H. Brief overview of prostate cancer statistics, grading, diagnosis and treatment strategies. *Adv Exp Med Biol* (2018) 1095:1–14. doi: 10.1007/978-3-319-95693-0_1

4. McPartlin AJ, Li XA, Kershaw LE, Heide U, Kerkmeijer L, Lawton C, et al. MRI-Guided prostate adaptive radiotherapy - a systematic review. *Radiother Oncol* (2016) 119(3):371–80. doi: 10.1016/j.radonc.2016.04.014

5. Hall WA, Paulson ES, van der Heide UA, Fuller CD, Raaymakers BW, Lagendijk JJW, et al. MR linac Atlantic consortium and the ViewRay C2T2 research consortium. the transformation of radiation oncology using real-time magnetic resonance guidance: A review. *Eur J Cancer* (2019) 122:42–52. doi: 10.1016/j.ejca.2019.07.021

6. Zelefsky MJ, Kollmeier M, Cox B, Fidaleo A, Sperling D, Pei X, et al. Improved clinical outcomes with high-dose image guided radiotherapy compared with non-IGRT for the treatment of clinically localized prostate cancer. *Int J Radiat Oncol Biol Phys* (2012) 84(1):125–9. doi: 10.1016/j.ijrobp.2011.11.047

7. Mannerberg A, Persson E, Jonsson J, Gustafsson CJ, Gunnlaugsson A, Olsson LE, et al. Dosimetric effects of adaptive prostate cancer radiotherapy in an MR-linac workflow. *Radiat Oncol* (2020) 15(1):168. doi: 10.1186/s13014-020-01604-5

8. Tetar SU, Bruynzeel AME, Lagerwaard FJ, Slotman BJ, Bohoudi O, Palacios MA. Clinical implementation of magnetic resonance imaging guided adaptive radiotherapy for localized prostate cancer. *Phys Imaging Radiat Oncol* (2019) 9:69–76. doi: 10.1016/j.phro.2019.02.002

9. Cancer Institute N *Common terminology criteria for adverse events (CTCAE)* (2017). Available at: https://www.meddra.org/ (Accessed August 13, 2022).

10. de Mol van Otterloo SR, Christodouleas JP, Blezer ELA, Akhiat H, Brown K, Choudhury A, et al. Patterns of care, tolerability, and safety of the first cohort of patients treated on a novel high-field MR-linac within the MOMENTUM study: Initial results from a prospective multi-institutional registry. *Int J Radiat Oncol Biol Phys* (2021) 111(4):867–75. doi: 10.1016/j.ijrobp.2021.07.003

11. Bruynzeel AME, Tetar SU, Oei SS, Senan S, Haasbeek CJA, Spoelstra FOB, et al. A prospective single-arm phase 2 study of stereotactic magnetic resonance guided adaptive radiation therapy for prostate cancer: Early toxicity results. *Int J Radiat Oncol Biol Phys* (2019) 105(5):1086–94. doi: 10.1016/J.IJROBP.2019.08.007

12. Ugurluer G, Atalar B, Zoto Mustafayev T, Gungor G, Aydin G, Sengoz M, et al. Magnetic resonance image-guided adaptive stereotactic body radiotherapy for prostate cancer: Preliminary results of outcome and toxicity. *The British Journal of Radiology* (2021) 1:94. doi: 10.1259/bjr.20200696

13. Kishan AU, Ma TM, Lamb JM, Casado M, Wilhalme H, Low DA, et al. Magnetic resonance imaging-guided vs computed tomography-guided stereotactic body radiotherapy for prostate cancer: The MIRAGE randomized clinical trial. *JAMA Oncol* (2023) 12:373. doi: 10.1001/jamaoncol.2022.6558

14. Brand DH, Tree AC, Ostler P, van der Voet H, Loblaw A, Chu W, et al. Intensity-modulated fractionated radiotherapy versus stereotactic body radiotherapy for prostate cancer (PACE-b): acute toxicity findings from an international, randomised, open-label, phase 3, non-inferiority trial. *Lancet Oncol* (2019) 20 (11):1531–43. doi: 10.1016/S1470-2045(19)30569-8

15. Zilli T, Taussky D, Donath D, Le HP, Larouche RX, Béliveau-Nadeau D, et al. Urethra-sparing, intraoperative, real-time planned, permanent-seed prostate brachytherapy: toxicity analysis. *Int J Radiat Oncol Biol Phys* (2011) 81(4):377–383. doi: 10.1016/J.IJROBP.2011.02.037

16. Kataria T, Gupta D, Goyal S, Bisht SS, Chaudhary R, Chaudhary K, et al. Simple diagrammatic method to delineate male urethra in prostate cancer radiotherapy: an MRI based approach. *Br J Radiol* (2016) 89(1068):89. doi: 10.1259/BJR.20160348

17. Alongi F, Rigo M, Figlia V, Cuccia F, Giaj-Levra N, Nicosia L, et al. 1.5 T MR-guided and daily adapted SBRT for prostate cancer: feasibility, preliminary clinical tolerability, quality of life and patient-reported outcomes during treatment. *Radiat Oncol* (2020) 15(1). doi: 10.1186/S13014-020-01510-W

18. Tetar SU, Bruynzeel AME, Oei SS, Senan S, Fraikin T, Slotman BJ, et al. Magnetic resonance-guided stereotactic radiotherapy for localized prostate cancer: Final results on patient-reported outcomes of a prospective phase 2 study. *Eur Urol Oncol* (2021) 4(4):628–34. doi: 10.1016/J.EUO.2020.05.007

19. Meier RM, Bloch DA, Cotrutz C, Beckman AC, Henning GT, Woodhouse SA, et al. Multicenter trial of stereotactic body radiation therapy for low- and intermediate-risk prostate cancer: Survival and toxicity endpoints. *Int J Radiat Oncol Biol Phys* (2018) 102(2):296–303. doi: 10.1016/J.IJROBP.2018.05.040

20. Ghadjar P, Zelefsky MJ, Spratt DE, Munck af Rosenschöld P, Oh JH, Hunt M, et al. Impact of dose to the bladder trigone on long-term urinary function after high-dose intensity modulated radiation therapy for localized prostate cancer. *Int J Radiat Oncol Biol Phys* (2014) 88(2):339–44. doi: 10.1016/J.IJROBP.2013.10.042

21. Mariados N, Sylvester J, Shah D, Karsh L, Hudes R, Beyer D, et al. Hydrogel spacer prospective multicenter randomized controlled pivotal trial: Dosimetric and clinical effects of perirectal spacer application in men undergoing prostate image guided intensity modulated radiation therapy. *Int J Radiat Oncol Biol Phys* (2015) 92(5):971–7. doi: 10.1016/J.IJROBP.2015.04.030

22. Dearnaley D, Syndikus I, Mossop H, Khoo V, Birtle A, Bloomfield D, et al. Conventional versus hypofractionated high-dose intensity-modulated radiotherapy for prostate cancer: 5-year outcomes of the randomised, non-inferiority, phase 3 CHHiP trial. *Lancet Oncol* (2016) 17(8):1047–60. doi: 10.1016/S1470-2045(16)30102-4

23. Aluwini S, Pos F, Schimmel E, van Lin E, Krol S, van der Toorn PP, et al. Hypofractionated versus conventionally fractionated radiotherapy for patients with prostate cancer (HYPRO): acute toxicity results from a randomised non-inferiority phase 3 trial. *Articles Lancet Oncol* (2015) 16:274–83. doi: 10.1016/S1470-2045(14)70482-6

24. Geara FB, Bulbul M, Khauli RB, Andraos TY, Abboud M, Al Mousa A, et al. Nadir PSA is a strong predictor of treatment outcome in intermediate and high risk localized prostate cancer patients treated by definitive external beam radiotherapy and androgen deprivation. *Radiat Oncol* (2017) 12(1). doi: 10.1186/S13014-017-0884-Y

25. Ray ME, Thames HD, Levy LB, Horwitz EM, Kupelian PA, Martinez AA, et al. PSA nadir predicts biochemical and distant failures after external beam radiotherapy for prostate cancer: a multi-institutional analysis. *Int J Radiat Oncol Biol Phys* (2006) 64 (4):1140–50. doi: 10.1016/J.IJROBP.2005.07

frontiers | Frontiers in Oncology

TYPE Original Research
PUBLISHED 31 May 2023
DOI 10.3389/fonc.2023.1149961

OPEN ACCESS

EDITED BY
Samuel Chao,
Case Western Reserve University,
United States

REVIEWED BY
Raphael Pfeffer,
Assuta Medical Center, Israel
Gamze Ugurluer,
Acıbadem University, Türkiye

*CORRESPONDENCE
A. M. E. Bruynzeel
ame.bruynzeel@amsterdamumc.nl;
d.doppenberg@amsterdamumc.nl

RECEIVED 23 January 2023
ACCEPTED 22 May 2023
PUBLISHED 31 May 2023

CITATION
Doppenberg D, Lagerwaard FJ, van Dieren S, Meijerink MR, van der Vliet JJ, Besselink MG, van Tienhoven G, Versteijne E, Slotman BJ, Wilmink JW, Kazemier G and Bruynzeel AME (2023) Optimizing patient selection for stereotactic ablative radiotherapy in patients with locally advanced pancreatic cancer after initial chemotherapy - a single center prospective cohort.
Front. Oncol. 13:1149961.
doi: 10.3389/fonc.2023.1149961

Optimizing patient selection for stereotactic ablative radiotherapy in patients with locally advanced pancreatic cancer after initial chemotherapy - a single center prospective cohort

D. Doppenberg[1,2,3], F. J. Lagerwaard[1,2], S. van Dieren[3], M. R. Meijerink[2,4], J. J. van der Vliet[2,5,6], M. G. Besselink[2,3], G. van Tienhoven[1,2], E. Versteijne[1,2], B. J. Slotman[1,2], J. W. Wilmink[2,7], G. Kazemier[2,8] and A. M. E. Bruynzeel[1,2]*

[1]Amsterdam UMC, Department of Radiation Oncology, Vrije Universiteit Amsterdam, Amsterdam, Netherlands, [2]Cancer Center Amsterdam, Amsterdam, Netherlands, [3]Amsterdam UMC, Department of Surgery, University of Amsterdam, Amsterdam, Netherlands, [4]Amsterdam UMC, Department Intervention Radiology, Vrije Universiteit Amsterdam, Amsterdam, Netherlands, [5]Amsterdam UMC, Department of Medical Oncology, Vrije Universiteit Amsterdam, Amsterdam, Netherlands, [6]LAVA Therapeutics, Utrecht, Netherlands, [7]Amsterdam UMC, Department of Medical Oncology, University of Amsterdam, Amsterdam, Netherlands, [8]Amsterdam UMC, Department of Surgery, Vrije Universiteit Amsterdam, Amsterdam, Netherlands

Background: The role of stereotactic ablative radiation therapy (SABR) as local treatment option after chemotherapy for locally advanced pancreatic cancer (LAPC) is evolving. However adequate patient selection criteria for SABR in patients with LAPC are lacking.

Methods: A prospective institutional database collected data of patients with LAPC treated with chemotherapy, mainly FOLFIRINOX, followed by SABR, which was delivered using magnetic resonance guided radiotherapy, 40 Gy in 5 fractions within two weeks. Primary endpoint was overall survival (OS). Cox regression analyses were performed to identify predictors for OS.

Results: Overall, 74 patients were included, median age 66 years, 45.9% had a KPS score of ≥90. Median OS was 19.6 months from diagnosis and 12.1 months from start of SABR. Local control was 90% at one year. Multivariable Cox regression analyses identified KPS ≥90, age <70, and absence of pain prior to SABR as independent favorable predictors for OS. The rate of grade ≥3 fatigue and late gastro-intestinal toxicity was 2.7%.

Conclusions: SABR is a well-tolerated treatment in patients with unresectable LAPC following chemotherapy, with better outcomes when applied in patients with higher performance score, age <70 years and absence of pain. Future randomized trials will have to confirm these findings.

KEYWORDS

pancreatic cancer, LAPC, radiotherapy, SABR, MRgRT, patient selection

Background

Pancreatic ductal adenocarcinoma has a dismal prognosis. At diagnosis, approximately half of the patients have metastasized disease and at least one third of all patients is diagnosed with a non-metastatic, locally unresectable tumor: locally advanced pancreatic cancer (LAPC) (1). A small percentage of patients with LAPC may become eligible for resection following induction chemotherapy, however 85% remains locally unresectable (2). Treatment of these patients focusses on local control, prolongation of life and preservation of quality of life, in which single or multi-regimen systemic chemotherapy plays an important role (3, 4). Based on extrapolation from randomized controlled trials (RCTs) in patients with metastatic PDAC, the current National Comprehensive Cancer Network (NCCN) guideline for LAPC recommends (modified) FOLFIRINOX (a combination of leucovorin, fluorouracil, irinotecan and oxaliplatin) for patients with a good performance score (PS) and a combination of gemcitabine and nab paclitaxel for patients with a poorer Karnofsky performance score (KPS) (5, 6). Patients who do not develop metastases during their systemic treatment may benefit from radiotherapy to delay local progression. A review that reports on overall survival (OS) in patients with LAPC treated with FOLFIRINOX, describes that almost two-third of patients received subsequent radiotherapy or chemoradiotherapy (7). Stereotactic ablative body radiation therapy (SABR) has a number of advantages over conventional radiotherapy and is nowadays recognized as a standard-of-care option in the treatment of LAPC in several guidelines (5, 8–10). SABR allows high-precision high-dose delivery in only few fractions whilst avoiding surrounding radio-sensitive organs at risk (OARs) (11). As a result, SABR causes limited radiation induced toxicity and thus allows quick resumption of systemic therapy, if indicated (11, 12). However, international consensus regarding the role and timing of SABR in the treatment of LAPC is lacking, as well as patient selection criteria. In order to establish such patient selection parameters for SABR, this study analyzed outcomes in LAPC patients treated with upfront chemotherapy followed by SABR.

Materials and methods

Study design

Clinical and outcome data of patients with unresectable LAPC after chemotherapy followed by SABR between June 2016 and March 2022 were selected from a prospectively maintained, ethics committee approved, institutional database.

Study procedures

Patients were referred to the department of Radiation Oncology after a diagnosis of unresectable LAPC by consensus of a multidisciplinary tumor board. Patient characteristics prior to SABR collected in the database were age, gender, patient fitness scored as KPS (13), location of the tumor within the pancreas, use and duration of chemotherapy.

At our center SABR is delivered in the form of magnetic-resonance guided radiotherapy (MRgRT) aiming for a total dose of 40Gy in 5 fractions with dose escalation within the tumor. The objectives for target coverage were a V95% of the GTV ≥90% and a D2% up to 125% of the prescribed dose. Simulation imaging consisted of an Magnetic Resonance (MR)- and Computerized Tomography (CT) scan, both in supine position in shallow inspiration breath-hold. The gross tumor volume (GTV) is delineated on the simulation MR scan aided by diagnostic imaging in collaboration with a gastro-intestinal intervention radiologist. The GTV includes the tumor in the pancreas and any adjacent suspicious lymph nodes. No additional margin for microscopic tumor extension was applied for SABR. The planning target volume (PTV) was generated by the addition of a 3 mm margin around the GTV. The duodenum, stomach, bowel, liver, kidneys, and spinal cord were contoured as OARs. Maximum dose limits to the OARs (duodenum, bowel and stomach) were prioritized over target coverage (14). Radiation was delivered using respiratory gating during subsequent breath-hold periods in shallow inspiration. In addition to auditory feedback provided during treatment, gating of the

tumor is augmented by visual feedback which is performed with the aid of an in-room MR compatible monitor, showing the actual tumor motion on a sagittal cine-MR. Daily adaptive planning is our standard approach for MRgRT of pancreatic cancer patients, which consists of MR imaging and recontouring of the target volume and relevant organs at risk within 2 cm distance, followed by online radiation plan re-optimization. As described for the pretreatment planning, organs-at-risk constraints are prioritized above target coverage for each fraction. Detailed information about the high-dose OAR constraints and the adaptive workflow used for daily plan adaptation in this patient group, is described in our earlier work (14). Patients received dietary instructions as treatment was delivered after 2 hours fasting. It was standard to prescribe prophylactic ondansetron prior to each fraction.

Outcomes

Primary end point was overall survival (OS) defined as 1) time between date of diagnosis and date of death (of any cause) and 2) time between start date of SABR and date of death (of any cause). The secondary end points were local control rates according to RECIST criteria and toxicity (i.e. pain, nausea, diarrhea, fatigue) using the NCI-CTCAE toxicity criteria (version 5.0) (15, 16). Toxicity outcomes were collected both prior to and after SABR to assess the effect of SABR on these measures. The toxicity of all separate symptoms was corrected for the baseline absence or presence and severity. An increase as well as new occurrence of toxicity was noted as toxicity caused by SABR. Outcomes were collected at 6 weeks after SABR for 'acute' toxicity and during follow-up for 'late' toxicity.

Statistical aspects/analyses

Data were analyzed using IBM SPSS Statistics for Windows version 26.0 (IBM Corp., Orchard Road Armonk, New York, NY). Categorical data are presented as percentages and frequencies. Normally distributed continuous data are presented as means and standard deviations (SDs). Primary analyses consisted of OS assessment using Kaplan-Meier estimations from the date of diagnosis and start date of treatment with SABR until the date of death or last moment of follow-up. As data was prospectively collected from start of SABR, stratified Kaplan-Meier analyses were performed among subgroups on OS from start of MRgRT. Continuous variables were divided in subgroups based on the median. Subgroups consisted of high versus low age (≤70 years versus >70 years), high versus low KPS (<90 versus ≥90), absence of pain prior to SABR (pain versus no pain), GTV >37 cc and ≤37cc, interval between the end of chemotherapy and start of SABR (≤6 weeks versus >6 weeks after the last cycle of chemotherapy), and number of chemotherapy cycles (1-4 versus 5-8 versus >8 cycles).

Univariable and multivariable Cox proportional hazard analyses were performed to identify predictors for OS after SABR. Variables in these analyses included all aforementioned variables (see Kaplan-Meier analyses). Variables that were associated with OS at univariable analysis ($p<0.2$) were included in one single multivariable Cox proportional hazard model. Results of the Cox proportional hazard analyses are presented in hazard ratios (HR) with corresponding 95% confidence intervals (CI). A p-value lower than 0.05 was considered statistically significant. Backward selection was performed until the multivariable model comprised only significant parameters (i.e., $p<0.05$).

Results

Patient characteristics

Overall, 74 patients with unresectable LAPC who were initially treated with chemotherapy and subsequently with SABR were included. Median age was 66 years (range 36-81 years), 51.4% of patients were female. About half of patients had a KPS <90 (54.1%). Most patients had primary pancreatic head cancer (67.6%). The majority (87.8%) of patients received FOLFIRINOX, median number of cycles prior to SABR was 4. SABR was delivered with a median dose of 40 Gy (IQR 40-40) in 5 fractions within two weeks overall treatment time. In a single patient, treatment was stopped after 4 fractions because of grade 3 fatigue. In 4 patients an upfront decision was made to deliver 5 fractions of 7 Gy because of local ingrowth in the stomach or bowel (n=2) and because of tumor size (n=2). The delivered mean D2% (dose maximum) was 121% of the prescribed dose and mean GTV dose was 111% of the prescribed dose. Twenty-two patients received chemotherapy after treatment with SABR, mainly FOLFIRINOX (72.7%), ranging from 1 to 12 cycles. Patient characteristics are shown in Table 1.

Survival outcomes

Median follow-up time was 17.8 months from diagnosis and 10.5 months from SABR, no patients were lost to follow-up. A total of 63/74 (86.5%) patients died and 10 patients were censored for the survival analyses, only a single patient died following a non-pancreatic cancer related cause. Median OS from diagnosis was 19.6 months (95%CI 15.9-23.2 months) and 12.1 months (95%CI 9.3-14.8 months) from start of SABR (Figure 1). Kaplan-Meier analyses in separate subgroups revealed a better survival after start of SABR for patients with KPS ≥90 (17.3 versus 6.7 months, p<0.001), age ≤70 (15.4 versus 6.7 months p<0.001, >4 cycles of chemotherapy (13.2 versus 6.0 months, p<0.001), and absence of pain at the time of SABR (15.4 versus 7.6 months, p=0.010). Other tested variables did not affect OS in the Kaplan-Meier analyses, in particular also the time interval between induction chemotherapy and SABR was not significant (See supplementary file).

Cox proportional hazard analyses

Univariable Cox regression analyses revealed that age ≤70, KPS≥90, absence of pain prior to SABR, Type of chemo therapeutic regimen, >4 cycles of chemotherapy, and <6 weeks interval between last cycle of chemotherapy and date of the first

10.3389/fonc.2023.1149961

TABLE 1 Baseline characteristics in patients with localized PDAC treated with chemotherapy and SABR.

Characteristic	Cohort (n=74)
Age, years, median (range)	66 (36-81)
Female sex, *n* (%)	38 (51)
Performance score (KPS), *n* (%) KPS <90 KPS 90-100	 40 (54) 34 (46)
Tumor location, *n* (%) Head Body-tail	 50 (68) 24 (32)
GTV, cc, median (range)	36.8 (7-117)
Radiation dose, Gy, median (IQR)(range)	40 (40-40)(32-40)
Number of fractions*	5
Induction chemotherapy, *n* (%) FOLFIRINOX Gemcitabine based	74 (100) 65 (88) 9 (12)
Number of cycles of induction chemotherapy, median (IQR) 1-4, *n* (%) 5-8, *n* (%) >8, *n* (%)	4 (4-8) 38 (51) 23 (31) 13 (18)
Chemotherapy post SABR, *n* (%)	22 (30)
FOLFIRINOX	16 (22)
Gemcitabine based	6 (8)
Number of cycles chemotherapy post SABR, 1-4, *n* (%) 5-8, *n* (%) >8, *n* (%)	 12 (50) 6 (27) 4 (18)

* A single patient stopped after 4 fractions because of grade 3 fatigue.

fraction, (p<0.2) (Table 2). These variables were therefore included in the multivariable model. This model revealed that age ≤70 (HR 0.42, p=0.007), KPS ≥90 (HR 0.49, p=0.026), and absence of pain prior to SABR (HR 0.40, p=0.001) were independently associated with improved OS. Results are shown in Table 2. In order to identify (un-)favorable patient groups, a cumulative score of the number of favorable predictive factors (KPS ≥90, age ≤70 and absence of pain) was generated, thus ranging from 0 to 3. Kaplan-Meier analysis showed a division between patients having no or one favorable factor versus more than one (Figure 2). An unfavorable (0-1 factor) and a favorable (2-3 factors) group were thus identified. Median survival from SABR for the unfavorable group was 6.6 months (N=31; 95%CI 5.9 – 7.3 months) versus 17.3 months (N=43; 95%CI 13.8 – 20.9 months) for the favorable group (Figure 3).

Progression of disease and local control rates

Six patients experienced a local recurrence. The actuarial local control rate at one year was 90.8%. Isolated loco-regional progression was observed in three patients (4.1%); the other three patients had a simultaneous diagnosis of distant metastases. Distant metastases without local recurrence were observed in 52 patients (70.3%), in the liver in 21 patients, peritoneum in 25 patients, and lungs in 17 patients. Sixteen patients had distant metastases in more than 1 site.

Pain response

Prior to SABR, the distribution of abdominal pain was as follows: no pain in 51.4%, grade ≤2 in 47.2% and grade 3 in 1.4% of patients. Relief of pain was observed in 30 of 36 patients (83.3%) with pre-existing pain, either complete disappearance of complaints or allowing reduction of pain medication.

Pain indication prior to initial chemotherapy had a similar contribution compared to pain indicated prior to SABR: no pain in 45%, grade ≤2 in 53%, grade 3 in 0.0% and missing in 2% of patients.

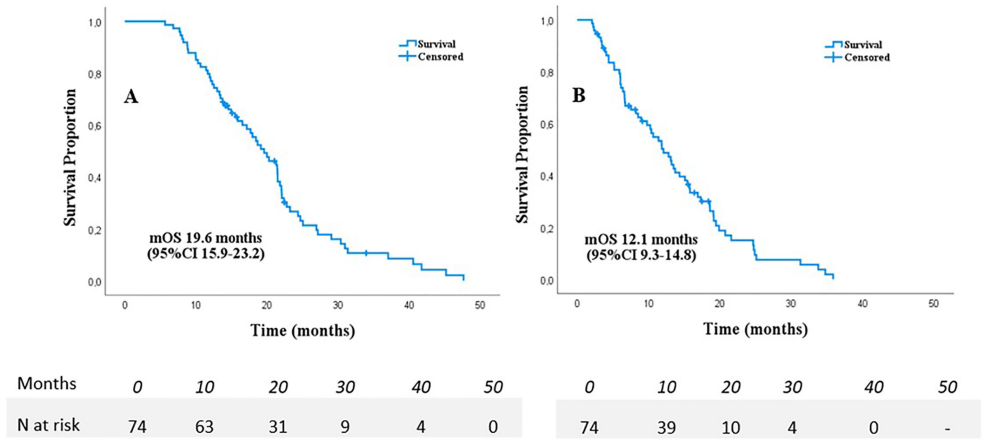

FIGURE 1
Overall survival from diagnosis **(A)** and start of SABR **(B)** in 74 patients with LAPC following chemotherapy.

TABLE 2 Univariable and multivariable Cox regression analyses on predictors for overall survival in patients with localized PDAC treated with chemotherapy and SABR.

		Univariable			Multivariable			Backward selection
	n(%)	HR	95%CI	p-value	HR	95%CI	p-value	
Sex (male)	36 (49)	0.77	0.46-1.28	0.310				
Age ≤70 years	48 (65)	0.39	0.22-0.68	**0.001**	0.39	0.21-0.73	**0.003**	**0.001**
KPS 90-100	34 (46)	0.42	0.25-0.70	**<0.001**	0.44	0.24-0.81	**0.008**	**0.003**
Absence of pain*	38 (51)	0.52	0.32-0.87	**0.012**	0.40	0.23-0.70	**0.001**	**0.003**
Tumor location (head)	49 (66)	0.76	0.45-1.30	0.320				
Tumor Volume (GTV) >37cc	36 (49)	1.33	0.78-2.28	0.297				
Type of Chemotherapy*^	65 (88)	1.75	0.84-3.64	**0.138**	1.36	0.73-2.33	0.460	Removed step 1
n of cycles chemotherapy* 1-4 cycles (reference) 5-8 cycles >8 cycles	38 (51) 23 (31) 13 (18)	 0.54 0.56	 0.31-0.96 0.26-1.22	**0.076** 0.034 0.145	 0.54 1.06	 0.29-0.99 0.47-2.40	0.102	Removed step 3
Longer interval chemo-SABR#	24 (32)	1.44	0.84-2.48	**0.183**	1.31	0.73-2.33	0.366	Removed step 2

HR, hazard ratio; CI, confidence interval; KPS, Karnofsky performance score; GTV, Gross tumor Volume; cc.
*Prior to SABR.
^FOLFIRINOX (reference) (n=65) versus Gemcitabine based chemotherapy (n=9).
#Interval between last cycle of chemotherapy and date of first fraction is ≥6 weeks.
Bold values in the univariable column mean that they were considered significant to be incorporated in the multivariable analysis. The bold values in the multivariable column mean that they are significant.

Toxicity

The only acute grade 3 toxicity that was observed was fatigue in two patients (2.7%); no grade 3 nausea, vomiting or diarrhea was seen. A transient increase or occurrence of abdominal pain was observed in 13/74 patients (17.6%) during or in the first weeks after treatment. This increase in pain did not exceed grade 2. Two patients (2.7%) experienced late grade 3 toxicity including one patient with gastrointestinal bleeding (1.4%) and one patient with suspicion of gastrointestinal obstruction (1.4%). No patient experienced late grade 3 pain, nausea, fatigue, or diarrhea.

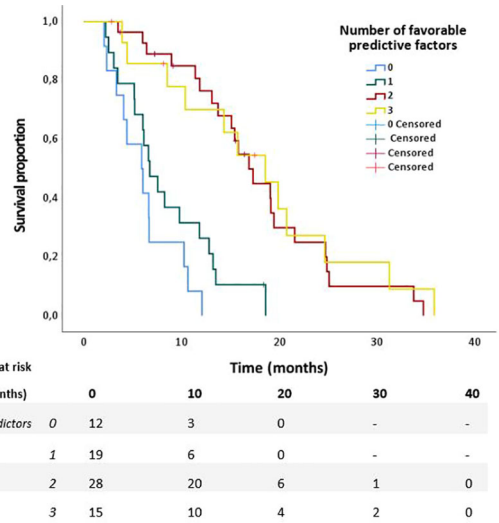

Numbers at risk						
Time (months)		0	10	20	30	40
N fav.predictors	*0*	12	3	0	-	-
	1	19	6	0	-	-
	2	28	20	6	1	0
	3	15	10	4	2	0

FIGURE 2
Overall survival of patients with 0 to 3 favorable predictors for survival from start of SABR in 74 patients with LAPC after chemotherapy.

Discussion

The role of radiotherapy in the treatment of LAPC is under debate in the current international guidelines. Two randomized trials in patients with LAPC comparing gemcitabine monotherapy with gemcitabine plus conventionally fractionated radiotherapy (CFRT) reported contradictory results with respect to OS (17, 18). Both trials were conducted in an era in which gemcitabine-based systemic therapy was predominantly administered, whereas currently FOLFIRINOX is, like in 88% of our (fitter) patients (5, 7). Gemcitabine-based regimens, with or without conventional radiation, have long been the standard of care, resulting in a median OS of 9–11 months in patients with LAPC (18, 19). The use of FOLFIRINOX chemotherapy has improved survival; however, the prognosis for patients with locally advanced pancreatic cancer remains poor, with a median OS of 12–14 months (18, 20). As current systemic treatment becomes more efficient, optimization of local control is increasingly important. With no randomized studies available to compare the efficacy and toxicity of CFRT and SABR in LAPC patients, an extensive systematic review and meta-analysis was performed recently by Tchelebi et al. (21) This study suggest that SABR may offer a modest improvement in 2-year OS (26.9% vs 13.7%) in combination with a favorable acute toxicity profile (5.6% vs 37.7%).

A retrospective cohort demonstrated improved loco-regional control in patients with LAPC who could be treated with a simultaneous integrated boost up to a biologically effective dose (BED_{10}) of more than 70 Gy (22). This dose-escalation was only

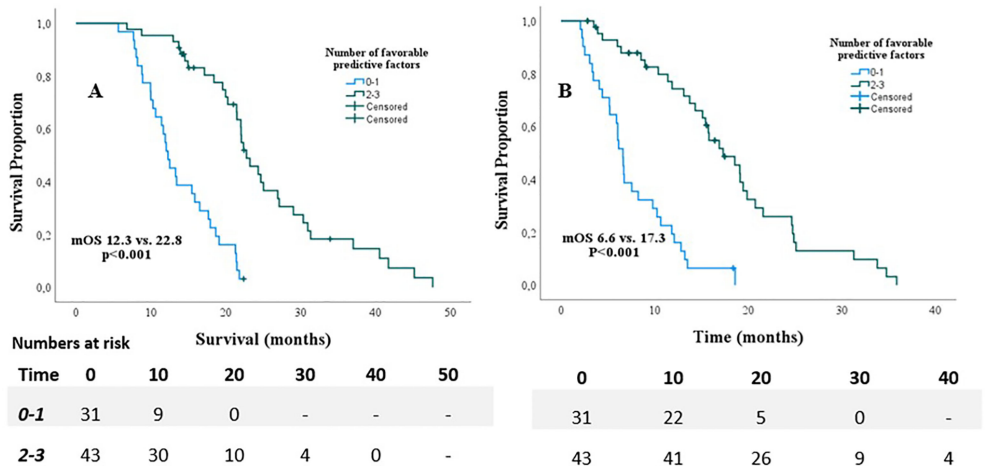

FIGURE 3
Overall survival from diagnosis **(A)** and start of SABR **(B)** for patients with <1 favorable predictor versus patients with 2 and 3 favorable predictors.

feasible in a quarter of the patients in whom the tumor was at more than 1 cm distance from the closest gastrointestinal mucosa. With local radiation dose-escalation in mind, the application of SABR may be a more promising approach. A systematic literature review of SABR for LAPC including more than 1000 patients showed a local control rate at one year of 72.3% (12). Although recent series suggest that further dose-escalation, e.g. using MR-guided radiotherapy as performed in this series, may allow for BED_{10} of more than 100 $Gy_{10,}$ we observed a local control rate of 90% with a BED_{10} of 72 Gy_{10} in five fractions (23, 24). Two similar retrospective studies included 149 and 62 patients also observed a high local control rates of respectively 86.0% and 87.9% at one year after SABR, and warrant the need for prospective evaluation (25, 26). The potential advantages and workflow of SABR performed as non-invasive MR-guided radiotherapy are outside the scope of this paper, but have been described previously (27, 28).

The findings of the present study should be interpreted in light of some limitations. First, a heterogeneous study population was included with possible selection bias due to the non-randomized single-arm design of this study. Differences in indication (primary LAPC and inoperable PC), use of chemotherapeutic regimen, and number of cycles of induction chemotherapy existed, however the present study did not find a prognostic relevance for the latter parameters. In addition, patients with higher age, larger tumors, and worse KPS were included, thus providing the possibility to compare outcomes in these subgroups. Moreover, by including a heterogeneous group treated with to a very similar/homogenous treatment with regard to dose, number of fractions and chemotherapeutic regimen, more can be concluded about the different clinical parameters. Second, it is desirable to find objective, rather than subjective, parameters to be incorporated in prediction models. However, in the present study absence of pain appeared to be a better predictive factor for survival compared to GTV (regardless incorporation of GTV as a continuous or categorized variable). No significant correlation was found between pain and GTV, hereafter both variables were included in the statistical analysis. Third, we were not able to include the value serum CA19-9 in our regression model due to a high proportion of invalid CA19-9 values. Given that CA19-9 levels and its reduction influence OS in PDAC, it would be interesting to find out if CA19-9 impacts survival and should be incorporated in patient selection for SABR (29, 30). Especially given that a high proportion of patients in the present study developed distant metastasis. Last, we were not able to compare these findings to a similar group treated with systemic therapy only, which is yet to be evaluated by a new, but still pending trial in unresectable LAPC comparing standard of care versus standard of care with SABR in unresectable PDAC (LAPSTAR), as well as pending trials comparing (m) FOLFIRINOX with or without additional SABR in the treatment of LAPC (NCT01827553 and NCT04986930).

The present study analyzed the outcomes in patients with LAPC, uniformly treated with initial chemotherapy followed by ablative SABR. Consistent with prior publications, SABR was well tolerated with low rates of acute and late toxicity, (<3%). The OS of 19.6 months is encouraging, but also underscores the need for clear clinical parameters to identify patients who may benefit from local ablative therapy following chemotherapy. The prognostic factors found, i.e. good performance, age younger than 70 years, and absence of pain, showing a substantial and relevant impact on survival in LAPC patients with almost one year median survival difference between the favorable and unfavorable groups. One issue to be addressed is the question whether the unfavorable group should be treated with SABR. The positive response to pain in 83% of patients, confirms the palliative effect of radiotherapy in prior studies, but palliative conventional RT may be sufficient (31, 32).

Conclusion

The impact of clinical parameters on survival of patients with LAPC after chemotherapy is considerable and should be taken into account in the selection for subsequent SABR. The value of SABR as local ablative therapy following chemotherapy should be investigated in randomized controlled trials, and patient

performance status, age, and absence of pain should be taken into account in the design of such trial.

Data availability statement

The raw data supporting the conclusions of this article will be made available by the authors, upon reasonable request.

Ethics statement

Ethical review and approval was not required for the study on human participants in accordance with the local legislation and institutional requirements. Written informed consent for participation was not required for this study in accordance with the national legislation and the institutional requirements.

Author contributions

Conceptualization, and design of the study: AB, FL, DD. AB, FL, DD have organized the database, performed the statistical analysis with the help of SD, and wrote the first draft of the manuscript. AB, FL, DD, SD, MM, EV, MB, GT, JV, BS, JW and GK wrote sections of the manuscript and revised the manuscript, all contributed equally. All authors have read and agreed to the published version of the manuscript.

Conflict of interest

The authors declare that the research was conducted in the absence of any commercial or financial relationships that could be construed as a potential conflict of interest.

Publisher's note

All claims expressed in this article are solely those of the authors and do not necessarily represent those of their affiliated organizations, or those of the publisher, the editors and the reviewers. Any product that may be evaluated in this article, or claim that may be made by its manufacturer, is not guaranteed or endorsed by the publisher.

Supplementary Material

The Supplementary Material for this article can be found online at: https://www.frontiersin.org/articles/10.3389/fonc.2023.1149961/full#supplementary-material

References

1. Tsai S, Evans DB. Therapeutic advances in localized pancreatic cancer. *JAMA Surg* (2016) 151(9):862–8. doi: 10.1001/jamasurg.2016.1113

2. Mizrahi JD, Surana R, Valle JW, Shroff RT. Pancreatic cancer. *Lancet* (2020) 395 (10242):2008–20. doi: 10.1016/S0140-6736(20)30974-0

3. Chen Z, Lv Y, Li H, Diao R, Zhou J, Yu T. Meta-analysis of FOLFIRINOX-based neoadjuvant therapy for locally advanced pancreatic cancer. *Med (Baltimore)* (2021) 100(3):e24068. doi: 10.1097/MD.0000000000024068

4. Damm M, Efremov L, Birnbach B, Terrero G, Kleeff J, Mikolajczyk R, et al. Efficacy and safety of neoadjuvant gemcitabine plus nab-paclitaxel in borderline resectable and locally advanced pancreatic cancer-a systematic review and meta-analysis. *Cancers (Basel)* (2021) 13(17):4326. doi: 10.3390/cancers13174326

5. Tempero MA. Pancreatic adenocarcinoma, version 1.2022, NCCN clinical practice guidelines in oncology national comprehensive cancer network: national comprehensive cancer network. (2022).

6. Conroy T, Desseigne F, Ychou M, Bouche O, Guimbaud R, Becouarn Y, et al. FOLFIRINOX versus gemcitabine for metastatic pancreatic cancer. *N Engl J Med* (2011) 364(19):1817–25. doi: 10.1056/NEJMoa1011923

7. Suker M, Beumer BR, Sadot E, Marthey L, Faris JE, Mellon EA, et al. FOLFIRINOX for locally advanced pancreatic cancer: a systematic review and patient-level meta-analysis. *Lancet Oncol* (2016) 17(6):801–10. doi: 10.1016/S1470-2045(16)00172-8

8. de Geus SWL, Eskander MF, Kasumova GG, Ng SC, Kent TS, Mancias JD, et al. Stereotactic body radiotherapy for unresected pancreatic cancer: a nationwide review. *Cancer* (2017) 123(21):4158–67. doi: 10.1002/cncr.30856

9. Expert Panel on Radiation O-G, Small WJr., Hayes JP, Suh WW, Abdel-Wahab M, Abrams RA, et al. ACR appropriateness Criteria(R) borderline and unresectable pancreas cancer. *Oncol (Williston Park)* (2016) 30(7):619–24, 27, 32.

10. Balaban EP, Mangu PB, Yee NS. Locally advanced unresectable pancreatic cancer: American society of clinical oncology clinical practice guideline summary. *J Oncol Pract* (2017) 13(4):265–9. doi: 10.1200/JOP.2016.017376

11. Rosati LM, Kumar R, Herman JM. Integration of stereotactic body radiation therapy into the multidisciplinary management of pancreatic cancer. *Semin Radiat Oncol* (2017) 27(3):256–67. doi: 10.1016/j.semradonc.2017.02.005

12. Petrelli F, Comito T, Ghidini A, Torri V, Scorsetti M, Barni S. Stereotactic body radiation therapy for locally advanced pancreatic cancer: a systematic review and pooled analysis of 19 trials. *Int J Radiat Oncol Biol Phys* (2017) 97(2):313–22. doi: 10.1016/j.ijrobp.2016.10.030

13. Friendlander AH, Ettinger RL. Karnofsky performance status scale. *Spec Care Dentist.* (2009) 29(4):147–8. doi: 10.1111/j.1754-4505.2009.00088.x

14. Bohoudi O, Bruynzeel AME, Meijerink MR, Senan S, Slotman BJ, Palacios MA, et al. Identification of patients with locally advanced pancreatic cancer benefitting from plan adaptation in MR-guided radiation therapy. *Radiother Oncol* (2019) 132:16–22. doi: 10.1016/j.radonc.2018.11.019

15. Eisenhauer EA, Therasse P, Bogaerts J, Schwartz LH, Sargent D, Ford R, et al. New response evaluation criteria in solid tumours: revised RECIST guideline (version 1.1). *Eur J Cancer* (2009) 45(2):228–47. doi: 10.1016/j.ejca.2008.10.026

16. *Common terminology criteria for adverse events (CTCAE) v5.0 Cancer.gov2017*. Available at: https://ctep.cancer.gov/protocoldevelopment/electronic_applications/docs/ctcae_v5_quick_reference_5x7.pdf.

17. Hammel P, Huguet F, van Laethem JL, Goldstein D, Glimelius B, Artru P, et al. Effect of chemoradiotherapy vs chemotherapy on survival in patients with locally advanced pancreatic cancer controlled after 4 months of gemcitabine with or without erlotinib: the LAP07 randomized clinical trial. *JAMA* (2016) 315(17):1844–53. doi: 10.1001/jama.2016.4324

18. Loehrer S.R. PJ, Feng Y, Cardenes H, Wagner L, Brell JM, Cella D, et al. Gemcitabine alone versus gemcitabine plus radiotherapy in patients with locally advanced pancreatic cancer: an Eastern cooperative oncology group trial. *J Clin Oncol* (2011) 29(31):4105–12. doi: 10.1200/JCO.2011.34.8904

19. Chauffert B, Mornex F, Bonnetain F, Rougier P, Mariette C, Bouche O, et al. Phase III trial comparing intensive induction chemoradiotherapy (60 gy, infusional 5-FU and intermittent cisplatin) followed by maintenance gemcitabine with gemcitabine alone for locally advanced unresectable pancreatic cancer. *Definitive results 2000-01 FFCD/SFRO study Ann Oncol* (2008) 19(9):1592–9. doi: 10.1093/annonc/mdn281

20. Rombouts SJ, Walma MS, Vogel JA, van Rijssen LB, Wilmink JW, Mohammad NH, et al. Systematic review of resection rates and clinical outcomes after FOLFIRINOX-based treatment in patients with locally advanced pancreatic cancer. *Ann Surg Oncol* (2016) 23(13):4352–60. doi: 10.1245/s10434-016-5373-2

21. Tchelebi LT, Lehrer EJ, Trifiletti DM, Sharma NK, Gusani NJ, Crane CH, et al. Conventionally fractionated radiation therapy versus stereotactic body radiation therapy for locally advanced pancreatic cancer (CRiSP): an international systematic review and meta-analysis. *Cancer* (2020) 126(10):2120–31. doi: 10.1002/cncr.32756

22. Krishnan S, Chadha AS, Suh Y, Chen HC, Rao A, Das P, et al. Focal radiation therapy dose escalation improves overall survival in locally advanced pancreatic cancer patients receiving induction chemotherapy and consolidative chemoradiation. *Int J Radiat Oncol Biol Phys* (2016) 94(4):755–65. doi: 10.1016/j.ijrobp.2015.12.003

23. Chuong MD, Bryant J, Mittauer KE, Hall M, Kotecha R, Alvarez D, et al. Ablative 5-fraction stereotactic magnetic resonance-guided radiation therapy with on-table adaptive replanning and elective nodal irradiation for inoperable pancreas cancer. *Pract Radiat Oncol* (2021) 11(2):134–47. doi: 10.1016/j.prro.2020.09.005

24. Rudra S, Jiang N, Rosenberg SA, Olsen JR, Roach MC, Wan L, et al. Using adaptive magnetic resonance image-guided radiation therapy for treatment of inoperable pancreatic cancer. *Cancer Med* (2019) 8(5):2123–32. doi: 10.1002/cam4.2100

25. Chuong MD, Herrera R, Kaiser A, Rubens M, Romaguera T, Alvarez D, et al. Induction chemotherapy and ablative stereotactic magnetic resonance image-guided adaptive radiation therapy for inoperable pancreas cancer. *Front Oncol* (2022) 12:888462. doi: 10.3389/fonc.2022.888462

26. Toesca DAS, Ahmed F, Kashyap M, Baclay JRM, von Eyben R, Pollom EL, et al. Intensified systemic therapy and stereotactic ablative radiotherapy dose for patients with unresectable pancreatic adenocarcinoma. *Radiother Oncol* (2020) 152:63–9. doi: 10.1016/j.radonc.2020.07.053

27. Bohoudi O, Bruynzeel AME, Senan S, Cuijpers JP, Slotman BJ, Lagerwaard FJ, et al. Fast and robust online adaptive planning in stereotactic MR-guided adaptive radiation therapy (SMART) for pancreatic cancer. *Radiother Oncol* (2017) 125(3):439–44. doi: 10.1016/j.radonc.2017.07.028

28. Bruynzeel AME, Lagerwaard FJ. The role of biological dose-escalation for pancreatic cancer. *Clin Transl Radiat Oncol* (2019) 18:128–30. doi: 10.1016/j.ctro.2019.04.020c

29. Ballehaninna UK, Chamberlain RS. The clinical utility of serum CA 19-9 in the diagnosis, prognosis and management of pancreatic adenocarcinoma: an evidence based appraisal. *J Gastrointest Oncol* (2012) 3(2):105–19. doi: 10.3978/j.issn.2078-6891.2011.021

30. Daamen LA, Dorland G, Brada LJH, Groot VP, van Oosten AF, Besselink MG, et al. Preoperative predictors for early and very early disease recurrence in patients undergoing resection of pancreatic ductal adenocarcinoma. *Hpb* (2022) 24(4):535–46. doi: 10.1016/j.hpb.2021.09.004

31. Ebrahimi G, Rasch CRN, van Tienhoven G. Pain relief after a short course of palliative radiotherapy in pancreatic cancer, the academic medical center (AMC) experience. *Acta Oncol* (2018) 57(5):697–700. doi: 10.1080/0284186X.2017.1400692

32. Ryckman JM, Reames BN, Klute KA, Hall WA, Baine MJ, Abdel-Wahab M, et al. The timing and design of stereotactic radiotherapy approaches as a part of neoadjuvant therapy in pancreatic cancer: is it time for change? *Clin Transl Rad Onco* (2021) 28:124–8. doi: 10.1016/j.ctro.2021.04.002

frontiers | Frontiers in Oncology

TYPE Opinion
PUBLISHED 24 October 2023
DOI 10.3389/fonc.2023.1274666

OPEN ACCESS

EDITED BY
Minesh P. Mehta,
Baptist Health South Florida, United States

REVIEWED BY
Anna Bruynzeel,
VU Medical Center, Netherlands

*CORRESPONDENCE
Enis Özyar
enis.ozyar@acibadem.com.tr

RECEIVED 08 August 2023
ACCEPTED 27 September 2023
PUBLISHED 24 October 2023

CITATION
Özyar E and Ben-David M (2023) Obituary: Frank J. Lagerwaard MD, PhD.
Front. Oncol. 13:1274666.
doi: 10.3389/fonc.2023.1274666

Obituary: Frank J. Lagerwaard MD, PhD

Enis Özyar[1]* and Merav Ben-David[2,3]

[1]Acıbadem University, Istanbul, Türkiye, [2]Oncology Institute, Assuta Medical Center, Tel-Aviv, Israel, [3]Faculty of Health Science, Ben-Gurion University of the Negev, Beer Sheva, Israel

KEYWORDS

obituary, Lagerwaard, MR-linac, prostate cancer, pancreas cancer

On July 27, 2023, with the passing of Dr. Frank J Lagerwaard, the profession of radiation oncology lost an outstanding clinician and a brilliant researcher.

Frank spent his childhood years in Rotterdam, Holland. He had graduated from St. Laurens College in 1981 and had earned his medical degree from the Erasmus University in Rotterdam in 1986. For a year between 1989-1990, Frank had worked at Militair Hospitaal Dr. A. Mathijsen as a Radiology Resident and had been a resident of Internal Medicine at the Ignatius Hospital until 1993. He stayed at the Daniel Den Hoed Cancer Center, Rotterdam to complete his radiation oncology training between 1993-2002 and his work resulted in a thesis that earned Lagerwaard a Doctor of Philosophy degree. After 2002, Lagerwaard started to work at the VU University Medical Center (VUMC).

Frank specialized in the treatment of CNS, lung, and pancreatic cancer. After 2006, he was involved in the development of the *MR Linac* program at VUMC. Many scholars are indebted to Lagerwaard for his pioneering work on ablative MR-guided adaptive radiotherapy. He had welcomed many departments within VUMC to share their initial experiences with this cutting edge technology.

Dr. Lagerwaard impact on the field was profound and far-reaching. He was a brilliant researcher, as is evident from the numerous condolences we have received from colleagues all around the world. Each of these contain a personal story of how Frank had positively contributed to their individual careers, professional organizations, and personal lives. His colleagues will always remember this bright, irreverent, kind, and warm-hearted scientist.

His contributions and his positive influence on the lives of many will be forever lasting. There can be no nobler legacy.

Author contributions

EO: Writing – original draft, Writing – review & editing. MB-D: Writing – original draft, Writing – review & editing.

Funding

The authors declare that no financial support was received for the research, authorship, and/or publication of this article.

Conflict of interest

The authors declare that the research was conducted in the absence of any commercial or financial relationships that could be construed as a potential conflict of interest.

Publisher's note

Frontiers in Oncology

Advances knowledge of carcinogenesis and tumor progression for better treatment and management

The third most-cited oncology journal, which highlights research in carcinogenesis and tumor progression, bridging the gap between basic research and applications to imrpove diagnosis, therapeutics and management strategies.

Discover the latest Research Topics

See more →

Frontiers

Avenue du Tribunal-Fédéral 34
1005 Lausanne, Switzerland
frontiersin.org

Contact us

+41 (0)21 510 17 00
frontiersin.org/about/contact